EQUIVALENT CIRCUITS FOR SLOTS IN RECTANGULAR WAVEGUIDE

ARTHUR A. OLINER

AUGUST 1951

AIR FORCE CAMBRIDGE RESEARCH CENTER

DISCLAIMER NOTICE

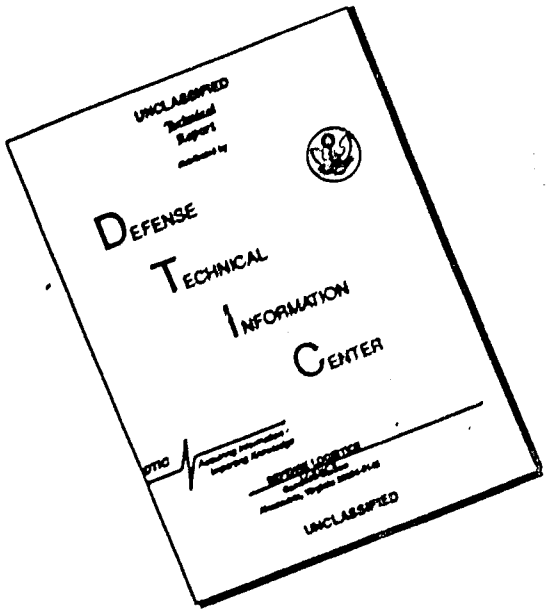

THIS DOCUMENT IS BEST QUALITY AVAILABLE. THE COPY FURNISHED TO DTIC CONTAINED A SIGNIFICANT NUMBER OF PAGES WHICH DO NOT REPRODUCE LEGIBLY.

R-234-50, PIB-179

ERRATA

for

EQUIVALENT CIRCUITS FOR SLOTS IN RECTANGULAR WAVEGUIDE

by

ARTHUR A. OLINER

Microwave Research Institute
Polytechnic Institute of Brooklyn

August 1951
Contract No. AF-19(604)-890

1. Page 72 bottom, eq. (3.32): In the $\underline{z}_o\underline{z}_o$ sums, the factor ϵ_m is missing.

2. Page 73 top, eq. (3.32): $\sum_{m=0}^{\infty} \sum_{n=-\infty}^{\infty}$ should read $\sum_{m=-\infty}^{\infty} \sum_{n=0}^{\infty}$

3. Page 114, eq. (3.107): The very last term in the expression for B_t/Y_o, namely $(\frac{\pi}{2} \frac{b'}{\lambda_{g3}})^2$, should be omitted.

4. Page 120: The expression for C should read

$$C = \frac{Ci\,(ka' + \pi) + Ci\,|ka' - \pi|}{2} \quad ;$$

the negative sign appearing in the original is incorrect.

5. Page 123, eq. (3.120): The factor $16/\pi^2$ should read $\pi^2/16$.

6. Page 123, eq. (3.122): A somewhat more accurate expression is

$$\frac{B_b}{Y_o} + \frac{B_a}{2Y_o} = \frac{1}{n_c^2} \frac{B_t}{Y_o} + \frac{1}{n_c^2} \frac{2b}{\lambda_g} \left[\ell n\, 2 + \frac{\pi o'}{6b} + \frac{3}{2} \left(\frac{b}{\lambda_g}\right)^2 \right]$$

EQUIVALENT CIRCUITS FOR SLOTS IN RECTANGULAR WAVEGUIDE

ARTHUR A. OLINER

MICROWAVE RESEARCH INSTITUTE
POLYTECHNIC INSTITUTE OF BROOKLYN

This work was performed for AFCRL under Contract AF19(122)-3

AUGUST 1951

AIR FORCE CAMBRIDGE RESEARCH CENTEI.
CAMBRIDGE, MASSACHUSETTS

TABLE OF CONTENTS

Acknowledgment

The research described by this report was conducted at the Microwave Research Institute of the Polytechnic Institute of Brooklyn under Contract No. AF-19(122)-3 sponsored by the Air Force Cambridge Research Laboratories.

I. INTRODUCTION

A. Scope of Research

The basic objective of this research is the investigation of the equivalent circuit behavior of rectangular slots of arbitrary dimensions located in a variety of positions in rectangular waveguide. Previous work on this subject has been reported by Watson and Stevenson[1], where the experimental investigation was primarily concerned with radiating slots near resonance, and where the theory restricts itself to narrow slots. The present work considers slots of arbitrary dimensions, both experimentally and theoretically, where the theoretical results are both more accurate and easier to use than those of Stevenson. This investigation was initiated under the direction of Dr. N. Marcuvitz approximately two years ago. However, due to the pressure of increased academic commitments, Dr. Marcuvitz has found it impossible to continue in this capacity, and he has been replaced by Dr. A. A. Oliner as supervisor.

The choices of equivalent circuit representation, method of measurement for the parameters of this representation, and method of theoretical calculation of these parameters for the rectangular slot program are the following. The equivalent circuit representations used are "invariant" ones (to be described later); the parameters for lossless slots are measured by means of the tangent relation method, while radiating slots are measured by a method described later; and the theoretical calculations are made by means of the variational method, due to J. Schwinger. Details of these methods will be discussed later, but it should be mentioned here that stress is laid on them because in some respects they are in themselves contributions to microwave techniques. The types (geometrical location) of slots investigated are the following:

a) Transverse slot (guide to guide coupling), as a function of aperture dimensions, angle of rotation, and thickness.

b) Transverse radiating slot (permitting radiation from the end of the guide): as a function of aperture dimensions and thickness.

---

1 For example, see:
Stevenson, A. F., "Theory of Slots in Rectangular Wave Guides" J. App. Phys., 19, 24 (1948)
Watson, W. H., "The Physical Principles of Wave Guide Transmission" Oxford University Press, 1947

c) Slot-coupled E plane Tee: as a function of aperture dimensions and thickness.

d) Slot radiating from the broad face of the guide (E plane): as a function of aperture dimensions and thickness.

Work is now proceeding in a fashion similar to c) and d) for slot-coupled H plane Tees and H plane radiating slots. The radiating slots of b) and d) couple the guide to a half space (infinite baffle) rather than a "full" space, primarily because the theoretical calculations are then much simpler. Typical slots are shown in Fig. 1.1.

A number of smaller progress reports have been issued some time back, but attention is called here to two major reports which are referred to later in the present report. They are:

1) "The Representation, Measurement, and Calculation of Equivalent Circuits for Waveguide Discontinuities with Application to Rectangular Slots", Final Report, R-193-49, PIB-137.

2) "Waveguide Circuit Theory: Coupling of Waveguides by Small Apertures", Report R-157-47, PIB-106.

The latter report was written by N. Marcuvitz, and gives a detailed presentation of the theoretical background necessary for setting up the required variational expressions. The report describes the rigorous formulation of an arbitrary electromagnetic field in terms of modes characteristic of the guide cross-section, and includes terms which account for sources within the guide due to obstacles and apertures. It is then shown how the fields everywhere may be solved for by means of an integral equation, from which one may easily obtain the corresponding variational expression. The report contains other material, such as the solution of the integral equations for small apertures (not rectangular, however), but these are not of direct interest. The former report was a group project, and contains information on the first portion of the slots program, information which will not be repeated in the present report. The experimental results presented there are for the transverse slot, as a function of aperture dimensions, angle of rotation, and thickness, and for the thin transverse slot radiating from an "infinite" baffle, as a function of aperture dimensions. Corresponding theoretical results are presented there, but they are neither as accurate nor as simple in form as those presented for the

TYPICAL SLOTS

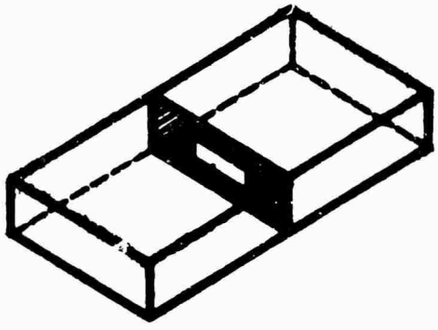

TRANSVERSE SLOT

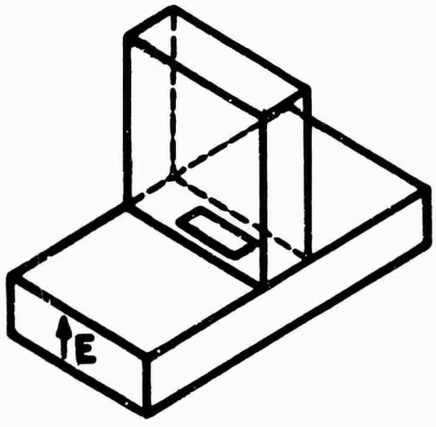

SLOT-COUPLED
E PLANE TEE

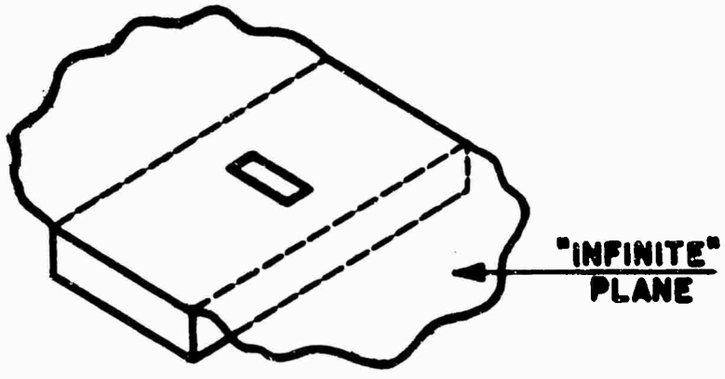

E PLANE RADIATING SLOT

Figure 1.1

transverse slot in the present report. The measurement method used is presented in considerable detail, including the tangent relation procedure itself, ways of obtaining the final parameters to within the ultimate precision of the data, the manner in which estimates of error are obtained, and a description of the equipment, together with the experimental techniques and the precautions to be observed. In addition, the "invariant" representation for the transverse slot is given (although not by that name), and the method of setting up the variational expression for transverse slots is described. The contents of these previous reports are listed here since in the present report reference to them is made frequently and it is tacitly assumed that they are available.

The term "invariant", applied to the equivalent circuit representations used in the slot program, is novel, and is introduced in this report. It is known that the parameters of an equivalent circuit representation can be changed by shifting the circuit reference planes. The purpose of the "invariant" representation is to obtain an equivalent circuit wherein the parameters are determined experimentally independently of any absolute distance measurements, i.e. the parameter values are "invariant" to absolute distance measurements, and depend only on electrical measurements. The absolute distance measurements, which are always less accurate, are then involved only in the location of the reference planes. As expected, the resultant representation is intimately connected with the measurement method, so that further details will be given in Part II. While it is of course true that the accuracy of the overall circuit, including the reference planes, is not improved in any way by the invariant representation, there are a number of distinct advantages:

a) For certain locations of reference planes, the circuit parameter values are critically dependent on the sources of error, and may change wildly for a very small error in, say, a distance measurement. It is known, however, that the overall accuracy is affected only slightly, so that the large change is spurious. It is therefore preferable to use a representation wherein the parameter values are insensitive to such small errors, and the invariant representation serves this purpose.

b) As mentioned above, the parameters depend only on the electrical measurements and are independent of the absolute distance measurements. Due to this separation of dependence,

it is much easier to estimate quantitatively the effect on the parameters of small sources of error, and therefore easier to estimate the accuracy of the final results.

c) The invariant representation results in an equivalent circuit which is simpler in form, and is consequently easier to use. This is especially true when several networks are compounded to form a composite network.

The measurement methods described in Part II are such as to result in an invariant representation and to lend themselves to a systematic procedure which obtains the final parameter values to within the precision of the data. The systematic precision procedure used for lossless structures is the tangent relation method described in detail in the above-mentioned Final Report. For lossy structures (slots which radiate), the tangent relation method is no longer satisfactory and a different method has been devised. It is applicable both to purely series or shunt representations (such as that for a thick radiating slot) and to general lossy structures. The latter precision method is not included in the present report but will be described in detail in a separate report devoted exclusively to precision measurements of dissipative structures. It should be added that for precision measurements one must not neglect the discontinuity produced by the end of the slot in the slotted section. A calibration procedure that takes this into account for lossless structures has been described in the above-mentioned Final Report. When lossy structures are being measured, the corrections to be applied to the slotted section readings are different from those of the lossless case. A method is given in Part II of obtaining the corrections to both the location of the minimum and to the VSWR, when lossy structures are being measured, which makes use of the calibration curve directly applicable to lossless structures.

As mentioned earlier, the theoretical results for the susceptances are derived from variational expressions. These are of the aperture type, and require the insertion of a trial electric field (in the aperture region) into the variational expression. A principal virtue of variational expressions is that the result (here a susceptance) is stationary about the correct field choice. In addition, since the trial field appears in both the numerator and denominator of the variational expressions, one need not know the amplitude of the trial field, but only its form. In some cases, one can formulate a maximum or a minimum principle for the susceptance, but such is

not available here since the kernels involved are not positive definite. It is to be stressed that the use of variational expressions reduces the calculation procedure to that of integrations rather than the solution of integral equations. However, the integrations involve infinite sums which are slowly convergent. There are a number of ways to deal with this problem, including that of transforming the sum to a more rapidly convergent one. Some methods of accomplishing the latter have been given in the Final Report mentioned above. An alternative procedure, that of approximating the guide Green's function (which involves the infinite sums) by a free space Green's function (in closed form) plus corrections, has also been given in that Final Report. In Part III of the present report a still different method is presented which is the most successful. The dyadic guide Green's function is first put into the form of a dyadic operator operating on a scalar function. This scalar function, an infinite double sum, is separated into a sum corresponding to what is obtained for a wide open (capacitive) slot, and a sum over the remaining higher modes. This latter sum is then transformed by means of a Poisson transformation into a much more convergent sum. As a result, the Green's function is separated into components in such a fashion as to make it possible to express the slot susceptance as the wide open slot result plus correction terms. Proof that this latest method of procedure is very successful is supplied by Part IV, where the experimental and theoretical results are compared, and where it is seen that the agreement is excellent over wide ranges of aperture dimensions.

Part V is devoted to somewhat different considerations. For the radiating slots discussed in Parts II to IV, the half space into which they radiate is considered simply as a terminating admittance, without regard to the propagation behavior in the half space itself. Part V investigates the half space itself in terms of spherical transmission lines, and furthermore considers the coupling of the half space to the rectangular waveguide. Evidently, the representation of the half space becomes comparatively simple if essentially only one mode must be considered. A transverse radiating slot, which was treated in Parts II to IV as a two terminal network, is considered as a four terminal network from this viewpoint. The first portion of Part V is concerned with how well and under what conditions a half space may be represented by a single spherical transmission line. It was found that the radiation pattern in the half space produced by a radiating slot was very well accounted for by only the H_{11} mode, and that more than 99 percent of the power radiated was carried by this mode. The equivalent circuit parameters of the four terminal structure representing the slot coupling element between the end of a rectangular guide and a half space have been measured and theoretically computed, both on the basis of the H_{11} mode only

in the half space. As seen in Part V, the agreement is good. Also included in Part V are some basic properties of spherical transmission lines. The study of spherical lines is continuing along the lines of determining the behavior of various transverse and longitudinal discontinuities in the half space. This will yield information on the effect of neighboring slots, and of removing the infinite baffle, on the equivalent circuit of a given slot.

B. Personnel

The members of the "Slots" program now include:

Professional

J. Blass, Research Assistant - MEE
L. Felsen, Research Assistant - MEE
H. Kurss, Research Assistant - EEE
A.A. Oliner , Research Associate - Ph D (Supervisor)

Technicians

Miss M. Crowell, Technician
Mrs. R. Haber, Computress - BA
Miss R. Hammond, Technician
Miss F. Okun, Computress - BA

Messrs. J. Blass and H. Kurss have been concerned essentially with the theoretical and experimental aspects, respectively, of the single slot investigation. Mr. L. Felsen has participated in the experimental portion of the single slot program, but has lately devoted himself to the spherical transmission line study of a half space. In the writing of this report, major credit should be given to J. Blass for Part III, and to L. Felsen for Part V.

Although Dr. N. Marcuvitz is not included in the list of personnel, and although it was mentioned earlier that he initiated the investigation, it should be stressed here that he is responsible directly for some of the work described in this report, as for example, the variational expressions discussed in Part III.

II. EQUIVALENT CIRCUIT REPRESENTATIONS AND MEASUREMENT PROCEDURES

A. E Plane Tee Structures

1. Equivalent Circuit Representations

A sketch of the structure and an equivalent circuit representation for it at centerline reference planes are shown in Figure 2.1.

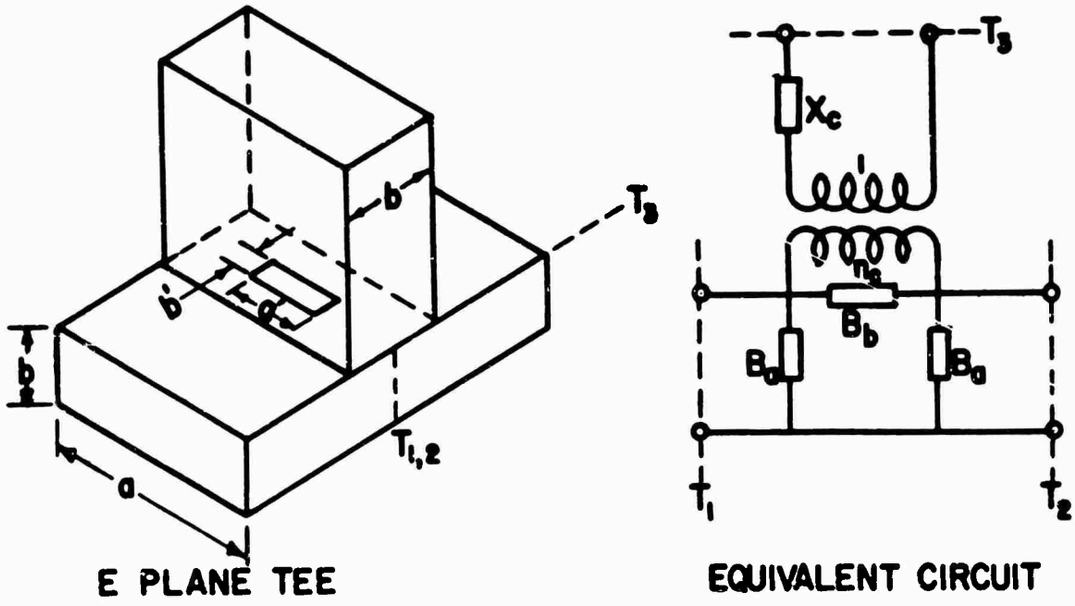

Figure 2.1

Since the considerations are restricted to symmetric structures the six-terminal network contains only four independent parameters. The fourth parameter appears as X_c rather than in susceptance form because X_c is a small quantity. The subscript c on the turns ratio signifies centerline representation. The centerline representation corresponds to the one used for the theoretical calculations in Part III, since the relations between the input and output fields are valid over a single surface.

For general use, as well as for measurement purposes, a different representation is preferable. This "invariant" representation, given in Figure 2.2, has the advantage that the values of the circuit parameters depend solely on electrical measurements (independent of any absolute distance measurements), while the less accurate mechanical measurements (or other methods of absolute distance measurement) affect only the location of the reference planes. In addition the circuit is much simpler in form. The

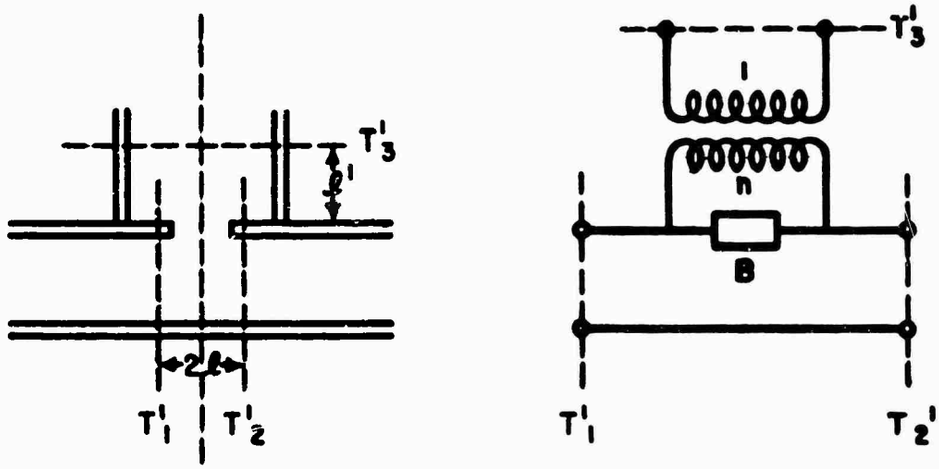

E PLANE TEE "INVARIANT" EQUIVALENT CIRCUIT

Figure 2.2

four independent parameters for the E plane Tee are B, n, 2ℓ, and ℓ', as indicated in Figure 2.2. A corresponding "invariant" representation for a symmetric lossless four-terminal network was given in Final Report,[2] R-193-49, PIB-137, Chap. II, Sec. D, 2. There, the circuit consisted of a single shunt element, whose value depended only upon the value of γ in the measurement procedure. The value of γ is that of the VSWR produced by the structure when a matched load is placed in back of it, and is thus seen to be independent of any reference plane locations. The reasons for the "invariant" nature of the parameters B and n of Figure 2.2 will be seen when the measurement procedure is discussed.

---

[2] Hereinafter referred to as "Final Report".

Since the theoretical calculations are made with the reference planes at the centerline, while the experimental results are obtained using the "invariant" representation, it is necessary to have available expressions relating the values of the parameters of one representation to those of the other. In Table 2-I the values of the parameters at the centerline representation are given in terms of the parameter values of the invariant representation, while the reverse is presented in Table 2-II. These expressions may be obtained in various ways. The relations given in Table 2-I are derived in the Appendix by two different methods in order to illustrate the possible approaches one can employ. The representations involved in Table 2-I were chosen simply as a typical example.

E PLANE TEE

TABLE 2-I

Parameters of the Centerline Representation in Terms of Those of the Invariant Representation

1. $$\frac{B_a}{Y_o} = -\tan \varkappa \ell \qquad , \qquad \varkappa = \frac{2\pi}{\lambda_g}$$

2. $$\frac{B_b}{Y_o} = \frac{\frac{B}{Y_o} - \frac{\tan \varkappa \ell'}{n^2}}{\left[1 + 2\left(\frac{B}{Y_o} - \frac{\tan \varkappa \ell'}{n^2}\right) \tan \varkappa \ell\right] \cos^2 \varkappa \ell}$$

3. $$-\frac{X_c}{Z_o} = \frac{\tan \varkappa \ell' + 2\left[\frac{B}{Y_o} \tan \varkappa \ell' + \frac{1}{n^2}\right] \tan \varkappa \ell}{1 + 2\left(\frac{B}{Y_o} - \frac{\tan \varkappa \ell'}{n^2}\right) \tan \varkappa \ell}$$

4. $$n_c = n \cos \varkappa \ell \cos \varkappa \ell' \left[1 + 2\left(\frac{B}{Y_o} - \frac{\tan \varkappa \ell'}{n^2}\right) \tan \varkappa \ell\right]$$

TABLE 2-II

Parameters of the Invariant Representation in Terms of Those of the Centerline Representation

1. $$2\ell = \frac{2}{\varkappa} \tan^{-1}\left(-\frac{B_a}{Y_o}\right) \quad , \quad \varkappa = \frac{2\pi}{\lambda_g}$$

2. $$\tan \varkappa \ell' = \frac{\frac{2}{n_c^2}\frac{B_a}{Y_o}}{1 + \frac{B_a}{Y_o}\left(\frac{B_a}{Y_o} + 2\frac{B_b}{Y_o}\right)} - \frac{X_c}{Z_o} \quad , \quad \ell' \text{ is the parameter.}$$

3. $$n = \frac{2}{n_c} \frac{\sin \varkappa \ell}{\sin \varkappa \ell'} \left[\frac{\tan \varkappa \ell'}{\tan \varkappa \ell' + \frac{X_c}{Z_o}}\right]$$

4. $$\frac{B}{Y_o} = \frac{\tan \varkappa \ell'}{n^2} + \frac{\frac{B_b}{Y_o}}{1 + \frac{B_a}{Y_o}\left(\frac{B_a}{Y_o} + 2\frac{B_b}{Y_o}\right)}$$

2. Measurement Method

The measurement procedure is based upon the representation shown in Figure 2.2, and follows the practise of reducing the measurement of a 2n-terminal structure to a series of four-terminal measurements.

In order to locate the reference planes T_1' and T_2' a variable short is placed at T_2' and adjusted until no power enters the Tee stub. Under this condition, open circuits occur at T_2' and at T_1', so that they are each located one quarter wavelength from the plane of the voltage null in the output and input guides, respectively. A tuning stub is placed in the stub arm and adjusted so as to maximize the sensitivity of the measurement. Care must be taken to maintain the symmetry of the curve of power detected in the stub guide versus position of the variable short about the point where no power enters the Tee stub, since minima are located by obtaining the average position between equal voltage levels on each side of the minimum.

This is necessary here even though the minimum point is sharp (as opposed to the minimum of a standing wave in the slotted line) because of possible backlash in the variable short. Since the structure is symmetric, T_1' and T_2' are symmetrically disposed with respect to the centerline. By this method of measurement, the symmetry plane, or centerline, need not be located mechanically. The actual determination of 2ℓ, the distance between T_1' and T_2', requires a measurement of the length of the section of guide containing the Tee structure. This length may be measured mechanically, or electrically if one covers up the slot opening. The latter has been found to be more accurate.

To locate the reference plane T_3', one first places a short circuit at T_2', and inserts a variable short in the stub guide. The stub guide short is then adjusted until a voltage null appears at T_1', indicating that a short circuit must then also be present at T_3'. The actual length ℓ' is then obtained from a knowledge of the length of the stub guide, which is determined electrically by placing the stub guide at the end of a slotted section and covering up the slot opening (with silver paint, say, if it is small). It should be noted that the relative location of the reference planes T_1', T_2', and T_3' do not involve any absolute distance measurements, while the parameters 2ℓ and ℓ' defining their absolute location do require their knowledge.

The remaining circuit parameters can be determined by the measurement method for a four-terminal structure described in the Final Report, Chap. II, Sec. D. A four-terminal structure between reference planes T_1' and T_3' is obtained by placing a fixed termination on T_2'. In particular, a short circuit at T_2' was chosen. The resulting equivalent circuit is shown in Figure 2.3.

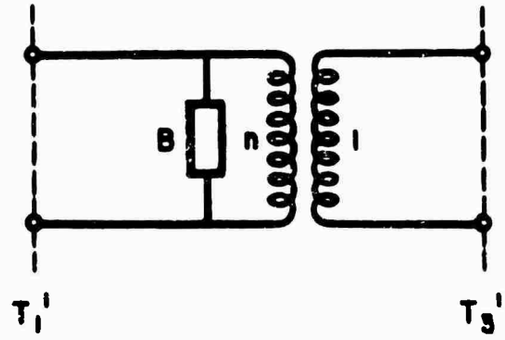

Figure 2.3

The tangent relation measurement technique yields three parameters, α and β, which depend upon the input and output terminal planes, respectively, and γ, which is independent of them. It is desired that the circuit parameters B and n be obtained in an "invariant" fashion, i.e., independently of any absolute distance measurement. The location of T_1' has been obtained in an invariant manner, namely, from a zero power measurement. Therefore α is known invariantly, and γ is always an invariant, being equal to the VSWR produced by the structure when a matched load is placed behind it. The value of β can be obtained from the relation between these parameters that holds when the network is a shunt one, namely (see Final Report, Chap. III, Sec. B, 1, a):

$$\beta = \alpha/\gamma \qquad (1.1)$$

The values of B and n are then determined from the values of α, β, and γ according to relations given in the above-mentioned section of the Final Report. It is stressed that these values of B and n do no depend on any absolute distance measurements.

The measurement procedure for the four-terminal network described above also yields a value for the location of the output reference plane T_2', so that if the length of the stub guide were known, ℓ' could be determined. Another method was given earlier for measuring ℓ', and it was found that the methods agreed well. Sensitivity calculations of the dependence of the parameters B, n, and ℓ' on the various sources of error in the measurement procedure are given in Part IV, and are used to determine the precision of the experimental results.

An alternative method of proceeding in an "invariant" fashion is to obtain α and β relative to the invariantly determined T_1' and T_2' (in the manner described earlier), and to use the already invariant γ, without imposing the restriction for a shunt circuit. The resulting equivalent circuit, however, would contain a series element which would be non-zero if any error occurred in the measurements, and for this reason was not employed.

3. Experimental Techniques

A portion of the experimental program consists of determining the equivalent circuit parameters for slot-coupled E plane Tees as a function of slot dimensions. Rather than use different coupling elements for each slot size, the same element was used for each slot width, while the slot length was successively increased. The first method used to change the slot size was to unsolder the stub connection, increase the size of the slot, and then resolder the Tee stub. This crude method was abandoned when it was found that the parameter values, especially that of ℓ', varied with the particular resoldering. Instead, an air chuck, a simplified drawing of which appears in Figure 2.4, was employed. A grooved metal plate is brazed to the main

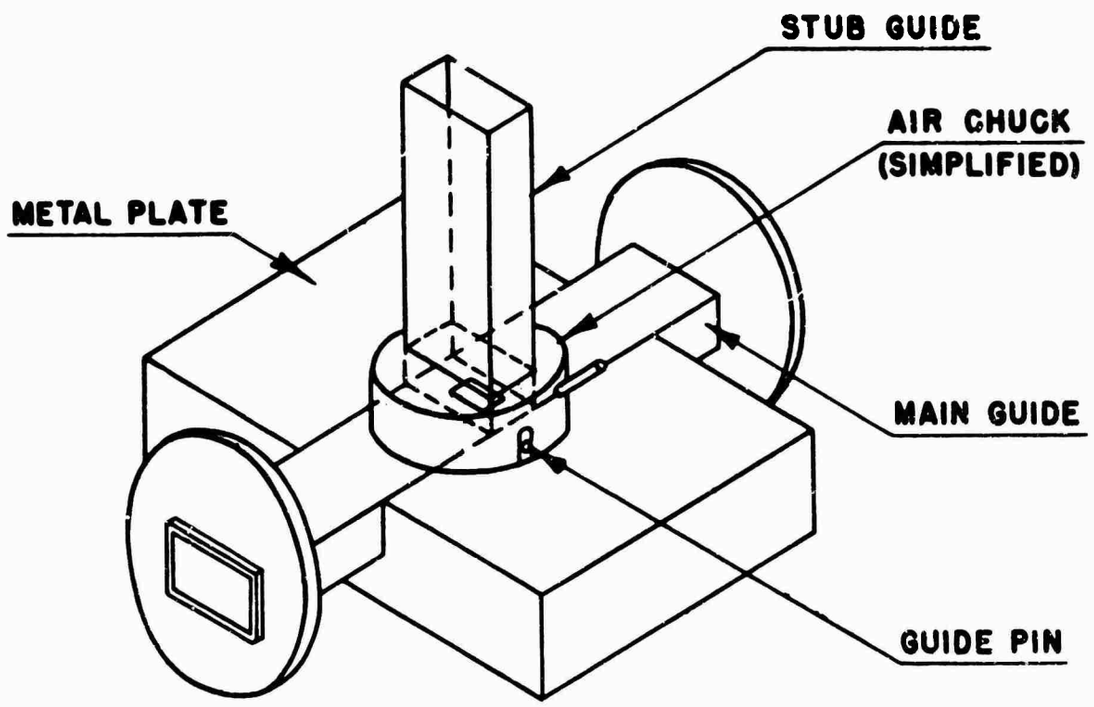

Figure 2.4

section of the Tee in a manner such that the top of the guide is in the same plane as the upper surface of the metal plate. The slot is machined in the top of the guide. The air chuck "B" is placed over the slot, and is properly oriented by means of a pair of guide pins. A section of waveguide is then continued from the top of the chuck, while electrical contact at the slot is maintained by the weight of the air chuck unit and the vacuum. It is then a relatively simple matter to remove the Tee section, change the size of the aperture , and afterwards replace the Tee stub.

Difficulties arose, however, with the use of the air chuck in connection with thin slots (wall thickness = .010"), where the top wall of the guide was found to buckle when the slot was enlarged by filing. (In order that the top of the guide be in the same plane as the metal plate, it is necessary to have the whole top of the guide the same thickness as the

slot wall itself, at least over the air chuck region.) The procedure finally adopted for thin slots was to construct the Tee section with a very small coupling hole. With the coupling aperture sealed by silver paint the effective "electrical" guide lengths are readily measured. Slot enlargements are then still made by filing, but are effected with the aid of a steel mandrel which fits the main guide and on whose top face are milled slots of the desired sizes.

The air chuck is employed, however, for the measurement of thick slots since there, no buckling questions arise. The physical arrangement is slightly different from that shown in Figure 2.4, and Figure 2.5 indicates the actual structure, omitting the air chuck itself since it is the same as that in Figure 2.4. A photograph of the thick slot is shown in Figure 2.6, where the slot thickness has been reduced to the point where some of the construction features are evident. The photograph in Figure 2.7 illustrates the arrangement of the equipment for the taking of data, specifically the zero power measurement for the location of reference planes T_1' and T_2'.

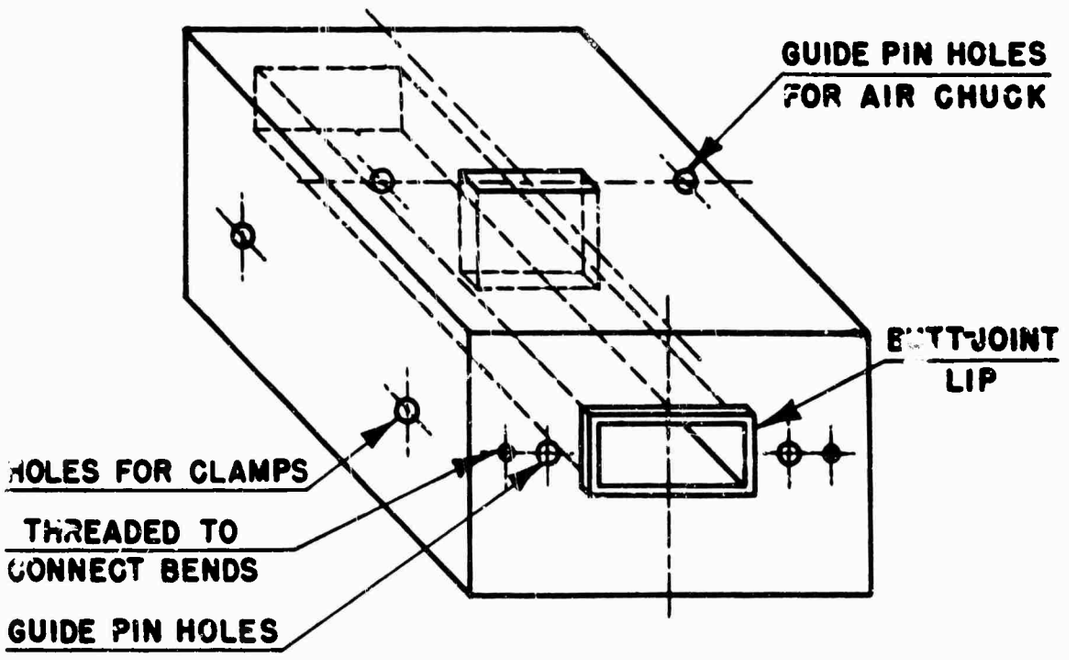

Figure 2.5

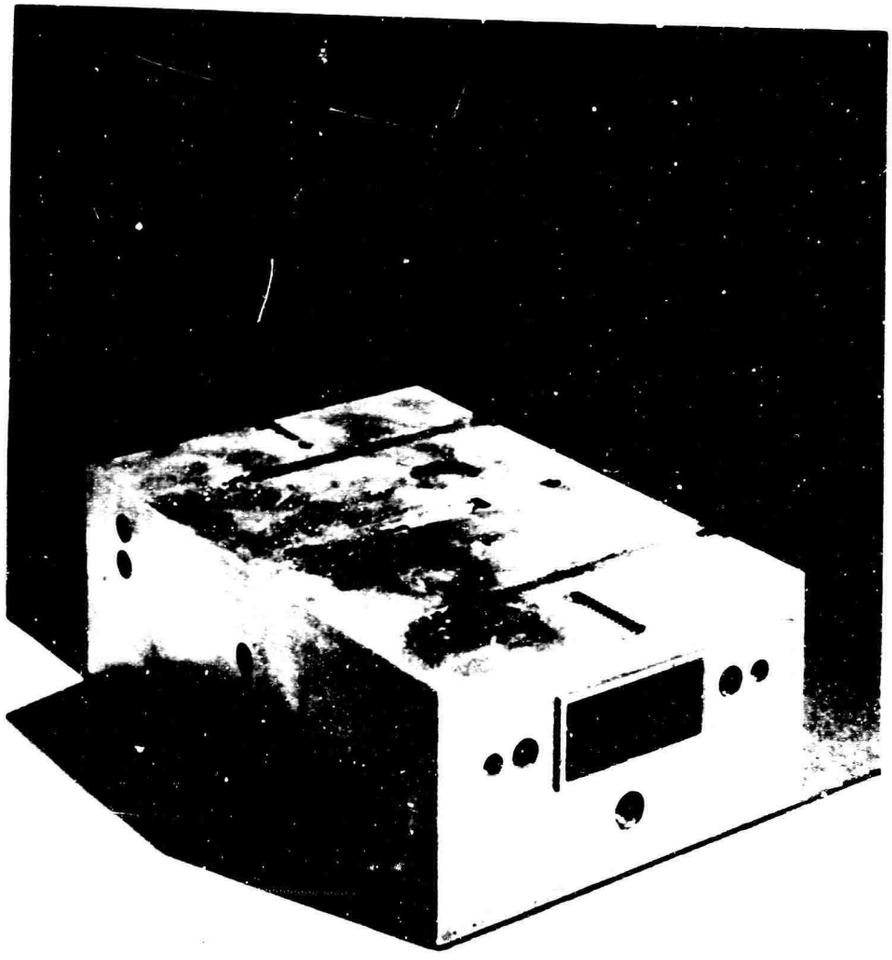

Figure 2.6

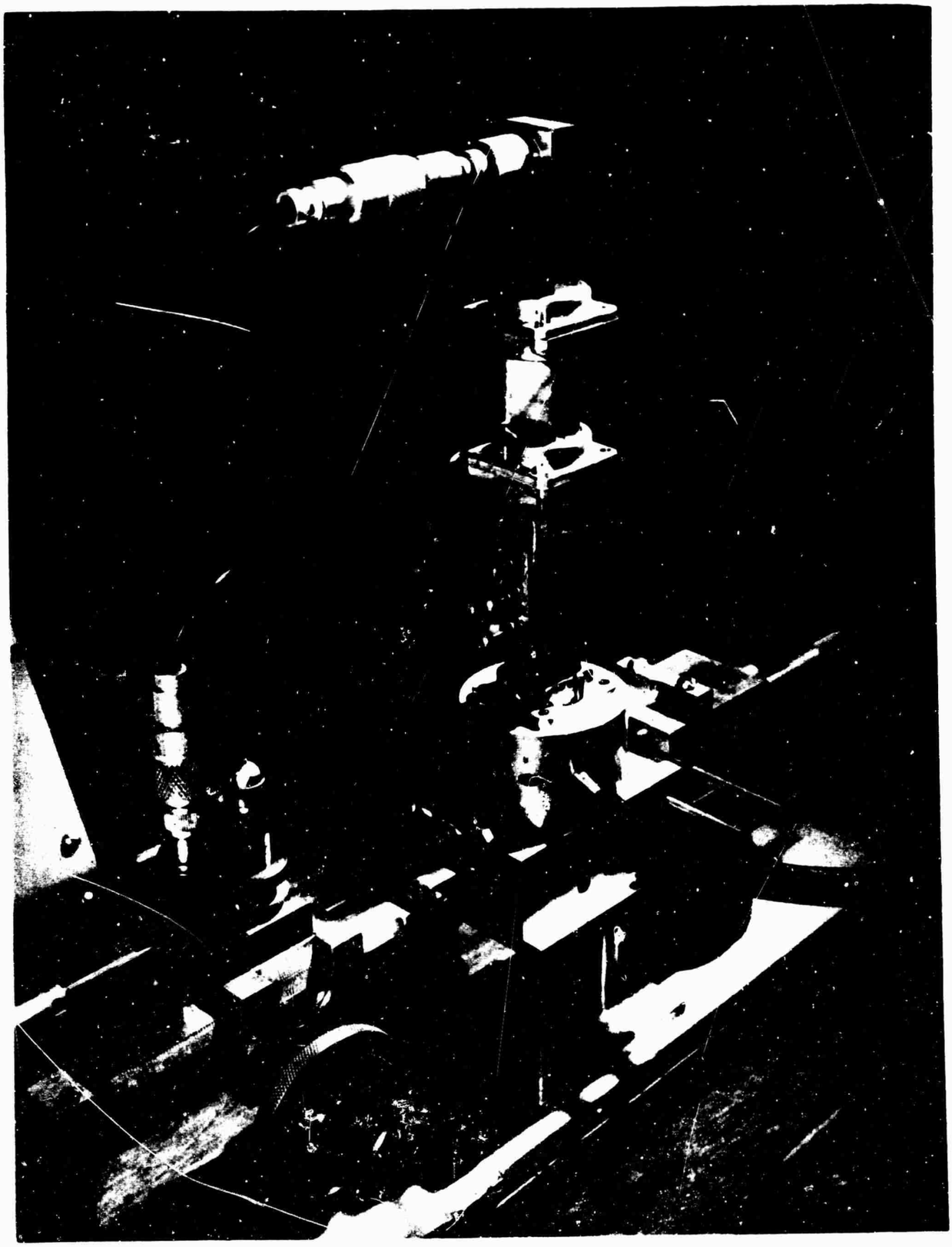

FIGURE 2.7

4. The Thick Slot

The thick slot-coupled E plane Tee, whose physical structure is given in Figure 2.8, may be considered as a whole or in terms of its component parts. Its "invariant" equivalent circuit representation, when considered as a whole, is also given in Figure 2.8. The measurement procedure

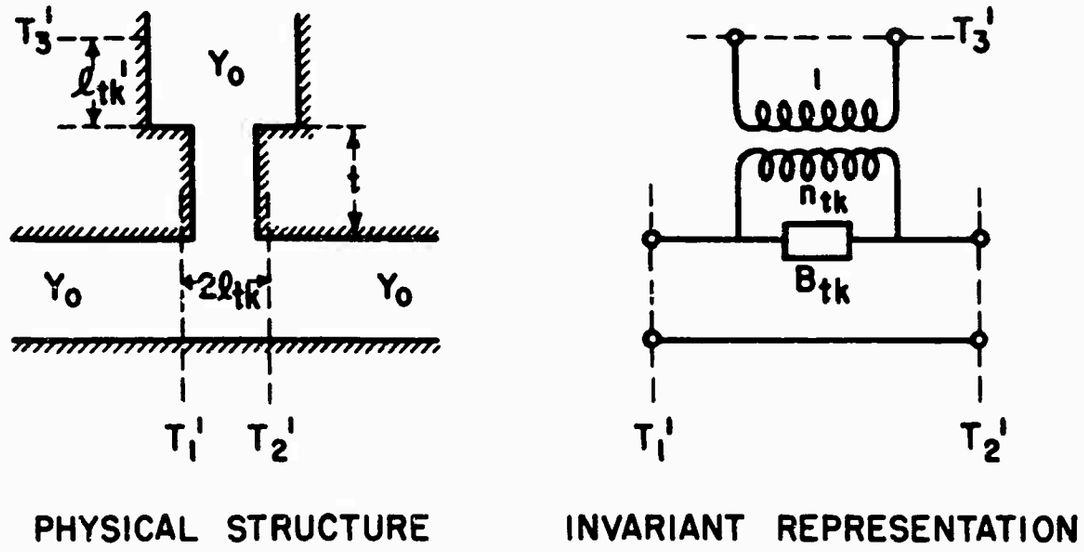

Figure 2.8

used to obtain the parameters of this network is identical to that described for thin slots in Sec. 2. The component parts of this structure are an E plane Tee junction (with no slot), joined by a transmission line of length t, equal to the slot thickness, to a change of cross-section junction in the stub guide. If one knows the circuit parameters for all the component parts of the structure, he can obtain the parameter values for the "invariant" representation of the overall structure. Alternatively, from the knowledge of the parameters of the overall structure and of the change of cross-section, one can obtain the parameters for the E plane Tee junction. In fact, a check on the measurement is obtained by seeing whether or not these latter parameters are independent of the slot thickness t, for values of t large enough so that no interaction occurs between the Tee junction and the change of cross-section junction. Both of these methods of utilizing the data are employed in Part IV.

The equivalent circuit for the change in guide cross-section is shown in Figure 2.9 (a) (see Final Report, Chap. V). The reference plane

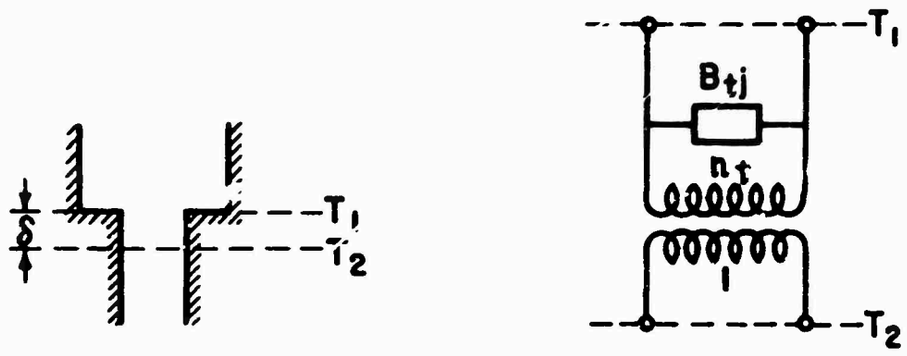

Figure 2.9 (a)

shift δ is very small, and is usually negligible. The turns ratio n_t (where the t stands for "transverse") is given by:

$$n_t^2 = \frac{a'b'}{a\,b}\left[\frac{4}{\pi}\,\frac{\cos(\pi\, a'/2a)}{1-(a'/a)^2}\right]^2 \qquad (2.1)$$

where a' and b' are the smaller guide dimensions, and a and b the larger guide dimensions. The value of susceptance B_{tj} is to a good approximation equal to .55 times the susceptance value B_t of a thin transverse slot with aperture dimensions equal to the smaller cross-section.

The equivalent circuit for the E plane Tee junction, at centerline reference planes, is given in Figure 2.9 (b), and may be regarded as corresponding to an infinitely thick slot. The parameter values are distinguished from those in the slot-coupled case by the subscript "j" meaning "junction". Centerline reference planes are chosen because comparison will be made between the theoretical values for the junction above and for the thin slot-coupled E plane Tee, where the stub guide dimensions above are equal to the slot dimensions. The length of transmission line represented by the slot proper has a propagation constant γ' related to its dimensions in the usual manner, and a characteristic admittance given by $Y_0' = \gamma'/\omega\mu$.

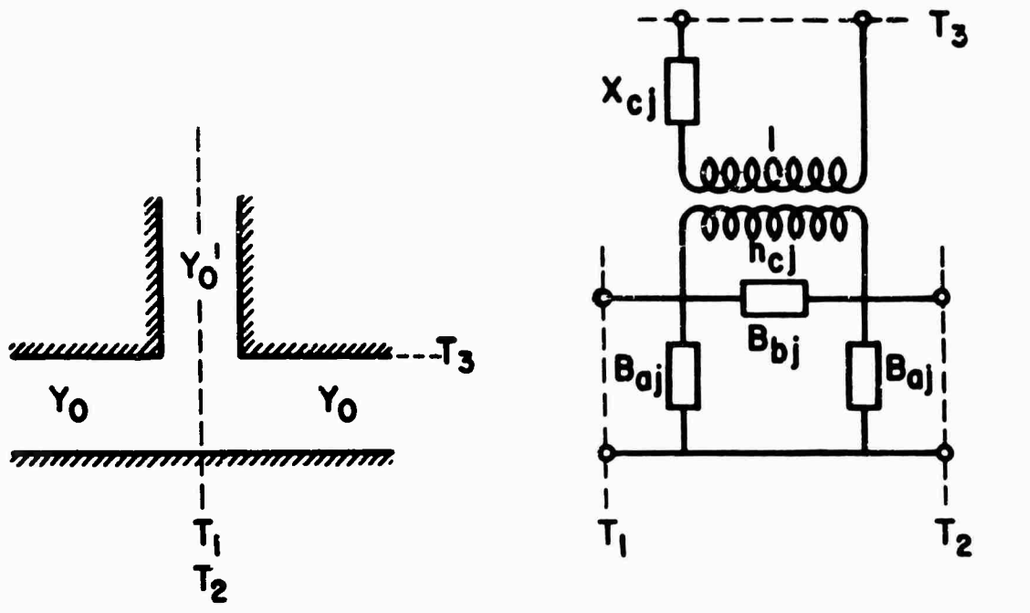

E PLANE TEE JUNCTION

EQUIVALENT CIRCUIT AT CENTERLINE REFERENCE PLANES

Figure 2.9 (b)

The parameters of the "invariant" representation for the overall structure are obtainable from a knowledge of the change of cross-section circuit, the thickness and cross-section dimensions of the slot, and the parameters of the thin slot-coupled E plane Tee of identical slot dimensions. The result is approximate but is adequate for engineering applications as is shown in Part IV. The parameters for the E plane Tee junction of Figure 2.9 (b) are related approximately to those of the slot -coupled E plane Tee by the following:

Junction Tee		Slot-coupled Tee
B_{aj}	=	B_a
B_{bj}	=	$B_b - \frac{B_t}{2n_o^2}$
$n_{cj} = n_t J_o(\pi b'/2)$	;	$n_c = J_o(\pi b'/2)$
$X_{cj} = 0$	;	$X_c = 0$

(2.2)

The reasons for these relations will be given in Part III. It is there pointed out that the relations above apply only for large α ($\alpha > .5$), but are valid for arbitrary β, where α is a'/a and β is b'/b. The reason for the restriction in range of aperture dimensions is that the field assumption used for large α is not valid in the range of small α. The corresponding relations in the range of small α have not yet been determined. The turns ratio n_t is the value involved in the change of cross-section network of Figure 2.9 (a), and the expression for it is given in Equation (2.1). The susceptance B_t is that for a zero-thickness transverse slot of identical dimensions.

Appropriate relations must be developed in order to obtain the parameters of the overall network from those of the composite one. Rather than relate directly the overall network at invariant reference planes to the composite network at centerline reference planes, it is more convenient to first transform the E plane Tee junction network to invariant reference planes and then to relate the overall and composite networks. The E plane Tee junction at invariant reference planes is given in Figure 2.9(c), and, as seen, the parameters are B_j, n_j, ℓ'_j, and $2\ell_j$. The turns ratio n_j is not equal to n_{cj} of Figure 2.9(b), since the reference plane locations

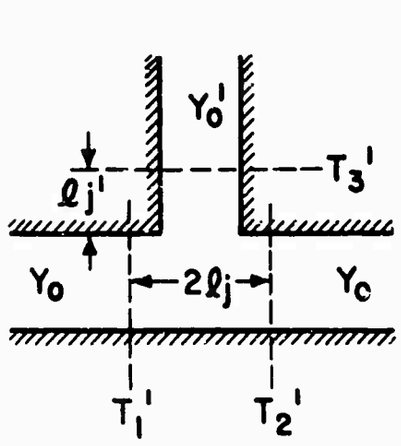

E PLANE TEE JUNCTION

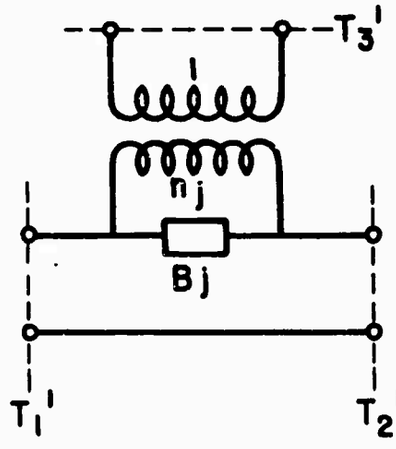

EQUIVALENT CIRCUIT AT INVARIANT REFERENCE PLANES

Figure 2.9 (c)

E PLANE TEE JUNCTION

TABLE 2-V

Parameters of the Invariant Representation in Terms of Those of The Centerline Representation

1. $$\ell_j = -\frac{1}{\varkappa}\tan^{-1}\left(\frac{B_{aj}}{Y_o}\right)$$

2. $$\ell'_j = \frac{1}{\varkappa'}\tan^{-1}\left[\frac{\frac{Y'_o}{Y_o}\;\frac{\frac{2}{n_j^2}\;\frac{B_{aj}}{Y_o}}{1+\frac{B_{aj}}{Y_o}\left(\frac{B_{aj}}{Y_o}+2\frac{B_{bj}}{Y_o}\right)}-\frac{X_{cj}}{Z_o}}{}\right]$$

3. $$n_j = -\frac{2}{n_{cj}}\frac{Y'_o}{Y_o}\;\frac{\sin\varkappa\ell_j}{\sin\varkappa'\ell'_j}\left[\frac{\tan\varkappa'\ell'_j}{\tan\varkappa'\ell'_j+\frac{X_{cj}}{Z_o}\frac{Y'_o}{Y_o}}\right]$$

4. $$\frac{B_{ij}}{Y_o} = \frac{1}{n_j^2}\frac{Y'_o}{Y_o}\tan\varkappa'\ell'_j+\frac{\frac{B_{bj}}{Y_o}}{1+\frac{B_{aj}}{Y_o}\left(\frac{B_{aj}}{Y_o}+2\frac{B_{bj}}{Y_o}\right)}$$

TABLE 2-VI

Parameters of the Centerline Representation in Terms of Those of The Invariant Representation

1. $$\frac{B_{aj}}{Y_o} = -\tan\varkappa\ell_j$$

2. $$\frac{X_{cj}}{Z_o} = \frac{Y_o}{Y'_o}\left[\frac{\tan\varkappa'\ell'_j+2\left(\frac{B_{ij}}{Y_o}\tan\varkappa'\ell'_j+\frac{1}{n_j^2}\frac{Y'_o}{Y_o}\right)\tan\varkappa\ell_j}{1+2\left(\frac{B_{ij}}{Y_o}-\frac{1}{n_j^2}\frac{Y'_o}{Y_o}\tan\varkappa'\ell'_j\right)\tan\varkappa\ell_j}\right]$$

3. $$n_{cj} = n_j\left[1+2\left(\frac{B_{ij}}{Y_o}-\frac{Y'_o}{Y_o}\frac{\tan\varkappa'\ell'_j}{n_j^2}\right)\tan\varkappa\ell_j\right]\cos\varkappa'\ell'_j\cos\varkappa\ell_j$$

4. $$\frac{B_{bj}}{Y_o} = \frac{\frac{B_{ij}}{Y_o}-\frac{Y'_o}{Y_o}\frac{1}{n_j^2}\tan\varkappa'\ell'_j}{\left[1+2\left(\frac{B_{ij}}{Y_o}-\frac{Y'_o}{Y_o}\frac{1}{n_j^2}\tan\varkappa'\ell'_j\right)\tan\varkappa\ell_j\right]\cos^2\varkappa\ell}$$

B. E Plane Radiating Slots

1. Equivalent Circuit Representations

A sketch of a slot radiating from the broad face of rectangular guide, and an equivalent circuit representation for it at centerline reference planes are shown in Figure 2.11. This representation, which corresponds

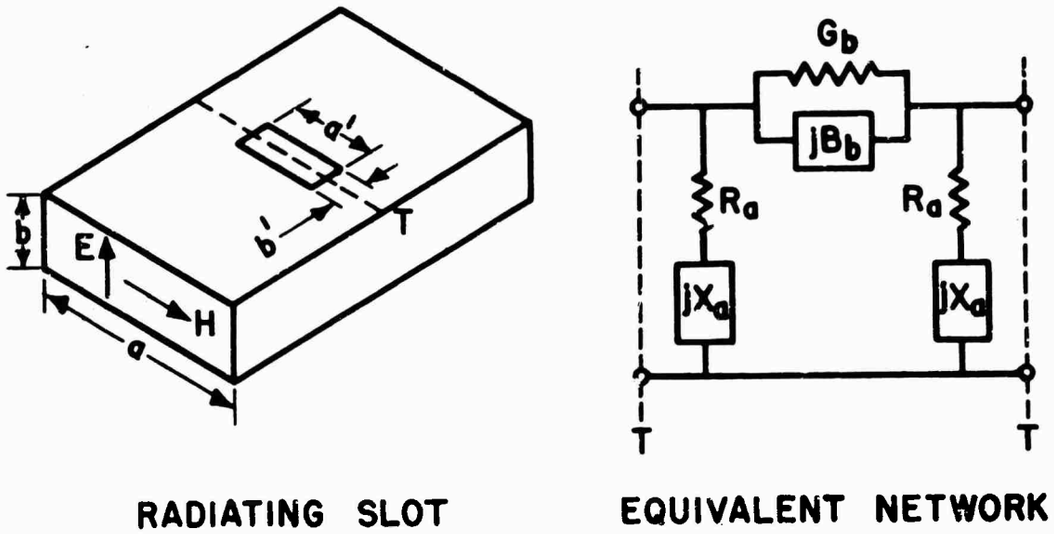

Figure 2.11

to that of a symmetrical lossy four-terminal structure, is most suitable for theoretical calculations (as was the centerline representation for the E plane Tee). However, for dissipative structures there exist a variety of "invariant" representations, the choice depending on the particular application. A useful representation is the one given in Figure 2.12, obtained from the centerline representation by a suitable shift of reference planes. This particular representation was chosen because as the loss approaches zero, the representation becomes purely series. In addition, as is discussed later under thick radiating slots, the shunt arms vanish for the thick slots, resulting again in a purely series representation.

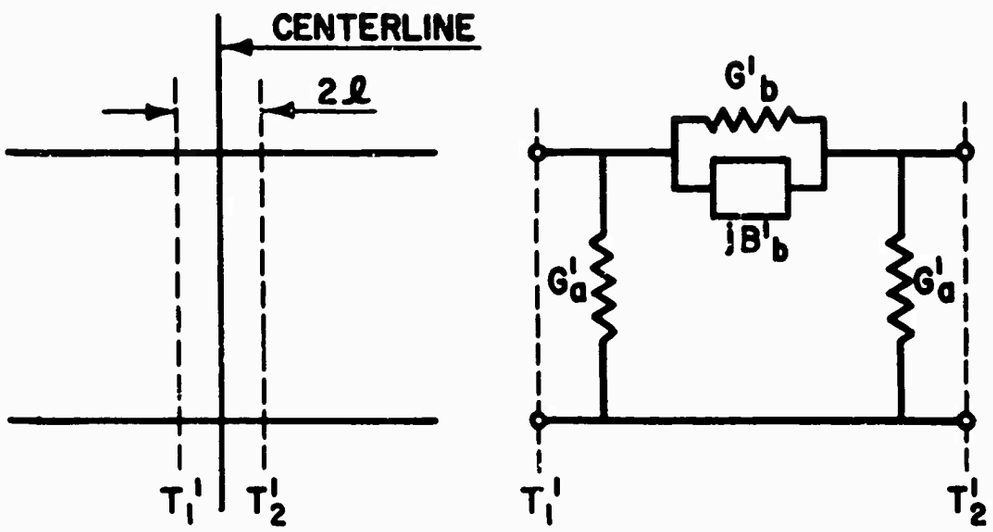

Figure 2.12

The values of the parameters of the centerline representation in terms of those of the representation of Figure 2.12, and vise versa, are given in Tables 2-VIII and 2-VII, respectively. Also included in the Tables are limiting values for some of the parameters for small G_a or R_a.

E PLANE RADIATING SLOT

TABLE 2-VII

Parameters of the Invariant Representation in Terms of Those of The Centerline Representation

1a. $$2\ell = \frac{1}{\varkappa} \tan^{-1} \left[\frac{2 \frac{B_a}{Y_o}}{(\frac{G_a}{Y_o})^2 + (\frac{B_a}{Y_o})^2 - 1} \right]$$

2a. $$\frac{G'_a}{Y_o} = \frac{\frac{G_a}{Y_o}(1 + \tan^2 \varkappa \ell)}{(1 - \frac{B_a}{Y_o} \tan \varkappa \ell)^2 + (\frac{G_a}{Y_o} \tan \varkappa \ell)^2}$$

1b. $$2\ell = \frac{1}{\varkappa} \tan^{-1} \left[\frac{2 \frac{X_a}{Z_o}}{(\frac{R_a}{Z_o})^2 + (\frac{X_a}{Z_o})^2 - 1} \right]$$

2b. $$\frac{R'_a}{Z_o} = \frac{\frac{R_a}{Z_o}(1 + \tan^2 \varkappa \ell)}{(1 - \frac{X_a}{Z_o} \tan \varkappa \ell)^2 + (\frac{R_a}{Z_o} \tan \varkappa \ell)^2}$$

3. $$\frac{R'_b}{Y_o} = \frac{\frac{B_b}{Y_o}(1 - \tan^2 \varkappa \ell) - 2\left[(\frac{B_b}{Y_o})(\frac{B_a}{Y_o} + \frac{B_b}{Y_o}) + \frac{G_b}{Y_o}(\frac{G_b}{Y_o} + \frac{G_a}{Y_o})\right] \tan \varkappa \ell}{\left[1 - (\frac{B_a}{Y_o} + 2\frac{B_b}{Y_o}) \tan \varkappa \ell\right]^2 + (\frac{G_a}{Y_o} + 2\frac{G_b}{Y_o})^2 \tan^2 \varkappa \ell}$$

4. $$\frac{G'_b}{Y_o} = \frac{\frac{1}{2}(\frac{G_a}{Y_o} + 2\frac{G_b}{Y_o})(1 + \tan^2 \varkappa \ell)}{\left[1 - (\frac{B_a}{Y_o} + 2\frac{B_b}{Y_o}) \tan \varkappa \ell\right]^2 + (\frac{G_a}{Y_o} + 2\frac{G_b}{Y_o})^2 \tan^2 \varkappa \ell}$$

NOTE I. $(R_a + j X_a)(G_a + j B_a) = 1$, i.e., $G_a = \frac{R_a}{R_a^2 + X_a^2}$, $B_a = \frac{-X_a}{R_a^2 + X_a^2}$

$(R'_a\ G'_a) = 1.$ $\qquad R_a = \frac{G_a}{G_a^2 + B_a^2}$, $X_a = \frac{-B_a}{G_a^2 + B_a^2}$

NOTE IIa. When $\frac{G_a}{Y_o} \ll 1$ and $\frac{B_a}{Y_o} \ll 1$, $\ell \to \frac{1}{\varkappa}\left(\frac{B_a}{Y_o}\right)$ and $\frac{G'_a}{Y_o} \to \frac{G_a}{Y_o}$

IIb. When $\frac{X_a}{Z_o} \gg \frac{R_a}{Z_o}$ and $\frac{X_a}{Z_o} \gg 1$, $\ell \to \frac{1}{2\varkappa}\left(\frac{Z_o}{X_a}\right)$ and $\frac{R'_a}{Z_o} \to \left(\frac{X_a}{Z_o}\right)^2 \left(\frac{Z_o}{R_a}\right)$

E PLANE RADIATING SLOT

TABLE 2-VIII

Parameters of the Centerline Representation in Terms of Those of The Invariant Representation

1a. $$\frac{G_a}{Y_o} = \frac{\frac{G'_a}{Y_o}(1 + \tan^2 \varkappa\ell)}{1 + \left(\frac{G'_a}{Y_o}\right)^2 \tan^2 \varkappa\ell}$$

2a. $$\frac{B_a}{Y_o} = \frac{\left[\left(\frac{G'_a}{Y_o}\right)^2 - 1\right] \tan \varkappa\ell}{1 + \left(\frac{G'_a}{Y_o}\right)^2 \tan^2 \varkappa\ell}$$

1b. $$\frac{R_a}{Z_o} = \frac{\frac{R'_a}{Z_o}(1 + \tan^2 \varkappa\ell)}{1 + \left(\frac{R'_a}{Z_o}\right)^2 \tan^2 \varkappa\ell}$$

2b. $$\frac{X_a}{Z_o} = \frac{\left[\left(\frac{R'_a}{Z_o}\right)^2 - 1\right] \tan \varkappa\ell}{1 + \left(\frac{R'_a}{Z_o}\right)^2 \tan^2 \varkappa\ell}$$

3. $$\frac{G_b}{Y_o} = \frac{\frac{1}{2}\left(\frac{G'_a}{Y_o} + 2\frac{G'_b}{Y_o}\right)(1 + \tan^2 \varkappa\ell)}{\left(1 + 2\frac{B'_b}{Y_o} \tan \varkappa\ell\right)^2 + \left(\frac{G'_a}{Y_o} + 2\frac{G'_b}{Y_o}\right)^2 \tan^2 \varkappa\ell} - \frac{1}{2}\frac{G_a}{Y_o}$$

4. $$\frac{B_b}{Y_o} = \frac{1}{2}\left[\frac{\left(1+2\frac{B'_b}{Y_o} \tan \varkappa\ell\right)\left(2\frac{B'_b}{Y_o} - \tan \varkappa\ell\right) + \left(\frac{G'_a}{Y_o} + 2\frac{G'_b}{Y_o}\right)^2 \tan \varkappa\ell}{\left(1 + 2\frac{B'_b}{Y_o} \tan \varkappa\ell\right)^2 + \left(\frac{G'_a}{Y_o} + 2\frac{G'_b}{Y_o}\right)^2 \tan^2 \varkappa\ell} - \frac{B_a}{Y_o}\right]$$

NOTE: Same as NOTE I of Table 2-VII.

2. Measurement Method

As mentioned earlier, an "invariant" measurement method is one in which the equivalent circuit parameters are determined independent of any absolute distance measurements, i.e., where the latter affect only the location of the reference planes. There are two ways by which such a measurement method may procede: (a) Some invariant method is used to obtain the relative location of the reference planes for the invariant representation. The values of D_{or} and S_{or} in the tangent relation procedure are then evaluated at these reference planes. (b) The data is so treated that the parameters are evaluated independently of D_{or} and S_{or}. Then the relative location of the reference planes need not be known. An example of the former method is the E plane Tee, when the relative location of reference planes was obtained by a zero power measurement. An example of the latter method is the symmetrical, lossless four-terminal network where the invariant representation involves a single shunt element whose susceptance depends only on γ, and is therefore independent of D_o and S_o. The latter quantities affect the reference plane locations.

Work is now progressing on a satisfactory method for determining in an invariant fashion the parameters of a general lossy four-terminal network, and in particular the symmetric one representing the thin radiating slot. Such a method has already been devised for the series network representing a thick radiating slot, and will be described in the section on thick slots. For the thin radiating slot it has therefore been necessary to measure the parameters at the centerline representation and then by the relations given in Table 2-VII to obtain the representation of Figure 2.12.

The problem still remains of how to obtain the final parameter values to within the precision of the data for a lossy structure. The details of the tangent relation method as applied to a lossless structure have been given in the Final Report mentioned earlier. Some information was given in the Final Report concerning the application of the tangent relation method to lossy structures but, as mentioned there, the procedure is quite involved and is therefore considered unsatisfactory. Further work on this method has produced certain simplifications, but the result is still far from satisfactory. Several other methods have been devised, and are now being tested, so that they will not be reported at this time. It has been necessary therefore, for the while, to use the two-point method (for a symmetric structure) in determining the experimental values given in Part IV. The two-point method has been described in the Final Report, in Chap. II, Sec. C.

3. Experimental Techniques

One of the purposes served by the precision experimental results is that of checking the accuracy of theoretical calculations. Since the

theoretical calculations are greatly simplified when the slots radiate from the guide into a half-space, the experimental arrangement should therefore be such as to approximate a half-space. In addition, this experimental arrangement corresponds to many physical situations of interest. The first results were obtained with the slots described in Figure 2.4, i.e., with the grooved metal plate attached, but without the addition of the air chuck. In fact, the measurements were taken immediately after the E plane Tee measurements, before the slot size was changed. For small loss (little radiation) this arrangement is probably a good approximation to a half-space.

The radiation from a slot in the top of the guide into an actual half-space was achieved in the manner indicated in the sketch of Figure 2.13 and the photograph of Figure 2.14. As seen, the guide is essentially bent

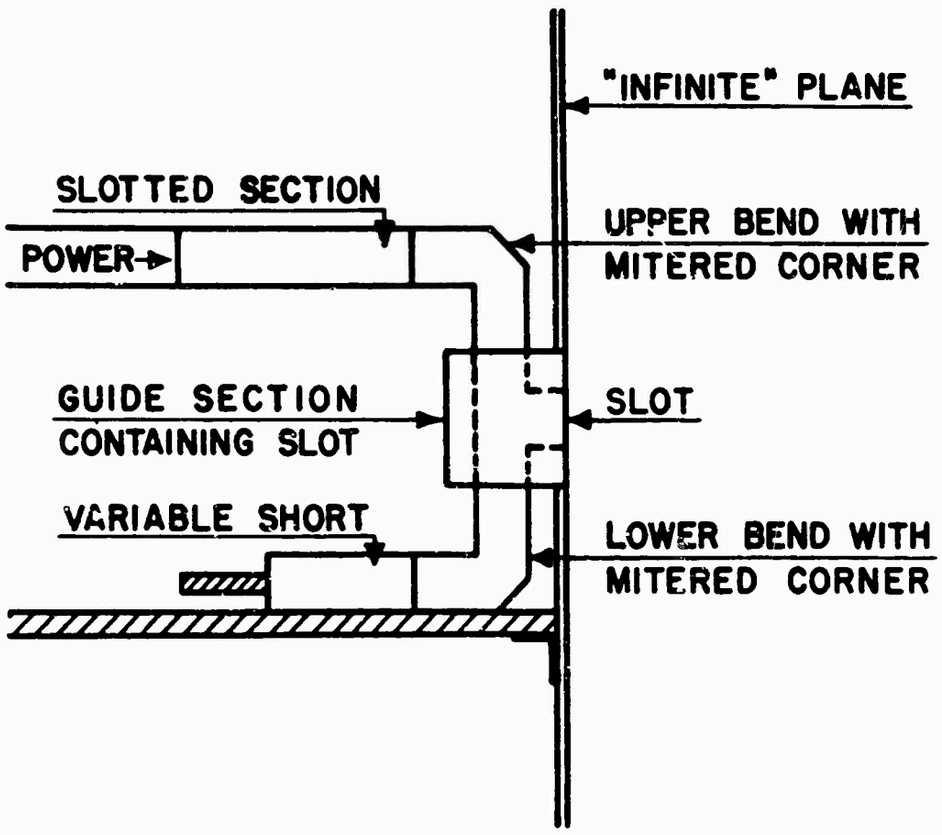

Figure 2.13

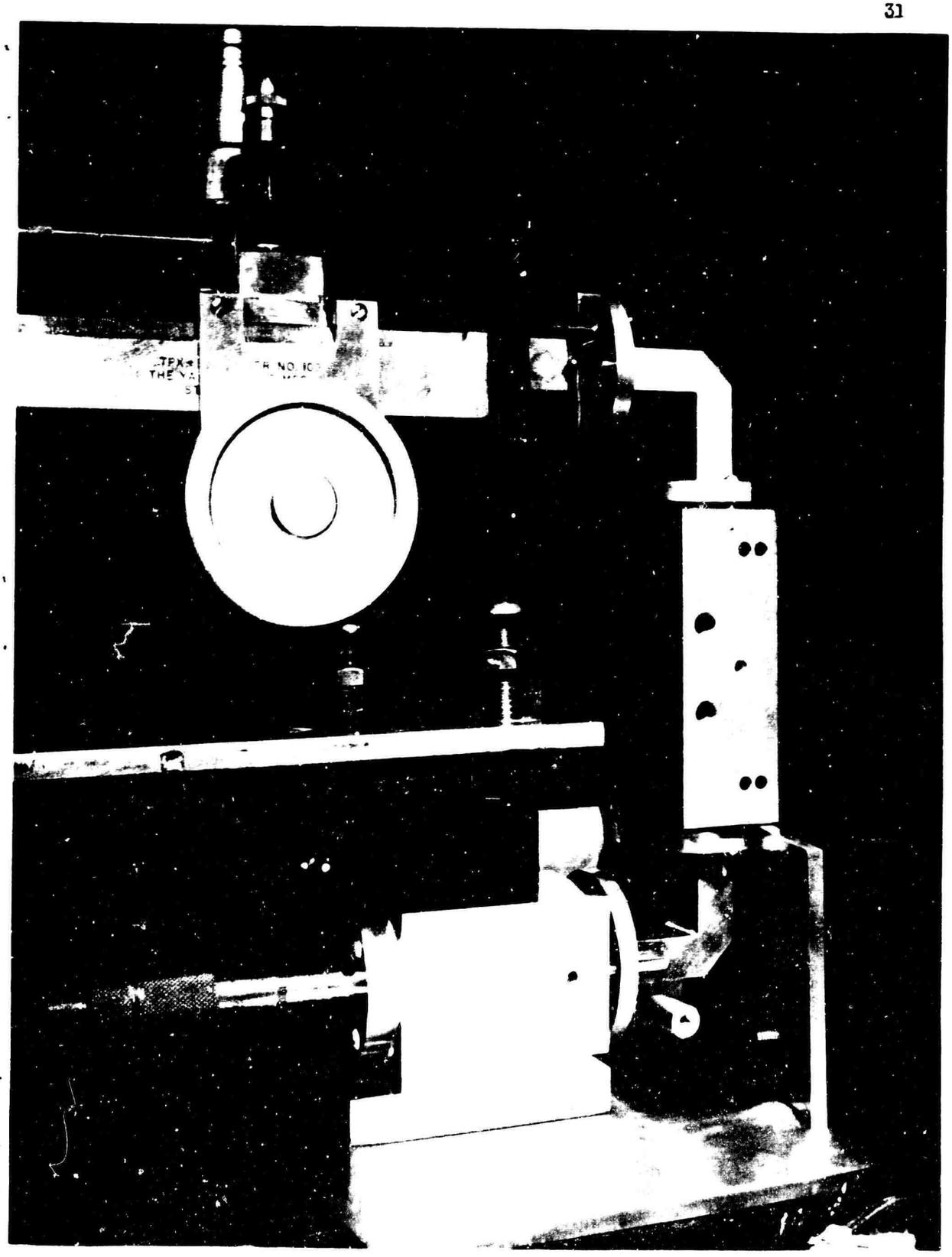

FIGURE 2.14

around so that the section of guide containing the slot is vertical. This is necessary since the "infinite" conducting plane available was first used in connection with slots radiating from the end of the guide, and was therefore placed vertically. Its use in this connection has been described in the Final Report, Chap. IV. The sections containing the bends are made with mitered corners so as to be reflectionless at the operating frequency. The design dimensions were obtained from p. 133 of "Microwave Transmission Design Data", put out by the Sperry Gyroscope Co. In accordance with a diagram given there on p. 134, a value of d = .325" was chosen for a right angle bend in a .900" by .400" guide, operating at λ = 3.20 cms. The guide section containing the slot is made the same size as the hole in the "infinite" plane, and to insure continuity of surface current flow on the "infinite" plane strips of thin (.002" or .003") copper are placed over the contact regions, and are held in place with scotch tape. Figures 2.13 and 2.14 show the application to a thick radiating slot. The thick slot was investigated as a function of thickness, while maintaining the cross-section dimensions constant. This was achieved by successively grinding down the surface until the thicknesses desired were obtained.

It will be recalled that slotted section measurements are always corrected for by a calibration curve that accounts for the presence of the slot and other possible discontinuity effects inherent in the apparatus. The details of this calibration procedure have been given in the Final Report, Chap. IV. It is there assumed that the distance to voltage minimum measurements in the output guide, defined by the distance S, were as indicated by the variable short and therefore needed no correction. However, as seen from Figure 2.13 or 2.14, in these measurements the structure to be measured is not followed directly by the variable short, but one of the bends appears there also. In addition, the other of the bends appears between the slotted section and the structure to be measured, thereby invalidating the calibration curve for the slotted section alone. Therefore, both the S readings and the D readings (distance to voltage minimum in the input guide, i.e., slotted section) must be corrected. The calibration procedure is the following.

First, the apparatus is arranged as in Figure 2.15-(a). A run of

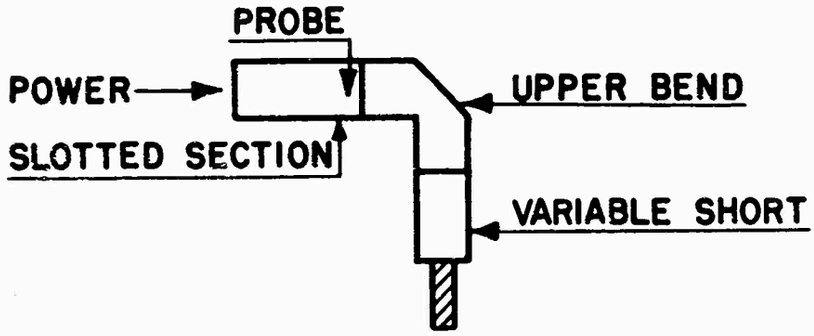

Figure 2.15 (a)

D vs. S is taken, and the calibration curve of - (D + S) vs. D is plotted. The ordinate of this curve then gives the correction to be added to any subsequent D reading obtained when some structure is inserted between the variable short and the upper bend, in order to obtain the correct D value. The correction curve for the values of S is obtained by arranging the equipment as in Figure 2.15-(b).

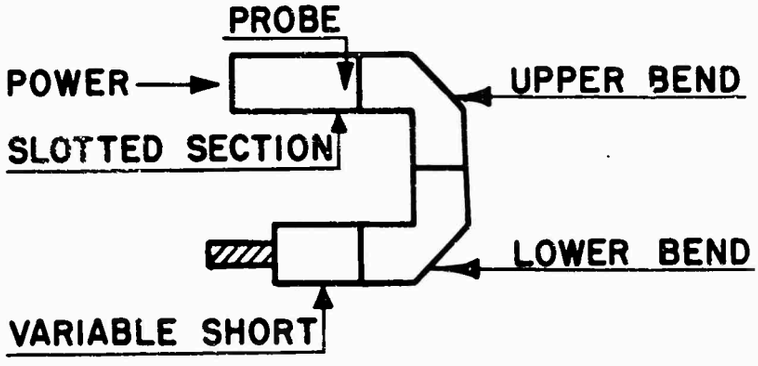

Figure 2.15 (b)

The calibration procedure now corrects for the presence of discontinuity effects in the lower bend. A run of D vs. S is taken, and the D values are corrected by using the calibration curve obtained from the arrangement of

Figure 2.15-(a). The ordinate of the calibration curve of - (D + S) vs. S then gives the correction to be added to any subsequent S reading to yield the correct S value.

The above calibration procedure is valid for the measurement of lossless structures, since the calibration techniques involve only lossless components. When the structure to be measured is dissipative, the calibration curve is altered. In addition, input VSWR measurements are necessary, and the presence of the discontinuities inherent in the measuring equipment affects somewhat the VSWR values. When the structure to be measured is dissipative, the calibration curve for the values of ΔD is the one valid for the lossless case, multiplied by the factor $(r^2 + 1)/(r^2 - 1)$, where r is the measured input VSWR corresponding to the D value in question. It is seen that for large VSWR the correction is negligible. The correction to the VSWR is obtained also from the calibration curve for the lossless case. The correction to be added to the VSWR is given by 4π times the VSWR, multiplied by the ordinate (in input guide wavelengths) of the calibration curve at an eigth-wavelength preceding the corresponding D value. The derivation of these corrections, together with a discussion on the use of this calibration curve, will be given in a report to be issued soon.

4. The Thick Radiating Slot

The thick radiating slot may be represented by a purely series equivalent circuit (shown in Figure 2.16), rather than the one containing resistive shunt arms representing the thin radiating slot. One can consider the thick slot as being composed of an E plane Tee junction coupling to a

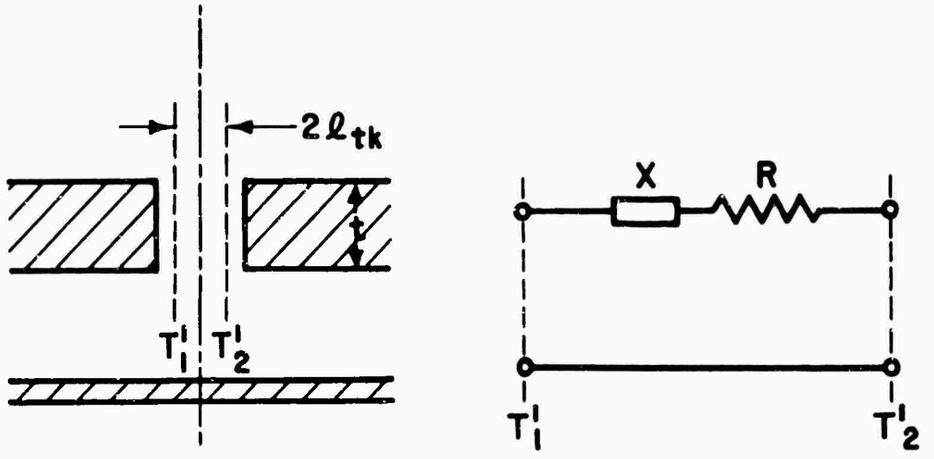

Figure 2.16

section of transmission line of length t, equal to the slot thickness, and terminated by a two-terminal radiating network. When the E plane Tee junction is represented by the "invariant" network of Figure 2.9-(c), it is clear that the overall network for the thick radiating slot can be of the form of Figure 2.16, where the $2\ell_{ik}$ is the same as that for a thick E-plane Tee structure of identical slot dimensions. When the slot thickness t becomes so small that interaction occurs between the higher modes excited by the radiating junction and the Tee junction in the guide, then the purely series representation is no longer valid, and resistive shunt arms appear in the equivalent circuit, as in the thin slot case.

The measurement method for the thick radiating slot is based on the representation of Figure 2.16. As in all the other measurement methods, data is taken of the input VSWR and location of minimum, for a series of output reactances, obtained by varying the location of the short circuit in a variable short. A plot of the resulting reciprocal VSWR vs. S, the location of the output short circuit, is of the form shown in Figure 2.17.

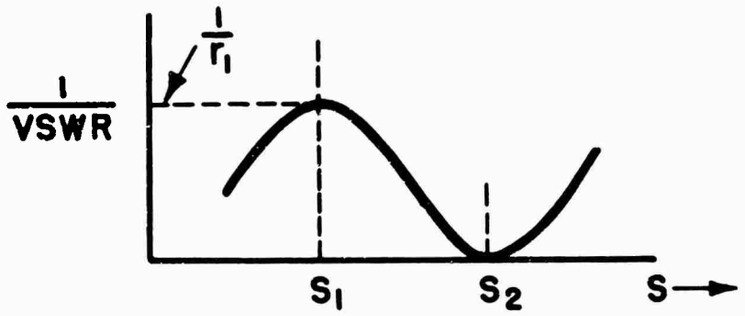

Figure 2.17

It is first recognized that when the input VSWR is a minimum, the input impedance is purely real. (This may be seen from a constant resistance curve in the reflection coefficient plane. The constant resistance curve is applicable since the output is always purely reactive.) From the reciprocal VSWR curve, it is seen that the minimum VSWR occurs at $S = S_1$. For a fixed S_1 in the output guide, a purely resistive impedance is obtained at voltage maxima and voltage minima in the input guide. Therefore, the relative location of the input reference plane T_1' is given either by the input minimum location D_1 corresponding to S_1, or by $D_1 \pm 1/4$ (where D and S are given in units of guide wavelength). The term "relative" is

used because the location is known relative to some fixed point, namely the end of the physical structure, but not relative to the symmetry plane of the structure. The latter requires an absolute distance measurement, i.e. the overall length of the structure. D_1 corresponding to S_1 may be obtained from a plot of D vs. S. At input reference plane T_1', the value of input resistance is constant independent of S (which corresponds to a pure reactance). Therefore, one can obtain T_1' by calculating the input resistance corresponding to two different values of S, at D_1 and at $D_1 \pm 1/4$, and noting for which location the input resistance is constant. However, it is simpler to determine whether T_1' is at D_1 or $D_1 \pm 1/4$ by referring to the value of D corresponding to S_2. Since an open circuit placed at T_1' results in an infinite input VSWR, T_1' is located as being a quarter wavelength from the value of D corresponding to S_2 (see Figure 2.17). However, since the value of S_2 is not accurately determinable from Figure 2.17, this procedure is not used to determine the exact location of T_1', but rather to determine whether T_1' occurs at D_1 or $D_1 \pm 1/4$. The value of R in the equivalent circuit is obtained from r_1, the minimum value of VSWR, or $1/r_1$, depending on the location of T_1'. If T_1' is at D_1, then $R = 1/r_1$; while if T_1' is at $D_1 \pm 1/4$, $R = r_1$. This is so since R is a minimum when the voltage is a minimum.

At S_2, in Figure 2.17, the VSWR is infinite, indicating an open circuit at T_1', and therefore one at T_2' (from the purely series nature of the equivalent circuit). Hence, the reading of S_2 corresponds to $T_2' \pm 1/4$. This method of obtaining the relative location of the output reference plane is not as accurate, however, as the location of T_1', since the data is inaccurate for very high VSWR's. Therefore, since the structure is symmetric, a more accurate value of T_2' is obtained by reversing the section and repeating the measurements. This is valid since the location relative to the physical end of the structure is involved. In this way one also obtains a check on the values of R and X. The value of X is determinable in two ways, once T_2' is located. First, the value of X is equal to the input reactance at T_1' corresponding to a short circuit at T_2'. Or else, one may obtain the amount S is changed in going from the short circuit position, $S_2 \pm 1/4$, to the position for resonance, S_1. X is then given by tan 2π (shift in S). Since the values of R and X are determined independent of any absolute distance measurement, the representation is seen to be "invariant"

To determine the actual value of 2ℓ, however, it is necessary to measure the overall length of the section containing the structure. The value of 2ℓ is then given by the difference between the overall length and the sum of the distances between T_1' and T_2' and the respective physical ends of the structure.

section of transmission line of length t, equal to the slot thickness, and terminated by a two-terminal radiating network. When the E plane Tee junction is represented by the "invariant" network of Figure 2.9-(c), it is clear that the overall network for the thick radiating slot can be of the form of Figure 2.16, where the $2\ell_k$ is the same as that for a thick E-plane Tee structure of identical slot dimensions. When the slot thickness t becomes so small that interaction occurs between the higher modes excited by the radiating junction and the Tee junction in the guide, then the purely series representation is no longer valid, and resistive shunt arms appear in the equivalent circuit, as in the thin slot case.

The measurement method for the thick radiating slot is based on the representation of Figure 2.16. As in all the other measurement methods, data is taken of the input VSWR and location of minimum, for a series of output reactances, obtained by varying the location of the short circuit in a variable short. A plot of the resulting reciprocal VSWR vs. S, the location of the output short circuit, is of the form shown in Figure 2.17.

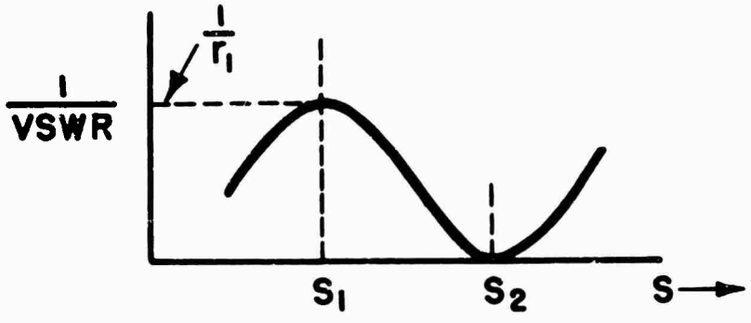

Figure 2.17

It is first recognized that when the input VSWR is a minimum, the input impedance is purely real. (This may be seen from a constant resistance curve in the reflection coefficient plane. The constant resistance curve is applicable since the output is always purely reactive.) From the reciprocal VSWR curve, it is seen that the minimum VSWR occurs at $S = S_1$. For a fixed S_1 in the output guide, a purely resistive impedance is obtained at voltage maxima and voltage minima in the input guide. Therefore, the relative location of the input reference plane T_1' is given either by the input minimum location D_1 corresponding to S_1, or by $D_1 \pm 1/4$ (where D and S are given in units of guide wavelength). The term "relative" is

used because the location is known relative to some fixed point, namely the end of the physical structure, but not relative to the symmetry plane of the structure. The latter requires an absolute distance measurement, i.e. the overall length of the structure. D_1 corresponding to S_1 may be obtained from a plot of D vs. S. At input reference plane T_1', the value of input resistance is constant independent of S (which corresponds to a pure reactance). Therefore, one can obtain T_1' by calculating the input resistance corresponding to two different values of S, at D_1 and at $D_1 \pm 1/4$, and noting for which location the input resistance is constant. However, it is simpler to determine whether T_1' is at D_1 or $D_1 \pm 1/4$ by referring to the value of D corresponding to S_2. Since an open circuit placed at T_1' results in an infinite input VSWR, T_1' is located as being a quarter wavelength from the value of D corresponding to S_2 (see Figure 2.17). However, since the value of S_2 is not accurately determinable from Figure 2.17, this procedure is not used to determine the exact location of T_1', but rather to determine whether T_1' occurs at D_1 or $D_1 \pm 1/4$. The value of R in the equivalent circuit is obtained from r_1, the minimum value of VSWR, or $1/r_1$, depending on the location of T_1'. If T_1' is at D_1, then $R = 1/r_1$; while if T_1' is at $D_1 \pm 1/4$, $R = r_1$. This is so since R is a minimum when the voltage is a minimum.

At S_2, in Figure 2.17, the VSWR is infinite, indicating an open circuit at T_1', and therefore one at T_2' (from the purely series nature of the equivalent circuit). Hence, the reading of S_2 corresponds to $T_2' \pm 1/4$. This method of obtaining the relative location of the output reference plane is not as accurate, however, as the location of T_1', since the data is inaccurate for very high VSWR's. Therefore, since the structure is symmetric, a more accurate value of T_2' is obtained by reversing the section and repeating the measurements. This is valid since the location relative to the physical end of the structure is involved. In this way one also obtains a check on the values of R and X. The value of X is determinable in two ways, once T_2' is located. First, the value of X is equal to the input reactance at T_2' corresponding to a short circuit at T_2'. Or else, one may obtain the amount S is changed in going from the short circuit position, $S_2 \pm 1/4$, to the position for resonance, S_1. X is then given by tan 2π (shift in S). Since the values of R and X are determined independent of any absolute distance measurement, the representation is seen to be "invariant"

To determine the actual value of 2ℓ, however, it is necessary to measure the overall length of the section containing the structure. The value of 2ℓ is then given by the difference between the overall length and the sum of the distances between T_1' and T_2' and the respective physical ends of the structure.

The above described method yields only the first approximation values for the parameters R and X, and the reference plane locations, T_1' and T_2'. A correction procedure to determine these values to within the precision of the data has been devised, but it will be presented in a later report on precision dissipative measurements.

As mentioned previously, the thick radiating slot may be considered as a whole, for which the invariant representation is given in Figure 2.16, or in terms of its component parts, resulting in a composite representation. This composite representation consists of the E plane Tee junction described in Figure 2.9-(c), connected to a length of transmission line equal to the slot thickness t terminated by a two-terminal network representing the junction between the slot guide proper and a half space. This two-terminal network is shown in Figure 2.18. From a knowledge of the parameters of

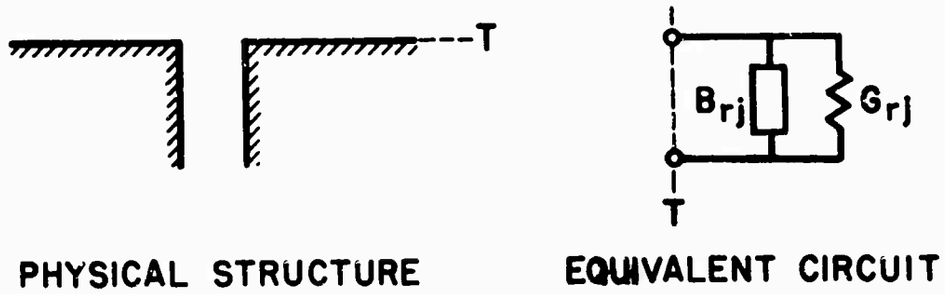

Figure 2.18

the networks of Figures 2.18 and 2.9-(c), and from the slot dimensions, one can obtain the parameters for the invariant overall network of Figure 2.16. The expressions involved are listed in two different ways in Table 2-IX.

Alternatively, the parameters of the two-terminal radiating network (a transverse radiating junction) may be obtained from the overall invariant network and the invariant representation for the E plane Tee junction. The method of determining the latter is described in Sec. A, 4) of this Part. The resulting composite network for the thick radiating slot is given in Figure 2.19, while the overall invariant network is that in Figure 2.16. Applying a short circuit bisection to each network and equating input admittances at T_1', one obtains the required relations, which

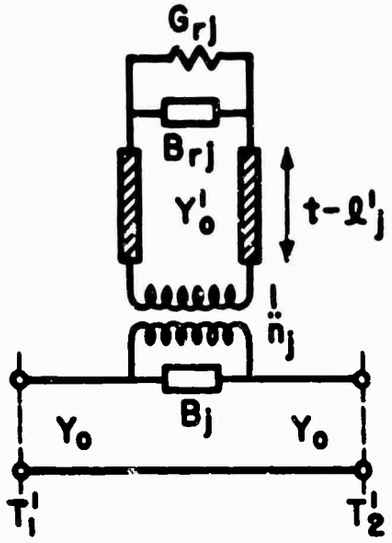

Figure 2.19

are given in two different ways in Table 2-X. The parameters G_{tk} and B_{tk} now correspond to the experimentally determined parameters, X and R, and are related to them by:

$$G_{tk} = \frac{R}{R^2 + X^2} \quad , \quad B_{tk} = - \frac{X}{R^2 + X^2} \qquad (2.3)$$

Note that the parameters of the transverse radiating junction are normalized in Table 2-X to the characteristic admittance of the main guide and not the slot guide.

THICK E PLANE RADIATING SLOT

TABLE 2-IX

Parameters of the Thick Radiating Slot in Terms Those of its Component Parts

$$1a.\quad \frac{G_{tk}}{Y_o} = \frac{\frac{1}{n_j^2}\left(\frac{Y'_o}{Y_o}\right)^2 \left(\frac{G'_{rj}}{Y_o}\right)^2 \left(1 + \tan^2 \alpha' t'\right)}{\left(\frac{Y'_o}{Y_o}\right)^2 + \left(\frac{G'_{rj}}{Y_o}\right)^2 \tan^2 \alpha' t'}$$

$$2a.\quad \frac{B_{tk}}{Y_o} = \frac{B_j}{Y_o} + \frac{1}{n_j^2}\frac{Y'_o}{Y_o}\left[\frac{\left(\frac{Y'_o}{Y_o}\right)^2 - \left(\frac{G'_{rj}}{Y_o}\right)^2}{\left(\frac{Y'_o}{Y_o}\right)^2 + \left(\frac{G'_{rj}}{Y_o}\right)^2 \tan^2 \alpha' t'}\right] \tan \alpha' t'$$

where $t' = t - \ell'_r - \ell'_j$

$$\ell'_r = \frac{1}{2\alpha'} \tan^{-1}\left[\frac{2\,\frac{B_{rj}}{Y_o}\,\frac{Y'_o}{Y_o}}{\left(\frac{B_{rj}}{Y_o}\right)^2 + \left(\frac{G_{rj}}{Y_o}\right)^2 - \left(\frac{Y'_o}{Y_o}\right)^2}\right]$$

$$\frac{G'_{rj}}{Y_o} = \frac{\left(\frac{Y'_o}{Y_o}\right)^2 \left(\frac{G_{rj}}{Y_o}\right)\left(1 + \tan^2 \alpha' \ell'_r\right)}{\left[\frac{Y'_o}{Y_o} - \frac{B_{rj}}{Y_o} \tan \alpha' \ell'_r\right]^2 + \left(\frac{G_{rj}}{Y_o}\right)^2 \tan^2 \alpha' \ell'_r}$$

$$1b.\quad \frac{G_{tk}}{Y_o} = \frac{\frac{1}{n_j^2}\left(\frac{Y'_o}{Y_o}\right)^2 \left(\frac{G_{rj}}{Y_o}\right)\left[1 + \tan^2 \alpha' (t - \ell'_j)\right]}{\left[\frac{Y'_o}{Y_o} - \frac{B_{rj}}{Y_o} \tan \alpha' (t - \ell'_j)\right]^2 + \left(\frac{G_{rj}}{Y_o}\right)^2 \tan^2 \alpha' (t - \ell'_j)}$$

$$2b.\quad \frac{B_{tk}}{Y_o} = \frac{B_j}{Y_o} + \frac{1}{n_j^2}\frac{Y'_o}{Y_o}\left\{ \frac{\frac{B_{rj}}{Y_o}\frac{Y'_o}{Y_o}\left[1 - \tan^2 \alpha'(t-\ell'_j)\right]}{\left[\frac{Y'_o}{Y_o} - \frac{B_{rj}}{Y_o}\tan \alpha'(t-\ell'_j)\right]^2 + (\frac{G_{rj}}{Y_o})^2 \tan^2 \alpha'(t-\ell'_j)} + \right.$$

$$\left. + \frac{\left[(\frac{Y'_o}{Y_o})^2 - (\frac{B_{rj}}{Y_o})^2 - (\frac{G_{rj}}{Y_o})^2\right]\tan \alpha'(t-\ell'_j)}{\text{same denominator}} \right\}$$

$$3.\quad 2\ell_{tk} = 2\ell_j$$

NOTE: $(G_{tk} + j\,B_{tk})(R + jX) = 1,\ R = \frac{G_{tk}}{G_{tk}^2 + B_{tk}^2},\ X = -\frac{B_{tk}}{G_{tk}^2 + B_{tk}^2}$

THICK E PLANE RADIATING SLOT

TABLE 2-X

Parameters of the Transverse Radiating Junction in Terms of Those of The Thick Radiating Slot and The Composite Representation

$$1a.\quad \frac{G_{rj}}{Y_o} = \frac{\frac{G'_{rj}}{Y_o}(\frac{Y'_o}{Y_o})^2(1 + \tan^2 \alpha' \ell'_r)}{(\frac{Y'_o}{Y_o})^2 + (\frac{G'_{rj}}{Y_o})^2 \tan^2 \alpha' \ell'_r}$$

$$2a.\quad \frac{B_{rj}}{Y_o} = \frac{(\frac{Y'_o}{Y_o})\left[(\frac{G'_{rj}}{Y_o})^2 - (\frac{Y'_o}{Y_o})^2\right]\tan \alpha' \ell'_r}{(\frac{Y'_o}{Y_o})^2 + (\frac{G'_{rj}}{Y_o})^2 \tan^2 \alpha' \ell'_r}$$

where $\ell'_r = t - \ell'_j - \frac{\phi}{\alpha'}$

$$\frac{G'_{rj}}{Y_o} = \frac{Y'_o}{Y_o}\left\{ \frac{\frac{1}{n_j^2}\frac{Y'_o}{Y_o}\frac{G_{tk}}{Y_o}(1 + \tan^2 \phi)}{\left[\frac{1}{n_j^2}\frac{Y'_o}{Y_o} + (\frac{B_{tk}}{Y_o} - \frac{B_j}{Y_o})\tan \phi\right]^2 + (\frac{G_{tk}}{Y_o})^2 \tan^2 \phi} \right\}$$

$$\phi = \frac{1}{2} \tan^{-1} \left\{ \frac{\frac{2}{n_j^2} \frac{Y'_o}{Y_o} \left(\frac{B_{tk}}{Y_o} - \frac{B_j}{Y_o}\right)}{\left(\frac{1}{n_j^2} \frac{Y'_o}{Y_o}\right)^2 - \left(\frac{B_{tk}}{Y_o} - \frac{B_j}{Y_o}\right)^2 - \left(\frac{G_{tk}}{Y_o}\right)^2} \right\}$$

1b. $$\frac{G_{rj}}{Y_o} = \frac{Y'_o}{Y_o} \frac{G_{tk}}{Y_o} \left\{ \frac{\frac{1}{n_j^2} \frac{Y'_o}{Y_o} \left[1 + \tan^2 \alpha'(t - \ell'_j)\right]}{\left[\frac{1}{n_j^2} \frac{Y'_o}{Y_o} + \left(\frac{B_{tk}}{Y_o} - \frac{B_j}{Y_o}\right) \tan \alpha'(t - \ell'_j)\right]^2 + \left(\frac{G_{tk}}{Y_o}\right)^2 \tan^2 \alpha'(t - \ell'_j)} \right\}$$

2b. $$\frac{B_{rj}}{Y_o} = \frac{Y'_o}{Y_o} \left\{ \frac{\frac{1}{n_j^2} \frac{Y'_o}{Y_o} \left[\frac{B_{tk}}{Y_o} - \frac{B_j}{Y_o}\right] \left[1 - \tan^2 \alpha'(t - \ell'_j)\right]}{\left[\frac{1}{n_j^2} \frac{Y'_o}{Y_o} + \left(\frac{B_{tk}}{Y_o} - \frac{B_j}{Y_o}\right) \tan \alpha'(t - \ell'_j)\right]^2 + \left(\frac{G_{tk}}{Y_o}\right)^2 \tan^2 \alpha'(t - \ell'_j)} + \right.$$

$$\left. + \frac{\left[\left(\frac{G_{tk}}{Y_o}\right)^2 + \left(\frac{B_{tk}}{Y_o} - \frac{B_j}{Y_o}\right)^2 - \left(\frac{1}{n_j^2} \frac{Y_o}{Y_o}\right)^2\right] \tan \alpha'(t - \ell'_j)}{\text{same denominator}} \right\}$$

C. Transverse Radiating Slots

The case of radiation from thin transverse slots at the end of rectangular waveguide has been discussed in the above mentioned Final Report, in Chaps. IV and V. In these chapters the measurement method for determining the parameters of the two-terminal network representing the thin slot is given, including the method of attaching the slot to an "infinite" baffle to insure radiation into a half space. The vacuum chuck used to achieve the latter is described in detail. In Chap. V, the experimental results are given.

In this report, the case of thick radiating transverse slots is considered. The physical structure of these slots is shown in Figure 2.20.

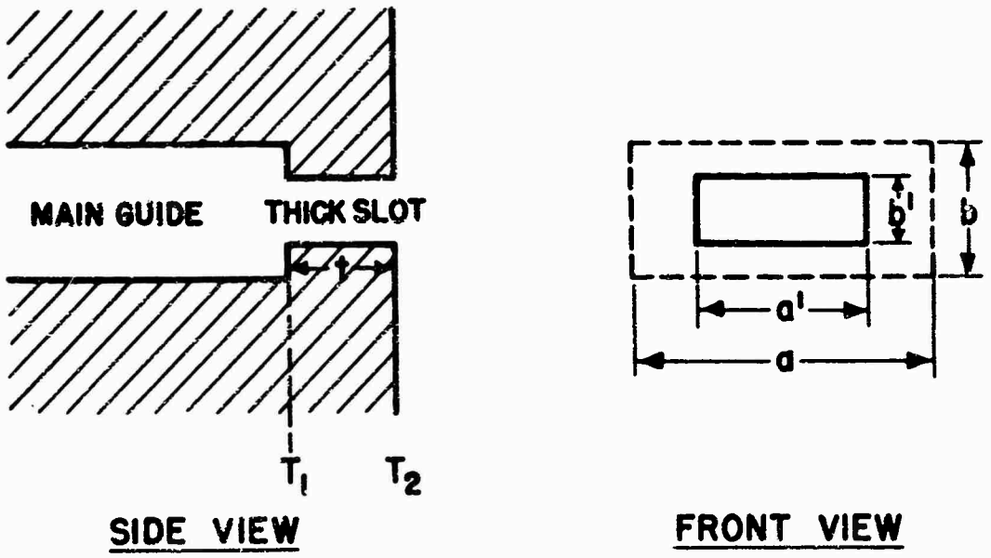

PHYSICAL STRUCTURE

Figure 2.20

The network equivalent may be considered as a lossy two-terminal circuit Y_{rtk} for the overall structure at reference plane T_1, or in one of the composite forms given in Figure 2.21.

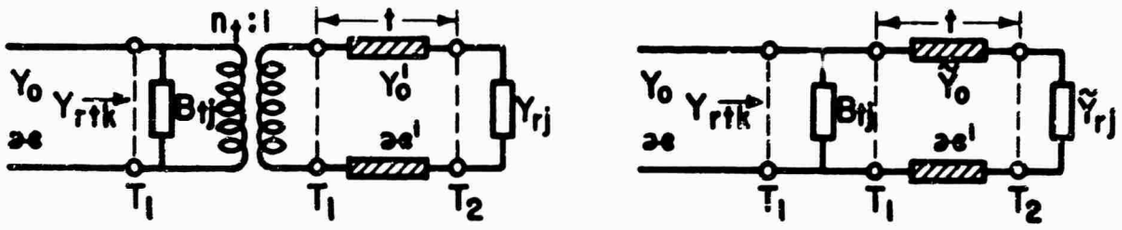

COMPOSITE EQUIVALENT NETWORK FOR THE THICK TRANSVERSE RADIATING SLOT

Figure 2.21

The difference between the two circuits is that in (b) the transformer of (a) has been eliminated. This requires that the characteristic admittance Y'_o and terminal admittance Y_{rj} of (a) be multiplied by the factor $1/n_t^2$ (n_t is the transformer turns ratio) in order to obtain the correct corresponding values of (b).

The discussion below is based on the simpler network (b) of Figure 2.21, which is seen to consist of the following components: 1) the susceptance B_{tj} introduced by the change in cross-section at terminal plane T_1 ; 2) a transmission line of length t, characteristic admittance $\tilde{Y}_o$, and propagation constant γ' representing the slot proper; and 3) a terminating admittance $\tilde{Y}_{rj}$ which accounts for all effects to the right of terminal plane T_2. As mentioned above, the transformer with turns ratio n_t, which appears between terminal planes T_1 to the right of B_{tj} in the equivalent circuit for the change in cross-section at T_1 (cf. Final Report, Chap. VI, Sec. B), has been removed to the right so that the characteristic admittance for the slot guide relative to that of the main guide is given by:

$$\frac{\tilde{Y}_o}{Y_o} = \frac{\lambda_g \, a \, b}{\lambda'_g \, a' \, b'} \left[\frac{\pi}{4} \frac{1 - (\frac{a'}{a})^2}{\cos(\frac{\pi \, a'}{2a})} \right]^2 \qquad (2.4)$$

The susceptance B_{tj}/Y_o is approximately equal to one-half the relative susceptance of a thin aperture coupling two identical guides. However, it was found experimentally from precision measurements on thick transverse slots within rectangular waveguide that the effect of change in cross-section is more closely equal to .55x (susceptance of thin slot), for $t > .1^{a}$ (see Final Report Chap. V, Sec. A, 3. The reference plane shift δ discussed in this section is considered negligibly small.).

The purpose of the measurements on these thick radiating slots is to check experimentally the validity of the equivalent circuits of Figure 2.21, and to obtain an experimental value for the junction between the "intervening" slot guide and a half space, i.e. for $\tilde{Y}_{rj}/Y_o$. If the thick slot can indeed be represented by a single mode transmission line of length t connecting the terminal admittance $\tilde{Y}_{rj}$ with the main guide, then, for a given cross-section, $\tilde{Y}_{rj}$ should be constant for all t provided that t is large enough to permit higher mode interaction effects to be neglected. This requirement of constancy for $\tilde{Y}_{rj}$ constitutes a very severe check not only of the parameters B_{tj} and $\tilde{Y}_o$, but also of the experimental measurements which yield the input admittance Y_{rtk} at terminal plane T_1 (Figure 2.21), from which $\tilde{Y}_{rj}$ is computed. Thus, a reasonable check of the validity of the network picture for a thick slot as given in Figure 2.21 may be taken to exist as long as the computed value of $\tilde{Y}_{rj}$ deviates from a constant value within the limits of experimental accuracy and the tolerances on the pertinent parameters. The measured data of the input admittance Y_{rtk}/Y_o is utilized in another way to check the network picture of Figure 2.21. The theoretical values of $\tilde{Y}_{rj}/Y_o$, $\tilde{Y}_o/Y_o$ and B_{tj}/Y_o are used in the equivalent circuit and computed values of Y_{rtk}/Y_o are obtained which are then compared to the measured values. Such a comparison for various values of thickness is given in Part IV. One notes that the latter check on the network picture requires the theoretical value for $\tilde{Y}_{rj}/Y_o$, while the former does not.

For a given thickness t, the relative input admittance Y_{rtk}/Y_o to the thick slot is computed from experimental measurements in the manner indicated in the Final Report, Eqs. (5.4). From a knowledge of Y_{rtk}/Y_o the terminal admittance $\tilde{Y}_{rj}/Y_o$ is determined as follows, making use of standard transmission line relationships:

$$\frac{\tilde{Y}_{rj}}{Y_o} = \frac{\tilde{Y}_o}{Y_o} \frac{j - \left(\frac{Y_{rtk}}{Y_o} - j\frac{B_{tj}}{Y_o}\right)\frac{Y_o}{\tilde{Y}_o}\cot \beta' t}{j\left(\frac{Y_{rtk}}{Y_o} - j\frac{B_{tj}}{Y_o}\right)\frac{Y_o}{\tilde{Y}_o} - \cot \beta' t} = \frac{\tilde{G}_{rj}}{Y_o} + j\frac{\tilde{B}_{rj}}{Y_o} \qquad (2.5a)$$

where $Y_{rtk} = G_{rtk} + j B_{rtk}$, $\beta' = \frac{2\pi}{\lambda'_g}$, $\lambda'_g = \frac{\lambda}{\sqrt{1 - \left(\frac{\lambda}{2a'}\right)^2}}$.

If Equation (2.5a) is written explicitly in terms of $\tilde{G}_{rj}/Y_o$ and $\tilde{B}_{rj}/Y_o$, one obtains:

$$\frac{\tilde{G}_{rj}}{Y_o} = \frac{\frac{G_{rtk}}{Y_o}\csc^2 \gamma' t}{\left[\cot \gamma' t + \frac{Y_o}{\tilde{Y}_o}\left(\frac{B_{rtk}}{Y_o} - \frac{B_{tj}}{Y_o}\right)\right]^2 + \left[\frac{Y_o}{\tilde{Y}_o}\frac{G_{rtk}}{Y_o}\right]^2} \tag{2.5b}$$

$$\frac{\tilde{B}_{rj}}{Y_o} = \frac{\frac{Y_o}{\tilde{Y}_o}\cot \gamma' t\left[\left(\frac{G_{rtk}}{Y_o}\right)^2 + \left(\frac{B_{rtk}}{Y_o} - \frac{B_{tj}}{Y_o}\right)^2\right] - \left[\frac{\cot \gamma' t}{\left(\frac{Y_o}{\tilde{Y}_o}\right)}\right] + \left[\frac{B_{rtk}}{Y_o} - \frac{B_{tj}}{Y_o}\right](\cot^2 \gamma' t - 1)}{\left[\cot \gamma' t + \frac{Y_o}{\tilde{Y}_o}\left(\frac{B_{rtk}}{Y_o} - \frac{B_{tj}}{Y_o}\right)\right]^2 + \left[\frac{Y_o}{\tilde{Y}_o}\frac{G_{rtk}}{Y_o}\right]^2} \tag{2.5c}$$

If the slot is beyond cutoff, then

$$\gamma' = -j|\gamma'| \quad ; \quad \frac{\tilde{Y}_o}{Y_o} = -j\left|\frac{\tilde{Y}_o}{Y_o}\right| \quad ; \quad \cot \gamma' t = -j \coth |\gamma'| t \tag{2.6}$$

so that for large thicknesses, $\coth |\gamma'| t \cong 1$. In that case, Equation (2.5a) becomes indeterminate, and if one solves it for Y_{rtk}, it is seen that it is independent of $\tilde{Y}_{rj}$, i.e.:

$$\frac{Y_{rtk}}{Y_o} \cong j\frac{B_{tj}}{Y_o} + \frac{\tilde{Y}_o}{Y_o} \quad , \tag{2.7}$$

and one cannot solve uniquely for $\tilde{Y}_{rj}$ from a knowledge of Y_{rtk}. Equation (2.7) expresses the fact that the input admittance to a beyond cutoff slot for which $\gamma' t \gg 1$ is independent of the terminating admittance Y_{rj}.

The value of Y_{rtk}, for the overall thick slot, is obtainable from the composite network of Figure 2.21-(b) if one knows the theoretical values for $\tilde{Y}_{rj}$, the junction to the half space, and B_{tj}, the change in cross-section. The value to choose for B_{tj} has been discussed above, and the value for $\tilde{Y}_{rj}$ may be obtained in the following manner. $\tilde{G}_{rj}/Y_o$ is to be taken equal to G_r/Y_o, the conductance of a thin radiating slot of identical dimensions (see Figure 2.22). $\tilde{B}_{rj}$ is given by

$$\frac{\tilde{B}_{rj}}{Y_o} = \frac{B_r}{Y_o} - \frac{B_{tj}}{Y_o} \tag{2.8}$$

which follows from Equation (2.5c) for $t = 0$ (B_{rtk} becomes B_r for zero thickness). The expression relating Y_{rtk} to the other parameters is:

$$\frac{Y_{rtk}}{Y_o} = j\frac{B_{tj}}{Y_o} + \frac{\tilde{Y}_o}{Y_o}\left[\frac{j + \frac{\tilde{Y}_{rj}}{Y_o}\frac{Y_o}{\tilde{Y}_o}\cot\chi' t}{\cot\chi' t + j\frac{\tilde{Y}_{rj}}{Y_o}\frac{Y_o}{\tilde{Y}_o}}\right] \tag{2.9}$$

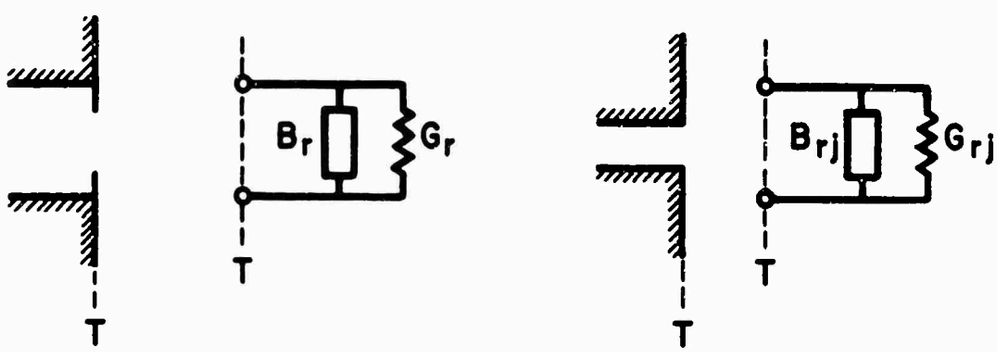

Figure 2.22

Although the experimental procedure for measuring the admittance of thick apertures radiating into a half space from the end of a guide is identical with that followed in measurements on thin slots, a modified method has to be employed for holding the thick apertures to the end of the guide. For this purpose, two separate vacuum chucks were constructed: chuck A bolted to the infinite plane, which holds in place a .005" brass sheet that provides electrical contact between the far side of the aperture and the infinite plane; and chuck B, mounted to the end of the slotted section, which makes good contact with the near side of the aperture (see Figure 2.23). As in the case of thin slots the vacuum chucks eliminate the need for screws in the mounting of the apertures. The two separate chucks are better suited for this type of measurement than the single composite vacuum chuck used with thin slots since they can be adapted to apertures of different thicknesses.

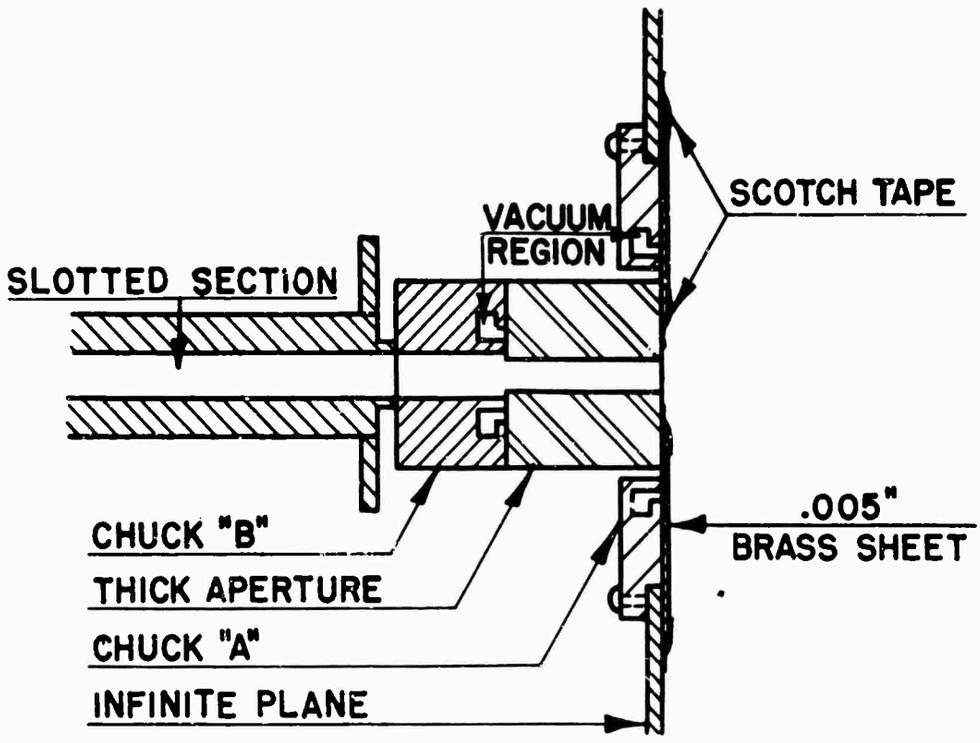

Figure 2.23

APPENDIX: Transformations between Equivalent Representations

(H. Kurss)

Two techniques for obtaining the transformations between equivalent representations are discussed here.

The classical approach consists of first appending transmission lines to the terminals so as to obtain two equivalent networks at the same set of reference planes. The various transformations are then obtained upon equating corresponding input admittances or voltages when the corresponding terminals of the two networks are terminated in the same but arbitrary admittances. A judicious choice of these terminations will greatly reduce the labor involved and simplify the resulting relations. This method of "special terminations" is often accessible to further simplification through use of the bisection theorems.

The alternative approach is based upon the method for obtaining the parameters of a quadrupole at a shifted set of reference planes by means of certain shifting formulae which have been discussed in the Final Report, Chap. III, Sec. A. These shifting formulae may be more compactly given in matrix form as will be shown in a future report. The original multipole networks can be reduced to quadrupoles by recourse to the bisection theorems or "special terminations" described above.

The method based upon the quadrupole shifting formulae is the more routine of the two methods, and results in a completely explicit set of transformation formulae. However the "special terminations" technique generally involves much less work when properly applied, and is capable of yielding a semi-explicit set of transformation formulae which are simpler in form than the completely explicit set.

From the infinity of possible representations there can be isolated a finite number of preferred representations to which all representations of the structure can be reduced by reference plane shift. The two preferred representations chosen for this report are the so-called "centerline" and "invariant" representations. When the impedance parameters are derived from the field equations together with the boundary conditions imposed by the physical structure, the reference planes are most naturally located at the discontinuity surfaces or the centerline planes, so that the "centerline" representation is best suited for theoretical purposes. The "invariant" representation is particularly of value when the parameters are to be obtained from a set of experimental data. The reasons for the latter statement are given in Part I, and also elsewhere in Part II.

A typical transformation is to be derived in detail by both methods to illustrate their main features. The transformation chosen relates the parameters of the E plane Tee centerline representation to those of the corresponding invariant representation, and is given below.

Derivation of the transformation equations relating the parameters of the invariant representation to those of the centerline representation for the E plane Tee.

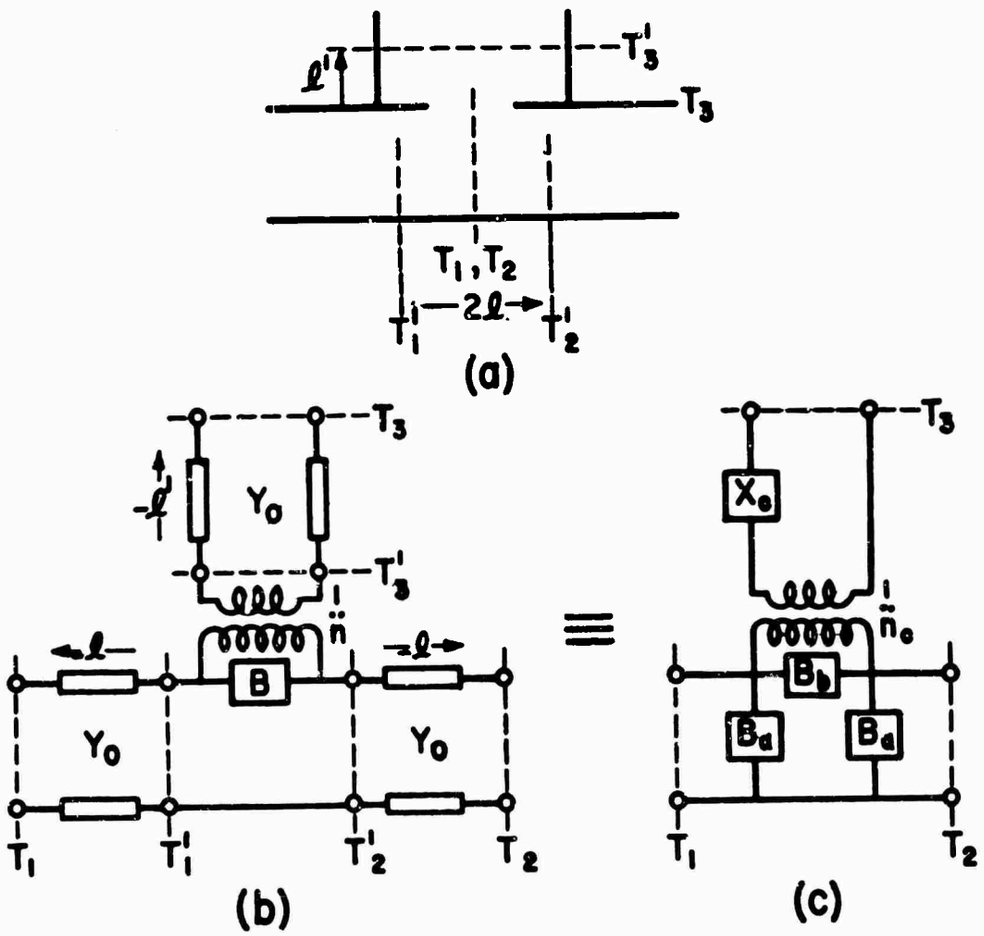

Figure 1

Figure 1-(a) shows the physical structure of the slot-coupled E plane Tee together with the location of the reference planes for both the centerline representation (unprimed) and the invariant representation (primed). The centerline representation is given in (c), while in (b)

lengths of line have been added to the invariant representation so that the outer reference planes become those of the centerline representation, permitting the equivalence indicated.

a) Method I. Special Terminations:

An open circuit bisection applied to Figures 1-(b) and 1-(c) yields the equivalence shown in Figure 2, so that

$$B_a/Y_0 = -\tan \alpha \ell \qquad (1)$$

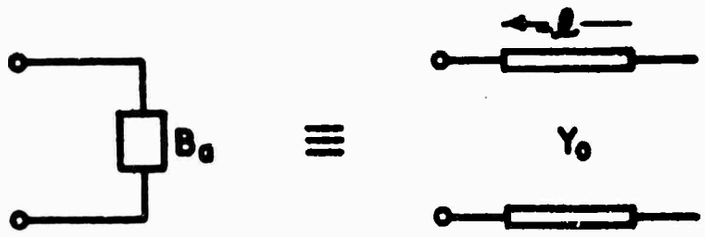

Figure 2

A short circuit bisection results in the equivalence shown in Figure 3.

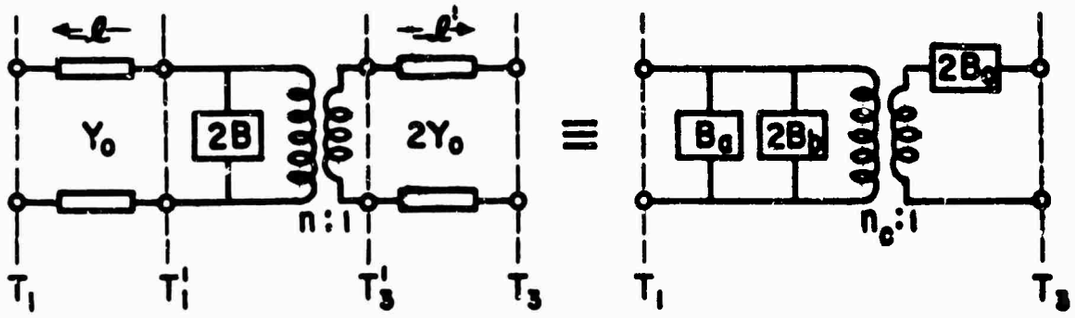

Figure 3

When an open circuit is placed at T_3 of each network of Figure 3 the input admittances at T_1 are

$$j\,(B_a + 2\,B_b) = \left[\frac{2\,j\,(B - \frac{Y_o}{n^2}\tan \varkappa \ell') - j\,Y_o \tan \varkappa \ell}{Y_o + 2\,(B - \frac{Y_o}{n^2}\tan \varkappa \ell')\tan \varkappa \ell}\right] Y_o \qquad (2)$$

which simplifies into

$$\frac{B_b}{Y_o} = \frac{\frac{B}{Y_o} - \frac{\tan \varkappa \ell'}{n^2}}{\left[1 + 2\,(\frac{B}{Y_o} - \frac{\tan \varkappa \ell'}{n^2})\tan \varkappa \ell\right]\cos^2 \varkappa \ell} \qquad (3)$$

upon use of Equation (1). When a short circuit is placed at T_1 of each network of Figure 3 the input admittances at T_3 are

$$2\,j\,B_c = \left[\frac{j\,n^2\left[2B + Y_o \cot \varkappa \ell\right] - j\,2\,Y_o \tan \varkappa \ell'}{2\,Y_o + n^2\left[2\,B + Y_o \cot \varkappa \ell\right]\tan \varkappa \ell'}\right] 2\,Y_o \qquad (4)$$

or

$$\frac{B_c}{Y_o} = \frac{1 + 2\left[\frac{B}{Y_o} - \frac{\tan \varkappa \ell'}{n^2}\right]\tan \varkappa \ell}{\tan \varkappa \ell' + 2\left[\frac{B}{Y_o}\tan \varkappa \ell' + \frac{1}{n^2}\right]\tan \varkappa \ell} \qquad (5)$$

When an open circuit is placed at each T_3 then the voltage at T_1 become

$$V_1 = n_c V_3 = V_3 \cos \varkappa \ell \; n \cos \varkappa \ell \left[1 + \left(\frac{2B}{Y_o} - 2 \frac{\tan \varkappa \ell'}{n^2} \right) \tan \varkappa \ell \right] \qquad (6)$$

or

$$\frac{n_c}{n} = \left\{ 1 + 2 \left[\frac{B}{Y_o} - \frac{\tan \varkappa \ell'}{n^2} \right] \tan \varkappa \ell \right\} \cos \varkappa \ell \; \cos \varkappa \ell' \qquad (7)$$

The transformation relations are then given by Equations (1), (3), (5), and (7), from which the parameters of the centerline representation are obtainable from those of the invariant representation.

b) Method II. Use of the Quadrupole Shifting Formulae:

When a reactance of $-X_c$ is placed at T_3 of Figures 1-(b) and (c), the equivalence shown in Figure 4 is obtained. The magnitude of B_{se} does

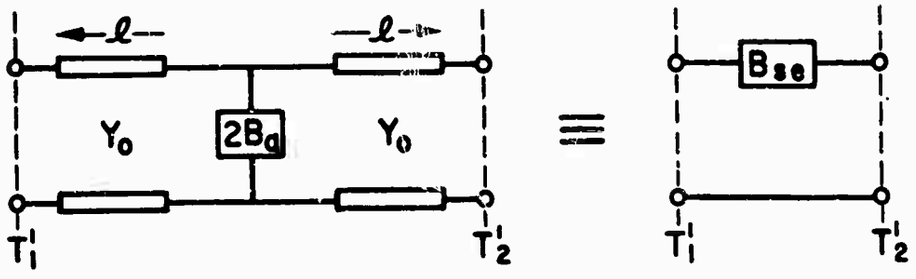

Figure 4

not enter into the determination of the relation between ℓ and B_a. The network parameters (see the Final Report, Chap. II, Eq. (18) and Chap. III Sec. A) on an admittance basis, for the purely shunt network, are $1/a = 0$, $c/a = 1$, and $b/a = -2 B_a/Y_o$, while for the purely series network, $b' = 0$. Setting $b' = 0$ (see Final Report, Chap. III, Eq. (6c)), setting $\alpha_o = \beta_o = \tan \varkappa \ell$, and using the above network parameters, results in $\tan \varkappa \ell = \infty$ or $B_a/Y_o = -\tan \varkappa \ell$. The latter is clearly the desired relation and it agrees with Equation (1).

The admittance parameters of the short circuit half (see Figure 3) between reference planes T_1' and T_2' are, from Figure 3.2 of Chap. III and Equation (18) of Chap. II, both of the Final Report,

$$b/c = -2B/Y_0$$
$$a/c = 2/n^2 \qquad (8)$$
$$1/c = 0$$

The transformed parameters, between reference planes T_1 and T_3, are, similarly:

$$\frac{B_a}{Y_0} + 2\frac{B_b}{Y_0} = -\frac{b'}{c'}$$
$$\frac{B_c}{Y_0} = c' \qquad n_c^2 = \frac{2c'^2}{b' + a'c'} \qquad (9)$$

The parameters indicative of the reference plane shifts are (Eq. (5a) of Chap. III, Final Report) $\alpha_0 = \tan \varphi(-\ell)$ and $\beta_0 = \tan \varphi(-\ell')$ or:

$$\alpha_0 = -\tan \varphi \ell$$
$$\beta_0 = -\tan \varphi \ell' \qquad (10)$$

The parameters for the network between T_1 and T_3 are related to those existing between T_1' and T_2' by Equation (6c) of the Final Report, Chap. III, which can be written in simplified form, since $1/c = 0$, as:

$$\frac{B_a}{Y_0} + 2\frac{B_b}{Y_0} = -\frac{b'}{c'} = -\frac{b/c - \alpha_0 - \beta_0 a/c}{1 + \alpha_0 b/c - \alpha_0 \beta_0 a/c}$$
$$\frac{B_c}{Y_0} = c' = \frac{1 + \alpha_0 b/c - \alpha_0 \beta_0 a/c}{-\alpha_0 a/c - \beta_0 - \alpha_0 \beta_0 b/c} \qquad (11)$$
$$n'^2 = \frac{2c'^2}{b' + a'c'} = \frac{2(c/a)(1 + \alpha_0 b/c - \alpha_0 \beta_0 a/c)^2}{(1 + \alpha_0^2)(1 + \beta_0^2)}.$$

These reduce directly to the expressions presented under Method I, upon substitution of Equations (8) and (10) into (11).

III. VARIATIONAL CALCULATIONS OF THE EQUIVALENT CIRCUIT PARAMETERS FOR THIN SLOTS

(J. Blass)

A. Network Considerations Appropriate to Thin Slot Structures

It is well known that the magnetic and electric fields in a uniform waveguide can be expressed as an infinite sum of orthogonal modes wherein the transverse magnetic and electric field mode amplitudes I_i and V_i satisfy transmission line equations involving the longitudinal variable. The transverse magnetic and electric mode functions which shall be designated by $\underline{h}_i'$, $\underline{h}_i''$ and $\underline{e}_i'$, $\underline{e}_i''$, respectively (the primes indicate E modes, the double primes H modes), and the longitudinal mode functions $\underline{h}_{iz}''$ and $\underline{e}_{iz}'$ are curvilinear functions of the transverse variables (x,y). Waveguide systems are usually operated at frequencies which permit the propagation of only the dominant mode, which for the rectangular waveguide is the H_{10} mode. The field far from any discontinuity consists therefore of only one dominant mode, although in the vicinity of a discontinuity the field consists of an infinite number of modes. The primary problem in the study of discontinuities is to relate the voltage and current of the dominant mode on one side of the discontinuity to the voltage and current on the other side. In these cases of uniform waveguides the dominant mode amplitudes V, I at one terminal plane progress to any other terminal plane along a transmission line whose propagation constant $(j\mathcal{K})$ and characteristic admittance Y_0 are determined by the waveguide dimensions and the frequency. Since linearity and reciprocity relations exist it is possible to represent a discontinuity, as far as V and I are concerned, by a lumped network inserted into the line at some predetermined terminal plane or planes.

If the waveguide structure is of the two terminal plane type, namely one input and one output plane, the dominant mode network representation of the discontinuity is a two terminal pair circuit. Thus, structures such as a change of guide cross section, a radiating slot, or a thick obstacle, for example, may be represented at a given frequency by lumped circuits such as either of those schematically presented in Figures 3.1(a) and (b).

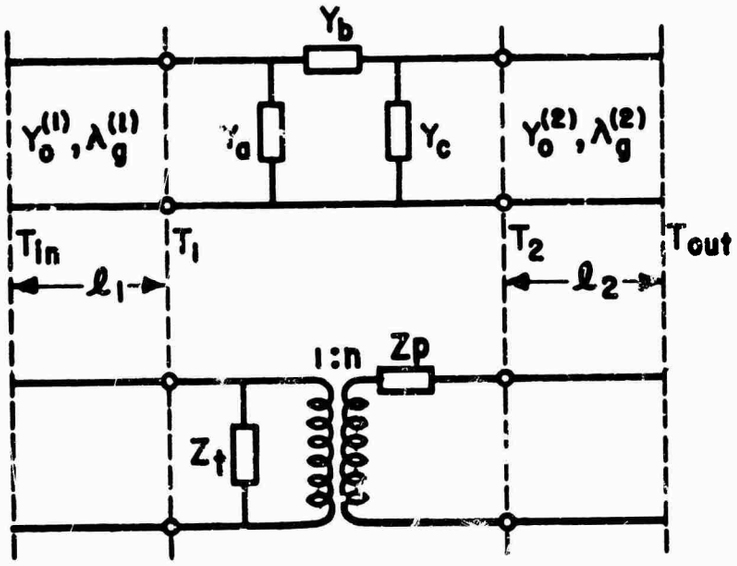

Figure 3.1(a)

Figure 3.1(b)

T_{in} and T_{out} are the waveguide input and output terminal planes, (T_1,T_2) are the terminal planes at which the above network represents the discontinuity, and ℓ_1 and ℓ_2 are lengths of transmission line between T_{in}, T_{out} and T_1, T_2 respectively. The above circuits may be altered to different, but equally valid, ones if T_1 and T_2 are shifted to some other points, in order to yield simpler or more convenient representations. T_{in} and T_{out} do not enter directly into the calculation of the admittance, but have been included in the above figures for the purpose of illustrating the relative location of the network.

The E-plane and H-plane Tees fall into a different classification since they are examples of three terminal plane waveguide structures whose equivalent circuit representations are three terminal pair networks. Again, this assumes that only the dominant mode propagates in both the main and stub guides. A particular schematic representation of a symmetrical three terminal pair structure is given in Figure 3.2. T_1 and T_2 represent terminal planes in the main guide structure which are separated by equal distances from the plane of symmetry, while T_3 refers to the terminal plane in the stub guide. For the variational calculations T_1, T_2 have been chosen at the plane of symmetry and T_3 has been made coincident with the plane of the iris. A discussion of terminal plane transformations in

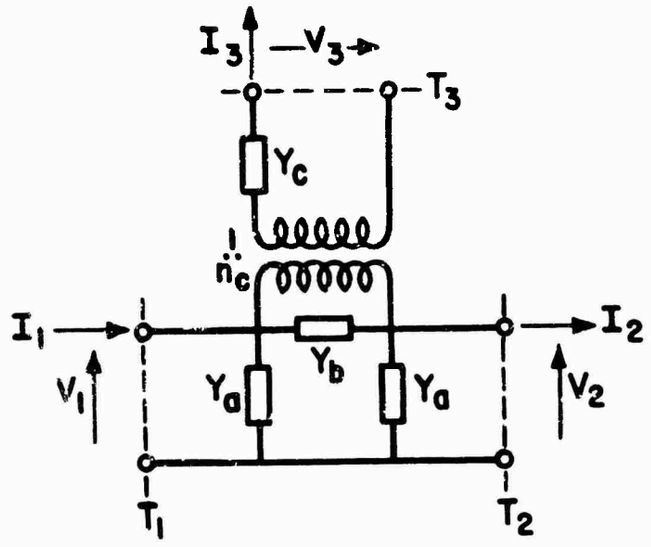

Figure 3.2

connection with invariant representations of such networks is given in Part II.

The representations of planar slot discontinuities which have been chosen for the variational calculations have the planes T_1 and T_2 coinciding with the plane of symmetry. The resulting networks can be shown to be simplified versions of the general circuits of Figures 3.1 and 3.2 and before proceeding to the analytical aspects of the problem the reasons for the simplifications will be made clear.

The transverse slot which couples two identical guides is considered first. Suppose that the electric field generated in the slot is due

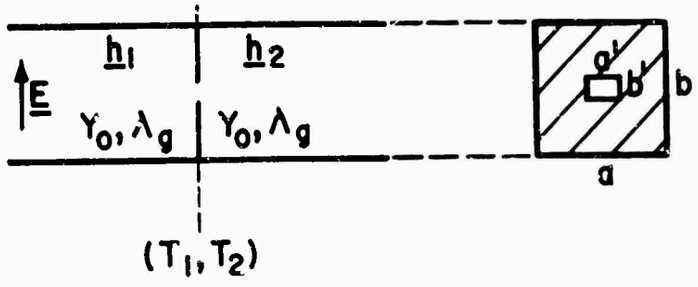

Figure 3.3

to a source far to the left. From the symmetry of the structure it is seen that (see Final Report, Chap. I):

$$V_1 = \iint_{ap.} \underline{z}_o \times \underline{E} \cdot \underline{h}_1 \, dS$$

$$V_2 = \iint_{ap.} \underline{z}_o \times \underline{E} \cdot \underline{h}_2 \, dS = V_1 \qquad (3.1)$$

since $\underline{h}_1 = \underline{h}_2$ for identical input and output guides. If the source were on the right the same electric field would be excited and the same relationships would exist. That is, if a source on the right resulted in voltages V_1', V_2' then $V_1' = V_2'$. The network equations

$$V_1 = Z_{11} I_1 + Z_{12} I_2$$

$$V_2 = Z_{21} I_1 + Z_{22} I_2 \qquad (3.2)$$

become

$$V_1 = Z (I_1 + I_2) = V_2.$$

Therefore, the network becomes purely shunt, and Figure 3.1(a), with $Y_b = \infty$, or Figure 3.1(b) with $Z_p = 0$, and $n = 1$, are representative of the structure.

If the two guides are not identical as in the structure of Figure 3.4, the circuit representation is no longer simply shunt. As before, consider first a source on the left which generates an electric field $\underline{E}$ in the aperture. The equations for the dominant mode voltages are then

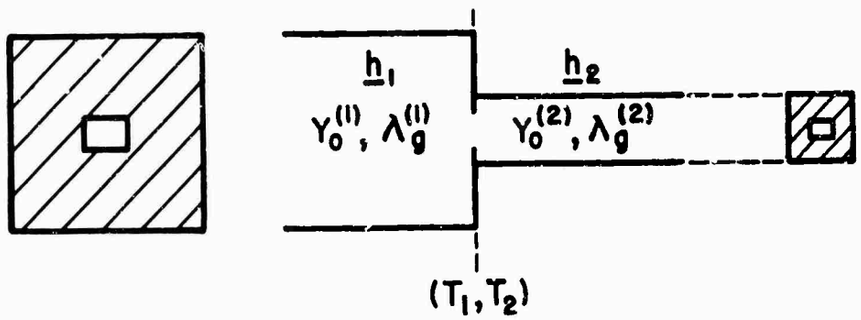

Figure 3.4

$$V_1 = \iint_{ap.} \underline{z}_0 \times \underline{E} \cdot \underline{h}_1 \, dS \cdot$$

$$V_2 = \iint_{ap.} \underline{z}_0 \times \underline{E} \cdot \underline{h}_2 \, dS \cdot \qquad (3.3a)$$

A source field on the right will excite a slot field $\underline{E}'$. The voltages to the left and right of the discontinuity, respectively, are

$$V_1' = \iint_{ap.} \underline{z}_0 \times \underline{E}' \cdot \underline{h}_1 \, dS$$

$$V_2' = \iint_{ap.} \underline{z}_0 \times \underline{E}' \cdot \underline{h}_2 \, dS \qquad (3.3b)$$

Since in general $\underline{E}' \neq \underline{E}$ and $\underline{h}_1 \neq \underline{h}_2$, it follows that $V_1 \neq V_2$, $V_1' \neq V_2'$ and furthermore that $V_1/V_2 \neq V_1'/V_2'$. Hence no simplification of the circuits of Figure 3.1 is possible. If, however, the slot is small and not near one of the guide walls, the energizing fields are almost constant over the slot region so that the induced electric fields $\underline{E}$ and $\underline{E}'$ differ approximately at most by a constant factor. For a small slot, therefore, it is seen from Equations (3.3) that

$$\frac{V_1}{V_2} = \frac{V_1'}{V_2'}$$

This implies, by Equations (3.2), that $Z_{11}/Z_{21} = Z_{12}/Z_{22}$, but since $Z_{12} = Z_{21}$, the general impedance matrix reduces to

$$\begin{vmatrix} Z_{11} & \sqrt{\frac{Z_{22}}{Z_{11}}}\, Z_{11} \\ \sqrt{\frac{Z_{22}}{Z_{11}}}\, Z_{11} & \left(\frac{Z_{22}}{Z_{11}}\right) Z_{11} \end{vmatrix}$$

The corresponding equivalent circuit is the one of Figure 3.1(b) in which $z_p = 0$ and

$$n = \sqrt{\frac{z_{22}}{z_{11}}}$$

The equivalent network of a symmetrical two terminal pair structure may also be analyzed by first reducing it to two one terminal pair networks by a method described in the next paragraph in its application to three terminal pair structures.

The slot coupled E plane Tee, shown in Figure 3.5, has a symmetrical three terminal pair network equivalent.

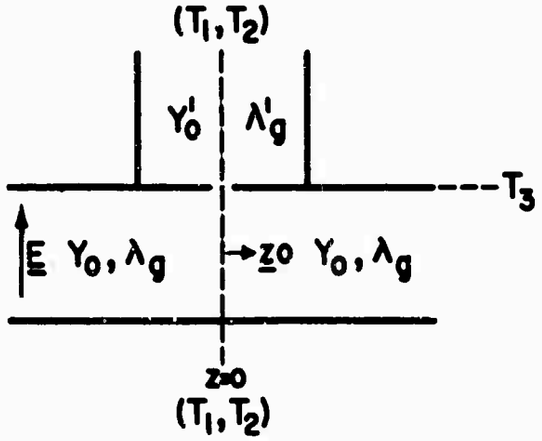

Figure 3.5

Bartlett's bisection theorem can be employed in order to determine more easily the elements of the network. If symmetric current excitation is used in the main guide, $I_1 = I_2$ (See Figure 3.2). This is equivalent to inserting a shorting plane ($V = 0$) at (T_1, T_2). The composite circuit can then be considered to be a pair of two terminal pair structures. Examination of the induced aperture electric field due to this excitation shows that it is similar in form to that obtained for Figure 3.4. The electric field excited in the slot by the stub source or by the main guide source will differ approximately by a constant amplitude factor if the slot dimension in the z direction is small compared to the guide wave length and the guide dimensions. The resulting equivalent network is therefore the shunt transformer circuit of Figure 3.6(a).

When symmetric voltage excitation is applied in the main guide, the circuit of Figure 3.2 is then open circuited at the plane (T_1, T_2). The circuit is now reduced to two one-terminal pair structures independently of the slot size, as shown in Figure 3.6(b). It is seen that such a separation is purposeful since the variational method can be just as well applied to the determination of the parameters of these reduced circuits.

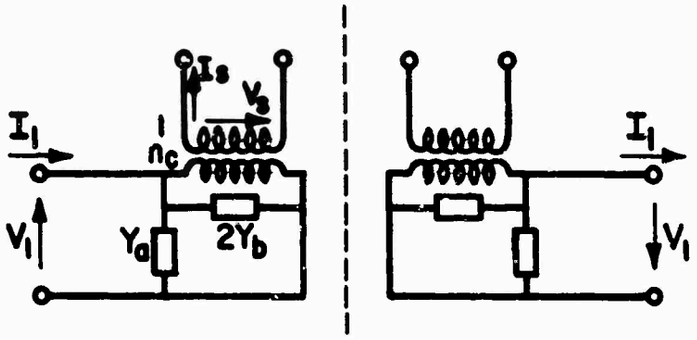

Figure 3.6(a)

Symmetrical H excitation

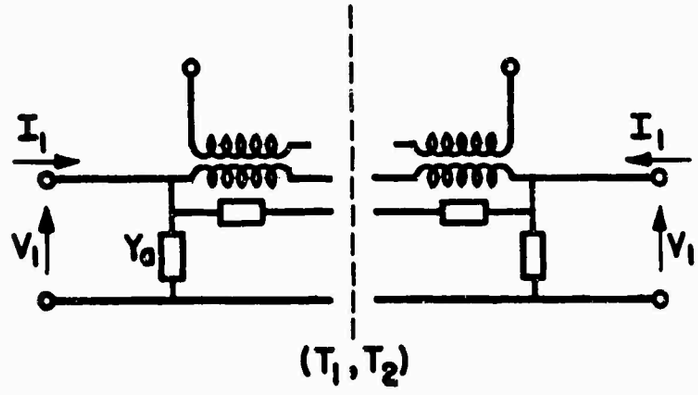

Figure 3.6(b)

Symmetrical E excitation

B. Variational Formulations

The boundary value problem associated with the discontinuity field can be simply formulated as an integral equation, but can rarely be solved in a simple manner. The integral equations, nevertheless, may be employed to obtain the desired circuit parameters by means of variational expressions whose relative insensitivity to the slot fields forms the basis for an approximation procedure.

The field excitation in a transverse slot can be regarded as equivalent to a distribution of magnetic current dipoles. The field excitation in a longitudinal slot is equivalent to both a magnetic and electric current dipole distribution. For this reason the transverse slot and the longitudinal slot are discussed separately.

1. Transverse Slot

Consider the transverse discontinuity of Figure 3.7(a) and the corresponding equivalent circuit in Figure 3.7(b).

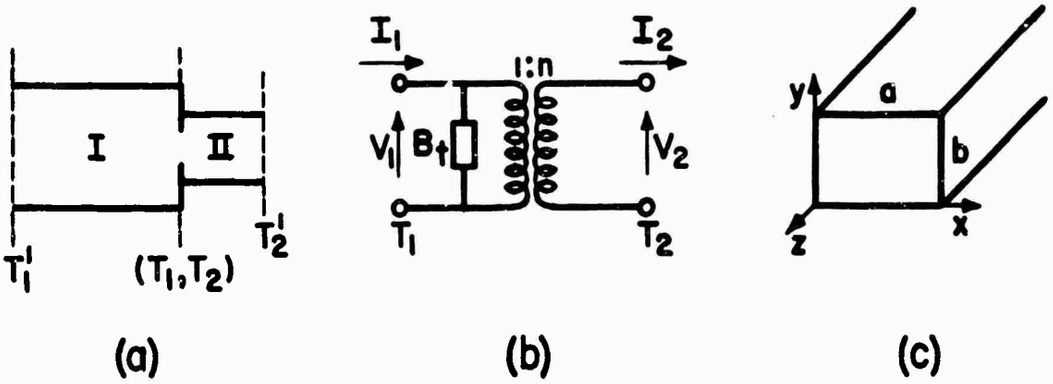

Figure 3.7

The electromagnetic field everywhere in regions I and II can be expressed, by a well known uniqueness theorem, in terms of the tangential component of either $\underline{E}$ or $\underline{H}$ on the boundary of the given region. The boundary of region I is the plane T_1', the metal walls, and the surface T_1. The boundary of region II is T_2, the metal walls and T_2'. The magnetic field at the outer

boundaries is just the dominant mode field if they are sufficiently far removed from the discontinuity so that the higher modes excited there have completely attenuated. The electric field is zero on the boundary except over the aperture region and on the planes T_1', T_2'. It is possible by a modal analysis to relate the magnetic field at T_1', T_2' to the electric field in the slot. The transverse magnetic field in region I in terms of the modes of this region is

$$\underline{H}_{t1} = I_1(z)\,\underline{h}_1(x,y) + \sum{}' I_{i1}(z)\,\underline{h}_{i1}(x,y) \tag{3.4a}$$

and in region II it is

$$\underline{H}_{t2} = I_2(z)\,\underline{h}_2(x,y) + \sum{}' I_{i2}\,\underline{h}_{i2}(x,y) \tag{3.4b}$$

where $\underline{h}_{i1}$ and $\underline{h}_{i2}$ are the vector mode functions appropriate to regions I and II, respectively. The primed sum includes all modes except the dominant one.

Since the higher mode waves are rapidly attenuated, the line presents a match to these modes in both directions from (T_1, T_2). The higher mode current on the left at T_1 is therefore related to the corresponding mode voltage by the relation

$$I_{i1} = -Y_{i1} V_{i1} \tag{3.5a}$$

while on the right,

$$I_{i2} = Y_{i2} V_{i2} \tag{3.5b}$$

The change in sign is appropriate to the indicated positive directions of current and voltage shown in Figure 3.7(b). However, V_i is related simply to the slot field by

$$V_i(o) = \iint_{\text{slot}} \pm\, \underline{M} \cdot \underline{h}_i \, dS' \tag{3.6}$$

where $\underline{M}$, the magnetic current density, is equal to

$$\underline{M} = \underline{n} \times \underline{E}. \tag{3.7}$$

and $\underline{n}$ is a vector normal to the surface out of the region. The positive sign is chosen when $\underline{n}$ is in the $\underline{z}_o$ direction and the negative sign when in the $-\underline{z}_o$ direction. Also $V_i(z) = V_i(o)\, e^{-j\beta_i |z|}$ for all but the dominant mode.

If the substitutions of Equations (3.5a) and (3.5b) are made in Equation (3.4a) and (3.4b), respectively, and the voltage is expressed as the integral of Equation (3.6), the integral representation of Equation (3.8a) and (3.8b) for the magnetic field is possible. The vector mode functions have been combined under the integral sign.

$$\underline{H}_{t1}(x,y,z) = I_1(z)\underline{h}_1 = \iint_{\text{slot}} \underline{M}_1 \cdot \sum_I' Y_{i1}\, \underline{h}_{i1}\, \underline{h}_{i1}\, e^{-j\beta_{i1}|z|}\, dx'dy' \tag{3.8a}$$

$$\underline{H}_{t2}(x,y,z) = I_2(z)\, \underline{h}_2 - \iint_{\text{slot}} \underline{M}_2 \cdot \sum_I' Y_{i2}\, \underline{h}_{i2}\, \underline{h}_{i2}\, e^{-j\beta_{i2}(z)}\, dx'dy' \tag{3.8b}$$

where

$$\underline{M}_1 = \underline{z}_o \times \underline{E}\ ,\ \underline{M}_2 = -\underline{z}_o \times \underline{E}$$

$$\underline{M}_1 = -\underline{M}_2 = \underline{M}$$

It is necessary to satisfy the continuity requirement of the magnetic field over the slot. Thus

$$\underline{H}_{t1}(x,y,o) = \underline{H}_{t2}(x,y,o)$$

which provides a means of eliminating the total magnetic field and thereby obtaining an integral equation for $\underline{M}$. Let

$$j\underline{\underline{B}}_t = \sum_i' \left\{ Y_i'\, \underline{h}_i'\, \underline{h}_i' + Y_i''\, \underline{h}_i''\, \underline{h}_i'' \right\} , \tag{3.9}$$

where the primes indicate E modes and the double primes H modes, and where the subscript "t" indicates the transverse dyadic suceptance in the vicinity of a short circuit plane. If Equation (3.8b) is subtracted from (3.8a) in the slot region ($z = 0$) the following equation for $\underline{M}$ is obtained:

$$0 = I_1(o)\underline{h}_1 - I_2(o)\underline{h}_2 - j\iint_{slot} \underline{M} \cdot (\underset{\sim}{\mathcal{B}}_{t1} + \underset{\sim}{\mathcal{B}}_{t2})\,dS' \qquad (3.10)$$

This result may be derived independently in terms of the dyadic waveguide Green's function. In the above equation the dominant mode contributions of the Green's functions have been lumped into the far field terms. The dyadic susceptances indicated are respectively the imaginary part of the transverse component of the waveguide Green's functions in the left and right hand semi-infinite regions.

If the two waveguides are identical, the modes functions are the same, i.e. $\underline{h}_2 = \underline{h}_1$. If the waveguides are not identical, a simple treatment is effected in the case of a small slot since then

$$\underline{h}_2 = n\,\underline{h}_1$$

over the slot region, where n is independent of slot size and is exactly equal to $\sqrt{b_1/b_2}$ when the change is a change in guide height. As indicated in the previous section, the series element Z_p of Figure 3.1(b) can then be neglected, and the representation of Figure 3.7(b) is valid. However, even if the slot is not small in size, the series element is small. Equation (3.10) can then be rewritten as:

$$\left[I_1(o) - n\,I_2(o)\right]\underline{h}_1 = \iint_{slot} \underline{M} \cdot j\left\{\underset{\sim}{\mathcal{B}}_{t1} + \underset{\sim}{\mathcal{B}}_{t2}\right\} dS' \qquad (3.11)$$

If both sides of Equation (3.11) are multiplied by the vector magnetic current density in a scalar product fashion and integrated over the slot region the left side becomes (using Equation (3.6)).

$$\left[I_1(o) - n\,I_2(o)\right] V_1(o) = P_t$$

where P_t designates the reactive power flow in the discontinuity. Then,

$$\frac{P_t}{V(o)^2} = \frac{I_1(o) - n\,I_2(o)}{V(o)} = j\,B_t$$

These considerations immediately lead to the variational expression for B_t,

namely,

$$j B_t = \frac{P_t}{V^2(o)} = j \frac{\iint_{slot}\iint_{slot} \underline{M} \cdot \left\{\underline{\mathcal{B}}_{t1}+\underline{\mathcal{B}}_{t2}\right\}\cdot \underline{M}\, dS\, dS'}{\left[\iint_{slot} \underline{M}\cdot \underline{h}_1\, dS\right]^2} \qquad (3.12)$$

Note that the double surface integral represents the reactive power flow in the discontinuity. It can be shown that the incremental variation of the susceptance B_t, due to a change in $\underline{M}$ (or $\underline{E}$) is proportional to the square of the increment of $\underline{E}$, that is, the susceptance is stationary about the correct slot electric field.

2. Longitudinal Slot

The longitudinal slot discontinuity is a junction between two regions, the main guide and the stub guide, where the latter includes as a special case a half space region.

The total magnetic field induced at any point in a rectangular waveguide, which propagates only one mode, by a magnetic surface current source at (x',y',z') and dominant mode sources located an integral number of wavelengths from $z = 0$ is (See Report R-157-47, pp. 16, 17):

$$\underline{H}(x,y,z) = \left(\frac{I_1+I_2}{2}\right)\underline{h}^{(1)}(x,y,z) - jY\left(\frac{V_1-V_2}{2}\right)\underline{h}^{(2)}(x,y,z) - j\iint \underline{M}\cdot \underline{\mathcal{B}}_g\, dS' \qquad (3.13a)$$

where

$$\left.\begin{aligned} \underline{h}_i^{(1)} &= \underline{h}_i'' \cos\varkappa_i z - \left(\frac{k_{ci}}{\varkappa_i}\right)\underline{h}_{iz}'' \sin\varkappa_i z \\ \underline{h}_i^{(2)} &= \underline{h}_i'' \sin\varkappa_i z + \left(\frac{k_{ci}}{\varkappa_i}\right)\underline{h}_{iz}'' \cos\varkappa_i z \end{aligned}\right\} \qquad (3.13b)$$

and $\underline{\mathcal{B}}_g$, now the total guide dyadic susceptance or the higher mode total magnetic field response of a unit magnetic dipole is

$$\underset{\sim}{\mathcal{B}}_g = \sum_I \left\{ \frac{1}{2} Y_i' \, \underline{h}_i' \, (s) \, \underline{h}_i'(s') e^{-j\varkappa_i |z - z'|} \right.$$

$$\left. + \frac{1}{2} Y_i'' \left[\underline{\bar{h}}_i^{(1)} (s, z>) - j \, \underline{\bar{h}}_i^{(2)} (s, z>) \right] \left[\underline{\bar{h}}_i^{(1)} (s, z<) + j \, \underline{\bar{h}}_i^{(2)} (s, z<) \right] \right\} \tag{3.13c}$$

where

$$(s, z>) \equiv \begin{cases} (s, z) & z > z' \\ (-', z') & z < z' \end{cases}$$

$$(s, z<) \equiv \begin{cases} (s', z') & z' < z \\ (s, z) & z' > z \end{cases}$$

and where s represents the transverse coordinates in the slot. It should be pointed out that in the reference given above the direction of V_2 is opposite to the one used here (See Figure 3.2) to obtain the expression of Equation (3.13a), and also that here the symbols $\underline{h}^{(1)}$ and $\underline{h}^{(2)}$ are introduced to make the notation more compact. V and I are equal to the magnetic and electric dominant mode amplitudes at integral multiples of a guide wavelength from the plane z = 0, and their positive directions are indicated in Figure 3.2. This general representation is needed in order to specify the field in a slot on the top or on the side of a waveguide. The magnetic field in the stub region, as has already been shown since it corresponds to the transverse slot case, can be evaluated in terms of the magnetic current distribution $\underline{M}$ as follows:

$$\underline{H}_s = I_s \, \underline{h}_s - j \iint_{\text{slot}} \underline{M} \cdot \underset{\sim}{\mathcal{B}}_s \, d S' \tag{3.14}$$

where the subscript "s" signifies stub guide. The spatial susceptance indicated in Equation (3.14) is essentially the transverse component of the spatial susceptance of Equation (3.13c) but is now relative to the modes in the stub guide.

If the Tee structure is to be considered as a two terminal pair network between the planes T_1 and T_2 (See Figure 3.2), that is, there are no dynamic sources in the stub which need be considered, the magnetic field in the stub is best described by lumping the scattered dominant mode field with the higher mode field, so that

$$\underline{H}_s = - j \iint_{\text{Slot}} \underline{M} \cdot \underset{\sim}{\mathcal{Y}}_s \, d S' \tag{3.15}$$

$\underset{\sim}{y}_s$ will include a resistive term if a radiating or propagating mode is present in the stub guide. Thus, for example, if the stub is a half space region $\underset{\sim}{y}_s$ will include a radiation resistance term, while if it is a Tee stub beyond cutoff $\underset{\sim}{y}_s$ will be purely reactive. If the stub region is a half space

$$\underset{\sim}{y}_s = \frac{1}{2\pi\omega}\left[-\nabla\nabla' + k^2\,\underset{\sim}{\epsilon}\right]\frac{e^{jk|\underline{r}-\underline{r}'|}}{|\underline{r}-\underline{r}'|} \tag{3.16}$$

where the identity dyadic $\underset{\sim}{\epsilon}$ is

$$\underset{\sim}{\epsilon} = \underline{x}_0\,\underline{x}_0 + \underline{y}_0\,\underline{y}_0 + \underline{z}_0\,\underline{z}_0 \tag{3.17}$$

The integral equation for the magnetic current distribution follows from the continuity condition

$$\underline{H}(x,y,z) - \underline{H}_s(x,y,z) = 0 \tag{3.18}$$

where $\underline{H}$ is the magnetic field just off the aperture in the main guide direction and $\underline{H}_s$ is the magnetic field just off the aperture in the stub guide direction. The integral equation now becomes (using Eqs. (3.13a) and (3.14)).

$$0 = \left(\frac{I_1+I_2}{2}\right)\underline{h}^{(1)} - jY\left(\frac{V_1-V_2}{2}\right)\underline{h}^{(2)} - I_s\,\underline{h}_s - j\iint_{\text{slot}} \underline{M}\cdot\left[\underset{\sim}{\mathfrak{G}}_L + \underset{\sim}{\mathfrak{G}}_s\right] dS' \tag{3.19}$$

where $\underline{M} = \underline{n} \times \underline{E}_{\text{slot}}$, and $\underline{n}$ points out of the main guide, and where $\underset{\sim}{\mathfrak{G}}_L$ is actually the $\underset{\sim}{\mathfrak{G}}_g$ of Eq. (3.13c), but signifies "longitudinal" here. For the E plane discontinuity $y = b$, $\underline{n} = \underline{y}_0$; for the H plane discontinuity $x = a$, $\underline{n} = \underline{x}_0$.

It has been previously pointed out that the problem of determining the parameters of a symmetrical E plane Tee network is simplified if the structure is investigated separately by means of a symmetrical electric field and a symmetrical magnetic field excitation in the main guide. For symmetrical electric field excitation $V_1 = -V_2$, $I_1 = -I_2$ (see Fig. 3.2) so that Eq. (3.19) can be expressed as

$$j Y V_1 \underline{h}^{(2)} + I_s \underline{h}_s = -j \iint_{slot} \underline{M} \cdot (\underset{\sim}{\mathcal{B}}_L + \underset{\sim}{\mathcal{B}}_s)\, dS' \qquad (3.20)$$

In the case of symmetrical magnetic field excitation

$$V_1 = V_2, \quad I_1 = I_2$$

and Eq. (3.19) reduces to

$$I_1 \underline{h}^{(1)} - I_s \underline{h}_s = j \iint_{slot} \underline{M} \cdot (\underset{\sim}{\mathcal{B}}_L + \underset{\sim}{\mathcal{B}}_s)\, dS' \qquad (3.21)$$

The magnetic current $\underline{M}$ of Eq. (3.21) differs from that of Eq. (3.20) since the exciting fields are not alike.

It was shown that Y_a of Fig. (3.2) may be calculated independently of the stub excitation if symmetrical electric field excitation is employed (see Fig. (3.6b)). It can be shown that for the above excitation (see report R-157-47, p. 58, Eq. (60))

$$2 I_1 = j Y \iint_{slot} \underline{M}_{s.e.} \cdot \underline{h}^{(2)}\, dS \qquad (3.22)$$

where the subscript s.e. designates symmetrical electric field excitation. If therefore I_s, the stub guide current is set equal to zero, (This is necessary since a dominant mode excitation in the stub guide produces anti-symmetric voltage excitation in the main guide, in contradiction to the assumed main guide excitation.) and Eq. (3.20) multiplied in a

scalar product fashion by $\underline{M}_{s.e.}$ and then integrated over the aperture region, the result is

$$V_1(2\,I_1) = -\,j \iint_{slot} \underline{M}_{s.e.} \cdot (\underset{\sim}{B}_L + \underset{\sim}{B}_s) \cdot \underline{M}_{s.e.}\, dS dS' \quad (3.23)$$

The variational expression for $1/Y_a$ results if both sides are divided by $(2I_1)^2$:

$$\frac{1}{2Y_a} = \frac{V_1}{2I_1} = j\, \frac{\iint_{slot} \underline{M}_{s.e.} \cdot (\underset{\sim}{B}_L + \underset{\sim}{B}_s) \cdot \underline{M}_{s.e.}\, dS dS'}{Y^2 \left[\iint_{slot} \underline{M}_{s.e.} \cdot \underline{h}^{(2)}\, dS\right]^2} \quad (3.24)$$

This result is also stationary about the correct value of the slot electric field.

For the case of symmetric magnetic field excitation, it may be shown that

$$2\,V_1 = \iint_{slot} \underline{M}_{s.h.} \cdot \underline{h}^{(1)}\, dS \quad (3.25)$$

where the subscript s.h. denotes symmetrical magnetic field excitation. The dominant mode voltage in the stub guide at the slot plane is always defined by

$$V_s = \iint_{slot} -\underline{M} \cdot \underline{h}_s\, dS \quad (3.26)$$

where the $\underline{n}$ now points into the main guide (out of the stub guide region). Consequently, if Eq. (3.21) is multiplied by $\underline{M}_{s.h.}$ in dot product fashion, where the $\underline{n}$ points into the stub guide, and the result is integrated over the slot region, the result when Eqs. (3.25) and (3.26) are used becomes:

$$2 V_1 I_1 - I_s V_s = j \iiiint_{\text{slot}} \underline{M}_{s.h.} \cdot (\underset{\sim}{B}_L + \underset{\sim}{B}_s) \cdot \underline{M}_{s.h.} \, dS dS' \qquad (3.27)$$

From the network of Fig. 3.6a it is seen that

$$\frac{V_1}{V_s/2} = n_c \qquad (3.28a)$$

Furthermore, it is evident from network considerations that

$$Y_a + 2 Y_b = \frac{I_1 - I_s/n_c}{V_1} \qquad (3.28b)$$

where the indicated current directions are given in Fig. 3.2 or in 3.6a. Thus, if Eq. (3.27) is divided by $(2V_1)^2$ and Eqs. (3.25), (3.28a) and (3.28b) are used, the variational expression for $(Y_a/2 + Y_b)$ is obtained i.e.,

$$\frac{Y_a}{2} + Y_b = \frac{j \iiiint_{\text{slot}} \underline{M}_{s.h.} \cdot (\underset{\sim}{B}_L + \underset{\sim}{B}_s) \cdot \underline{M}_{s.h.} \, dS dS'}{\left[\iint_{\text{slot}} \underline{M}_{s.h.} \cdot \underline{h}^{(1)} \, dS \right]^2} \qquad (3.29)$$

The variational expressions (3.12), (3.24), and (3.29) are employed in Sec. D for the calculation of the transverse slot susceptance B_t, and the longitudinal slot susceptances $1/B_a$ and $(B_a/2 + B_b)$, respectively. The transformer turns ratio n_c for the longitudinal slot may be computed from Eq. (3.28a). This expression, however, is not variational, that is, the value of n_c is not stationary about the correct electric field, even though it is seen that n_c is independent of the amplitude of the slot electric field. Using Eqs. (3.25) and (3.26), the expression for n_c becomes

$$n_c = \frac{\iint_{slot} \underline{M}_{s.h.} \cdot \underline{h}^{(1)} \, dS}{\iint_{slot} \underline{M}_{s.h.} \cdot \underline{h}_s \, dS} \qquad (3.30)$$

where $\underline{n}$ in both numerator and denominator points into the stub guide region.

C. Simplification of the Dyadic Spatial Susceptances (Green's Functions)

Once a slot field is chosen, the analytical problem becomes one of evaluating the necessary integrals, numerically or otherwise. The evaluation of the susceptances may be carried out by substituting the series representation of the spatial susceptances as given in Eq. (3.9) or (3.13c) into the variational integrals, integrating term by term and then summing the results of the integrals; or alternatively, by transforming these dyadic sums into some closed form so that the susceptance can be evaluated in closed form. Since the series which result from the former method are too slowly convergent to be of practical use the latter procedure is employed in this report.

The procedure, to be described in this section, of transforming the dyadic susceptances into a form suitable for calculations, may be summarized as follows. The spatial susceptances, which have been given in a mixed dyadic form, are first expressed as a dyadic operator acting on a double scalar sum of trigonometric functions. This sum separates naturally into a sum of (o,n), (1,n) and ($m \geq 2$,n) modes. The former two sums correspond to the kernels for already solved problems, and it is shown in Sec. D that results corresponding to them may be simply looked up in the Waveguide Handbook. The Poisson transformation permits the latter series, the (m,n), to be converted into a series of Bessel functions of the second kind of imaginary argument, which converges rapidly enough to be approximated by a single (rather than a double) infinite sum. This transformed kernel, when employed in the variational integrals, will again contribute an infinite series whose sum, however, can be readily approximated. It is also shown in this section that the singularity of the guide spatial admittance is equal to the free space spatial admittance, indicating that for approximate results the free space spatial admittance may be substituted for the guide expression.

The dyadic susceptance of Eq. (3.13c) can be rewritten as follows in a form which is more suitable for summation. The transverse E and H mode functions are expressed in terms of vector operators (see Report R-157-47, pp. 17, 18). The center of coordinates is illustrated in Fig. (3.7c).

$$\underline{h}_i' = \frac{-\underline{z}_o \times \nabla_t e_{iz}'}{k_{ci}'}, \quad \underline{h}_i'' = \frac{-\nabla_t h_{iz}''}{k_{ci}''}, \quad \underline{h}_{iz} = \underline{z}_o h_{iz} \qquad (3.31)$$

where

$$e_{iz}' = \frac{2}{\sqrt{ab}} \sin \frac{m\pi}{a} x \sin \frac{n\pi}{b} y$$

$$h_{iz}'' = \sqrt{\frac{2\,e_{nm}}{ab}} \cos \frac{m\pi}{a} x \cos \frac{n\pi}{b} y$$

$$k_{ci} = \sqrt{(\frac{m\pi}{a})^2 + (\frac{n\pi}{b})^2}$$

$$\nabla_t = \underline{x}_o \frac{\partial}{\partial x} + \underline{y}_o \frac{\partial}{\partial y}$$

Since the vector mode functions are seen to be expressed in terms of vector operators and scalars it is possible to separate out the vector operators by straightforward algebraic operations. The general dyadic spatial susceptance, can then be rewritten as:

$$\underline{\beta}_g = \frac{1}{ab\omega\mu} \operatorname{Im} \left\{ \left[-\nabla\nabla' + k^2 \underline{z}_o \underline{z}_o \right] \sum_{m=0}^{\infty} \sum_{n=-\infty}^{\infty} \cos \frac{m\pi}{a} x \frac{\cos \frac{m\pi}{a} x' \cos \frac{n\pi}{b} y \cos \frac{n\pi}{b} y' \exp \phi}{\sqrt{k^2 - k_{ci}^2}} \right.$$

$$\left. + k^2 \underline{x}_o \underline{x}_o \sum_{m=0}^{\infty} \sum_{n=-\infty}^{\infty} \frac{\sin \frac{m\pi x}{a} \sin \frac{m\pi x'}{a} \cos \frac{n\pi}{b} y \cos \frac{n\pi}{b} y' \exp \phi}{\sqrt{k^2 - k_{ci}^2}} \right.$$

$$+ k^2 Y_o Y_o \sum_{n=0}^{\infty}{}' \sum_{n=-\infty}^{\infty} \frac{\cos \frac{n\pi x}{a} \cos \frac{n\pi x'}{a} \sin \frac{n\pi y}{b} \sin \frac{n\pi y'}{b}}{\sqrt{k^2 - k_{ci}^2}} \exp \phi \Bigg\} \quad (3.32)$$

where $\phi = -j\sqrt{k^2 - k_{ci}^2}\ |z - z'|$

The series that must be summed are now purely scalar. In the above form they are seen to converge quite slowly when $|z-z'|$ is small. The Poisson transformation (Eq. (1) of the Appendix) can be applied to the (m,n) series, where $m=2, n \geq 0$, to obtain a more rapidly convergent expression. The Poisson transformation can be best applied to a series of functions which do not suffer a singularity over the closed interval of summation. In this connection, it is seen that if $m \geq 2$ and only the dominant mode propagates, i.e., $k^2-(m\pi/a)^2 < 1$, that for no real value of n, integral or otherwise, can.

$$\sqrt{k^2 - \left(\frac{m\pi}{a}\right)^2 - \left(\frac{n\pi}{b}\right)^2}$$

equal zero, that is, there will be no branch point of (n) along the real axis. A typical application of the transformation to the series of Eq. (3.32) is illustrated below in Eq. (3.33), where Z is equal to (z-z'), and Y is equal to (y-y') or (y+y'). The Fourier integral which must be evaluated is identical to the one of Eq. (7) of the Appendix.

$$\sum_{n=-\infty}^{\infty} \frac{\cos \frac{n\pi}{b} Y}{\sqrt{\left(\frac{n\pi}{b}\right)^2 - \alpha_m^2}} \exp \left[-\sqrt{\left(\frac{n\pi}{b}\right)^2 - \alpha_m^2}\ |Z|\right] = \frac{2b}{\pi} \sum_{\ell=-\infty}^{\infty} K_o \left[|\alpha_m| \sqrt{(Y+2\ell b)^2 + Z^2}\right] \quad (3.33)$$

where $\alpha_m^2 = k^2 - \left(\frac{m\pi}{a}\right)^2 < 0$, i.e. $m \geq 2$, and where K_o is a Bessel function of the second kind of imaginary argument. The virtue of this transformation is that $K_o(u)$ decreases exponentially for large argument so that it is possible to approximate quite accurately the infinite trignometric sum by a finite sum of Bessel functions. It will turn out that the major contribution to the susceptances in the variational integrals comes from

those terms whose argument may for some allowable values of Y and Z become zero. The only term for which this is true is $\ell = 0$.

Equation (3.34) is a representation of the dyadic component containing the $(m \geq 2, n)$ modes when $y=y'=b$. It is this component $\underset{\sim}{\mathcal{G}}^{L}_{mn}$ that is required for the calculation of the parameters of a slot in the top guide wall. The transverse dyadic susceptance $\underset{\sim}{\mathcal{G}}_t$ is twice the transverse component of the total dyadic susceptance considered at $z=z'=0$. Twice the value need be taken for the following reason. $\underset{\sim}{\mathcal{G}}_g$ is essentially the dyadic magnetic field response at any point (x,y,z) in the infinite waveguide due to a magnetic dipole located at (x',y',z'). When the waveguide is shorted at one end, thus creating a semi-infinite guide, an image term must be included. In particular when the shorting plane is at $z'=0$ and the magnetic current dipole is located on the plane the contribution of the image is equal to the initial contribution. Note that the images associated with the walls of the guide have already been included in the general representation. The $(m \geq 2, n)$ modal component $\underset{\sim}{\mathcal{G}}^{t}_{mn}$ of the transverse spatial susceptance is given in Eq. (3.35).

$$\underset{\sim}{\mathcal{G}}^{L}_{mn} = \frac{2}{ma\omega\mu}\left[-\nabla\nabla'+k^2\,\underline{x}_o\underline{x}_o\right]\sum_{m=2}^{\infty}\cos\frac{m\pi x}{a}\cos\frac{m\pi x'}{a}\,K_o\left[\varkappa_m|z-z'|\right]$$

$$+\,k^2\,\underline{x}_o\underline{x}_o\sum_{m=2}^{\infty}\sin\frac{m\pi x}{a}\sin\frac{m\pi x'}{a}\,K_o\left[\varkappa_m|z-z'|\right] \qquad (3.34)$$

where $\underset{\sim}{\mathcal{G}}_L = \underset{\sim}{\mathcal{G}}^{L}_{on} + \underset{\sim}{\mathcal{G}}^{L}_{ln} + \underset{\sim}{\mathcal{G}}^{L}_{mn}$

$$\underset{\sim}{\mathcal{G}}^{t}_{mn} = 2\,\underset{\sim}{\mathcal{G}}_{mn}\Big|_{z=z'=0}, \text{ where } \underset{\sim}{\mathcal{G}}_t = \underset{\sim}{\mathcal{G}}^{t}_{on} + \underset{\sim}{\mathcal{G}}^{t}_{ln} + \underset{\sim}{\mathcal{G}}^{t}_{mn}.$$

$$= \frac{2}{ma\omega\mu}\left\{-\nabla_t\nabla_{t'}\sum_{m=2}^{\infty}\cos\frac{m\pi x}{a}\cos\frac{m\pi x'}{a}\left[K_o(\varkappa_m|y-y'|)+K_o(\varkappa_m|y+y'|)\right]\right.$$

$$+ k^2 \underline{x}_o \underline{x}_o \sum_{m=2}^{\infty} \sin \frac{m\pi x}{a} \sin \frac{m\pi x'}{a} \left[K_o(\alpha_m |y-y'|) + K_o(\alpha_m |y+y'|) \right]$$

$$+ k^2 \underline{y}_o \underline{y}_o \sum_{m=2}^{\infty} \cos \frac{m\pi x}{a} \cos \frac{m\pi x'}{a} \left[K_o(\alpha_m |y-y'|) - K_o(\alpha_m |y+y'|) \right] \Bigg\} \quad (3.35)$$

The most significant terms, are the ones of argument $|y-y'|$ since the Bessel function diverges along the line $y=y'$. The other argument is zero only at the point $y=y'=0$.

Since the Poisson transformation finds its best application with the $(m \geq 2, n)$ modes the separation from the general form of the component of the dyadic which includes these modes follows naturally. The remaining dyadic component may be again separated into (o,n) and $(1,n)$ modes. Thus:

$$\underset{\sim}{\mathcal{G}} = \underset{\sim}{\mathcal{G}}_{on} + \underset{\sim}{\mathcal{G}}_{1n} + \sum_{m \geq 2} \underset{\sim}{\mathcal{G}}_{mn} \quad (3.36)$$

The important additional virtue of this separation is that with the field choices used the contribution to the susceptance parameters of the first term is zero, while that of the second term is just the susceptance of the wide open capacitive iris. Therefore, calculations involving these terms can be avoided since the parameters of the wide open capacitive iris are already available. The contribution of the $(m \geq 2, n)$ modes is then a correction to the well known "unperturbed" results. The calculation of this correction term is the major consideration of this part of the report.

The singularity of the spatial admittance occurs at $x=x'$, $y=y'$, $z=z'$, i.e., in the neighborhood of the magnetic current dipole, the magnetic field becomes infinite. In the vicinity of the singularity the spatial dyadic admittance (which includes the dominant mode term) approaches:

$$j\,(-\nabla\nabla' + k^2\underset{\sim}{\epsilon})\,\frac{1}{\pi a\omega\mu}\sum_{-\infty}^{\infty}\cos\frac{n\pi}{a}(x-x')K_0\left[\kappa_n\sqrt{(y-y')^2+(z-z')^2}\right] \tag{3.37}$$

But this sum converges and diverges together with the integral

$$(-\nabla\nabla' + k^2\underset{\sim}{\epsilon})\,\frac{1}{\pi^2\omega\mu}\int_{-\infty}^{\infty}\cos\left[(x-x')t\right]K_0\left[\sqrt{t^2-k^2}\,\sqrt{(y-y')^2+(z-z')^2}\right]dt \tag{3.38}$$

But from Eq. (8) of the Appendix this is seen to be

$$\frac{1}{4\pi\omega\mu}\,(-\nabla\nabla' + k^2\underset{\sim}{\epsilon})\quad\frac{e^{-jk\sqrt{(x-x')^2+(y-y')^2+(z-z')^2}}}{\sqrt{(x-x')^2+(y-y')^2+(z-z')^2}} \tag{3.39}$$

Thus the guide spatial admittance behaves like the free space admittance in the vicinity of x',y',z'. The ambiguity concerning the sign of the exponential may be simply resolved by noting that the resistive term of the spatial admittance must be positive. This is obtained if the exponential is $-j$. The guide spatial susceptances as used in the variational calculations will have a singularity equal to twice the imaginary part of the above result since the image contributions at any of the metal walls will contribute a like amount. Thus

$$\underset{\sim}{\beta}_L \to \underset{\sim}{\beta}_t \to \frac{1}{2\pi\omega\mu}\,(-\nabla\nabla' + k^2\,\underset{\sim}{\epsilon})\,\frac{\cos k\,|r-r'|}{|r-r'|} \tag{3.40}$$

where for the former $y=y'=b$, and for the latter $z=z'=0$.

This treatment is a mathematical justification of the frequent approximation of the guide dyadic spatial susceptance by the half space spatial susceptance.

D. Evaluation of the Circuit Parameters

1. The Trial Fields

It is now possible to evaluate the equivalent circuit parameters of the slots discussed in the previous sections in a relatively straightforward manner, wherein the results are expressed as corrections to the formulae for wide open capacitive irises. Before proceeding with the integration of the variational expressions, a choice must be made for the electric field descriptive of the slot excitation. This choice is somewhat facilitated by certain restraints which the expression for the true field must satisfy, such as: a) When $a'/a = 1$, the field should reduce to that of the wide open capacitive iris, and for the transverse slot when $b'/b = 1$, it should reduce to that for the wide open inductive slot. b) At the slot boundary, the electric field must be purely normal to the edge and be infinite (for a zero thickness slot). c) The slot electric field should be proportional in some way to the magnetic field $\underline{H}_0$ that would be present in the neighborhood of the slot (unperturbed magnetic field) if the slot was covered.

The problem of determining the slot field for the case where the unperturbed magnetic field has some cosine variation over the aperture, and is in the ξ direction indicated in Figure 3.8,

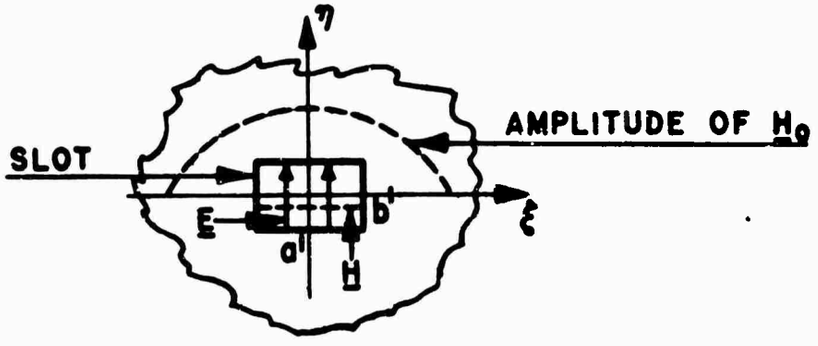

Figure 3.8

is almost similar to that of determining the slot field in the wide open capacitive or inductive irises since the unperturbed magnetic field, as well as the geometry, is similar. The choice of electric field is decided to a large extent by the relative dimensions of b' and a'. In contrast to Sec. C, from now on all functions will be referred to a center of coordinates at the mid-point of the slot. When $a' >> b'$ the slot electric field is chosen to be

$$\underline{E}_{slot} \propto \underline{\eta}_0 \frac{\cos \frac{\pi \xi}{a'}}{\sqrt{\left(\frac{b'}{2}\right)^2 - \eta^2}} \tag{3.41}$$

which for $a' = a$ reduces to the static electric field excited in a wide open capacitive slot. When $b' \gg a'$, the electric field is assumed to be identical to the static one excited in an inductive iris, i.e.,

$$\underline{E}_{slot} \propto \underline{\eta}_0 \sqrt{\sin^2 \frac{\pi}{2} \frac{a'}{a} - \sin^2 \frac{\pi \xi}{2a}} \tag{3.42}$$

Note that the condition of an infinity at the edge has not been satisfied. This is permissible since the singularity is integrable and of not too much consequence.

The true field will certainly have more than one component, but it is expected that for most cases the slot fields will be essentially unidirectional, so that the above fields are sufficiently close to them to permit the variational principle to hold. In some of the calculations it was expedient to use (3.42) instead of (3.41) since the integrals could be more readily evaluated, even though it may have been somewhat more correct to use the latter.

For the excitations for which the unperturbed magnetic field is not almost entirely unidirectional, such as in the case of the slot-coupled E plane Tee when the main guide is excited by a symmetrical electric field, the induced slot field is not expected to be unidirectional either. The difference between the induced fields generated as a result of this latter excitation and the one which is caused by the excitation discussed

in the previous paragraph is best illustrated by the rigorous results obtained for a small circular slot on the top of a guide (see Report R-157-47, p. 68). The bicomponent field of Eq. (24) of that report is the electric field produced by symmetrical E excitation; and the single component field of Eq. (19) is the electric field produced by symmetrical H excitation.

It can be shown that the field in the small E plane slot generated by a symmetrical dominant mode electric field must be expressed as a gradient field, i.e.,

$$\underline{E} \propto - \nabla_t \phi \tag{3.43}$$

where ϕ is a function which vanishes on the rim. For the slot of Fig. 3.9(a), excited as shown in Fig. 3.9(b), the scalar function ϕ is

$$\phi = \sqrt{\left(\frac{b'}{2}\right)^2 - z^2} \cos \frac{\pi x}{a'} \tag{3.44}$$

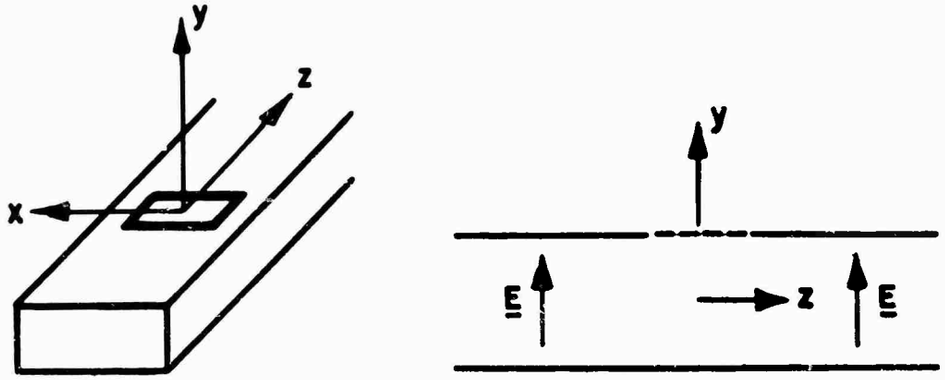

(a) (b)

Fig. 3.9

The reason for the gradient field may be seen from the following. The susceptance B_a is obtained by summing the contributions from the H modes and the E modes. For small slots, the H mode contribution would tend to predominate, resulting in this case in a capacitive susceptance. However, from a rigorous analysis of small elliptical E plane apertures it is known that B_a must be inductive. Thus, the choice of a trial field must be such that it vanishes when integrated with the H mode terms.

A typical H mode dyadic term (from Eq. (3.32)) is

$$\nabla \nabla' f(x,z)\, f(x',z')$$

The vector function $\underline{M}$ which satisfies the condition

$$\iint \underline{M} \cdot \nabla f(x,z)\, dS = 0$$

is the one which must be chosen for the variational expression. Now,

$$\iint \underline{M} \cdot \nabla f(x,z)\, dS = \iint \nabla \cdot \left[\underline{M} f(x,z) \right] dS - \iint f(x,z)\, \nabla \cdot \underline{M}\, dS$$

and since

$$\iint_{\nabla} \cdot \left[\underline{M} f(x,z) \right] dS = \oint \underline{M}\, f(x,z) \cdot \underline{n}\, d\ell$$

it is evident that $\underline{M}$ must satisfy the conditions:

$$\left.\begin{aligned} &\underline{M} \cdot \underline{n} = 0 \quad \text{on } \ell, \text{ the slot periphery} \\ &\nabla \cdot \underline{M} = 0 \end{aligned}\right\} \qquad (3.45)$$

But the condition $\nabla \cdot \underline{M} = 0$ can be satisfied by $\underline{M} = \nabla \times (\underline{z}_0 \phi)$. Lastly, since $\underline{M} = \underline{z}_0 \times \underline{E}$, we have Eq. (3.43), namely $\underline{E} = -\nabla\phi$. The condition $\underline{M} \cdot \underline{n} = 0$ on the periphery is satisfied by choosing ϕ along the periphery slot to be constant (in particular zero), which is equivalent to saying that the tangential components of the electric field at the slot edge are zero.

When the slot is not small, the field has two components whose functional dependence on the slot variables is the same as that for the small slot, but whose relative amplitudes are now different. The relative amplitudes can be determined by the application of the Rayleigh-Ritz procedure given in the Appendix, with the result that if the field $\underline{E}$ can be written as $\underline{E} = \underline{E}_1 + c\,\underline{E}_2$, the value of c is

$$c = \frac{\pi}{a'} \left[1 - \left(\frac{a'}{a}\right)^2 \right]$$

and the resultant slot electric field becomes

$$\underline{E} \propto \underline{x}_0 \left(\frac{\pi}{a'}\right)\left[1-\left(\frac{a'}{a}\right)^2\right]\sqrt{\left(\frac{b'}{2}\right)^2 - z^2} \quad \sin \frac{\pi x}{a'} + \underline{z}_0 \frac{z \cos \frac{\pi x}{a'}}{\sqrt{\left(\frac{b'}{2}\right) - z^2}} \tag{3.46}$$

It is seen that for long thin slots, i.e. a'/a near unity, the field becomes unidirectional. As pointed out previously, the absolute amplitude of $\underline{E}$ is unimportant to the variational calculations, and only the relative amplitudes are of significance.

2. The Transverse Slot

The field choices for centered slots have been of the form

$$\underline{E} = \underline{y}_0 E_1(x) E_2(y)$$

For slot dimensions within the range $b'/b < 0.5$ and $a'/a > 0.5$, the field choice is

$$\underline{E} \propto \underline{y}_0 \frac{\cos \frac{\pi}{a'} x}{\sqrt{1 - (\frac{2y}{b'})^2}} \tag{3.47}$$

while for the remaining range

$$\underline{E} \propto \underline{y}_0 \sqrt{\sin^2 \frac{\pi}{2} \frac{a'}{a} - \sin^2 \frac{\pi x}{a}} \tag{3.48}$$

The geometry is indicated in Fig. 3.10.

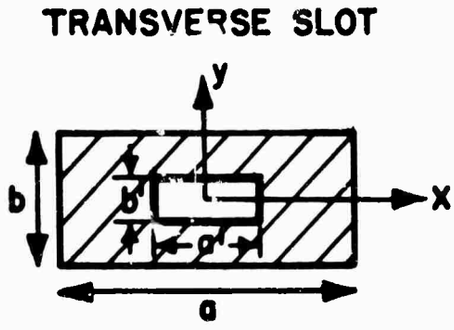

Figure 3.10

As has been noted the latter field does not satisfy the condition of becoming infinite at an edge, but since the singularity is integrable, the result is not sensitive to this condition.

Since the trial fields are unidirectional, and in this case $\underline{x}_0 \times \underline{E}$ is in the $\underline{x}_0$ direction, only the $\underline{x}_0 \underline{x}_0$ component of the dyadic admittance is retained, and $\mathcal{B}_{on}^{t}$ is therefore dropped from consideration. Since the fields are symmetric about the axes passing thru the center of the slots, they are orthogonal to all antisymmetric modes, i.e. (m,n) modes in which m is even, n odd.

The variational expression (3.12) for the susceptance, after

breaking up the dyadic susceptance according to Eq. (3.36), then becomes:

$$\frac{B_t}{2} = \frac{\iiint \underline{E}(x,y)\underline{E}(x',y')\underline{\underline{B}}_{in}^{t}\, dS dS'}{V^2} + \frac{2}{\pi a \mu} \frac{\int dx \int dx' \int dy \int dy' \left\{ \underline{E}(x,y)\underline{E}(x',y') \sum \right\}}{V^2} \tag{3.49}$$

where $$\sum = \sum_{m=3}^{\infty} \left[k^2 - \left(\frac{m\pi}{a}\right)^2 \right] \cos \frac{m\pi x}{a} \cos \frac{m\pi x'}{a} \left[K_0(\gamma_m |y-y'|) + 2\, K_0(\gamma_m |b-(y+y')|) \right]$$

where the first term may be written as

$$\frac{4\pi e^2}{ab\mu} \frac{\iint E_1(x)\, E_1(x') \cos \frac{\pi x}{a} \cos \frac{\pi x'}{a}\, dx\, dx'}{\left[\int E_1(x) \cos \frac{\pi x}{a}\, dx \int E_2(y) \sqrt{\frac{2}{ab}}\, dy \right]^2} \tag{3.50}$$

$$\times \iint E_2(y) E_2(y') \sum_{n=1}^{\infty} \frac{\cos \frac{n\pi y}{b} \cos \frac{n\pi y'}{b}}{\sqrt{\left(\frac{n\pi}{b}\right)^2 - \gamma^2}}\, dy\, dy'$$

where as always $\gamma_e^2 = k^2 - \left(\frac{\pi}{a}\right)^2$, and the limits go from $-a'/2$ to $a'/2$, and $-b'/2$ to $b'/2$. Note that in Eq. (3.50) the integral over (x,x') is independent of the integral over (y,y') and cancels the squared integral in x in the denominator. If $\underline{E}$ of Eq. (3.47) is chosen for the trial field, so that the $E_2(y)$ is then correct to a first order for the wide open capacitive slot field, this term is equal to half the susceptance of a capacitive iris. By assuming the small argument approximation for $K_0(\gamma_m |y-y'|)$ (see Eq. (4b) of the Appendix), valid since b'/b for this field assumption is less than 0.5, and neglecting all other terms by comparison, the correction to the capacitive result, i.e. the second term of Eq. (3.49), for this field choice is:

$$\frac{1}{2} B_{corr} = \frac{2b}{\lambda_g} Y_o \left(\frac{\lambda_g}{\lambda_{g3}}\right)^2 \left(\frac{\cos \frac{3\pi}{2}\alpha}{\cos \frac{\pi}{2}\alpha} \cdot \frac{1-\alpha^2}{1-9\alpha^2}\right)^2$$

$$\left\{\left[1 + \left(\frac{\pi}{2}\frac{b'}{\lambda_{g3}}\right)^2\right] \log \frac{4}{\gamma\pi}\left(\frac{\lambda_{g3}}{b}\right) + \left(\frac{\pi}{2}\frac{b'}{\lambda_{g3}}\right)^2\right\} \qquad (3.51)$$

where λ_{g3} is the absolute value of the guide wavelength for the third (m=3, n=0) mode, $\alpha = a'/a$, $\gamma = 1.781$, and $Y_o = \sigma\ell/\omega\mu$. This result has been obtained by assuming that the variation in the x direction of the slot field, for slots for which $a'/a > 0.5$, is adequately described by the m=1 and m=3 modes. In other words, the stored energy is contained in the (1,n) and (3,n) modes for the most part.

When $a'/a < 0.5$ it is necessary to consider the contribution of the other higher modes. It is better in this range, as well as for $a'/a > 0.5$ and $b'/b > 0.5$, to make the field choice of Eq. (3.48). The resultant sum over m, after integration in the variational expression, can be conveniently summed. The integral which results upon the insertion of the inductive type trial field of Eq. (3.48) into Eq. (3.49) may be evaluated quite accurately by extending the integrals in y over an infinite region and then expanding the integrand of the remainder integral in asymptotic form See Eq. (5) of the Appendix). The susceptance is obtained in terms of a correction to the susceptances of both a capacitive and an inductive iris, i.e.,

$$\frac{B_t}{Y_o} = \frac{1}{\beta}\frac{B_L}{Y_o} + \frac{B_c}{Y_o} + \frac{1}{\beta^2} T(\alpha) - \frac{1}{\beta^2} L(\beta) \cos^4 \frac{\pi}{2}\alpha \qquad (3.52a)$$

B_L/Y_o is the relative susceptance of an aperture of width $\alpha = a'/a$ and height $\beta = b'/b = 1$, and B_c/Y_o is a capacitive correction. Specifically,

$$B_L/Y_0 = -\frac{\lambda_g}{a}\left[1-\frac{3}{4}\left(1-\sqrt{1-\left(\frac{2a}{3\lambda}\right)^2}\right)\sin^2\pi\alpha\right]\cot^2\frac{\pi}{2}\alpha \qquad (3.52b)$$

$$B_0/Y_0 = \frac{4b}{\lambda_g}\left(\frac{p}{\beta}\right)^2\left[\log\frac{0.715}{p} + 0.26\,p^2 + \left(\frac{b}{\lambda_g}\right)^2\sin^2\pi p\right] \qquad (3.52c)$$

$$T(\alpha) = \frac{2}{\pi^3}\frac{\lambda_g}{b}\left[\frac{\sin\pi\alpha - \pi\alpha\cos\pi\alpha}{\sin^4\frac{\pi}{2}\alpha} - \pi\right] \qquad (3.52d)$$

$$L(\beta) = \frac{6}{\pi}\frac{\lambda_g}{a}\sqrt{1-\left(\frac{2a}{3\lambda}\right)^2}\left[\beta K_1(\gamma_3 b') + (1-\beta) K_1(\gamma_3|b-b'|)\right. \qquad (3.52e)$$

$$\left. -\frac{\pi}{\sqrt{2}}\beta\,\mathrm{Erf}_c(\sqrt{\gamma_3 b'}) - (1-\beta)\frac{\pi}{\sqrt{2}}\,\mathrm{Erf}_c(\sqrt{\gamma_3(b-b')})\right]$$

where

$$\mathrm{Erf}_0(x) = \frac{2}{\sqrt{\pi}}\int_x^\infty e^{-t^2}\,dt = 1 - \mathrm{Erf}(x).$$

and

$$p = \frac{1}{2} - \left|\frac{1}{2} - \beta\right|$$

The capacitive correction B_c/Y_0 is obtained from the term of Eq. (3.50), but is not the Waveguide Handbook result for a capacitive slot since the field choice is only very approximately the true capacitive field. However, for values of a'/a approaching unity the value of B_t/Y_0 must approach that for a wide open capacitive iris, while for smaller a'/a values the term B_c/Y_0 becomes relatively unimportant, and the term $(1/\beta)\,B_L/Y_0$ becomes dominant. For these reasons, it is appropriate to replace the B_c/Y_0 of Eq. (3.52c) by the Waveguide Handbook result for a capacitive iris for application in Eq. (3.52a). The above results are valid when $\beta > [1/3\pi\ a/b] \approx .2$ since the asymptotic expansion of $K_0(\gamma_3 b')$ is not valid for smaller values. When $\beta > 0.9$ the correction terms other than B_c/Y_0 may be

neglected. The contribution of $L(\beta)$ is always less than 20 percent and usually less than 10 percent, so that for rough calculations a much simplified expression can be used.

3. The Slot-Coupled E Plane Tee

a.) Expression for $(B_b + B_a/2)$

From energy considerations alone it may be seen that the susceptance of a transverse aperature is closely related to $B_b + B_a/2$ of a longitudinal slot. It has been shown that the susceptance of any reactive circuit component is equal to the rate of change of stored energy divided by the square of the voltage. In the case of the slot apertures the stored energy depends upon the slot electric field and the surrounding boundaries. When an E plane slot is excited by a symmetric current source the slot field induced is very similar to the field induced in the transverse slot. This is true at least for slots whose dimension parallel to the long dimension of the guide cross-section is not too small. The boundary of the region surrounding the slot in both cases is also seen to be fairly similar, the major difference being that in the case of the transverse slot there is the metal boundary of the upper and lower walls of the guide while in the case of the longitudinal slot there is no equivalent boundary, but rather a guide which extends to infinity in both directions. The stored energy of the lower order modes is more affected by the difference in the boundary conditions than is the stored energy of the higher order modes. Thus it is expected that the higher mode correction to the wide open slot susceptance for $B_b + B_a/2$ will be almost identical for the two cases. The major difference in the susceptances should be accounted for by the difference in the susceptance of the wide open slots, where (1, n) modes alone are excited. The mathematical justification of this can be seen by comparing the higher mode components of the transverse and longitudinal spatial susceptances. In the former case, terms involving $K_o\left[b - |y + y'|\right]$, which accounts for the images due to the top and bottom wall, appear as well as $K_o\left[|y - y'|\right]$. In the latter case, only terms involving $K_o\left[|z - z'|\right]$ occur. It is recognized that the $K_o\left[|y - y'|\right]$ in general results in a contribution which is greater than the contribution of $K_o\left[b - |y + y'|\right]$, so that if terms involving the latter expression were neglected the higher mode stored energy of the longitudinal slot would be equal to the higher mode stored energy of the transverse slot provided the slot field choice was the same. The (x, z) coordinates of the longitudinal E plane slot correspond to the (x, y) coordinates of the transverse slot.

For the range of aperture sizes $a'/a > 0.5$, $b'/b < 0.5$, the results of the transverse slot were obtained by justifiably neglecting the image terms of the upper and lower walls. The correction term to the wide open slot result is given in Equation (3.51).

When the E plane slot is excited by a symmetric current source, the unperturbed magnetic field in the vicinity of the aperture is

$$\underline{H}_o = I\,\underline{h}^{(1)} = I\,(\underline{h}\cos\beta z + j\,Y_g\,\underline{h}_z\,Z_o\sin\beta z)$$

$$\simeq I\,\underline{h}\cos\beta z = \underline{x}_o\,I\sqrt{\frac{2}{a\,b}}\cos\frac{\pi x}{a}\cos\beta z \qquad (3.53)$$

The induced electric field is in space quadrature with the inducing magnetic field and should satisfy the same conditions as did the transverse slot which was similarly excited. Note that in order to satisfy Maxwell's equations and the boundary conditions a bicomponent field must be excited, but for this range of aperture sizes it is assumed that by far the major contribution to the variational result comes from a single component, namely,

$$\underline{E} \propto \underline{z}_o\,\frac{\cos\frac{\pi x}{a'}}{\sqrt{(\frac{b'}{2})^2 - z^2}} \qquad (3.54)$$

which is the same field as that chosen for the transverse slot. From Equation (3.29)

$$B_b + \frac{B_a}{2} = \frac{\iiiint \underline{M}\cdot\{\underline{B}^L_{1n}+\underline{B}^L_{mn}\}\cdot\underline{M}\;dS\;dS'}{(\iint \underline{M}\cdot\underline{h}^{(1)}\,dS)^2} + \frac{\iiiint \underline{M}\cdot\{\underline{B}^t_{1n}+\underline{B}^t_{mn}\}\cdot M\;dS\;dS'}{(\iint \underline{M}\cdot\underline{h}^{(1)}\,dS)^2} \qquad (3.55)$$

where $\underline{B}_L = \underline{B}^L_{1n} + \underline{B}^L_{mn}$, and $\underline{B}_t = \underline{B}^t_{1n} + \underline{B}^t_{mn}$

The first term is the ratio of the rate of change of stored energy in the main guide to the dominant mode voltage across the slot at the center line, and the second term is the ratio of the rate of change of stored energy on the stub guide side of the slot (when the slot is radiating the radiation power is included in this term) to the same voltage. Since it has been stated that the contribution from both (m, n) terms are the same, it is possible to add them together to be just twice the higher mode contribution of the second term. The denominator, the square of the voltage, differs from the voltage across a transverse slot because of the factor ($\cos\beta z$).

If the substitution (see Equations(3.28a) and (3.30))

$$n_c = \frac{\iint \underline{M} \cdot \underline{h}^{(1)} \, dS}{\iint \underline{M} \cdot \underline{h} \, dS} = \frac{(2V)}{(V_t)} \tag{3.56}$$

is made, it is possible to obtain the expression given above relative to the characteristic admittance of the main guide. Thus

$$n_c^2 \left(\frac{B_b}{Y_o} + \frac{B_a}{2Y_o}\right) = \frac{\iiiint \underline{M} \cdot \left\{\underline{E}^L_{in} + \underline{E}^t_{in}\right\} \cdot \underline{M} \, dS \, dS'}{Y_o (V_t)^2} + \frac{B^t_{corr.}}{Y_o} \tag{3.57}$$

where $B^t_{corr.}/Y_o$ is given in Equation (3.51) for a slot located transversely in a guide of the same dimensions as the main guide. The first term on the right hand side of Equation (3.57) is the normalized susceptance $(B_b/Y_o + B_a/2Y_o)$ when $a'/a = 1$, and can be found in the Waveguide Handbook. Since

$$B_t = (B_t)_{\frac{a'}{a}=1} + B^t_{corr.}$$

and

$$n_c^2 \left(\frac{B_b}{Y_o} + \frac{B_a}{2Y_o}\right) = \left(\frac{B_b}{Y_o} + \frac{B_a}{2Y_o}\right)_{\frac{a'}{a}=1} + \frac{B^t_{corr.}}{Y_o} \tag{3.58}$$

it is possible to express the result as a correction to the transverse slot result, i.e.,

$$n_c^2 \left(\frac{B_b}{Y_o} + \frac{B_a}{2Y_o}\right) = \frac{B_t}{Y_o} + \left\{\left(\frac{B_b}{Y_o} + \frac{B_a}{2Y_o}\right) - \frac{B_t}{Y_o}\right\}_{\frac{a'}{a}=1}. \tag{3.59a}$$

For the field choice indicated in Equation (3.54)

$$n_c^2 = J_o^2 \left(\frac{\alpha b'}{2}\right) . \tag{3.59b}$$

When the E plane slot dimensions are in the range $a'/a < 0.5$, all b'; and $a'/a > 0.5$, $b'/b > 0.5$, the slot electric field induced by symmetric current excitation is chosen to be

$$\underline{E} = \underline{z}_0 \sqrt{\sin^2 \frac{\pi a'}{2a} - \sin^2 \frac{\pi x}{a}} \tag{3.60}$$

which is the same field, except that now the direction is appropriate to a slot on top of a guide, that was chosen for the transverse slot of the same dimensions. For this slot range, there are two slight modifications of the previous results indicated in Equation (3.59a). One involves taking into account the lack of the top and bottom wall image terms in the main guide spatial susceptance, and the other is to directly calculate the wide open slot result for this field choice. The higher mode component of the longitudinal dyadic susceptance can be written as

$$\underset{\sim}{B}^L_{mn} = \underset{\sim}{B}^t_{mn} - \underset{\sim}{B}_I \tag{3.61}$$

where $\underset{\sim}{B}_I$ indicates the image correction. It is necessary only to calculate separately at this point the contribution of the image correction and subtract it from the result of Equation (3.59a). Thus

$$n_c^2 \left(\frac{B_b}{Y_0} + \frac{B_a}{2Y_0}\right) = \frac{B_t}{Y_0} + \left(\frac{B_b}{Y_0} + \frac{B_a}{2Y_0} - \frac{B_t}{Y_0}\right)_{\frac{a'}{a}=1} - \frac{1}{Y_0} \frac{\iiiint \underline{M}^* \cdot \underset{\sim}{B}_I \cdot \underline{M} \, dS \, dS'}{V_t^2} \tag{3.62}$$

B_t/Y_0 is given in Equation (3.52). With the field choice of Equation (3.60),

$$\left(\frac{B_b}{Y_0} + \frac{B_a}{2Y_0}\right)_{\frac{a'}{a}=1} = \frac{2b}{\lambda_g}\left[\ell_n \frac{1.43b}{b'} + \frac{1}{2}\left(\frac{2b}{\lambda_g}\right)^2\right] + \frac{1}{2}\left(\frac{B_t}{Y_0}\right)_{\frac{a'}{a}=1} \tag{3.63}$$

Note that this expression in this form indicates the separate contributions of the main guide and the stub guide energies to the wide open slot susceptance. The last term of Equation (3.62) has been calculated and is equal to

$$\frac{1}{2}\left(\frac{b}{b'}\right)^2 \cos^4 \frac{\pi}{2}\frac{a'}{a}\left\{L\left(\frac{b'}{b}\right) - \frac{6}{\pi}\frac{\lambda}{a}\sqrt{1-\left(\frac{2a}{3\lambda}\right)^2}\,\frac{b'}{b}\left[K_1(\alpha_3 b') - \frac{\pi}{\sqrt{2}}\mathbf{H}_1(\sqrt{\alpha_3 b'})\right]\right\} \tag{3.64}$$

where $L(b'/b)$ is defined in Equation (3.52e). For this field choice, n_c is changed to

$$n_c^2 = \frac{\sin^2\left(\frac{\alpha b'}{2}\right)}{\left(\frac{\alpha b'}{2}\right)^2} \tag{3.65}$$

These results have been obtained on the basis that

$$(b - b')\,K_1(\alpha_3\,|b - b'|) << 1/\alpha_3$$

which is true if $|b - b'|$ is not too close to zero, so that the results of Equation (3.64) are strictly valid only when $b'/b < 0.9$. For $b'/b > 0.9$,

$$n_c^2\left(\frac{B_b}{Y_o} + \frac{B_a}{2Y_o}\right) = \frac{b}{b'}\frac{B_L}{Y_o} + \left\{\frac{B_b}{Y_o} + \frac{B_a}{2Y_o} - \frac{B_t}{Y_o}\right\}_{\frac{a'}{a}\approx 1} \tag{3.66}$$

where B_L is the susceptance of a transverse inductive slot of width a'; and where the latter term of the above expression may be obtained from data in the Waveguide Handbook.

b.) The Shunt Element, B_a.

The susceptance B_a is obtained by using the bicomponent field of Equation (3.46) in the variational expression Equation (3.24). The dyadic spatial admittance of each guide has been approximated by the "quasi-static" half space spatial admittance in the aperture $y = y' = b$, i.e.,

$$\underset{\sim}{B}_L + \underset{\sim}{B}_t \cong \frac{1}{\text{mesh}} \left[-\nabla\nabla' + k^2 \underset{\sim}{\zeta} \right] \frac{1}{\sqrt{(x - x')^2 + (z - z')^2}} \qquad (3.67)$$

The justification for this approximation is as follows. The guide spatial susceptance may be represented rigorously by the half space susceptance plus a constant plus a power series in r and r^n where r^n contains terms of the form $(x + x')$, $(z + z')$. Since the slot field for this case is anti-symmetrical within the slot, all even power terms cancel in the integrations. The contribution from the constant correction term therefore vanishes and it turns out that the major contribution is just from the static term. As seen, the cosine factor of Equation (3.40) is made unity in Equation (3.67). This is strictly valid only for small slots, but it turns out that the result for the susceptance using (3.67) differs little from that obtained when the cosine term is included. When the integrations are carried out, the following expression represents the major portion of the result:

$$\frac{B_a}{Y_o} = -\frac{b}{\lambda_g} \left(\frac{b'}{b}\right)^2 J_o^2\left(\frac{\pi b'}{2}\right)\left(\frac{a'}{a}\right) \left\{ \frac{\cos \frac{\pi}{2} \frac{a'}{a}}{1 - \left(\frac{a'}{a}\right)^2} \right\}^2 \left\{ 1 + \left(\frac{\lambda_g}{2a}\right)^2 \left[1 - \left(\frac{a'}{a}\right)^2 \right] \right\} \qquad (3.68)$$

c.) Main Guide and Stub Guide of Different Cross-section

The change in cross-section, i.e., when the stub guide dimensions are different from those of the main guide, does not introduce any new difficulties. The parameter $(B_b + B_a/2)$ is determined from the rate of change of higher mode stored energies in the two guides due to a given field in the slot when this field is induced by a symmetric current excitation. If the field induced in the slot is independent of the stub guide (an assumption which is reasonable as long as results are obtained variationally), the rate of change of stored energy in the main guide is also independent of the stub geometry. The rate of change of energy stored in the stub guide may be obtained directly from transverse slot considerations, since the longitudinal slot, relative to the stub guide, is a transverse discontinuity.

The susceptance parameters, for symmetric magnetic field excitation, relative to the main guide characteristic admittance, for a change in cross-section, are

$$j\left(\frac{B_b}{Y_o} + \frac{B_a}{2Y_o}\right) = \frac{P_L}{Y_o(2V)^2} + \frac{P_s}{Y_o(2V)^2} \tag{3.69}$$

where P_L is the rate of change of stored energy in the main guide, and P_s is the rate of change of stored energy in the stub guide. This equation is the symbolic equivalent of Equation (3.29). The susceptance of a transverse slot located in a guide of the dimensions of the stub guide is

$$\frac{B_t}{Y_{os}} = \frac{2P_s}{V_s^2}\,\frac{1}{Y_{os}} \tag{3.70}$$

and is known. V_s is the dominant mode voltage excited in the stub guide by the aperture field. Thus Equation (3.69) can be written as

$$j\left(\frac{B_b}{Y_o} + \frac{B_a}{2Y_o}\right) = \frac{P_L}{Y_o(2V)^2} + \frac{P_s}{Y_{os}V_s^2}\left(\frac{Y_{os}}{Y_o}\right)\left(\frac{V_s}{2V}\right)^2$$

$$j\left(\frac{B_b}{Y_o} + \frac{B_a}{2Y_o}\right) = j\frac{B_\ell}{Y_o} + j\frac{B_a}{2Y_o} + j\frac{1}{2}\frac{B_t}{Y_{os}}\left(\frac{Y_{os}}{Y_o}\right)\frac{1}{n_{cs}^2} \tag{3.71}$$

where the turns ratio $n_{cs} = 2V/V_s$, B_t/Y_{os} is the susceptance of a transverse slot located in the stub guide, and B_ℓ is the contribution of the main guide to the series element, as indicated in Figure 3.11. The figure expresses the four terminal equivalent circuit obtained by symmetrical main guide magnetic field excitation in terms of the notation of Equation (3.71). If the B_a/Y_o terms are dropped from Equation (3.71), it can be rewritten as:

$$\frac{B_b}{Y_o} = \frac{B_\ell}{Y_o} + \frac{B_t}{2Y_{os}}\left(\frac{Y_{os}}{Y_o}\right)\frac{1}{n_{cs}^2} \tag{3.72}$$

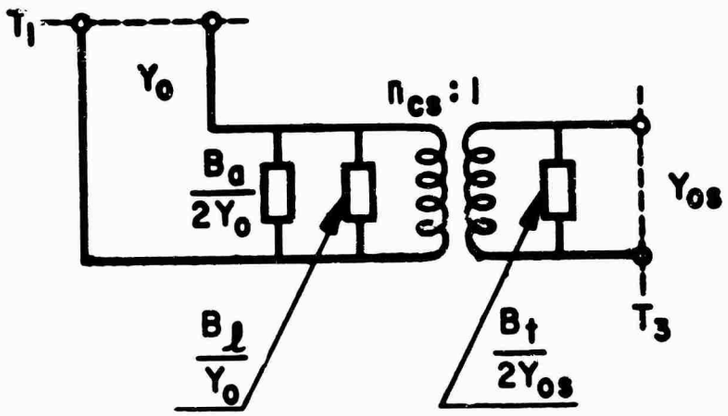

Figure 3.11

The susceptance element B_ℓ is determined from the rate of change of stored energy in the main guide alone, and is to a first order independent of the change in stub guide dimensions, since it is assumed that the form of the slot field remains unchanged. Thus, B_ℓ/Y_o may be obtained simply by subtracting the stub guide susceptance contribution from B_b/Y_o according to Equation (3.72), or by using Equation (3.71) in a similarly appropriate manner. In this way, once B_ℓ/Y_o is known for a given slot size, the value of B_b/Y_o is obtainable readily for any stub guide size. An explicit expression for B_ℓ/Y_o is given in Section E. The equivalent circuit for the complete Tee is shown in Figure 3.12.

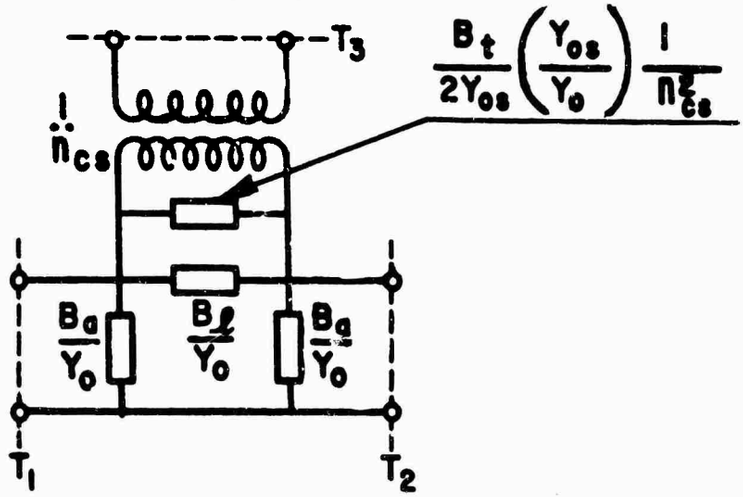

Figure 3.12

If the long dimension of the stub guide is c and the short dimension d, then the turns ratio n_{cs} is given by

$$n_{cs}^2 = J_o^2 \left(\frac{\varepsilon b'}{2}\right) \frac{c\,d}{a\,b} \left[\frac{\cos(\pi\, a'/2\, a)}{\cos(\pi\, a'/2\, c)}\right]^2 \left[\frac{1 - (a'/c)^2}{1 - (a'/a)^2}\right]^2 \qquad (3.73)$$

A thick slot-coupled E plane Tee can be considered as a length of guide, equal to the slot thickness, connecting an E plane Tee junction and a transverse slot which is simply a change in cross-section. The Tee junction referred to is shown in Figure 2.9 (b), and is seen to be a special case of the type of Tee considered above, namely, when the stub guide cross-section dimensions are identical to those of the slot itself. The susceptance B_t/Y_o for this case is to a first order equal to zero, so that from Equation (3.72)

$$\frac{B_{bj}}{Y_o} = \frac{B_\ell}{Y_o} \qquad (3.74)$$

where the subscript j is added to signify "junction", in accordance with the notation of Part II. The expression (3.74) for the turns ratio n_{cs} now becomes

$$n_{cj}^2 = J_o^2 \left(\frac{\varepsilon b'}{2}\right) \frac{a'b'}{a\,b} \left[\frac{4}{\pi} \frac{\cos(\pi\, a'/2\, a)}{1 - (a'/a)^2}\right]^2 \qquad (3.75)$$

The parameter B_a/Y_o is assumed unchanged, because the energy stored in the waveguide structure, when the slot is excited by a symmetric voltage source, is in the immediate vicinity of the aperture and is relatively unaffected by the presence of the walls. For the case of a Tee junction it would seem that the proximity of the walls of the stub guide to the slot should alter the value of B_a/Y_o, but it is probably still true that the half space dyadic susceptance is a good approximation to the guide dyadic susceptance in the variational integrals, thereby only slightly influencing the B_a/Y_o value.

4. Transverse Slot Radiating into a Half Space

(H. Kurss)

When considered as a waveguide termination, the equivalent circuit for a transverse slot radiating from the end of the guide into a half space is a two terminal network. The admittance element $Y_r = G_r + j B_r$ consists of a radiation conductance in parallel with a susceptance, as shown in Figure 3.13.

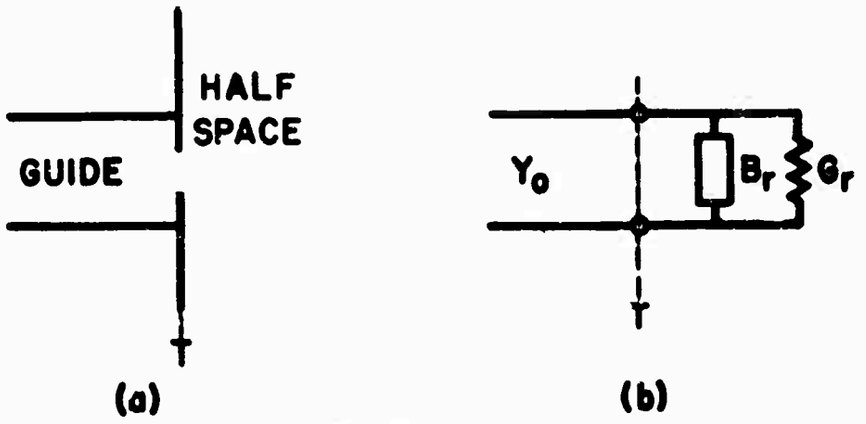

Figure 3.13

In a manner somewhat analogous to the derivations for the other variational expressions given above, the variational formulation for this admittance element is obtained as:

$$Y_r = G_r + j B_r = \frac{\iint dS \iint dS' \; \underline{n} \times \underline{E}(\underline{r}) \cdot (\underset{\sim}{y}_g + \underset{\sim}{y}_h) \cdot \underline{n} \times \underline{E}(\underline{r}')}{\left[\iint dS \; \underline{n} \times \underline{E}(\underline{r}) \cdot \underline{h}(\underline{r})\right]^2} \qquad (3.76)$$

where

$\underset{\sim}{y}_g = j \underset{\sim}{B}_g$ = imaginary dyadic spatial guide admittance.

$\underset{\sim}{y}_h = \underset{\sim}{G}_r + j \underset{\sim}{B}_h$ = complex dyadic spatial half space admittance.

$\underline{E}(\underline{r})$ = the slot trial electric field.

The slot electric field may be considered real in the variational expression since any complex amplitude factor which is independent of space coordinates cancels out. It is readily demonstrated that both G_r and B_r

are stationary about the correct slot electric field which satisfies the integral equation

$$I\,\underline{h} = \int dS' \left(\underline{\underline{y}}_g + \underline{\underline{y}}_h\right) \cdot \underline{n} \times \underline{E}\,(\underline{r}') \qquad (3.77)$$

where I is the complex current corresponding to the real field $\underline{E}\,(\underline{r}')$.

It is convenient to decompose the admittance element represented by Equation (3.76) in a manner analogous to those expressions given earlier for the transverse slot and the slot-coupled E plane Tee as

$$Y_r = \frac{VI}{V^2} = \frac{I}{V} = \frac{P_t}{V^2} + \frac{P_h}{V^2} \qquad (3.78)$$

where P_t is the rate of change of stored energy in the waveguide side of the aperture, and P_h is the rate of change of stored energy in the half space plus an additional quantity which is a measure of the radiated power. The imaginary part of Y_r, i.e., the shunt susceptance, is

$$j B_r = \frac{P_t}{V^2} + I_m \left[\frac{P_h}{V^2}\right] \qquad (3.79)$$

It is recognized that the first term, which is purely reactive, is half the susceptance of a transverse slot of the same dimensions; the second term is the susceptance calculated by using the imaginary part of the half space spatial admittance. The two terms are almost equal for small slots since the guide spatial admittance then can be approximated by the half space kernel as shown in Equation (3.40).

The radiation conductance G_h (which is also equal to G_r) is:

$$G_h = Re \left[\frac{I}{V}\right] = Re \left[\frac{P_h}{V^2}\right] \qquad (3.80)$$

and is the term contributed to the variational expression (3.76) by the dyadic half space conductance so that

$$G_h = \frac{\iint dS \iint dS'\, \underline{n} \times \underline{E}\,(\underline{r}) \cdot \underline{\underline{G}}_h \cdot \underline{n} \times \underline{E}\,(\underline{r}')}{\left[\iint dS\, \underline{n} \times \underline{E}\,(\underline{r}) \cdot \underline{h}\,(\underline{r})\right]^2} \qquad (3.81)$$

where $\underset{\sim}{G}_h = \frac{\omega\varepsilon}{2\pi}\left(\underset{\sim}{\varepsilon} + \frac{\nabla\nabla}{k^2}\right)\frac{\sin k\,|\underline{r} - \underline{r}'|}{|\underline{r} - \underline{r}'|}$

It may be shown that the insertion of any trial electric field in (3.81) different from the true electric field yields a value of G_h greater than the true value. This statement assumes both that the correct Green's function is used and that the integrations are evaluated exactly. This minimum property for the conductance can be derived simply,[1] once it is shown that the insertion of any completely arbitrary aperture electric field in (3.81) always yields a positive result for G_h. This is sufficient since this proof for the minimum property involves the insertion of a difference field into the numerator of the variational expression. The difference field being the difference between the trial and the exact aperture fields. A proof that the result of Equation (3.81) is positive for arbitrary aperture electric fields is given below. The proof given here is only one of several that could be given, and is certainly not the simplest of them, but is most direct in that it involves the real part of the half space spatial susceptance itself.

The transverse component of the half space dyadic conductance in the plane $z = z' = 0$ is:

$$(\underset{\sim}{G}_h)_t = \frac{\omega\varepsilon}{2\pi}\left(\underset{\sim}{\varepsilon} + \frac{\nabla_t\,\nabla_t}{k^2}\right)\frac{\sin k\,|\underline{r} - \underline{r}'|}{|\underline{r} - \underline{r}'|} \qquad (3.82)$$

where $\underset{\sim}{\varepsilon} = \underline{i}\,\underline{i} + \underline{j}\,\underline{j}$

$$\nabla_t = \underline{i}\,\frac{\partial}{\partial x} + \underline{j}\,\frac{\partial}{\partial y}$$

$$|\underline{r} - \underline{r}'| = \sqrt{(x - x')^2 + (y - y')^2}$$

Let us utilize certain integral expressions, namely,[2]

$$\frac{\sin k\,|\underline{r} - \underline{r}'|}{|\underline{r} - \underline{r}'|} = \int_0^k \frac{J_0\left(|y - y'|\,t\right)\cos\sqrt{k^2 - t^2}\,(x - x')}{\sqrt{k^2 - t^2}}\,t\,dt \qquad (3.83)$$

---

1 See, for example, Miles, J.W., "Plane Discontinuities in Cylindrical Tubes", J. Acous. Soc. Am., 17, 259-271, (Jan 1946).

2 Watson, G.N., "A Treatise on the Theory of Bessel Functions", 1922, p. 416.

and[3]

$$J_o(|y - y'|\, t) = \frac{2}{\pi}\int_o^t \frac{\cos w(y - y')}{\sqrt{w^2 - t^2}}\, dw \qquad (3.84)$$

These two results can be combined into the expression:

$$\frac{\sin k|\underline{r} - \underline{r}'|}{|\underline{r} - \underline{r}'|} = \frac{2}{\pi}\int_o^k dt \cos(x-x')t \int_o^{\sqrt{k^2-t^2}} \frac{\cos(y - y')\, w\, dw}{\sqrt{k^2 - t^2 - w^2}} \qquad (3.85)$$

The dependence of the integrand upon the primed and unprimed co-ordinates can be exhibited in a symmetric product when the parameters

$$S \equiv x\,t + y\,w \qquad D \equiv x\,t - y\,w$$

$$S' \equiv x'\,t + y'\,w \qquad D' \equiv x'\,t - y'\,w$$

are introduced, for then

$$2\cos(x-x')t\cos(y-y')w = \cos D\cos D' + \sin D\sin D' + \cos S\cos S' + \sin S\sin S' .$$

A typical term in the conductance expression (3.81) then becomes:

$$K\int_o^k dt \int_o^{\sqrt{k^2-t^2}} \frac{dw}{\sqrt{k^2-t^2-w^2}} \left[(1-\frac{t^2}{k^2})C_D^2(E_x) + \frac{2wt}{k^2} C_D(E_x)C_D(E_y) + (1-\frac{w^2}{k^2})C_D^2(E_y)\right] \qquad (3.86)$$

where $C_D(E_x) = \iint E_x(x,y)\cos D\, dx\, dy$

$\underline{z}_o \times \underline{E} = \underline{i}\, E_x(x,y) + \underline{j}\, E_y(x,y)$

$\underline{E}$ = aperture field

K = a positive number.

However, since $w^2 + t^2 \leq k^2$ it is easily shown that the integrand is positive for non-vanishing $E_x(x,y)$ and $E_y(x,y)$. The conductance is essentially the sum of such typical terms and is consequently also positive.

---

[3] ibid, p. 48.

As implied by Equation (3.79), the susceptance of the transverse radiating slot of Figure 3.13, relative to the characteristic admittance of the waveguide, is composed of two parts, namely,

$$\frac{B_r}{Y_o} = \frac{B_t}{2Y_o} + \frac{B_h}{Y_o} \tag{3.87}$$

This breakup follows naturally from the variational expression (3.76). The first term, $B_t/2Y_o$, is half the susceptance of a transverse slot of the same aperture dimensions within the waveguide, and was calculated in 2) of this section. The second term, which involves the imaginary part of the half space spatial admittance, depends solely on the stored energy in the half space region, and is given by:

$$\frac{B_h}{Y_o} = \frac{\iiiint \underline{n} \times \underline{E}(\underline{r}) \cdot \underset{\sim}{B}_h \cdot \underline{n} \times \underline{E}(\underline{r}') \, dS \, dS'}{Y_o \left[\iint \underline{n} \times \underline{E}(\underline{r}) \cdot \underline{h}(\underline{r}) \, dS \right]^2} \tag{3.88}$$

where

$$\underset{\sim}{B}_h = \frac{\pi\epsilon}{2\pi} \left(\underset{\sim}{\epsilon} + \frac{\nabla\nabla}{k^2} \right) \frac{\cos k |\underline{r} - \underline{r}'|}{|\underline{r} - \underline{r}'|}$$

$$Y_o = \frac{\beta\epsilon}{\omega\mu}$$

The mode function $\underline{h}(\underline{r})$ involved in the denominator applies to the waveguide region, and is that of the dominant mode therein, thus permitting normalization of B_h to that mode. Identical considerations apply to the expression (3.81) for G_h, where both sides must be divided by $Y_o = \beta\epsilon/\omega\mu$ to complete the normalization.

The trial aperture electric field $\underline{E}(\underline{r})$ for expressions (3.81) and (3.88) was chosen as

$$\underline{E} \propto \underline{y}_o \cos \frac{\pi x}{a} \tag{3.89}$$

where the origin of coordinates lies at the center of the slot. The choice was dictated largely by the ability to evaluate the resulting integrals.

The trial fields (3.47) and (3.48) used in the evaluation of B_t/Y_o, although expected to be slightly more accurate than that of (3.89), led to integration difficulties.

If the geometry of the transverse radiating slot is as shown in the solid lines of Figure 3.14, then the equivalent circuit is similar to that shown in Figure 3.13, but the normalization desired is to the slot waveguide characteristic admittance Y_o', rather than that of the main waveguide, Y_o. Figure 3.14 illustrates a possible application as a

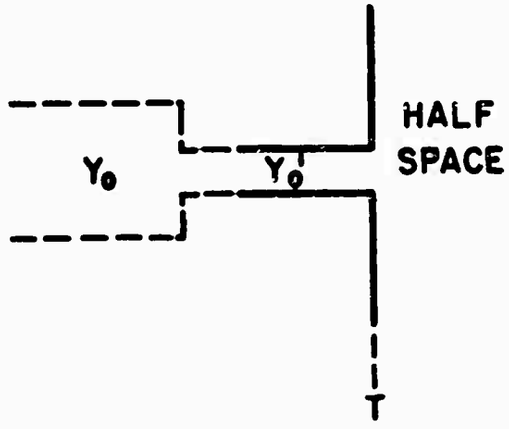

Figure 3.14

portion of a thick slot. In order to obtain normalization to Y_o', the term Y_o in expression (3.88) is replaced by $Y_o' = \gamma e'/\omega\mu$, where $\gamma e'$ is the propagation wavenumber of the slot guide, and the mode function $\underline{h}$ in the denominator is replaced by $\underline{h}'$, corresponding to the dominant mode in the slot guide. Similar considerations apply to the expression (3.81) for the conductance. Comparison of the expressions involved shows that Y_r/Y_o for the slot of Figure 3.13 is related to Y_r/Y_o' for the slot of Figure 3.14 by

$$\frac{Y_r}{Y_o} = \frac{1}{n_t^2}\,\frac{Y_o'}{Y_o}\,\frac{Y_r}{Y_o'} \tag{3.90}$$

where the expression for n_t^2 involves the ratio of the denominators and is defined in Equation (32b) of the Final Report, Chap. VI. For the special

case of the trial field of Equation (3.89), the $B_t/2Y_o'$ term vanishes since the trial field is then the dominant mode field of the slot guide and is orthogonal to all the higher modes constituting the guide spatial susceptance. Furthermore, the expression for n_t^2 is then given directly by Equation (35) of the Final Report, Chap. VI. Since the direct waveguide contribution vanishes for the Y_r/Y_o' term, and the geometry involved is that of a junction between the slot guide and the half space, the quantity Y_r/Y_o' will be denoted by Y_{rj}/Y_o'.

The evaluation of the integrals involved in the variational expressions (3.81) and (3.88) are now discussed. The differentiations involved in the half space dyadic susceptance are readily removed by an integration by parts procedure as shown in the Final Report, Chap. VI, p. 4. The remaining quadruple integrals are directly reduced to double integrals when new variables $x - x'$, $x + x'$, $y - y'$, $y + y'$ are introduced. This leads to the expression:

$$\frac{Y_r}{Y_o} = \frac{j\,2}{n_t^2 \mathscr{L} b'} \left\{ (C^2 - 1) \left[\int_0^{r\pi} d\eta \left(r - \frac{\eta}{\pi}\right) \int_0^{\pi} d\xi \left(1 - \frac{\xi}{\pi}\right) \frac{\cos \xi \; e^{-j C \sqrt{\xi^2 + \eta^2}}}{\sqrt{\xi^2 + \eta^2}} \right] \right.$$

$$\left. + (C^2 + 1) \left[\int_0^{r\pi} d\eta \left(r - \frac{\eta}{\pi}\right) \int_0^{\pi} \frac{d\xi \sin \xi \; e^{-j C \sqrt{\xi^2 + \eta^2}}}{\pi \sqrt{\xi^2 + \eta^2}} \right] \right\} \tag{3.91}$$

where $C = \frac{ka'}{\pi} = \frac{2a'}{\lambda}$; $r = \frac{b'}{a'}$; $\frac{1}{\mathscr{L}} = \frac{\lambda}{2\pi \sqrt{1 - \left(\frac{\lambda}{2a}\right)^2}} = \frac{\lambda_g}{2\pi}$;

$$\xi = \frac{\pi}{a'}(x - x') , \quad \eta = \frac{\pi}{a'}(y - y') ;$$

and n_t^2 is given in Equation (35) of Chap. VI of the Final Report. The integrals are evaluated by approximating the integrands by the first few terms of a convergent power series.

When $r = b'/a'$ is greater than unity the first integration involves the evaluation of the integrals

$$I_1 = \int_0^{r\pi} \left(r - \frac{\eta}{\pi}\right) \frac{\sin C\sqrt{\xi^2 + \eta^2}}{\sqrt{\xi^2 + \eta^2}}\, d\eta$$

$$I_2 = \int_0^{r\pi} \left(r - \frac{\eta}{\pi}\right) \frac{\cos C\sqrt{\xi^2 + \eta^2}}{\sqrt{\xi^2 + \eta^2}}\, d\eta$$

Since[4]

$$\int_0^{\infty} \frac{\sin C\sqrt{\xi^2 + \eta^2}}{\sqrt{\xi^2 + \eta^2}}\, d\eta = \frac{\pi}{2} J_0(C\xi)$$

$$\int_0^{\infty} \frac{\cos C\sqrt{\xi^2 + \eta^2}}{\sqrt{\xi^2 + \eta^2}}\, d\eta = -\frac{\pi}{2} Y_0(C\xi)$$

an integration by parts results in:

$$I_1 = \frac{r\pi}{2} J_0(C\xi) - \frac{\cos C\xi}{C\pi} - \frac{r}{C} \int_{\infty}^{r\pi} \frac{\cos C\sqrt{\xi^2 + \eta^2}}{\eta^2}\, d\eta$$

$$I_2 = -\frac{r\pi}{2} Y_0(C\xi) + \frac{\sin C\xi}{C\pi} + \frac{r}{C} \int_{\infty}^{r\pi} \frac{\sin C\sqrt{\xi^2 + \eta^2}}{\eta^2}\, d\eta$$

---

[4] Watson, G. N., loc. cot., p. 180.

When $C\xi$ is small then:[5]

$$J_0(C\xi) \cong 1 - \frac{C^2\xi^2}{4}$$

$$\frac{\pi}{2} Y_0(C\xi) \cong \left(1 - \frac{C^2\xi^2}{4}\right)(\log C\xi + \gamma - \log 2) + \frac{C^2\xi^2}{4} .$$

Moreover, when $\xi < \pi, \eta > r\pi$, $r > 1$ then $\sqrt{\xi^2 + \eta^2} \cong \eta + \frac{1}{2}\frac{\xi^2}{\eta}$.

Consequently:

$$\int_{\infty}^{r\pi} \frac{\sin C\sqrt{\xi^2 + \eta^2}\, d\eta}{\eta^2} \cong \int_{\infty}^{r\pi} \frac{\sin C\eta\, d\eta}{\eta^2} + \frac{C\xi^2}{2} \int_{\infty}^{r\pi} \frac{\cos C\eta\, d\eta}{\eta^3}$$

$$\int_{\infty}^{r\pi} \frac{\cos C\sqrt{\xi^2 + \eta^2}\, d\eta}{\eta^2} \cong \int_{\infty}^{r\pi} \frac{\cos C\eta\, d\eta}{\eta^2} - \frac{C^2\xi^2}{2} \int_{\infty}^{r\pi} \frac{\sin C\eta\, d\eta}{\eta^3} .$$

With these approximations one finds

$$I_1 = \left(1 - \frac{C^2\xi^2}{4}\right)\left[\frac{\cos C r\pi}{C\pi} + r\,\mathrm{Si}(C r\pi)\right] - \frac{\cos C\xi}{C\pi} - \frac{\xi^2}{4}\frac{\sin C r\pi}{r\pi^2}$$

with a similar expression for I_2. The remaining integrations with respect to ξ are readily evaluated by integration by parts. For example:

$$\int_{\epsilon}^{\pi} \ln t \cos t\, dt = -\ln t \cos t \Big|_{\epsilon}^{\pi} + \int_{\epsilon}^{\pi} \frac{\cos t\, dt}{t}$$

$$= \ln \pi + \mathrm{Ci}(\pi) + \ln \epsilon \cos \epsilon - \mathrm{Ci}(\epsilon)$$

---

5 Jahnke, E. and Emde, F., "Tables of Functions", 1943, pp. 128, 132.

Upon allowing ϵ to approach zero one obtains

$$\int_0^{\pi} \ln t \sin t \, dt = \ln \pi + \mathrm{Ci}(\pi) - \ln \gamma$$

where $\ln \gamma = .5772.$

The final expressions for the admittance parameters are:

$$\frac{G_h}{Y_o} = \frac{\lambda_g}{\lambda} \frac{ab}{4\pi b'^2} \left[\frac{1-(\frac{a'}{a})^2}{\cos(\frac{\pi}{2}\frac{a'}{a})}\right]^2 \left\{\left[\cos(kb') - \frac{\sin(kb')}{kb'} + k b' \, \mathrm{Si}(kb')\right]\right.$$

$$\left. - (\frac{\pi^2 - 8}{\lambda^2}) a'^2 \left[\cos(kb') + \frac{\sin(kb')}{kb'} - kb' \, \mathrm{Si}(kb')\right]\right\} \qquad (3.92a)$$

$$\frac{B_h}{Y_o} = \frac{\lambda_g}{b'a'^2} \frac{ab}{16} \frac{\pi^2}{16} \left[\frac{1-(\frac{a'}{a})^2}{\cos(\frac{\pi}{2}\frac{a}{a})}\right]^2 \left\{\left[2 - \pi \, \mathrm{Si}(\pi) + \frac{1+\cos(ka')}{r} - \frac{2\cos(kb')}{(r\pi)^2}\right]\right.$$

$$\left. + (\frac{2a'}{\lambda})^2 \left[N_1 - (\frac{\pi^2 - 8}{2\pi^2}) \frac{\cos(ka')}{(r\pi)^2}\right] + (\frac{2a'}{\lambda})^4 \left[N_2 - (\frac{\pi^2 - 8}{2\pi^2}) A\right]\right\} \qquad (3.92b)$$

where $r = \frac{b'}{a'}$; $k = \frac{2\pi}{\lambda}$; $A = \mathrm{Ci}(kb') - \frac{\sin kb'}{kb'} - \ln \frac{\gamma a'}{\lambda}$; $\lambda_g = \frac{\lambda}{\sqrt{1-(\frac{\lambda}{2a})^2}}$

and

$$N_1 = \frac{1}{\pi^2}\left[\frac{\pi\,\mathrm{Si}(\pi)}{2} - \mathrm{Ci}(\pi) + 3\,\ell n\left(\frac{\pi}{\gamma}\right) - \pi^2\,\ell n\,\pi\right] = -.3482$$

$$N_2 = \frac{1}{\pi}\left[\frac{\mathrm{Si}(\pi)}{2} - \frac{\pi}{2}(1 - \ell n\,\pi) - \frac{3}{\pi} - \frac{2}{\pi}(\mathrm{Ci}(\pi) - \ell n\,\gamma\pi)\right] = .1632$$

The only restriction in these results is that $r = b'/a'$ is greater than unity. For this reason, the terms have been arranged so that when b' remains finite while $a' \to 0$ then only the first term in the braces is significant.

When the aperture area becomes vanishingly small ($a' \to 0$ and then $b' \to 0$) the conductance becomes

$$\frac{G_h}{Y_0} = \frac{2\pi}{3}\,\frac{\lambda_g\,ab}{\lambda^3} \tag{3.93}$$

in agreement with the result obtained in the Final Report, Chap. VI, p. 22.

When the slot width is $a' = \lambda/2$ (a half-wavelength slot) the admittance computation becomes simplified. The first integration involves the evaluation of

$$C_s(\eta, \pi) = \int_0^\pi \frac{\sin\xi\,\cos\sqrt{\xi^2+\eta^2}\;d\xi}{\sqrt{\xi^2+\eta^2}}$$

$$S_s(\eta, \pi) = \int_0^\pi \frac{\sin f\,\sin\sqrt{f^2+\eta^2}\;df}{\sqrt{f^2+\eta^2}}$$

Upon changing variables one can evaluate these as:[6]

$$C_s(\eta, \pi) = \frac{1}{2}\left[\mathrm{Si}\left(\sqrt{\pi^2+\eta^2}+\pi\right) + \mathrm{Si}\left(\sqrt{\pi^2+\eta^2}-\pi\right)\right] - \mathrm{Si}(\eta)$$

---

[6] Tables of Generalized Sine and Cosine Integral Functions, Harvard University Press, 1949, p. XIV.

$$S_s(\eta, \pi) = -\frac{1}{2}\left[\mathrm{Ci}\left(\sqrt{\pi^2+\eta^2}+\pi\right) + \mathrm{Ci}\left(\sqrt{\pi^2+\eta^2}-\pi\right)\right] + \mathrm{Ci}(\eta)$$

The integration with respect to η is performed by using the relations:

$$\frac{d\,C_s(\eta,\pi)}{d\eta} = -\frac{\sin\sqrt{\pi^2+\eta^2}}{\eta} - \frac{\sin\eta}{\eta}$$

$$\frac{d\,S_s(\eta,\pi)}{d\eta} = \frac{\cos\sqrt{\pi^2+\eta^2}}{\eta} + \frac{\cos\eta}{\eta}$$

so that

$$\int_0^a C_s(\eta,\pi)\,d\eta = a\,C_s(a,\pi) + 1 - \cos a + \int_0^a \sin\sqrt{\pi^2+\eta^2}\;d\eta$$

$$\int_0^a S_s(\eta,\pi)\,d\eta = a\,S_s(a,\pi) - \sin a - \int_0^a \cos\sqrt{\pi^2+\eta^2}\;d\eta$$

With these formulae it is readily deduced that:

$$\frac{G_h}{Y_o} = \frac{\pi ab}{4\lambda^2}\,\frac{\left[1-\left(\frac{\lambda}{2a}\right)^2\right]^{3/2}}{\cos^2\left(\frac{\pi\lambda}{4a}\right)}\left\{2\,S_s(r\pi,\pi) + \frac{2\sin r\pi}{r\pi} + \frac{2(1-\cos r\pi)}{(r\pi)^2}\right.$$

$$\left. + \frac{4}{r\pi}\int_0^{r\pi}\cos\sqrt{\pi^2+\eta^2}\;d\eta - \frac{2}{(r\pi)^2}\int_0^{r\pi}\eta\cos\sqrt{\pi^2+\eta^2}\;d\eta\right\}$$

(3.94a)

$$\frac{B_h}{Y_o} = \frac{\pi\, ab}{4\,\lambda^2}\,\frac{\left[1-\left(\frac{\lambda}{2a}\right)^2\right]^{3/2}}{\cos^2\frac{\pi\,\lambda}{4a}}\left\{2\,C_s(r\pi,\pi)+\frac{4}{r\,\pi}-\frac{2\sin r\pi}{(r\,\pi)^2}-\frac{2\cos r\pi}{r\,\pi}\right.$$

$$\left.+\frac{4}{r\,\pi}\int_0^{r\,\pi}\sin\sqrt{\pi^2+\eta^2}\;d\eta\;-\frac{2}{(r\,\pi)^2}\int_0^{r\,\pi}\eta\,\sin\sqrt{\pi^2+\eta^2}\;d\eta\right\} \tag{3.94b}$$

where no approximations have been made as yet in the integrations. However, for a half-wave slot, $r = b'/a'$ is always less than unity, and for this range of values the above expressions (3.94) can be well approximated by:

$$\frac{G_h}{Y_o} = \frac{\pi\, ab}{4\,\lambda^2}\,\frac{\left[1-\left(\frac{\lambda}{2a}\right)^2\right]^{3/2}}{\cos^2\left(\frac{\pi\,\lambda}{4a}\right)}\left\{\left[\ln(2\pi\gamma)-Ci(2\pi)\right]-\frac{\pi^2}{3\,\lambda^2}\,b'^2\right\} \tag{3.95a}$$

$$\frac{B_h}{Y_o} = \frac{\pi\, ab}{4\,\lambda^2}\,\frac{\left[1-\left(\frac{\lambda}{2a}\right)^2\right]^{3/2}}{\cos^2\left(\frac{\pi\,\lambda}{4a}\right)}\left\{Si(2\pi)-\frac{4\,\pi}{3\,\lambda}\,b'\right\} \tag{3.95b}$$

For the special case of $a = .9$, $b = .4$, $\lambda = 1.26$ these reduce to:

$$\frac{G_h}{Y_c} = .769 - .6[illegible]2\,b'^2 \tag{3.96a}$$

$$\frac{B_h}{Y_o} = .448 - 1.04\,b' \tag{3.96b}$$

When $r = b'/a'$ is less than unity the integrations are more difficult. The first integration involves the evaluation of the integrals:

$$I_1 + j I_2 = \int_0^{\pi} \frac{\cos\xi \; e^{-jc\sqrt{\xi^2+\eta^2}}}{\sqrt{\xi^2+\eta^2}} \, d\xi$$

$$I_3 + j I_4 = \int_0^{\pi} \frac{\xi \cos\xi \; e^{-jc\sqrt{\xi^2+\eta^2}}}{\sqrt{\xi^2+\eta^2}} \, d\xi$$

$$I_5 + j I_6 = \int_0^{\pi} \frac{\sin\xi \; e^{-jc\sqrt{\xi^2+\eta^2}}}{\sqrt{\xi^2+\eta^2}} \, d\xi$$

To evaluate these, the range of integration is broken up into $0 \leq \xi \leq \xi'$ and $\xi \leq \xi \leq \pi$ where $r\pi < \xi'$. In the range $\xi' \leq \xi \leq \pi$ the approximation $\sqrt{\xi^2+\eta^2} = \xi + \frac{1}{2}\frac{\eta^2}{\xi}$ is used, while in the range $0 \leq \xi \leq \xi'$ the small argument approximation for the trigonometric functions is used. A check on the integrations is provided by the fact that the terms containing ξ' must cancel since the original integrals are clearly independent of ξ'. The integrations proceed essentially in the fashion described in the Final Report, Chap. VI p.6. After the integrals I_1 to I_6 have been approximated in terms of powers of η and $\ln \eta$ all that remains is the evaluation of standard integrals between definite limits. Upon collecting results, one can express the final admittance parameters as follows.

$$\frac{G_h}{Y_o} = \frac{\lambda_g}{\lambda^2}\frac{b'}{n_t^2}\left\{\left(\frac{2\xi'}{k}\right)^2\left[\overline{Si}(ka'+\pi)+\overline{Si}(ka'-\pi)\right] - \frac{4\cos^2(ka'/2)}{ka'}\right.$$

$$\left. + \frac{1}{\pi}\left[1+\left(\frac{\lambda}{2a'}\right)^2\right]\left[Ci|ka'-\pi| - Ci(ka'+\pi) + \ln\left|\frac{ka'+\pi}{ka'-\pi}\right|\right] + O_G\left(\frac{b'}{a'}\right)^2\right\} \tag{3.97a}$$

where

$$Q_Q\left(\frac{b'}{a'}\right)^2 = \frac{1}{24}\left(\frac{b'}{a'}\right)^2\left\{\frac{2\pi^2 \sin ka'}{(ka')^2} - ka'\left(\frac{\alpha\epsilon'}{k}\right)^2 \cos ka'\right.$$

$$- ka'\left[1-3\left(\frac{\lambda}{2a'}\right)^2\right] + \frac{(ka')^2}{2\pi}\left(\frac{\alpha\epsilon'}{k}\right)^2\left[\pi\left[Si(ka'+\pi)+Si(ka'-\pi)\right]\left(\frac{\alpha\epsilon'}{k}\right)^2\right.$$

$$\left.\left. + \left[1+3\left(\frac{\lambda}{2a'}\right)^2\right]\left[Ci\,|ka'-\pi| - Ci(ka'+\pi) + \ell n\left|\frac{ka'+\pi}{ka'-\pi}\right|\right]\right]\right\}$$

$$\frac{R_h}{Y_o} = \frac{2b'\lambda_g}{\lambda^2}\frac{1}{n_t^2}\left\{\left(\frac{\alpha\epsilon'}{k}\right)^2\left[\frac{Ci(ka'+\pi) - Ci\,|ka'-\pi|}{2} + \frac{3}{2} - \ell n\frac{\gamma\,\alpha\epsilon' b'}{2}\right]\right.$$

$$\left. + \frac{\sin ka'}{ka'} + \left[1+\left(\frac{\lambda}{2a'}\right)^2\right]\left[\frac{Si(ka'+\pi) - Si(ka'-\pi)}{2\pi}\right] - \frac{2b'}{3a'}\left(\frac{\lambda}{2a'}\right)^2 - Q_B\left(\frac{b'}{a'}\right)^2\right\} \tag{3.97b}$$

where

$$Q_B\left(\frac{b'}{a'}\right)^2 = \frac{1}{24}\left(\frac{b'}{a'}\right)^2\left\{\left(\frac{\alpha\epsilon'}{k}\right)^2\left[ka'\sin ka' - \cos ka' + \pi\left[Si(ka'+\pi) - Si(ka'-\pi)\right]\right.\right.$$

$$\left.\left. + (ka')^2\left(\frac{\alpha\epsilon'}{k}\right)^2\left[\frac{Ci(ka'+\pi) - Ci\,|ka'-\pi|}{2} + \frac{19}{12} - \ell n\frac{\gamma\,\alpha\epsilon' b'}{2}\right]\right]\right.$$

$$\left. + \left[1+\left(\frac{\lambda}{2a'}\right)^2\right]\left[\frac{\sin ka'}{\pi} + \cos ka' + (ka')^2\left(\frac{\alpha\epsilon'}{k}\right)^2\left[\frac{Si(ka'+\pi) - Si(ka'-\pi)}{2\pi}\right]\right]\right\}$$

and

$$\varkappa' = 2\pi/\lambda_g' = \frac{2\pi}{\lambda}\sqrt{1-(\lambda/2a')^2} = \sqrt{k^2-(\pi/a)^2}$$

$$\frac{1}{n_t^2} = \frac{ab}{a'b'}\left[\frac{\pi}{4}\,\frac{1-(a'/a)^2}{\cos(\pi a'/2a)}\right]^2$$

A single formula for the conductance can be obtained which is valid for all aperture sizes, and which differs from the accurate expressions by 10 percent at most, this greatest error occurring for the wide open aperture. Agreement is excellent for small apertures. The expression is:

$$\frac{G_h}{Y_o} = \frac{2\pi}{3}\,\frac{\lambda_g\, ab}{\lambda^3}\left[\frac{1-(\frac{a'}{a})^2}{\cos\frac{\pi}{2}\frac{a'}{a}}\right]^2\left\{\left[1-.374(\frac{a'}{\lambda})^2+.130(\frac{a'}{\lambda})^4-.154(\frac{a'}{\lambda})^6\right]\right.$$

$$\left.-1.36\,(\frac{b'}{\lambda})^2\left[1-.268\,(\frac{a'}{\lambda})^2+.160\,(\frac{a'}{\lambda})^4\right]+.556\,(\frac{b'}{\lambda})^4\right\} \qquad (3.98)$$

This result is obtained by means of the approximation

$$\frac{\sin C\sqrt{\xi^2+\eta^2}}{\sqrt{\xi^2+\eta^2}} = C-\frac{C^3(\xi^2+\eta^2)}{6}+\frac{C^5(\xi^2+\eta^2)^2}{120}-\frac{C^7(\xi^2+\eta^2)^3}{5{,}040}\cdot$$

in the variational expression (3.31) for the conductance. This formula results in conductances which are too small for large apertures since the last term in the series approximation for the sine was negative.

5. E Plane Slot Radiating into a Half Space

When the E plane slot is excited by a symmetrical current source the field set up in the slot, to a first order, is identical to that for the transverse radiating slot, and also that in the slot-coupled E plane Tee. The symbolic expression for the variational formulation resulting from the above excitation, analogous to Equation (3.69), is

$$\left(\frac{Y_a}{2} + Y_b\right)_R = \frac{P_L}{(2V)^2} + \frac{P_h}{(2V)^2} \tag{3.99}$$

where the subscript R designates "radiating", while from Equation (3.71), we have

$$\frac{P_L}{(2V)^2} = j B_\ell + \frac{Y_a}{2} \tag{3.100}$$

and from Equations (3.79), (3.80), and (3.56),

$$\frac{P_h}{(2V)^2} = \frac{P_h}{(V_t)^2}\left(\frac{V_t}{2V}\right)^2 = (G_h + j B_h)\frac{1}{n_c^2} \tag{3.101}$$

Therefore, Equation (3.99) is rewritten as

$$\left(\frac{Y_a}{2} + Y_b\right)_R = j B_\ell + \frac{Y_a}{2} + (G_h + j B_h)\frac{1}{n_c^2} \tag{3.102a}$$

or

$$(Y_b)_R = j B_\ell + \frac{G_h + j B_h}{n_c^2} \tag{3.102b}$$

In Equations (3.102), all quantities may be written as relative to the main guide characteristic admittance Y_o. The quantity B_ℓ is discussed in Sec. 3) c. The expression for n_c is given by Equation (3.59b) or by (3.65), while expressions for B_h and G_h are given by Equations (3.92), or (3.95), or (3.97), depending upon the range of aperture dimensions. The four

terminal equivalent circuit for the E plane radiating slot in terms of the notation of this section is shown in Figure 3.15.

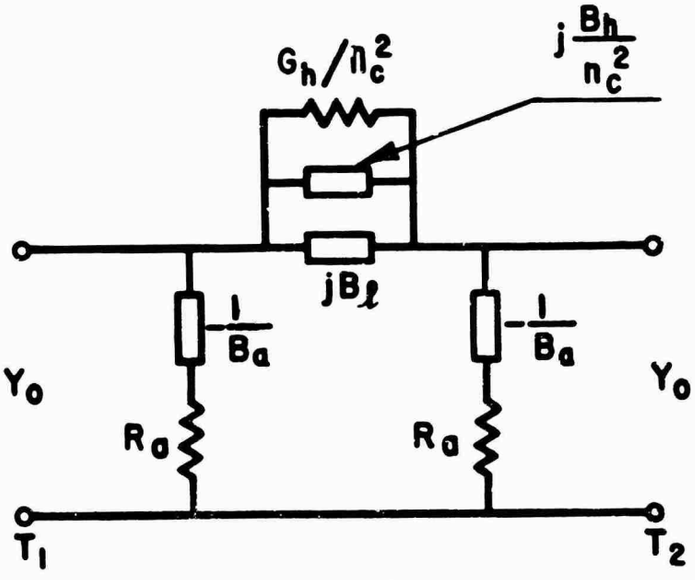

Figure 3.15

The shunt susceptance B_a/Y_0 is taken as identical to the one obtained for the E plane Tee, since the field and geometry considerations are the same as those in the case discussed in Sec. 3) c. We may also write $X_a = -1/B_a$ since X_a is large, and is $>>R_a$.

Since the field choice is real, i.e.,

$$\underline{M}_{s.c.} \propto \underline{x}_0 \frac{z}{\sqrt{(\frac{b'}{2})^2 - z^2}} \cos\frac{\pi x}{a'} + \underline{z}_0 \left[1-(\frac{a'}{a})^2\right] \frac{\pi}{a'}\sqrt{(\frac{b'}{2})^2 - z^2} \sin\frac{\pi x}{a} \tag{3.103}$$

the radiation resistance R_a/Z_0, relative to the guide characteristic impedance, is

$$\frac{R_a}{Z_o} = \mathrm{Re}\left[\frac{V\,I}{Z_o I^2}\right] = \frac{\frac{\omega\epsilon}{\pi k^2}\iint dS \iint dS'\, \underline{M}_{s.c.} \cdot (-\nabla\nabla' + k^2\, \underset{\sim}{\epsilon})\, \frac{\sin k\,|r - r'|}{|r - r'|}\, \underline{M}_{s.c.}}{Y_o \left[\iint \underline{M}_{s.c.} \cdot \underline{h}^{(2)}\, dS\right]^2} \tag{3.104}$$

This has been calculated and is approximately equal to

$$\frac{R_a}{Z_o} = \frac{2\pi\, ab}{3\lambda\, \lambda_g} \left[\frac{1 + (1 - \alpha^2)^2}{\left\{1 - \alpha^2 \left(\frac{\lambda}{2a}\right)^2\right\}^2}\right] \tag{3.105}$$

where $\alpha = a'/a$. As α approaches zero, the expression for R_a/Z_o reduces to

$$\frac{R_a}{Z_o} = \frac{4\pi}{3}\, \frac{ab}{\lambda\, \lambda_g} \tag{3.106}$$

E. Summary of Results for the Slot Parameters

1. Transverse centered slot coupling identical waveguides

(H_{10} mode propagating)

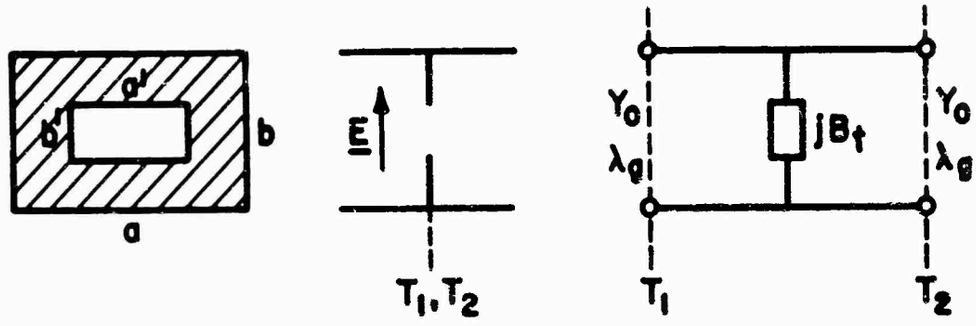

CROSS-SECTION SIDE VIEW EQUIVALENT NETWORK

Results:

The slot considered is a zero-thickness, centered, transverse aperture coupling identical rectangular waveguides. Its equivalent network at the reference planes coincident with the slot contains a single resonant-type shunt element. The susceptance of this element, relative to the characteristic admittance of the waveguide, for a slot of aperture dimensions a' and b' in a guide of dimensions a and b is given by two expressions, each valid for a different range of slot dimensions.

For the range of aperture dimensions $b'/b < 0.5$, $a'/a > 0.5$:

$$\frac{B_t}{Y_o} = \frac{4b}{\lambda_g}\left[\ell n \csc\frac{\pi b'}{2b} + \frac{1}{2}\left(\frac{b}{\lambda_g}\right)^2 \cos^4\frac{\pi}{2}\frac{b'}{b}\right] \qquad (3.107)$$

$$- \frac{4b}{\lambda_g}\left(\frac{\lambda_g}{\lambda_{g3}}\right)^2 \left[\frac{\cos\frac{3\pi}{2}\frac{a'}{a}}{\cos\frac{\pi}{2}\frac{a'}{a}} \cdot \frac{1-\left(\frac{a'}{a}\right)^2}{1-9\left(\frac{a'}{a}\right)^2}\right]^2 X$$

$$X \left\{\left[1 + \left(\frac{\pi}{2}\frac{b'}{\lambda_{g3}}\right)^2\right] \ell n \frac{4}{\gamma\pi}\left(\frac{\lambda_{g3}}{b'}\right) + \left(\frac{\pi}{2}\frac{b'}{\lambda_{g3}}\right)^2\right\}$$

where $\gamma = 1.781$. λ_g is the guide wavelength in the rectangular waveguide of dimensions a and b, and λ_{g3} is the absolute value of the guide wavelength for the third ($m = 3$, $n \neq 0$) mode, i.e.,

$$\lambda_{g3} = \left| \frac{\lambda}{\sqrt{1 - \left(\frac{3\lambda}{2a}\right)^2}} \right|$$

For the remaining range of slot dimensions:

$$\frac{B_t}{Y_o} = \frac{b}{b'} \frac{B_L}{Y_o} + \frac{B_c}{Y_o} + \left(\frac{b}{b'}\right)^2 \left[T\left(\frac{a'}{a}\right) - L\left(\frac{b'}{b}\right) \cos^4 \frac{\pi a'}{2a} \right] \qquad (3.108)$$

where:

$$\frac{B_L}{Y_o} = -\frac{\lambda_g}{a} \left[1 - \frac{3}{4}\left(1 - \sqrt{1 - \left(\frac{2a}{3\lambda}\right)^2}\right) \sin^2 \frac{\pi a'}{a} \right] \cot^2 \frac{\pi a'}{2a}$$

$$\frac{B_c}{Y_o} = \frac{4b}{\lambda_g} \left[\ell n \csc \frac{\pi b'}{2b} + \frac{1}{2}\left(\frac{b}{\lambda_g}\right)^2 \cos^4 \frac{\pi b'}{2b} \right]$$

$$T\left(\frac{a'}{a}\right) = \frac{2}{\pi^3} \frac{\lambda_g}{b} \left[\frac{\sin \frac{\pi a'}{a} - \frac{\pi a'}{a} \cos \frac{\pi a'}{a}}{\sin^4 \frac{\pi a'}{2a}} - \pi \right]$$

$$L\left(\frac{b'}{b}\right) = \frac{6}{\pi} \frac{\lambda_g}{a} \sqrt{1 - \left(\frac{2a}{3\lambda}\right)^2} \left[\frac{b'}{b} K_1(\alpha_3 b') + \left(1 - \frac{b'}{b}\right) K_1(\alpha_3 |b - b'|) \right.$$

$$\left. - \frac{\pi}{\sqrt{2}} \frac{b'}{b} \operatorname{Erf}_c\left(\sqrt{\alpha_3 b'}\right) - \left(1 - \frac{b'}{b}\right) \frac{\pi}{\sqrt{2}} \operatorname{Erf}_c\left(\sqrt{\alpha_3 (b - b')}\right) \right]$$

where $\alpha_3 = 2\pi/\lambda_{g3}$, where λ_{g3} is defined above,

K_1 is the Bessel function of the second kind of imaginary argument, and

$$Erf_c(x) = \frac{2}{\sqrt{\pi}} \int_x^\infty e^{-t^2} dt = 1 - Erf(x)$$

Restrictions:

The results have been obtained variationally. The two different expressions for B_t/Y_0 result from the insertion of two different trial aperture electric fields in the variational expression. For expressions (3.107) and (3.108), the trial fields (3.47) and (3.48), respectively, were used. In both cases, the spatial susceptance utilized was the modified guide one discussed in Sec. C.

2. Transverse centered slot coupling guides of different cross-section

(H_{10} mode propagating in at least one guide)

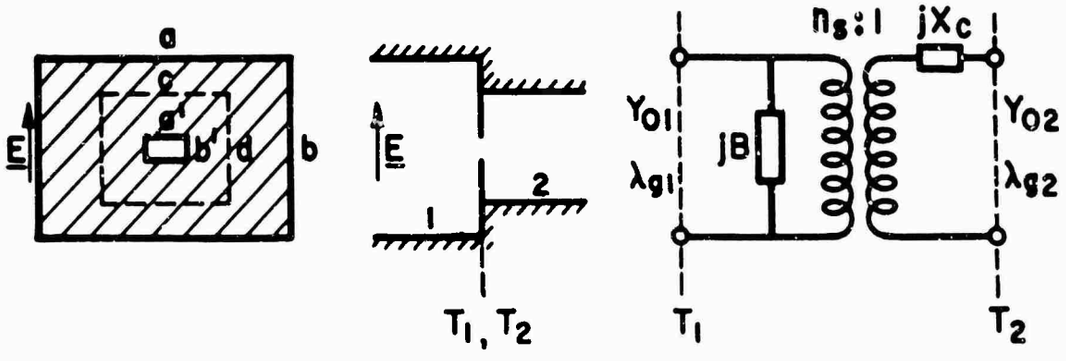

CROSS-SECTION SIDE VIEW EQUIVALENT NETWORK

Results:

An equivalent circuit referred to the junction plane of the two guides consists of an input susceptance B coupled by means of a transformer to an output series reactance. To a first order, the series reactance is zero and the susceptance is half the sum of the susceptance of a transverse slot in guide (1) and the susceptance of a transverse slot in guide (2) coupled thru a transformer whose turns ratio is $n_s : 1$. Thus

$$B = \frac{1}{2}\left(B_{t1} + \frac{1}{n_s^2} B_{t2}\right)$$

or

$$\frac{B}{Y_{01}} = \frac{1}{2}\left[\frac{B_{t1}}{Y_{01}} + \frac{1}{n_s^2}\,\frac{B_{t2}}{Y_{02}}\,\left(\frac{Y_{02}}{Y_{01}}\right)\right] \qquad (3.109)$$

where B_{t1}/Y_{01} and B_{t2}/Y_{02} are given by Equations (3.107) and/or (3.108), depending upon the dimensions of the slot relative to those of each guide. Also

$$X_c \cong 0$$

The turns ratio n_s is given by

$$n_s^2 = \left[\frac{\cos\frac{\pi}{2}\frac{a'}{a}}{1-\left(\frac{a'}{a}\right)^2} \cdot \frac{1-\left(\frac{a'}{c}\right)^2}{\cos\frac{\pi}{2}\frac{a'}{c}}\right]^2 \cdot \frac{c\,d}{a\,b} \qquad (3.110)$$

Restrictions:

These results have been obtained by assuming that the slot excitation for this case is the same as that for the transverse slot coupling identical guides, an assumption which should be sufficiently accurate for engineering applications.

The susceptance of a transverse change of cross-section can be calculated from the above formulae directly since the contribution to the susceptance from the guide whose cross-section dimensions are exactly those of the slot is almost zero. Thus the value for B becomes equal simply to $B_{t1}/2$. The ratio of the terms within the bracket in n_s^2 containing the dimension c becomes equal to $4/\pi$ when $c = a'$.

3. Transverse centered slot coupling rectangular waveguide to a half space.

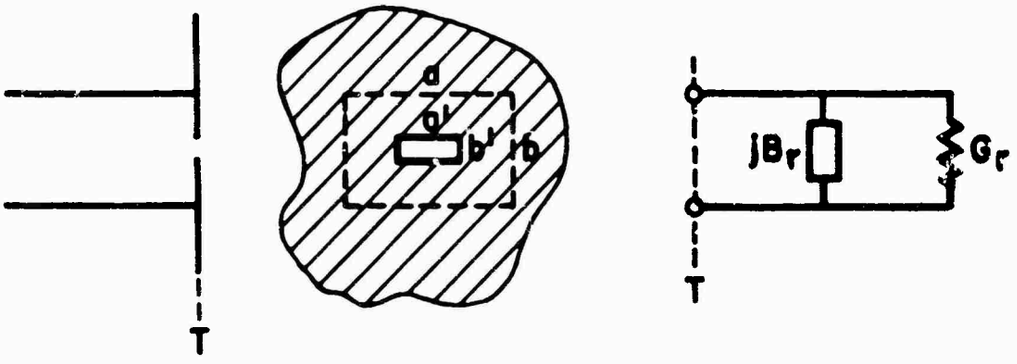

SIDE VIEW CROSS-SECTION EQUIVALENT NETWORK

Results:

The equivalent two terminal circuit is a resonant-type lossy network. The susceptance B_r, referred to the plane of the obstacle, is partially determined from the formula for the susceptance of a transverse aperture. The relative susceptance of a rectangular radiating aperture of width a' and height b' centrally located in a transverse plane in a rectangular waveguide of width a and height b is

$$\frac{B_r}{Y_o} = \frac{B_t}{2Y_o} + \frac{B_h}{Y_o} \qquad (3.111)$$

where B_t/Y_o is given by Equation (3.107) or (3.108) depending on the aperture dimensions, and where the expressions below for B_h/Y_o correspond to different ranges of aperture dimensions.

For $b' > a'$:

$$\frac{B_h}{Y_0} = \frac{\lambda_g}{a'} \frac{1}{n_t^2} \left\{ \left[\left[2 - \pi \, Si(\pi) + \frac{1 + \cos ka'}{b'/a'} - \frac{2 \cos kb'}{(\pi b'/a')^2} \right] \right.\right.$$

$$\left.\left. + \left(\frac{2a'}{\lambda}\right)^2 \left[N_1 - \left(\frac{\pi^2 - 8}{2\pi^2}\right) \frac{\cos ka'}{(\pi b'/a')^2} \right] + \left(\frac{2a'}{\lambda}\right)^4 \left[N_2 - \left(\frac{\pi^2 - 8}{2\pi^2}\right) A \right] \right\} \qquad (3.112)$$

where

$$\frac{1}{n_t^2} = \frac{ab}{a'b'} \left[\frac{\pi}{4} \frac{1 - (a'/a)^2}{\cos (\pi a'/2a)} \right]^2$$

$$N_1 = -.3482 \quad , \quad N_2 = .1632$$

$$A = Ci(kb') - \frac{\sin kb'}{kb'} - \ell n \frac{\gamma a'}{\lambda}$$

$$\ell n \, \gamma = .5772 \quad , \quad k = 2\pi/\lambda$$

and

$$Si(x) = \int_0^x \frac{\sin t}{t} \, dt$$

$$Ci(x) = \int_\infty^x \frac{\cos t}{t} \, dt$$

For $b' < a'$:

$$\frac{B_h}{Y_0} = \frac{2b' \lambda_g}{\lambda^2} \frac{1}{n_t^2} \left\{ \left(\frac{\pi x'}{k}\right)^2 \left[C + \frac{3}{2} - \ell n \frac{\gamma \pi x' b'}{2} \right] + \frac{\sin ka'}{ka'} \right.$$

$$\left. + \left[1 + \left(\frac{\lambda}{2a'}\right)^2 \right] (S_-) - \frac{2b'}{3a'} \left(\frac{\lambda}{2a'}\right)^2 - Q_B \left(\frac{b'}{a'}\right)^2 \right\} \qquad (3.113)$$

where

$$Q_B \left(\frac{b'}{a'}\right)^2 = \frac{1}{24}\left(\frac{b'}{a'}\right)^2 \left\{\left(\frac{\varkappa'}{k}\right)^2 \left[ka' \sin ka' - \cos ka' + 2\pi^2 S_- + (\varkappa' a')^2 \left[C + \frac{19}{12} - \ell n \frac{\gamma \varkappa' b'}{2}\right]\right] + \left[1 + \left(\frac{\lambda}{2a'}\right)^2\right]\left[\frac{\sin ka'}{\pi} + \cos ka' + (\varkappa' a')^2 S_-\right]\right\}$$

and

$$\varkappa' = 2\pi/\lambda_g' = \frac{2\pi}{\lambda}\sqrt{1 - (\lambda/2a')^2} = \sqrt{k^2 - (\pi/a')^2}$$

$$C = \frac{Ci\,(ka' + \pi) - Ci\,|ka' - \pi|}{2}$$

$$S_- = \frac{Si\,(ka' + \pi) - Si\,(ka' - \pi)}{2\pi}$$

and the other symbols are defined above.

For a half-wavelength slot, i.e., $a' = \lambda/2$:

$$\frac{B_h}{Y_o} = \frac{\pi a b \lambda}{4\lambda_g^3} \sec^2\left(\frac{\pi\lambda}{4a}\right)\left[Si\,(2\pi) - \frac{4\pi}{3\lambda} b'\right] \qquad (3.114)$$

The radiation conductance, G_r/Y_o relative to the waveguide characteristic admittance, is directly equal to G_h/Y_o. The expression for it, for the range of aperture sizes for which $b' > a'$, is:

$$\frac{G_r}{Y_o} = \frac{\lambda_g a' 4}{\lambda b' \pi^3}\frac{1}{n_t^2}\left\{\left[\cos kb' - \frac{\sin kb'}{kb'} + kb'\,Si(kb')\right] - \left(\frac{\pi^2 - 8}{\lambda^2}\right) a'^2 \left[\cos kb' + \frac{\sin kb'}{kb'} - kb'\,Si(kb')\right]\right\} \qquad (3.115)$$

For $b' < a'$:

$$\frac{G_r}{Y_o} = \frac{\lambda_g b'}{\lambda^2} \frac{1}{n_t^2} \left\{ \left(\frac{2\pi'}{k}\right)^2 S - \frac{4\cos^2(ka'/2)}{ka'} + \frac{1}{\pi}\left[1+\left(\frac{\lambda}{2a'}\right)^2\right]\left[L-2C\right] + O_G\left(\frac{b'}{a'}\right)^2 \right\} \tag{3.116}$$

where

$$O_G\left(\frac{b'}{a'}\right)^2 = \frac{1}{24}\left(\frac{b'}{a'}\right)^2 \left\{ \frac{2\pi^2 \sin ka'}{(ka')^2} - ka' \left(\frac{2\pi'}{k}\right)^2 \cos ka' - ka' \left[1 - 3\left(\frac{\lambda}{2a'}\right)^2\right] \right.$$

$$\left. + \frac{(2\pi' a')^2}{2\pi}\left[\pi\left(\frac{2\pi'}{k}\right)^2 S + \left[1 + 3\left(\frac{\lambda}{2a'}\right)^2\right]\left[L - 2C\right]\right] \right\}$$

and

$$S = Si(ka' + \pi) + Si(ka' - \pi)$$

$$L = \ell n \left| \frac{ka' + \pi}{ka' - \pi} \right|$$

and the other symbols are defined above.

For a half-wavelength slot, i.e., $a' = \lambda/2$:

$$\frac{G_r}{Y_o} = \frac{\pi a b \lambda}{4\lambda_g^3} \sec^2\left(\frac{\pi\lambda}{4a}\right)\left[\ell n\, 2\pi\gamma - Ci(2\pi) - \frac{\pi^2}{3\lambda^2} b'^2\right] \tag{3.117}$$

A single formula for the conductance which is valid for all aperture sizes is:

$$\frac{G_r}{Y_o} = \frac{\lambda_g a' b'}{\lambda^3} \frac{32}{3\pi} \frac{1}{n_t^2} \left\{ \left[1 - .374\left(\frac{a'}{\lambda}\right)^2 + .130\left(\frac{a'}{\lambda}\right)^4 - .154\left(\frac{a'}{\lambda}\right)^6\right] \right.$$

$$\left. - 1.36\left(\frac{b'}{\lambda}\right)^2\left[1 - .268\left(\frac{a'}{\lambda}\right)^2 + .160\left(\frac{a'}{\lambda}\right)^4\right] + .556\left(\frac{b'}{\lambda}\right)^4 \right\} \tag{3.118}$$

This latter expression differs from the accurate expressions above by 10 percent at most, this greatest error occurring for the wide open aperture, and is excellent for small apertures. The error is such that the conductance value predicted by (3.118) is too low.

Restrictions:

The results have been obtained variationally, wherein it was assumed that the form of the slot field is approximately that present in the transverse slot within the guide. Actually the trial field used was a cosine field, and therefore slightly different from the fields used for the calculation of B_t/Y_o. The spatial admittance used for computing B_h/Y_o and G_h/Y_o was the half space one.

4. Centered symmetrical slot-coupled E plane Tee

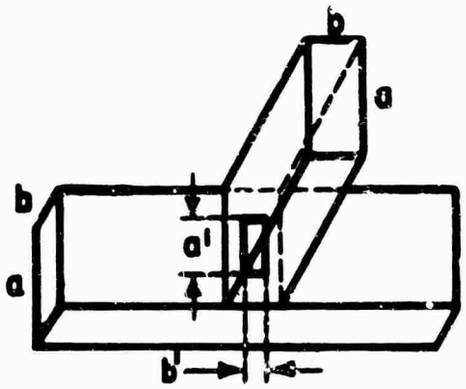

CUTAWAY VIEW

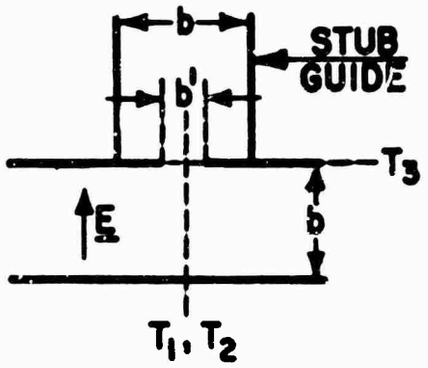

SIDE VIEW

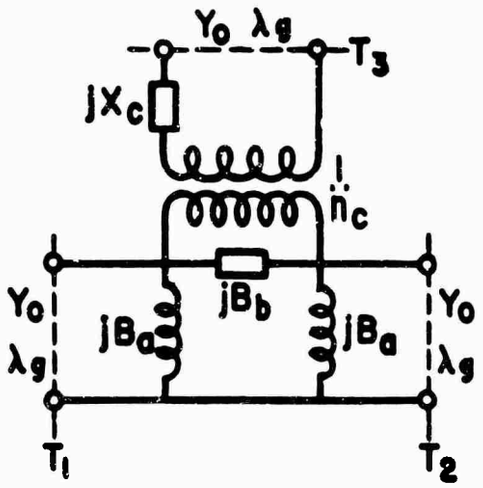

EQUIVALENT NETWORK

Results:

The equivalent network shown applies to the indicated reference planes, and is valid for a symmetrical E plane Tee. The resonant-type series element jB_b is the dominant one. Formulae for the parameters, relative to the waveguide characteristic admittance, are given below.

$$\frac{X_c}{Z_o} \cong 0 \tag{3.119}$$

$$-\frac{B_a}{Y_o} = \frac{Z_o}{X_a} = \frac{b'}{\lambda_g}\,\frac{16}{\pi^2}\,n_t^2\,J_o^2\left(\frac{\pi b'}{\lambda_g}\right)\left[\left(\frac{k}{\beta}\right)^2 - \left(\frac{\lambda_g}{2a'}\right)^2\left(\frac{a'}{a}\right)^2\right] \tag{3.120}$$

where

$$n_t^2 = \frac{a'b'}{a\,b}\left[\frac{4}{\pi}\,\frac{\cos(\pi a'/2a)}{1-(a'/a)^2}\right]^2$$

$$\beta = 2\pi/\lambda_g$$

$$-\frac{B_a}{Y_o} \cong \frac{b}{\lambda}\,\frac{\lambda_g}{\lambda}\left(\frac{b'}{b}\right)^2\left(\frac{a'}{a}\right), \qquad \text{for } a'/a,\ b'/b \ll 1 \tag{3.121}$$

Parameter B_b/Y_o occurs in combination with $B_a/2Y_o$, where the latter quantity is given above. The different expressions listed for $(B_b/Y_o + B_a/2Y_o)$ and for n_c are applicable for different ranges of aperture dimensions. For $a'/a > 0.5$, $b'/b < 0.5$:

$$\frac{B_b}{Y_o} + \frac{B_a}{2Y_o} = \frac{1}{n_c^2}\,\frac{B_t}{Y_o} + \frac{1}{n_c^2}\left[0.345 + \frac{1}{2}\left(\frac{b}{\lambda_g}\right)^2\right] \tag{3.122}$$

$$n_c = J_o\left(\frac{\pi b'}{\lambda_g}\right) \tag{3.123}$$

For $a'/a > 0.5$, $0.5 \leq b'/b < 0.9$:

$$\frac{B_b}{Y_o} + \frac{B_a}{2Y_o} = \frac{1}{2n_c^2}\frac{B_t}{Y_o} - \frac{1}{2n_c^2}\left(\frac{b}{b'}\right)\frac{\lambda_g}{a}\left[1 - \frac{3}{4}\left(1 - \sqrt{1-\left(\frac{2a}{3\lambda}\right)^2}\right)\sin^2\frac{\pi a'}{a}\right]\cos^2\frac{\pi a'}{2a}$$

$$+ \frac{1}{n_c^2}\left(\frac{b}{b'}\right)^2\left\{\frac{1}{2}\,T\left(\frac{a'}{a}\right) - \frac{3}{\pi}\frac{b'}{b}\frac{\lambda_g}{a}\sqrt{1-\left(\frac{2a}{3\lambda}\right)^2}\cos^4\frac{\pi}{2}\frac{a'}{a}\left[K_1\left(\frac{2\pi}{\lambda_{g3}}\,b'\right)\right.\right.$$

$$\left.\left. - \frac{\pi}{\sqrt{2}}\,\mathrm{Erf}_c\left(\sqrt{\frac{2\pi b'}{\lambda_{g3}}}\right)\right]\right\} + \frac{1}{n_c^2}\left(\frac{2b}{\lambda_g}\right)\left[\ln\frac{1.43b}{b'} + 2\left(\frac{b}{\lambda_g}\right)^2\right] \tag{3.124}$$

$$n_c = \frac{\lambda_g}{\pi b'}\sin\frac{\pi b'}{\lambda_g} \tag{3.125}$$

For $a'/a > 0.5$, $b'/b \geq 0.9$:

$$\frac{B_b}{Y_o} + \frac{B_a}{2Y_o} = \frac{1}{n_c^2}\frac{b}{b'}\left(\frac{B_t}{Y_o}\right)_{b'/b=1} + \frac{1}{n_c^2}\left[\frac{2b}{\lambda_g}\left\{\ln\frac{1.43b}{b'} + 2\left(\frac{b}{\lambda_g}\right)^2\right\} - \frac{1}{2}\left(\frac{B_t}{Y_o}\right)_{a'/a=1}\right] \tag{3.126}$$

The equation for n_c is that given by Equation (3.125). For $a'/a > 0.5$, $b'/b = 1.0$. Equation (3.126) reduces to:

$$\frac{B_b}{Y_o} + \frac{B_a}{2Y_o} = \frac{1}{n_c^2}\frac{B_t}{Y_o} + \frac{1}{n_c^2}\frac{2b}{\lambda_g}\left[\ln 1.43 + 2\left(\frac{b}{\lambda_g}\right)^2\right] \tag{3.127}$$

The equation for n_c is that given by Equation (3.125).

For the symbols involved: The B_t/Y_o is the relative susceptance of a transverse slot of the same dimensions as that for the slot-coupled Tee, except where otherwise indicated. For Equations (3.122) and (3.124) the B_t/Y_o values are given, respectively, by Equations (3.107) and (3.108). The B_t/Y_o values for Equations (3.126) and (3.127) are obtainable from the Waveguide Handbook. The symbols $T(a'/a)$, K_1, λ_{g3}, and Erf_c of Equation (3.124) are defined in connection with Equation (3.108). J_o^c is the Bessel function of the first kind of zero order.

Restrictions:

The results have been obtained variationally assuming that for symmetrical current excitation the field induced in the aperture is the same as that in the transverse slot, so that it has been possible to utilize the latter's results. To a first order the element X_c is zero.

The exact evaluation of X_c has not been attempted. The expression for B_a/Y_o was obtained by using a bicomponent aperture field together with the quasi-static half space spatial susceptance.

It will be noted that the expressions for $(B_b/Y_o + B_a/2Y_o)$ are specified for $a'/a > 0.5$ only. It was anticipated from the integrations that Equations (3.124), (3.126) and (3.127) would be valid for all a'/a values, but comparison with experiment indicates poorer agreement for $a'/a < 0.5$. The probable reason for this disagreement is that the field assumption used for the slots of larger a' is no longer valid for those of smaller a'. The corresponding expressions in the range of smaller a' have not been evaluated. This restriction applies also to n_c, but not to B_a/Y_o or X_c/Z_o.

5. Centered symmetrical slot-coupled E plane Tee, stub guide of arbitrary cross-section.

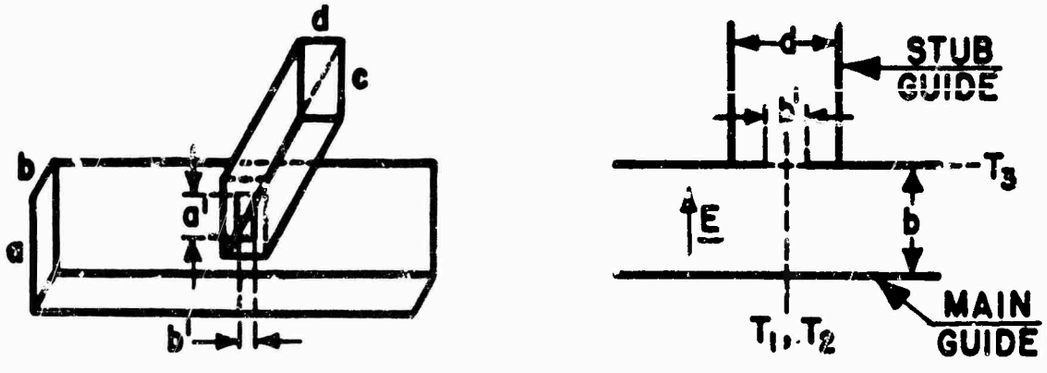

CUTAWAY VIEW

SIDE VIEW

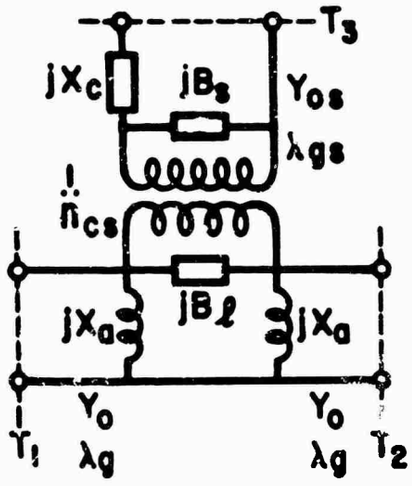

EQUIVALENT NETWORK

Results:

The equivalent circuit referred to the indicated reference planes is a symmetrical six terminal network with a series arm equal to $j\,(B_\ell + B_s/n_{cs}^2)$, and a shunt arm equal to $j\,X_a$. The formulae for the parameter relative to the characteristic admittance of the main guide are given below: Parameters X_c/Z_o and B_a/Y_o are given by Equations (3.119) and (3.120).

$$\frac{B_s}{Y_{os}} = \frac{1}{2}\,\frac{B_t}{Y_{os}} \tag{3.128}$$

B_t/Y_{os} is the susceptance of a transverse slot in a rectangular waveguide of dimensions c, d, and is obtained from Equation (3.107) when $a' > 0.5\ c$, $b' < 0.5\ d$; and from Equation (3.108) for all other slot sizes.

The parameter B_ℓ/Y_o is related to the parameter $(B_b/Y_o + B_a/2Y_o)$ of the slot-coupled E plane Tee for which the stub guide dimensions are those of the main guide by the following:

$$\frac{B_\ell}{Y_o} = \left(\frac{B_b}{Y_o} + \frac{B_a}{2Y_o}\right) - \frac{B_a}{2Y_o} - \frac{1}{n_c^2}\,\frac{B_t}{2Y_o} \tag{3.129}$$

where all quantities on the right hand side apply to the case in which the stub guide is of the same dimensions as the main guide. The values to be inserted depend on the slot dimensions relative to the main guide, and are given, respectively, by Equations (3.122), (3.124), (3.126) and (3.127) for $(B_b/Y_o + B_a/2Y_o)$. The value to be used for B_t/Y_o is discussed in connection with these equations; B_a/Y_o is given by Equation (3.120).

The turns ratio n^2_{cs} is given by: For $a'/a > 0.5$, $b'/b < 0.5$:

$$n^2_{cs} = J_o^2 \left(\frac{\pi b'}{\lambda_g}\right) \left[\frac{\cos(\pi a'/2a)}{1-(a'/a)^2} \cdot \frac{1-(a'/c)^2}{\cos(\pi a'/2c)}\right]^2 \frac{cd}{ab} \qquad (3.130)$$

For $a'/a > 0.5$, $b'/b > 0.5$:

$$n^2_{cs} = \left(\frac{\lambda_g}{\pi b'}\right)^2 \sin^2 \frac{\pi b'}{\lambda_g} \left[\frac{\cos(\pi a'/2a)}{1-(a'/a)^2} \cdot \frac{1-(a'/c)^2}{\cos(\pi a'/2c)}\right]^2 \frac{cd}{ab} \qquad (3.131)$$

When the stub guide dimensions are the same as those of the main guide, the expressions for X_a/Z_o and B_ℓ/Y_o are unchanged. B_s/Y_{os} is simply $B_t/2Y_o$, and Equations (3.130) and (3.131) for n^2_{cs} become, respectively, Equations (3.123) and (3.125) for n^2_o. When the stub guide dimensions are the same as those of the slot itself, the expressions for X_a/Z_o and B_ℓ/Y_o remain unchanged, B_s/Y_{os} reduces to zero, and in the expression for n^2_{cs} the ratio of the terms containing the dimension c becomes equal to $4/\pi$.

Restrictions:

The relations given are all obtained on a microwave network basis. It is assumed that the slot field does not change appreciably enough for the various stub guide sizes to invalidate the variational nature of the results. It is felt that this is a valid assumption, and it is born out by experimental data in conjunction with thick slots, involving a special case of the Tee considered here.

The expression for B_ℓ/Y_o becomes inaccurate for $a'/a < .5$ because the field assumption used for the slots of larger a' is no longer valid for those of smaller a'. The corresponding expression in the range of smaller a' has not been evaluated. This restriction applies also to n^2_{cs}, but not to the other parameters.

6. Centered E plane slot radiating into a half space.

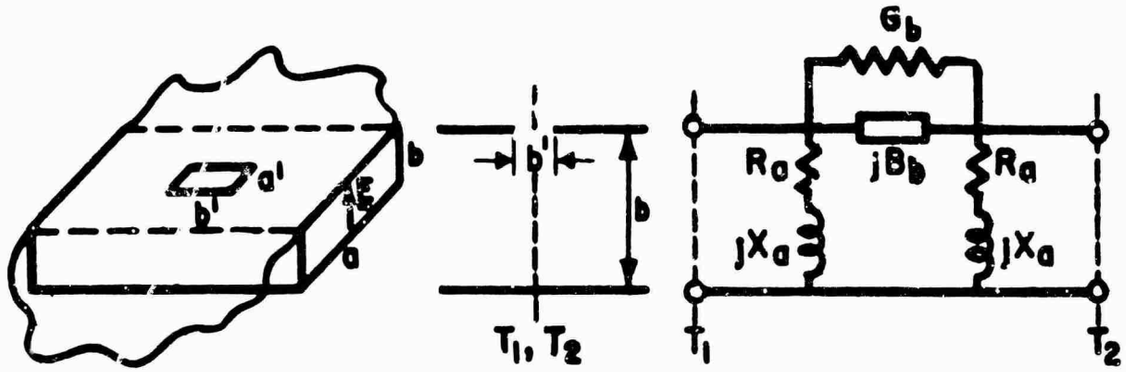

CUTAWAY VIEW SIDE VIEW EQUIVALENT NETWORK

Results:

The lossy four terminal equivalent circuit is approximately series. The series conductance G_b of the E plane radiating slot is determined quite simply from the conductance of the transverse radiating slot. The series susceptance B_b is also determined from previously obtained results. X_a is taken as the shunt reactance of the E plane Tee network, while R_a is the radiation resistance presented at the slot to symmetrical voltage excitation, since this excitation results in a two terminal network.

For a slot of width a' and length b' located in the broad face of a guide of width a and height b:

$$G_b = \frac{1}{n_c^2} G_h \tag{3.132}$$

$$B_b = B_\ell + \frac{1}{n_c^2} B_h \tag{3.133}$$

$$X_a = (X_a)_{\text{E plane Tee}} \tag{3.134}$$

$$B_a = \frac{2\pi ab}{3\lambda\lambda_g}\left[\frac{1 + (1-\alpha^2)^2}{\left[1-\alpha^2(\lambda/2a)^2\right]^2}\right] \qquad (3.135)$$

where $\alpha = a'/a$.

The n_c is that of Equation (3.123) or (3.125) B_ℓ is given by Equation (3.129), B_h by Equation (3.112), (3.113), or (3.114), and X_a by Equation (3.120). The choice of equations for n_c and B_h is decided by the slot size. All parameters are actually specified relative to the main guide characteristic admittance Y_o.

Restrictions:

It has been possible to combine the results of the previous sections because it is assumed that the form of the field excited in the slot-coupled E plane Tee and the E plane radiating slot are the same for various excitations. There was no change in the shunt reactance X_a since it has been shown that this result is more or less independent of the neighboring boundaries.

APPENDIX

1) Poisson - Transformation

$$\sum_{n=N_1}^{N_2} u(n) = \sum_{m=-\infty}^{\infty} \int_{N_1}^{N_2} u(z)\, e^{-j2\pi mz}\, dz \qquad (1)$$

provided u(z) is regular in the interval

$$N_1 \leq z \leq N_2$$

2) Properties of $K_n(x)$

$$K_n(x) = \frac{\pi}{2} j^{n+1} H_n^{(1)}(jx) \qquad (2)$$

$$K_0(x) = -\ln\frac{\gamma x}{2} I_0(x) + \sum_{1}^{\infty} \frac{(\frac{1}{2}x)^{2m}}{(m!)^2} \psi(m+1) \qquad (3)$$

where $\psi(m+1) = 1 + \frac{1}{2} + \frac{1}{m} - \ln\gamma$

$$\gamma = 1.781$$

$$K_n(x) \doteq \frac{(n-1)!}{2}\left(\frac{2}{x}\right)^n \quad , \quad 0<x<<1 \ , \quad n \geq 1 \qquad (4a)$$

$$K_0(x) \doteq \ln 2/\gamma x \quad , \quad 0<x<<1 \ , \quad n = 0 \qquad (4b)$$

$$K_n(x) \sim \sqrt{\frac{\pi}{2x}}\, e^{-x} \quad , \quad x>>1 \qquad (5)$$

$$\frac{d}{dx}\left[x^n K_n(kx)\right] = -k x^n K_{n-1}(kx) \qquad (6)$$

$$K_o\left[k\sqrt{x^2+y^2}\right] = \frac{1}{2}\int_{-\infty}^{\infty} \frac{e^{-jxu}\, e^{-\sqrt{y^2+u^2}\,y}}{\sqrt{k^2+u^2}}\, du \qquad (7)$$

3) Table of Integrals

$$\frac{1}{2\pi}\int_{-\infty}^{\infty} K_o\left[y\sqrt{t^2+v^2}\right] e^{jxt}\, dt = \frac{1}{2}\,\frac{e^{-\sqrt{y^2+x^2}\,v}}{\sqrt{y^2+x^2}} \qquad (8)$$

$$\frac{2}{\sqrt{\pi k}}\int_{1}^{0} \frac{e^{-kx}}{\sqrt{x}}\, dx = \frac{1}{k}\,\mathrm{Erf}_c\,(k^{1/2}) \qquad (9)$$

$$\int_{0}^{\infty} \cos xt\, \frac{e^{ja\sqrt{x^2+y^2}}}{\sqrt{x^2+y^2}}\, dx = \begin{cases} \frac{\pi j}{2} H_o^{(1)}\left(y\sqrt{a^2-t^2}\right) & a > t \\ K_o\left(y\sqrt{t^2-a^2}\right) & a < t \end{cases} \qquad (10)$$

4) Expression for the Relative Amplitudes for a Bicomponent Field

Let it be desired to determine the quantity

$$B = \frac{1}{\iint_S \underline{M}\cdot\underline{h}\, dS}$$

where $\underline{M}$ satisfies the following equation:

$$\underline{h}(S) = \iint_S \underline{M}(S') \cdot \underset{\sim}{\mathcal{B}}(S, S')\, dS'$$

where $\underset{\sim}{\mathcal{B}}$ is Hermitian, i.e.,

$$\iiiint \underline{M}_1 \cdot \underset{\sim}{\mathcal{B}} \cdot \underline{M}_2\, dS\, dS' = \iiiint \underline{M}_2 \cdot \underset{\sim}{\mathcal{B}} \cdot \underline{M}_1\, dS\, dS'$$

It can be shown that B expressed as

$$B = \frac{\iiiint_S \underline{M}(S') \cdot \underset{\sim}{\mathcal{B}} \cdot \underline{M}(S)\, dS\, dS'}{\left(\iint_S \underline{M} \cdot \underline{h}\, dS \right)^2}$$

is stationary about the correct value of $\underline{M}$; and it is evident that the result is independent of the absolute amplitude of $\underline{M}$.

In some applications of the variational method it is necessary, in order to partially satisfy the conditions of the boundary value problem, to choose a bicomponent trial field. The components themselves are usually chosen from some physical considerations. However, one must know also the relative amplitudes of the field components.

Let the bicomponent trial field be

$$\underline{M} = \underline{M}_1 + c\, \underline{M}_2$$

where c is the unknown relative amplitude, and $\underline{M}_1$ and $\underline{M}_2$ are given. If the following definitions are made:

$$\iint \underline{M}_1 \cdot \underline{h}\, dS = m_1 \quad , \iint \underline{M}_2 \cdot \underline{h}\, dS = m_2$$

$$\iiiint \underline{M}_1 \cdot \underset{\sim}{\mathcal{B}} \cdot \underline{M}_1 \, dS \, dS' = b_{11}$$

$$\iiiint \underline{M}_2 \cdot \underset{\sim}{\mathcal{B}} \cdot \underline{M}_2 \, dS \, dS' = b_{22}$$

and

$$\iiiint \underline{M}_1 \cdot \underset{\sim}{\mathcal{B}} \cdot \underline{M}_2 \, dS \, dS' = \iiiint \underline{M}_2 \cdot \underset{\sim}{\mathcal{B}} \cdot \underline{M}_1 \, dS \, dS' = b_{12} = b_{21}$$

then c can be calculated in a variational manner from

$$c = \frac{m_2 \, b_{11} - m_1 \, b_{12}}{m_1 \, b_{22} - m_2 \, b_{21}}$$

IV. COMPARISON OF THEORETICAL AND EXPERIMENTAL RESULTS

The measurements reported below have all been made at a wavelength of 3.20 cms. The experimental results for the thin transverse slot coupling identical guides and for the thin transverse radiating slot have been reported in the Final Report mentioned earlier. They are therefore given here only in graphical form, to allow comparison with the corresponding theoretical data. The other experimental data are listed in both graphical and tabular form, together with estimates of error wherever possible. The questions of choice of equivalent circuit representation, method of treating data, and the experimental techniques involved are discussed in Part II. The theoretical calculations together with the results are given in Part III.

The discussion below treats the thin slots separately from the thick slots. The reasons are that a) the variational (theoretical) calculations apply to the thin (specifically zero-thickness) slots, and b) the parameters for thick slots are obtainable from the parameters for the corresponding thin slots together with certain simple geometrical and microwave network considerations. Thus, the direct comparison between the theoretical and experimental results applies only to the thin slots, while the thick slot discussion utilizes in addition certain microwave network considerations. The discussion for the thick transverse slot coupling identical guides is omitted here as it has been given in the above-mentioned Final Report.

A. Thin Slots

1) The Transverse Slot

The experimental results for the transverse slot coupling identical guides, which have been reported together with estimates of error in the Final Report, have been obtained for slots of 0.005" wall thickness. The theoretical results have been computed for zero-thickness slots. The equivalent circuit for a zero-thickness slot is a pure shunt one, as shown in Figure 4.1-(a), while that for a slot with thickness requires an additional parameter (two additional parameters if the slot is unsymmetrical). This latter equivalent network may be in a Tee or Pi form, or may be in the form shown in Figure 4.1-(b). (See the discussion in the Final Report, Chap. II, Sec. D, 2.) The two parameters are B_t/Y_o and x, the distance between the input and output reference planes.

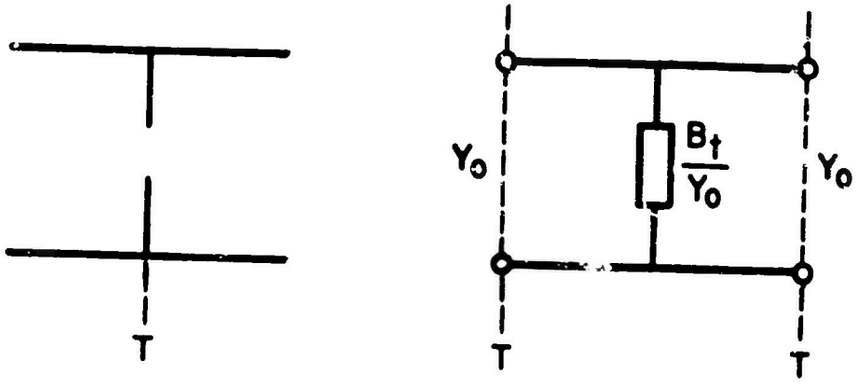

GEOMETRY EQUIVALENT CIRCUIT

Figure 4.1 (a) - Zero thickness transverse slot

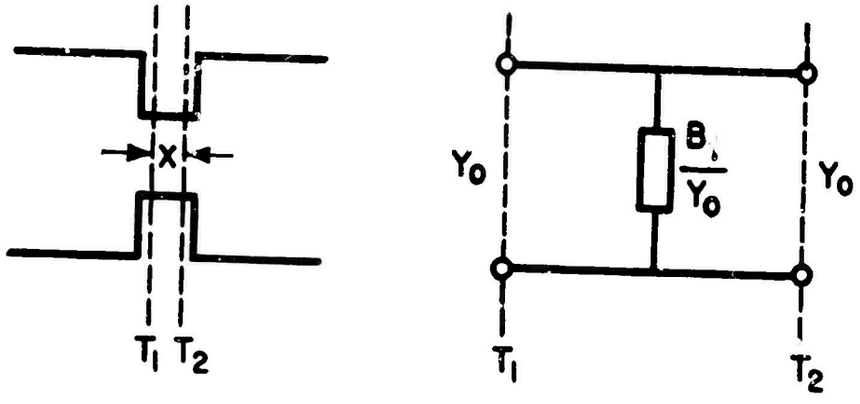

GEOMETRY EQUIVALENT CIRCUIT

Figure 4.1 (b) - Finite thickness transverse slot

When the slot thickness is small, as it is for the measured slots discussed here (0.005"), the value of parameter x is almost negligibly small since it is generally considerably smaller than the slot thickness itself. The smallness of parameter x implies that the value of B_t/Y_o is negligibly different from that which would be obtained if the slot thickness were actually zero. It is not known how to correct exactly for the shift in the B_t/Y_o value due to small but finite thickness, although a number of approximate methods are available, such as considering the slot width to be decreased by the slot thickness,[1] or considering the slot thickness as a length of slot guide coupling two main guides (actually not valid because of interaction effects at such small thicknesses). These approximate procedures indicate a negligible correction to the B_t/Y_o value so that it is therefore permissible to directly compare the theoretically and experimentally determined B_t/Y_o values. The discussion that follows will assume the situation of Figure 4.1-(a).

The theoretical results for B_t/Y_o are obtained from Equations (3.107) and (3.108), where the former expression is used for slots of dimensions $a'/a > 0.6$, $b'/b < 0.5$, while the latter one applies to slots of dimensions which lie outside of this range. The notation for the dimensions is indicated in Figure 4.2, where it is also seen that the slot is centered and oriented parallel to the sides of the guide. The parameters for off-center or rotated slots (at least for small slots), as well as for thick slots, may be obtained from the parameters of the zero-thickness centered slots together with appropriate microwave network considerations. An investigation of thick transverse slots and thin rotated transverse slots has been reported in the above-mentioned Final Report.

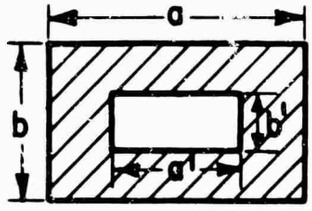

Figure 4.2 - The transverse slot: cross-section

A comparison of theoretical and experimental results for the relative susceptance B_t/Y_o of the transverse slot is given graphically in Figures 4.3 and 4.4. The theoretical results are obtained from Equations

---

[1] Found to be empirically valid for transverse inductive (i.e., b' = b) slots. See Montgomery, C. G., et al, "Principles of Microwave Circuits", Chap. 6, p. 166, McGraw-Hill, 1948.

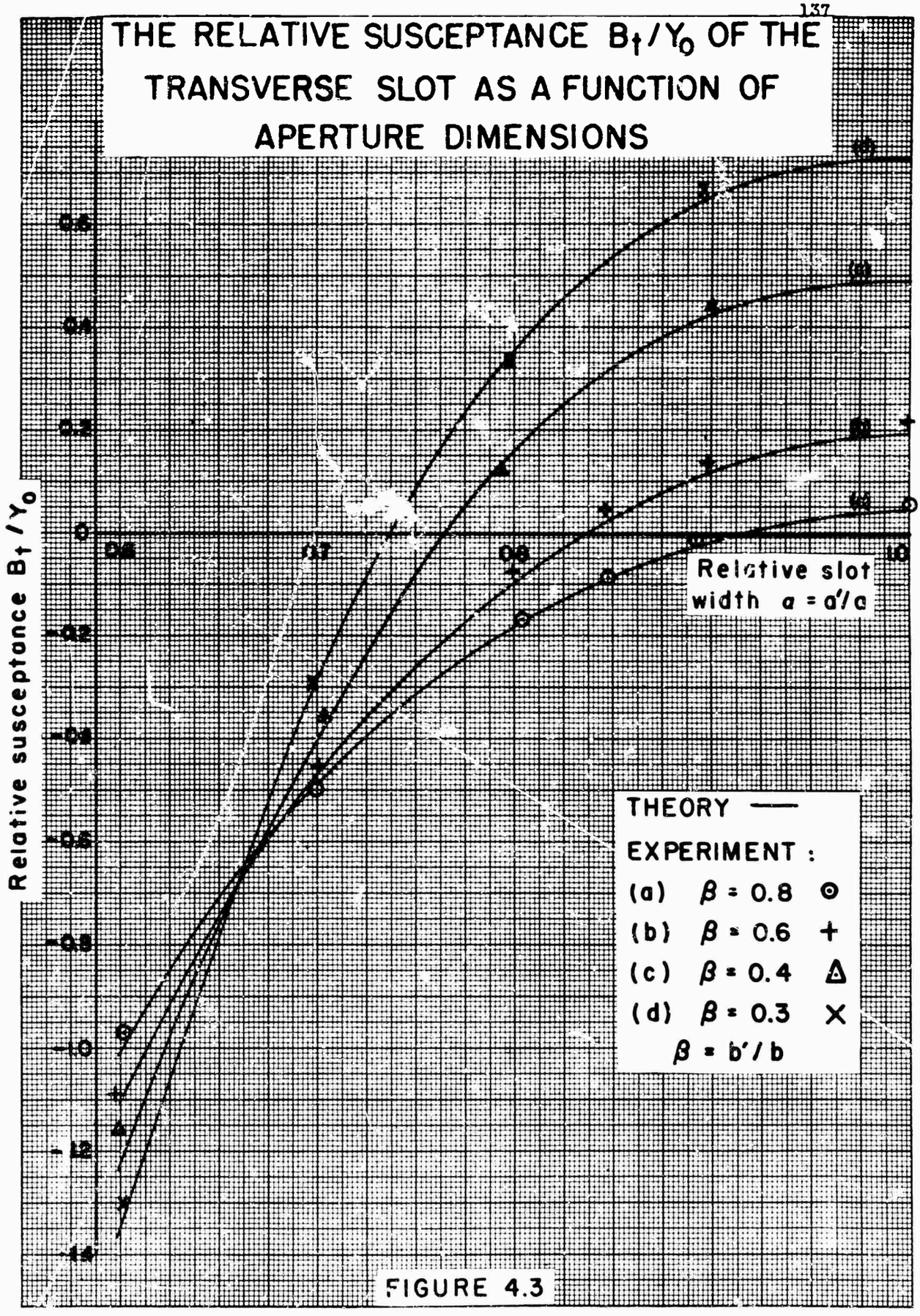
THE RELATIVE SUSCEPTANCE B_t/Y_0 OF THE TRANSVERSE SLOT AS A FUNCTION OF APERTURE DIMENSIONS
Relative susceptance B_t/Y_0
Relative slot width $a = a'/a$
THEORY
EXPERIMENT :
(a) $\beta = 0.8$
(b) $\beta = 0.6$
(c) $\beta = 0.4$
(d) $\beta = 0.3$
$\beta = b'/b$

FIGURE 4.3

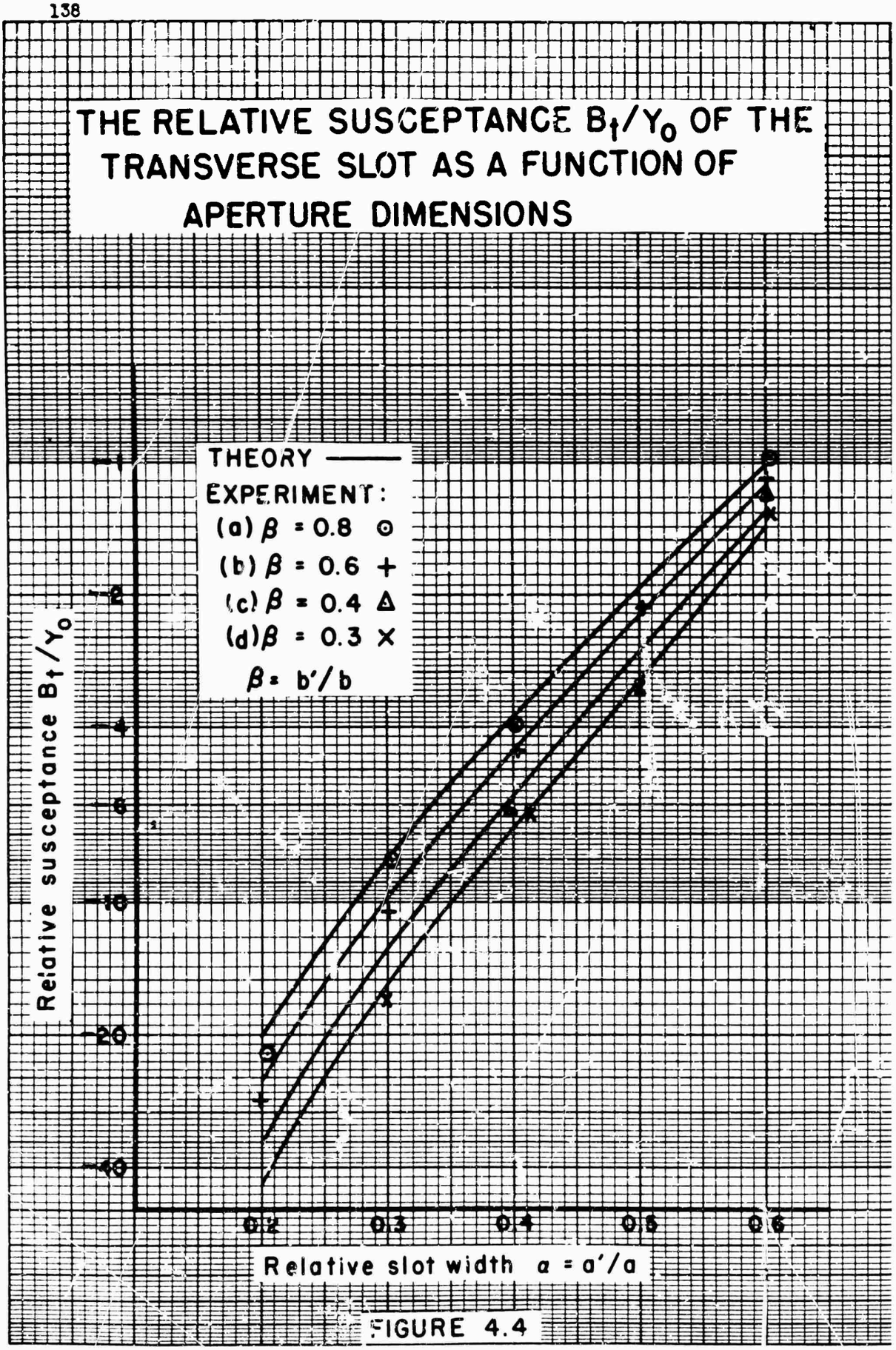
THE RELATIVE SUSCEPTANCE B_t/Y_0 OF THE TRANSVERSE SLOT AS A FUNCTION OF APERTURE DIMENSIONS
THEORY
EXPERIMENT:
(a) β = 0.8 ⊙
(b) β = 0.6 +
(c) β = 0.4 Δ
(d) β = 0.3 ×
β = b'/b
Relative susceptance B_t/Y_0
-1
-2
-4
-6
-10
-20
-40
0.2
0.3
0.4
0.5
0.6
Relative slot width $a = a'/a$

FIGURE 4.4

(3.107) and (3.108) for the appropriate ranges of a'/a and b'/b; the experimental results are taken from Table I of Chap. V of the Final Report. The theoretical data are represented by the solid lines, and the experimental data by the indicated points; both are plotted as a function of relative slot width $\alpha = a'/a$, with relative slot height $\beta = b'/b$ as a parameter. Since the values of B_t/Y_o vary over such a wide range, it is necessary to present the data on two graphs; Figure 4.3 applies for $0.6 \leq \alpha \leq 1.0$, while Figure 4.4 uses semi-log paper for the range $0.2 \leq \alpha \leq 0.6$. It is seen that over practically the whole range of slot dimensions excellent agreement is obtained.

Although the accuracy of both the theoretical and experimental data drops off for $\alpha < 0.3$, it is known from data not plotted in Figure 4.4 that the experimental data have a consistently greater absolute value than the theoretical data for slots for which $\alpha \leq 0.2$. One concludes from this that the theoretical data is reliable for $\alpha \geq 0.3$, and is questionable for slots of smaller width. The theoretical expressions were set up so as to force agreement with the accurate Waveguide Handbook[2] result for the wide-open transverse capacitive (i.e., $\alpha = a'/a = 1$) slots, so that the values of B_t/Y_o for $\alpha = 1$ will agree exactly with the Handbook results. In the integrations, however, approximations were made resulting in the accuracy dropping off slightly for $\beta > 0.9$, so that exact agreement is not obtained with the wide-open inductive (i.e., $\beta = b'/b = 1$) slot result given by the Handbook. However, the discrepancy is not at all serious, being only a few per cent over the range of α with the largest deviation occurring for α about 0.6; the Handbook values are slightly lower in absolute value. It may be noted that five of the experimental points shown in Figure 4.3 are not included in Table I of Chap. V of the Final Report, and that three of the points given there are not used in Figure 4.3. The latter points are ones which involved an error in calculation; the corrected values are plotted instead. The former points represent new data taken recently as a more complete check on the theoretical data.

A region of particular interest in Figure 4.3 is the resonant region. It is clear from the graphs that for certain values of slot dimensions a completely resonant slot can be obtained, i.e., the slot transmits all the power incident on it. This situation corresponds, of course, to $B_t/Y_o = 0$. The slot dimensions necessary for resonance are given in Figure 4.5, where the necessary relative slot width α is plotted as a function of relative slot height β. The solid curve represents the theoretical values obtained from Equations (3.107) and (3.108), while the indicated points represent experimental values. The latter are not obtained directly, but rather by interpolation of the other reported experimental data. It is seen that the agreement is excellent.

---

[2] Marcuvitz, N., "Waveguide Handbook", Chap. 5, p. 218, Vol. 10, R. L. Series, McGraw-Hill, in print.

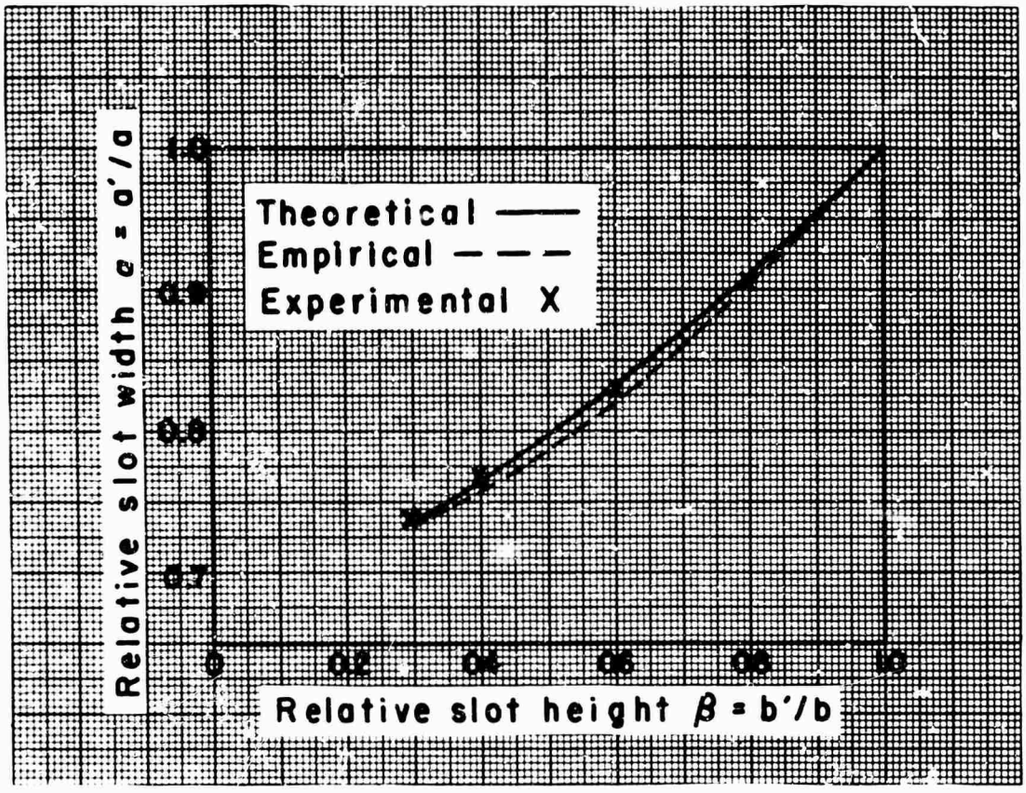

Figure 4.5 - Dimensions for resonance for the transverse slot

The dashed curve in Figure 4.5 is obtained from a well known empirical formula[3] for the dimensions for resonance. The formula is often written as

$$\frac{a}{b}\sqrt{1-\left(\frac{\lambda}{2a}\right)^2} = \frac{a'}{b'}\sqrt{1-\left(\frac{\lambda}{2a'}\right)^2} \qquad (4.1)$$

and can be rearranged as

$$\alpha^2 = \beta^2\left(\frac{\lambda}{\lambda_g}\right)^2 + \left(\frac{\lambda}{2a}\right)^2 \qquad (4.2)$$

---

[3] See, for example: Montgomery, C. G., et al., "Principles of Microwave Circuits", Chap. 6, p. 170, R. L. Series, Vol. 8, McGraw-Hill, 1948. Smullin, L. D. and Montgomery, C. G., "Microwave Duplexers", Chap. 3, p. 102, R. L. Series, Vol. 14, McGraw-Hill, 1948.

where $\alpha = a'/a$, $\beta = b'/b$. The dashed curve of Figure 4.5 was computed from Equation (4.2), and is a portion of a hyperbola. Further discussion of this hyperbola and its properties is given in the references of footnote 3. Equation (4.1) has also been given a pseudo-theoretical derivation,[4] to the effect that the characteristic impedance Z_o of rectangular waveguide is given by

$$Z_o = \sqrt{\frac{\mu}{\epsilon}} \frac{\lambda_g}{\lambda} \frac{b}{a} = \sqrt{\frac{\mu}{\epsilon}} \frac{b}{a} \frac{1}{\sqrt{1 - (\lambda/2a)^2}} \qquad (4.3)$$

Then, if a waveguide of cross-section dimensions a and b joins a second waveguide of cross-section dimensions a' and b' but with the same value of Z_o as given by definition (4.3), it is stated that no reflection will occur at the junction. Finally, application is made to the case of the slot by considering it as composed of two junctions separated by a slot guide of negligible length. Equating the Z_o values for the main and the slot guides according to (4.3) yields Equation (4.1).

Now, in the first place, even if (4.3) correctly and uniquely specified the Z_o of the waveguide, this would not guarantee a resonant junction or slot since a discontinuity is present which alters the mode form. An example of this is afforded by a junction of two coaxial lines of the same characteristic impedance (it is possible to uniquely specify this for TEM modes); such a junction is not reflectionless. In the second place, it must be emphasized that it is not possible to uniquely define characteristic impedance for a mode in a waveguide (except, of course, for a TEM mode). Hence, one must conclude that the correlation above is coincidental.

As seen in Figure 4.5, however, the empirical relation (4.2) affords a very good approximation for determining the dimensions for resonance, and in addition has the virtue of being simple in form. The largest deviation of the empirical curve from the theoretical curve is only about 2 percent. It is clear, therefore, that the empirical relation (4.2) rather than the accurate theory should be used for calculating the resonant dimensions because of the simplicity of the latter.

For the sake of convenience the theoretical values of B_t/Y_o are plotted in Figures 4.6 and 4.7 as a function of relative slot height β with relative slot width β as a parameter, in contrast to Figures 4.3 and 4.4.

---

[4] See the second reference of footnote 3. Also Slater, J. C., "Microwave Transmission", Chap. IV, pp. 184 - 6, Mc Graw-Hill, 1942.

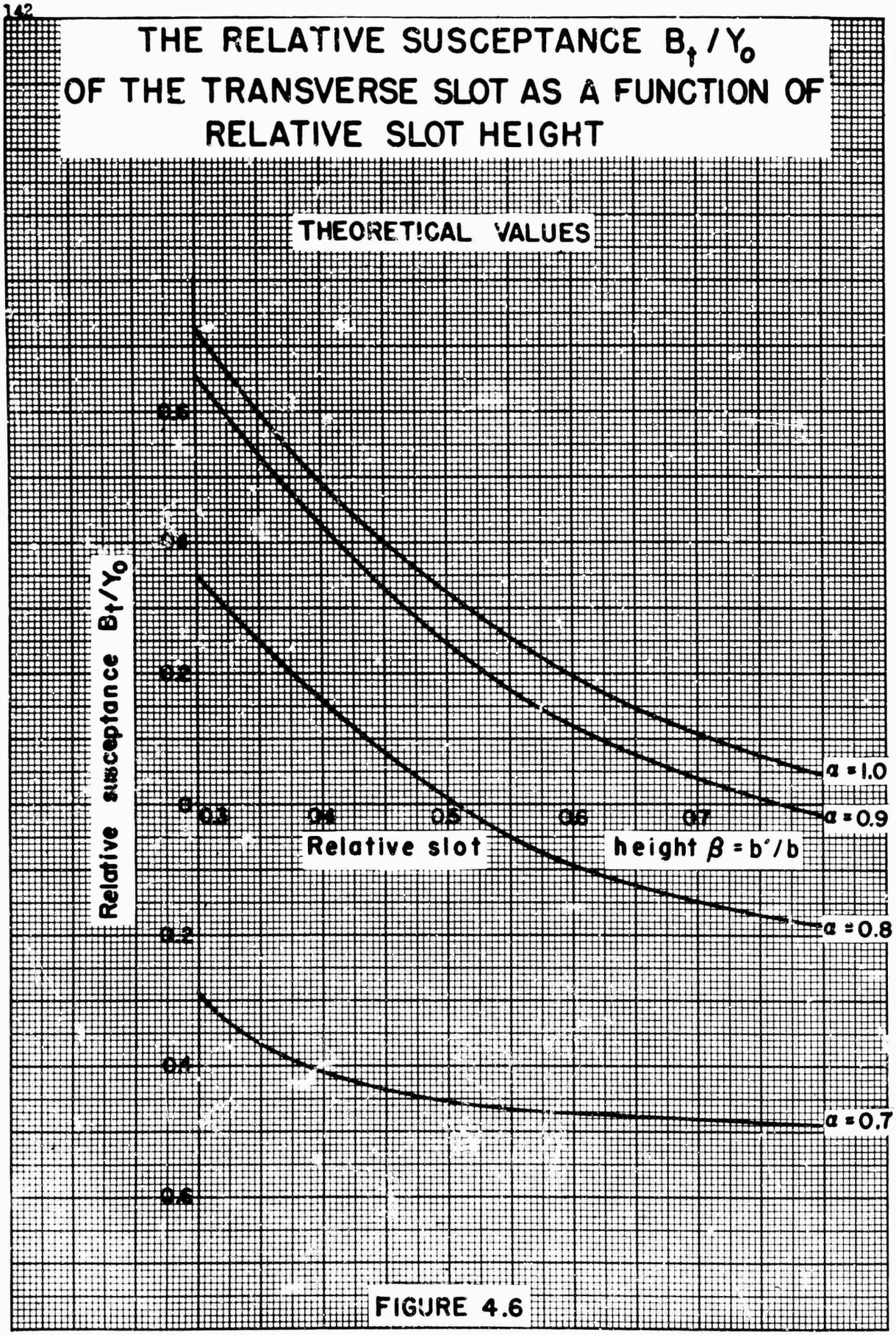
THE RELATIVE SUSCEPTANCE B_t / Y_o
OF THE TRANSVERSE SLOT AS A FUNCTION OF
RELATIVE SLOT HEIGHT
THEORETICAL VALUES
Relative susceptance B_t/Y_o
0.6
0.4
0.2
0.3
0.4
0.5
0.6
0.7
Relative slot height $\beta = b'/b$
$\alpha = 1.0$
$\alpha = 0.9$
$\alpha = 0.8$
$\alpha = 0.7$

FIGURE 4.6

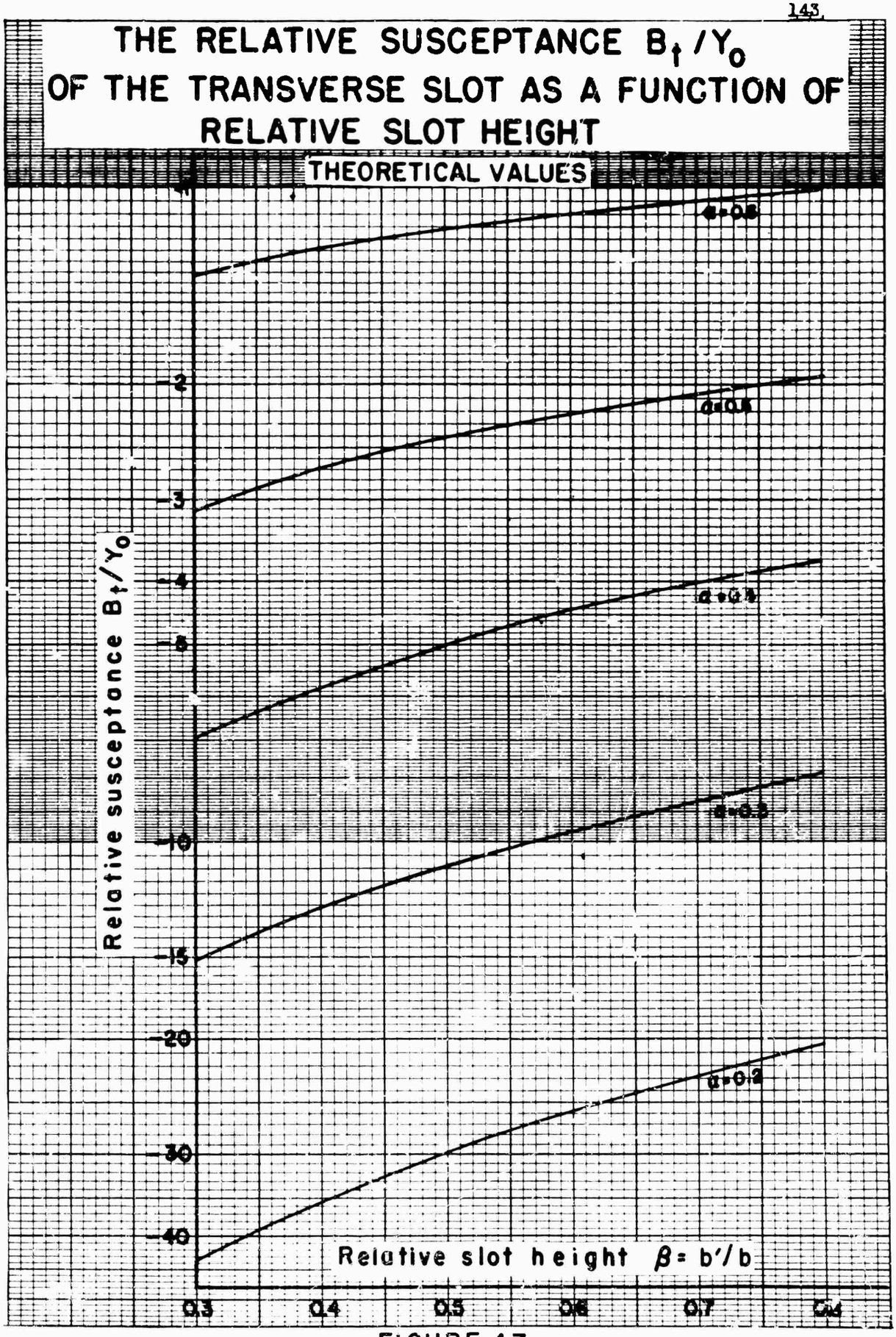
THE RELATIVE SUSCEPTANCE B_t/Y_0
OF THE TRANSVERSE SLOT AS A FUNCTION OF
RELATIVE SLOT HEIGHT
THEORETICAL VALUES
Relative susceptance B_t/Y_0
-1
-2
-3
-4
-5
-10
-15
-20
-30
-40
a=0.05
a=0.1
a=0.2
a=0.3
a=0.2
Relative slot height $\beta = b'/b$
0.3
0.4
0.5
0.6
0.7
0.4

FIGURE 4.7

The values for $\beta = 1.0$ are taken from the Waveguide Handbook;[5] the remainder of the curves from Equations (3.107) and (3.108). The use of Figures 4.3, 4.4, 4.6 and 4.7 permit one to obtain the value of B_t/Y_o for an arbitrary slot size with fair accuracy by interpolation of these graphs, without the necessity of computing the values. It must be recalled that these curves are valid at 3.20 cms. only; for other frequencies one must use Equation (3.107) or (3.108).

A comparison between theoretical and experimental results for the transverse slot has already been given in the Final Report, in Chap. I. The theoretical data given there are based upon results obtained variationally, but with the use of the free space dyadic spatial susceptance rather than the waveguide one. A better approximation is also given there involving corrections to the free space spatial susceptance. However, the theoretical results quoted in this report are considerably superior to those given in the Final Report, and should completely supersede them.

2) The Transverse Radiating Slot

The transverse radiating slot couples rectangular waveguide to a half space in such a way that radiation occurs from the end of the waveguide. For the measurements, the waveguide was terminated by an "infinite" plane baffle, and the radiation was directed into a region surrounded by absorbing walls. The mounting of the slots between the guide and the "infinite" plane was accomplished by means of a vacuum chuck. The details of the experimental arrangement have been described in the Final Report, Chap. IV, pp. 13-15. As was the case for the transverse slot located within the guide, the experimental results were obtained for slots of 0.005" wall thickness, while the theoretical results were computed for zero-thickness slots. In fact, as described in the Final Report, the same slots were used except for certain modifications.

The physical structure and the equivalent circuit for a zero-thickness slot are shown in Figure 4.8. As is seen, the equivalent circuit is a two terminal one, involving simply a conductance and a susceptance, at the reference plane T corresponding to the plane of the slot itself. The notation for the slot dimensions is that given in Figure 4.2 for the transverse slot. The slots considered are centered, oriented parallel to the edge, and of negligible thickness. Thick slots of this type are considered later in this report. Since the equivalent circuit is two terminal, the measurements are of a single point nature and cannot utilize the averaging procedure available for four terminal structures where a whole series of points are taken. That is, the input admittance only is needed, and that is obtained directly from the knowledge of the V.S.W.R. and the location of

---

[5] loc. cit., Chap. 5, p. 221

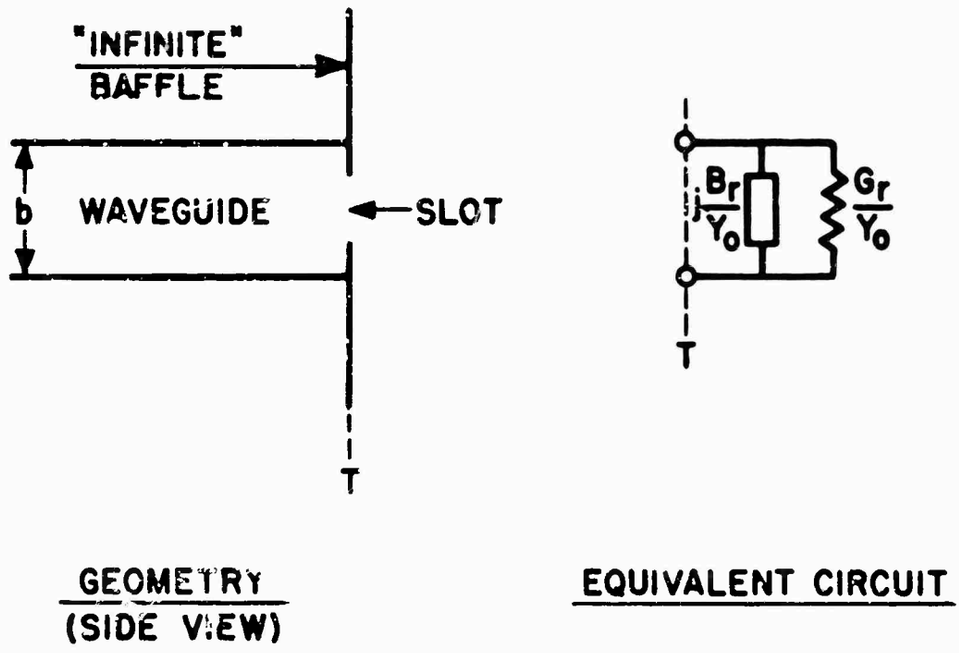

Figure 4.8 - The transverse radiating slot

the voltage minimum. The point nature of the data does not enable one to estimate the error of individual results, and the ± values attached to some of the results are obtained simply by repetition of the measurements. Furthermore, the results for the transverse radiating slot are therefore expected to be less accurate than those for the transverse slot within the guide. The experimental results, together with a further discussion of the measurement procedure and the possible errors involved, has been given in the Final Report, Chap. V, pp. 20-23.

Since the actual slots had finite thickness, the question arises as to what reference plane corresponds to the "plane of the slot". The form of the equivalent circuit is not affected by the choice of reference plane although the parameter values are. If the slot is thick enough a different treatment is preferable; this latter method is discussed in Sec. B of this part. It turns out here that the 0.005" thickness is so small that a shift of that magnitude in the reference plane produces a change in the input admittance of the order of the error in repeated measurements. Rigorously, however, the reference plane T, for the reported experimental data, coincides with the face of the slot in contact with the waveguide. This reference plane occurs naturally in the measurements as it is also the end of the slotted section.

The theoretical expressions for the admittance parameters are summarized in Sec. E, 3) of part III of this report. It is there pointed out that the variational expression breaks up naturally into two parts, one corresponding to the waveguide region and the other corresponding to the half space. The relative susceptance term then consists of a half space contribution given in the section referred to above, and a waveguide contribution equal to one-half of the relative susceptance B_t/Y_o of a transverse slot located within the waveguide. Comparison with experiment indicates that good agreement is obtained with this formulation; however, a slightly better agreement results when one takes the waveguide contribution to be 0.45, rather than 0.50, times B_t/Y_o. There seems to be no clearcut theoretical reason for this; it may be that the slot field for a slot within the guide is somewhat different from that for a slot radiating from the end of the guide. However, since the expression was variational, the effect of this difference should not be appreciable. It may be that at other frequencies the factor 0.50 is preferable. The theoretical data given in this section assumes the factor 0.45, so that

$$\frac{B_r}{Y_o} = \frac{B_h}{Y_o} + 0.45 \frac{B_t}{Y_o} \tag{4.4}$$

where the notation has been discussed in part III. It is stressed, however, that the effect of the alteration in the factor for B_t/Y_o is slight in any case; for certain ranges of α (for which B_t/Y_o is near resonance) the effect is, of course, negligible.

The expression for the relative conductance G_r/Y_o contains a contribution from the half space only. It is shown in Sec. D, 4) of part III the the theoretical result obtained for G_r/Y_o must be greater than the correct value provided that the integrations are carried through exactly. The correct value would be obtained if the trial slot field used was the actual one. Different expressions for B_r/Y_o and G_r/Y_o are applicable for different ranges of slot dimensions; these are given in Sec. E of part III as mentioned above. A simpler, although approximate, expression for G_r/Y_o, applicable over the complete range of slot dimensions, is also given. This latter expression yields values lower than the more accurate expression, but these values are in error by less than 10 percent at most. This largest error occurs for the wide open slot; for smaller slots the error rapidly decreases. In addition, there are available very simple and accurate expressions for G_r/Y_o and B_h/Y_o (see Equation (4.4)) for a half-wavelength slot, i.e., a slot with width $a' = \lambda/2$. These expressions are given by Equations (3.114) and (3.117).

THE RELATIVE SUSCEPTANCE B_r / Y_0 OF THE TRANSVERSE RADIATING SLOT AS A FUNCTION OF APERTURE DIMENSIONS

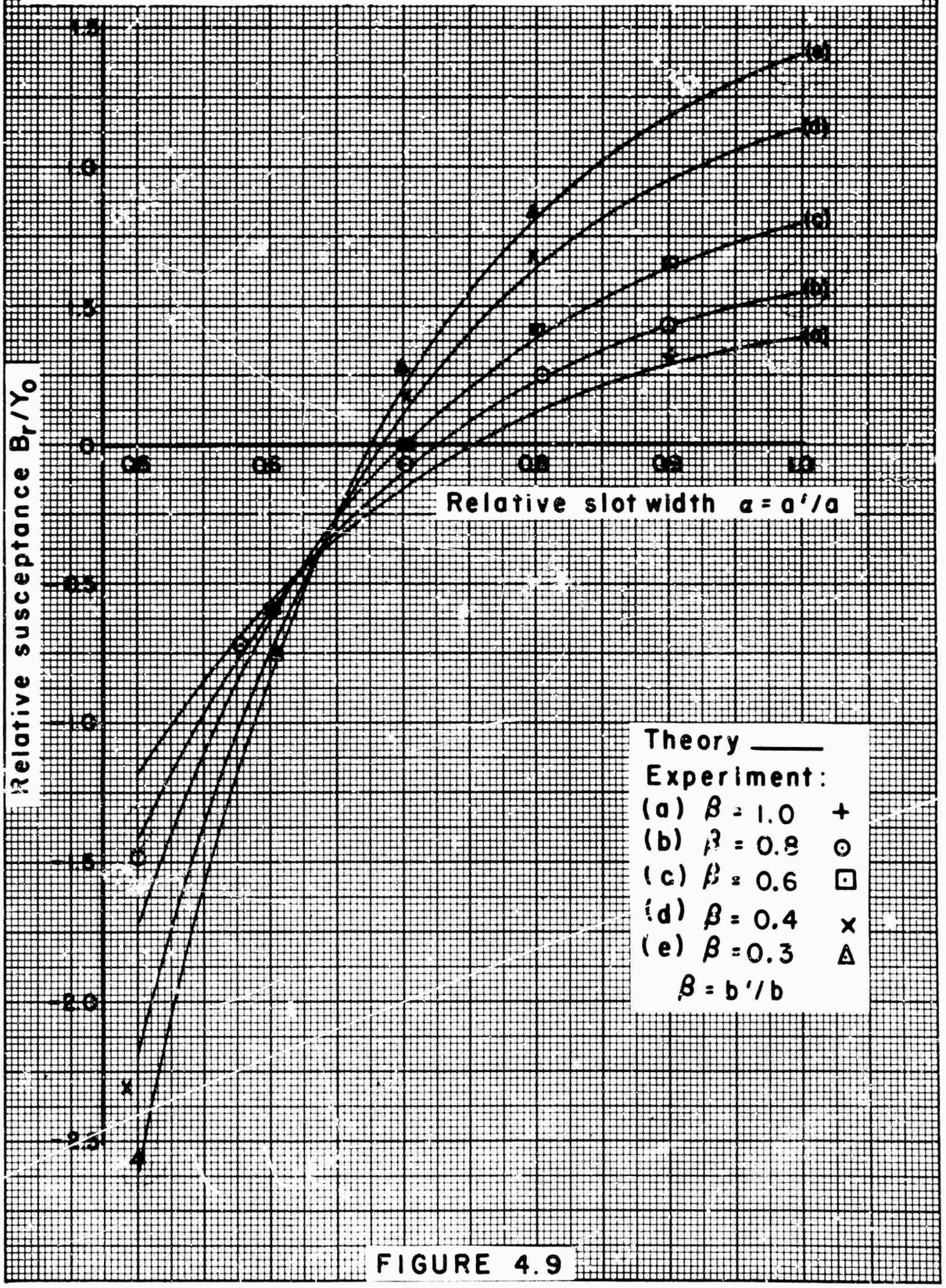

FIGURE 4.9

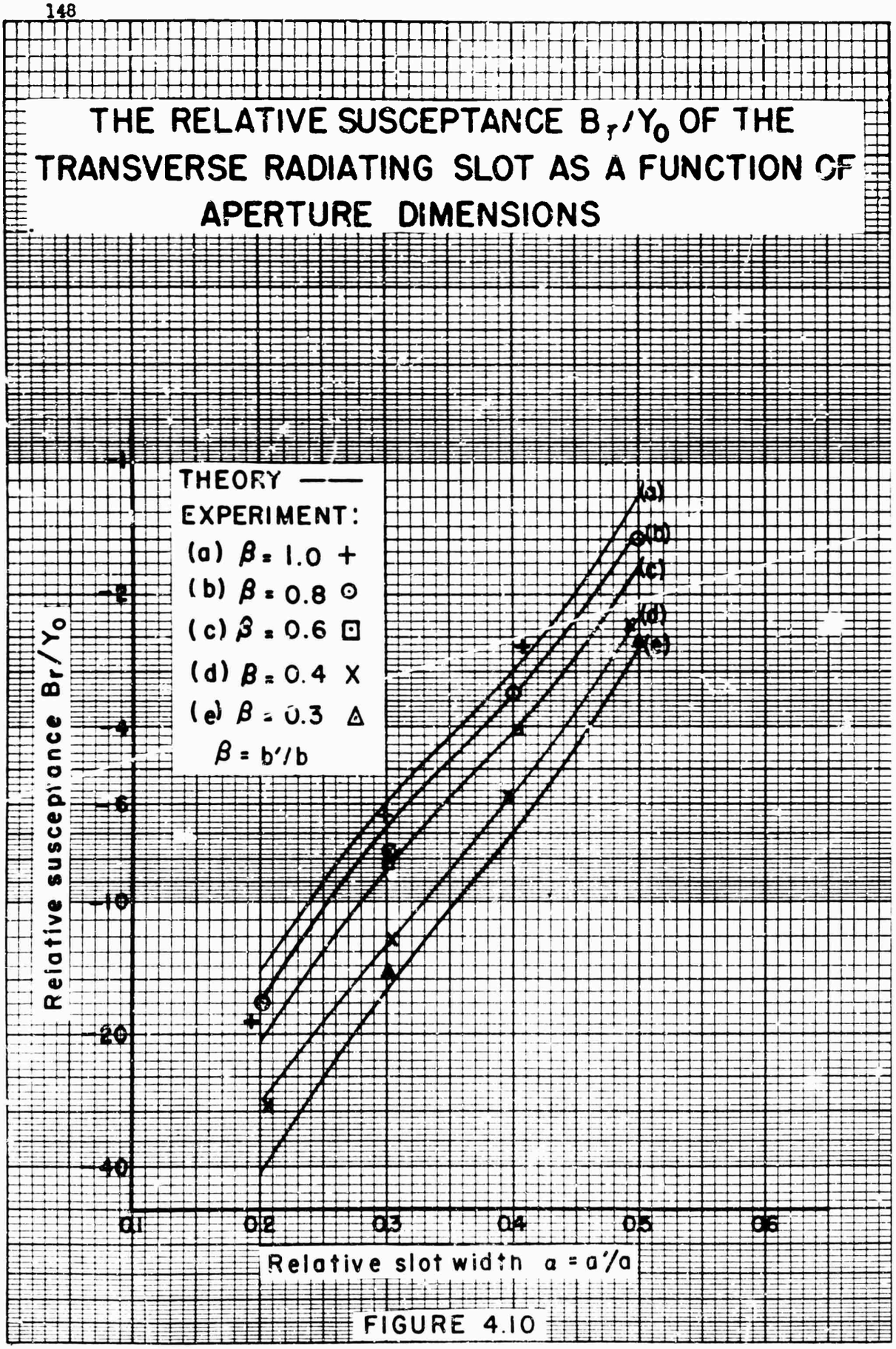
THE RELATIVE SUSCEPTANCE B_r/Y_0 OF THE TRANSVERSE RADIATING SLOT AS A FUNCTION OF APERTURE DIMENSIONS
THEORY ——
EXPERIMENT:
(a) β = 1.0 +
(b) β = 0.8 ⊙
(c) β = 0.6 ⊡
(d) β = 0.4 X
(e) β = 0.3 △
β = b'/b
Relative susceptance Br/Y0
-4
-6
-10
-20
-40
0.1
0.2
0.3
0.4
0.5
0.6
Relative slot width α = a'/a

FIGURE 4.10

A comparison of theoretical and experimental results for the susceptance B_r/Y_o (relative to the characteristic admittance of the waveguide) of the transverse radiating slot is given graphically in Figures 4.9 and 4.10. The theoretical results are obtained from Equations (3.112), (3.113), and (3.107), (3.108), using Equation (4.4), for the appropriate ranges of a'/a and b'/b; the experimental results are taken from Table VI of Chap. V of the Final Report. A rough guide for which theoretical expression for B_r/Y_o to use for which range of slot dimensions is the following: Equation (3.112) when $b'/a' > 1$, Equation (3.113) when $b'/a' < 1$. A more careful guide is afforded by the graph of Figure 4.11. The dashed line indicates the value $b'/a' = 1$; the lined portion corresponds to a region for which neither expression is accurate, although there Equation (3.112) is the somewhat better one. For Figure 4.10, the theoretical results corresponding to the lined region were obtained by estimating from neighboring data. The theoretical data of Figures 4.9 and 4.10 are represented by solid lines, and the experimental data by the indicated points; both are plotted as a function of relative slot width $\alpha = a'/a$, with the relative slot height $\beta = b'/b$ as a parameter. Since the values of B_r/Y_o vary over such a wide range, it is necessary to present the data on two graphs; Figure 4.9 applies to the range $0.5 \leq \alpha \leq 1.0$, while Figure 4.10 uses semi-log paper for $0.2 \leq \alpha \leq 0.5$. It is seen that practically over the whole range of slot dimensions excellent agreement is obtained.

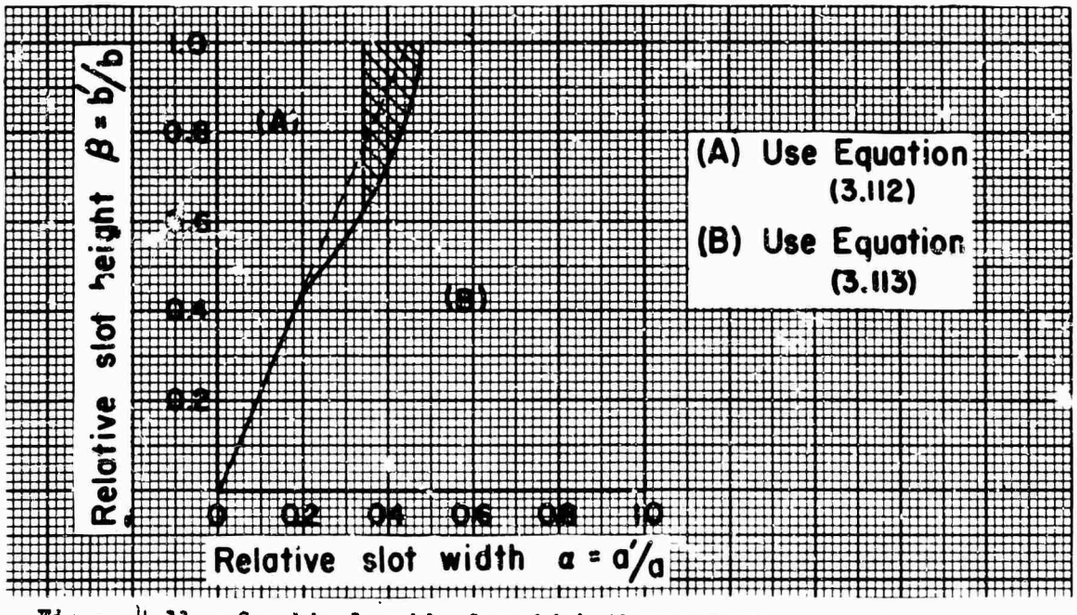

Figure 4.11 - Graphical guide for which theoretical expression to use.

The cross-over region for the curves in Figure 4.9 is seen to occur for α approximately equal to 0.63, as opposed to the case of the transverse slot within the guide (see Figure 4.3), where the cross-over region occurs near $\alpha = 0.67$. In addition, the susceptance value at the cross-over region is smaller in absolute value for the radiating slot. A comparison of Figures 4.9 and 4.3 indicates that the radiating slot is more capacitive in content than the slot within the guide; a consequence of this is that a slot for which $b' = b$ is always inductive if the slot is located within the guide, but may be either inductive or capacitive if the slot is radiating from the end of the guide. A slot for which $a' = a$ is always capacitive in both locations. A comparison of Figures 4.10 and 4.4 indicates great similarity in the behavior of small slots located within the guide and on the end of the guide. The susceptance of the radiating slot is somewhat smaller in absolute value in this range; for very small slots the susceptances of the slots in the two locations become equal.

In order to facilitate the determination of values of B_r/Y_0 for an arbitrary slot size by interpolation of graphs rather than by computation, the graphs of Figures 4.12 and 4.13 are given. In these graphs B_r/Y_0 is plotted as a function of relative slot height β, with relative slot width α as a parameter, in contrast to Figures 4.9 and 4.10.

A comparison of theoretical and experimental results for the relative conductance G_r/Y_0 of the transverse radiating slot is given graphically in Figure 4.14. The theoretical results are obtained from Equations (3.115) and (3.116) for the appropriate ranges of a'/a and b'/b; the experimental results are taken from Table VI of Chap. V of the Final Report. The theoretical data is again represented by the solid lines, and the experimental data by the indicated points; both are plotted as a function of relative slot width α, with relative slot height β as a parameter. It is seen that the conductance values do not extend over a wide range; they vary approximately from 0.65 to 0.90 over the whole range of slot dimensions. (Note that the ordinate scale does not extend to the origin.) No experimental values are given for α less than 0.6 because of the very low accuracy obtained there. In that range the conductance values are almost completely masked out by the susceptance values, which become large in absolute value for small α. Even in the range for which conductance values are reported, the accuracy of the experimental results is not high enough to afford a careful check on the theoretical calculations. This is largely due to the fact that the accuracy is limited because of the single point nature of the measurements. If the experimental values were perfectly accurate, and if the integrations for the

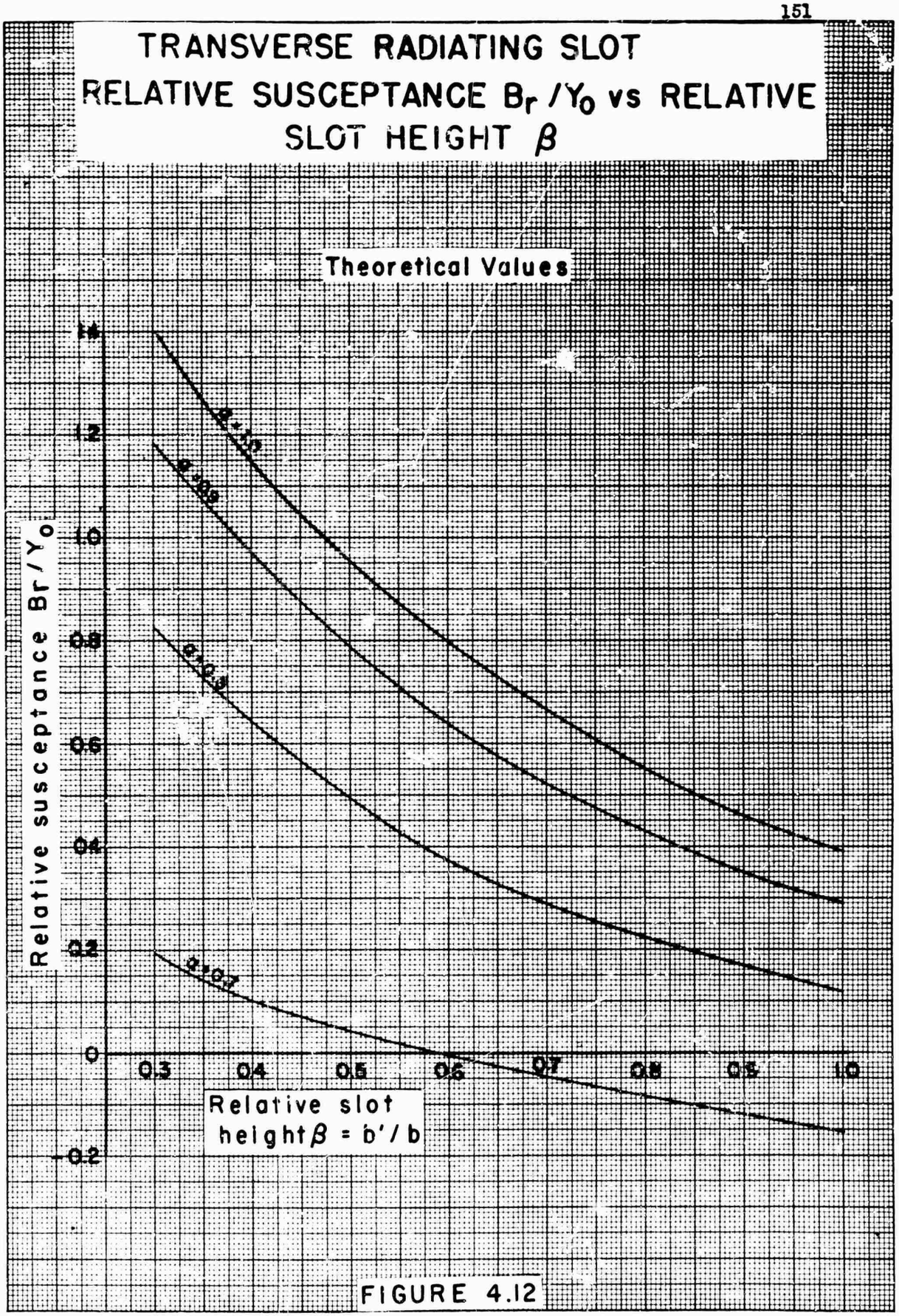
TRANSVERSE RADIATING SLOT
RELATIVE SUSCEPTANCE B_r / Y_0 vs RELATIVE SLOT HEIGHT β
Theoretical Values
Relative susceptance Br / Yo
1.4
1.2
1.0
0.8
0.6
0.4
0.2
0
-0.2
0.3
0.4
0.5
0.6
0.7
0.8
0.9
1.0
Relative slot height β = b' / b

FIGURE 4.12

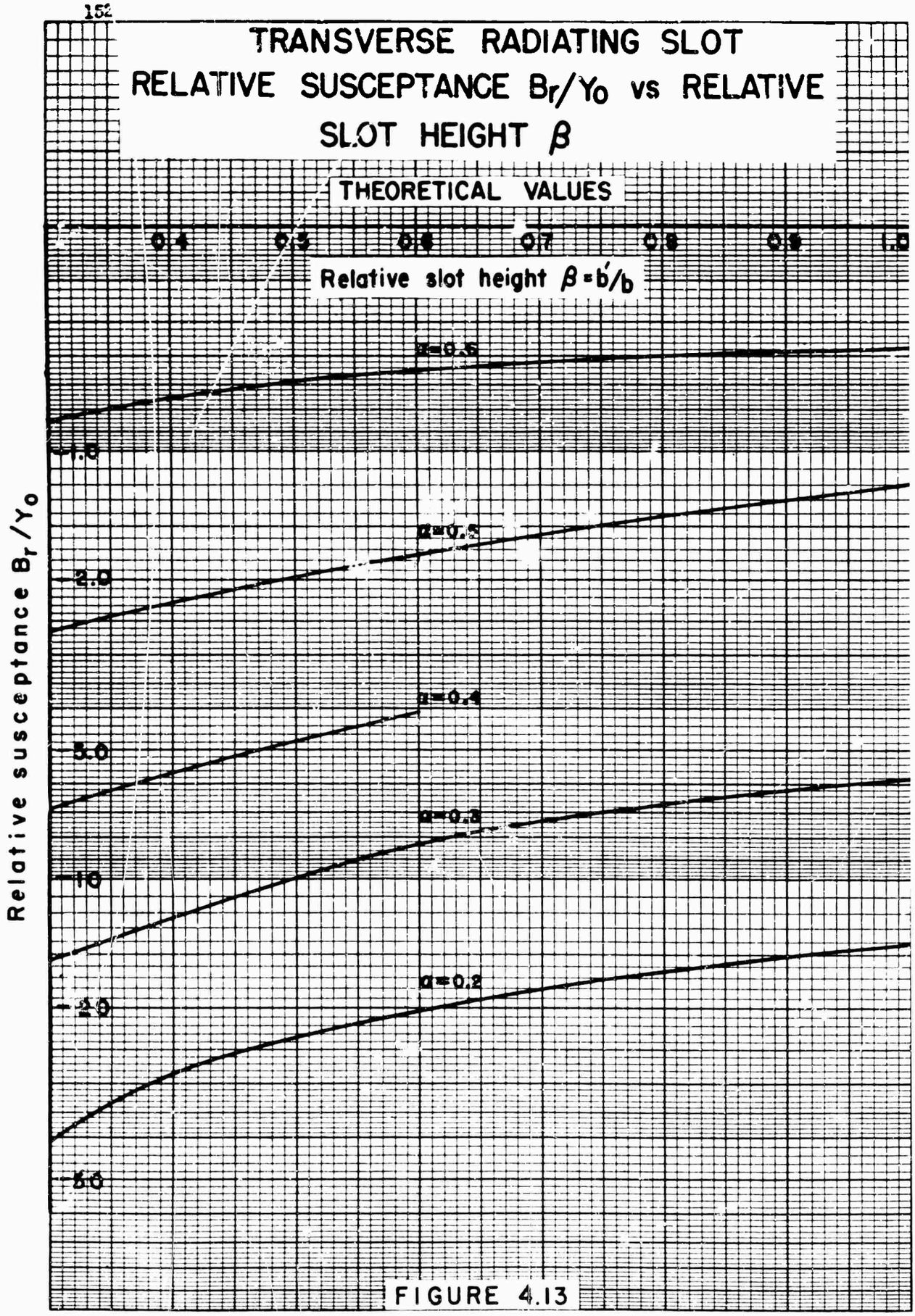
TRANSVERSE RADIATING SLOT
RELATIVE SUSCEPTANCE Br/Yo vs RELATIVE
SLOT HEIGHT β
THEORETICAL VALUES
0.4
0.5
0.6
0.7
0.8
0.9
1.0
Relative slot height β = b'/b
Relative susceptance Br/Yo
α=0.5
α=0.3
α=0.2
1.0
2.0
5.0
10
20
50

FIGURE 4.13

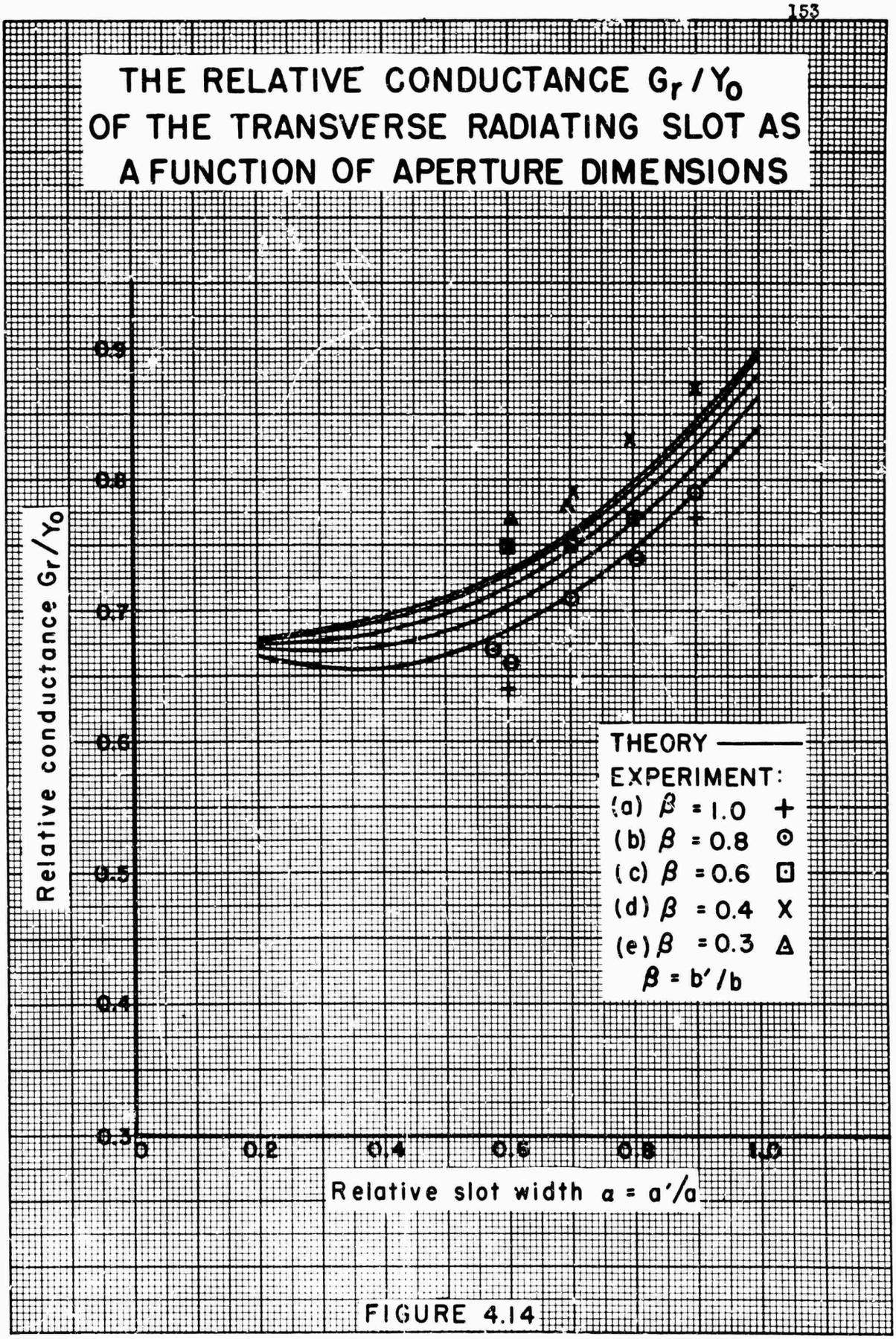
THE RELATIVE CONDUCTANCE G_r / Y_0 OF THE TRANSVERSE RADIATING SLOT AS A FUNCTION OF APERTURE DIMENSIONS
Relative conductance G_r/Y_0
0.9
0.8
0.7
0.6
0.5
0.4
0.3
0
0.2
0.4
0.6
0.8
1.0
Relative slot width $\alpha = a'/a$
THEORY
EXPERIMENT:
(a) β = 1.0 +
(b) β = 0.8 ⊙
(c) β = 0.6 ⊡
(d) β = 0.4 X
(e) β = 0.3 △
$\beta = b'/b$

FIGURE 4.14

theoretical expressions were carried out exactly, the experimental points would lie slightly below the theoretical curves due to the minimum property for the conductance. However, for some values of β this does not seem to be the case; an incorrect field choice cannot account for this as then the theoretical values would be raised further. One then suspects either the integrations or the measurements, but neither seem to be inadequate enough to produce this effect, and the actual reason is still undetermined. However, the practical effect of this is insignificant as the theoretical and experimental values agree to better than 5 percent or so. The theoretical expressions are therefore quite adequate for engineering applications.

3.) The Slot-coupled E Plane Tee

The geometry of the slot-coupled E plane Tee is indicated in the drawings of Figure 4.15. It is noted that two sets of reference planes are indicated: T_1, T_2 and T_3, and T_1', T_2' and T_3'. The former are the "centerline" reference planes and are those at which the theoretical data are reported; the latter, the primed reference planes, are the "invariant" ones and are those at which the experimental data are obtained. The equivalent circuit representation chosen for depicting the theoretical results is thus called the "centerline" representation and is given in Figure 4.16-(a). At the invariant reference planes this equivalent circuit simplifies to that shown in Figure 4.16-(b); this latter circuit is called the "invariant" representation. The invariant representation not only has the virtue of being simpler but in addition forms the basis for a precision measurement method. The advantages of utilizing the invariant representation in obtaining experimental data is discussed in part I; the details of the corresponding precision measurement method are given in part II, Sec. A, 2. In the discussion below, the experimental data will be given first, and will be followed by a consideration of the theoretical results and a comparison between the theoretical and experimental data.

The invariant equivalent circuit representation, the measurement method used to obtain the precision experimental data, and the various experimental techniques involved in altering the slot size, mounting the slot structure, etc., are all discussed in Sec. A of part II. All of the input data were corrected for the presence of the end of the slot in the slotted section, using a calibration curve for the slotted section. Since the theoretical data applies to a zero-thickness slot, the slot wall thickness was made as small as feasible. A 0.010" wall thickness was finally decided on; any smaller thickness resulted in a buckling of the slot. Measurements were taken for the following range of slot sizes: the relative slot width $\alpha = a'/a$ was varied in steps of a tenth from 0.3 to 1.0 for the values of relative slot height $\beta = b'/b$ equal to 0.3, 0.6 and 1.0 (see Figure 4.15 for the notation). The slot dimensions were altered by increasing the slot width while maintaining the slot height constant.

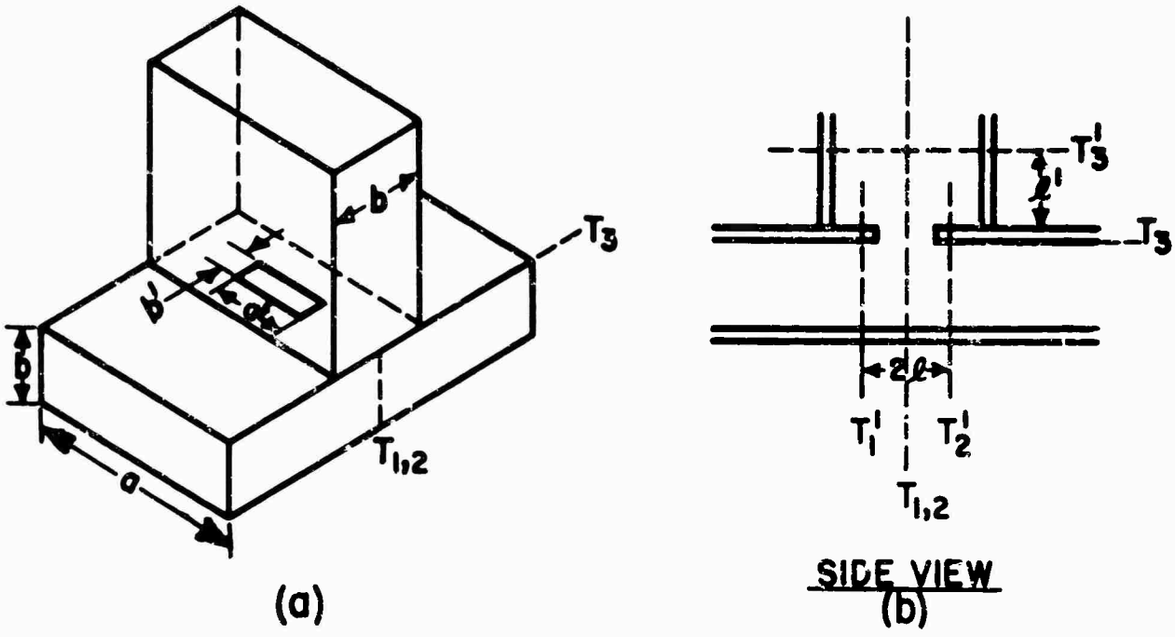

Figure 4.15 - Geometry of the slot-coupled E plane Tee.

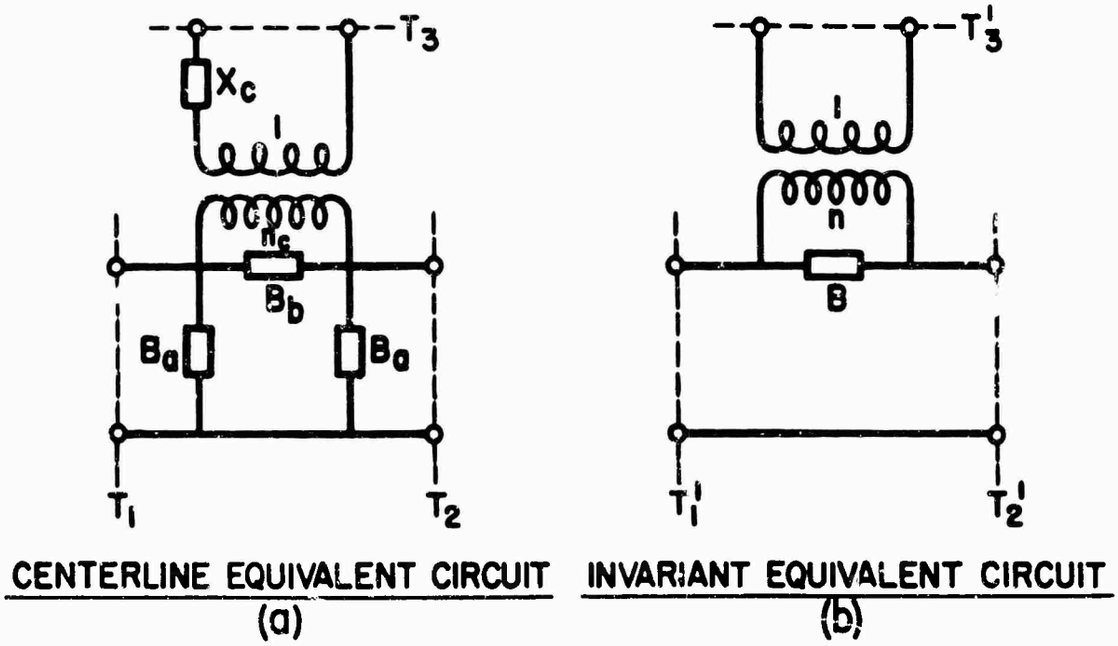

Figure 4.16 - Equivalent circuit representations for the slot-coupled E plane Tee.

The parameters of the invariant representation (see Figure 4.16-(b)) are B/Y_o, n , 2ℓ and ℓ' ; the latter two specify the location of the reference planes. An additional advantage obtained by using the invariant representation is that estimates can be made in a simple fashion of the error in the final parameter values in terms of the probable errors in the initial data. Expressions for estimating such errors for the slot-coupled E plane Tee are given in Table 4-I. The notation involved is that employed in the tangent relation method; the details of this notation, including similar expressions for estimates of error for the transverse slot, have been given in the Final Report, Chap. II. The experimental results for the parameter values discussed above are listed in Table 4-II. The $\pm$ values associated with the data are estimated using the expressions of Table 4-I.

TABLE 4-I

SLOT-COUPLED E PLANE TEE

Estimates of Error

The final parameters in terms of the data parameters are:

$$B/Y_o = \frac{\alpha\,(1 - \gamma^2)}{\alpha^2 + \gamma^2}$$

$$n^2 = \frac{\alpha^2 + \gamma^2}{(-\gamma)(\alpha^2 + 1)}$$

$$2\ell = \lambda_g \left[L \pm \frac{n}{2} + (D_{OC} - D_R)/\lambda_{gD} + (S_{OC} - S_R)/\lambda_{gS2} \right]$$

$$\ell' = \lambda_g \left[L_3 \pm \frac{m}{2} + (S_{SC3} - S_{R3})/\lambda_{gS3} \right]$$

$$\ell' = \lambda_g \left[L_3 \pm \frac{p}{2} + (S_O - S_{R3})/\lambda_{gS3} - s_o/\lambda_{gS3} \right]$$

where:

α = $\cot \beta \ (D_{OC} - D_O)$

β = $2\pi/\lambda_{gD}$

D_{OC} = value of D when no power flows in the stub guide

S_{OC} = value of S_2 when no power flows in the stub guide

D_R = value of D when a short circuit occurs at the end of the slotted line

$S_{R2,3}$ = value of $S_{2,3}$ when $D = D_R$

L = electrical length of the main guide (length/guide wavelength)

$L_{2,3}$ = electrical length of the stub guide (length/guide wavelength)

λ_g = guide wavelength in the arms of the Tee

λ_{gD} = guide wavelength in the slotted line

$\lambda_{gS2,3}$ = guide wavelength in the variable short on arm 2, 3.

D_o, S_o, γ = values obtained directly from the D vs. S curve

s_o/λ_{gS3} = $(1/2\pi) \tan^{-1} (\alpha/\gamma)$

n, m, p = an integer such that 2ℓ, ℓ', ℓ'' is small

The former of the two alternative expressions for ℓ' applies to a point determination; the latter occurs when the D vs. S run is used.

The most probable errors are given by:

$$\Delta B/Y_o = \sqrt{\left[\frac{\partial (B/Y_o)}{\partial \gamma} \Delta\gamma\right]^2 + \left[\frac{\partial (B/Y_o)}{\partial D_o} \Delta D_o\right]^2 + \left[\frac{\partial (B/Y_o)}{\partial D_{OC}} \Delta D_{OC}\right]^2}$$

$$\Delta n = \sqrt{\left[\frac{\partial n}{\partial \gamma} \Delta\gamma\right]^2 + \left[\frac{\partial n}{\partial D_o} \Delta D_o\right]^2 + \left[\frac{\partial n}{\partial D_{OC}} \Delta D_{OC}\right]^2}$$

$$\Delta 2\ell = \sqrt{\left[\lambda_g \Delta L\right]^2 + \left[\Delta(D_{OC} - D_R)\right]^2 + \left[\Delta(S_{OC} - S_{R2})\right]^2 + \left[(2\ell/\lambda_g)\Delta\lambda_g\right]^2}$$

$$\Delta\ell' = \sqrt{\left[\lambda_g \Delta L_3\right]^2 + \left[\Delta(S_{SC3} - S_{R3})\right]^2 + \left[(\ell'/\lambda_g)\,\Delta\,\lambda_g\right]^2}$$

The point measurement only for ℓ' has been included here. In the expressions for $\Delta 2\ell$ and $\Delta\ell'$, the ration of λ_g to λ_{gD}, λ_{gS2} and λ_{gS3} is assumed close to unity. In all of the expressions negligible error is assumed in λ_{gD}, λ_{gS2}, and λ_{gS3}. Many of the Δ's are independent of the slot size, but are a function of the accuracy of the measuring equipment. These are ΔD_{OC}, $\Delta(D_{OC} - D_R)$, $\Delta(S_{OC} - S_{R2})$, $\Delta(S_{SC3} - S_{R3})$, ΔL, ΔL_3, and $\Delta\lambda_g$; it is estimated that the first four of these and $\Delta\lambda_g$ are equal to approximately 0.001" or less, while ΔL and ΔL_3 are specified as 0.001 or less, the increased possible error arising because of the manner of covering the slot. The value of $\Delta\gamma$ is obtained directly from the ΔD vs. S error curve, while ΔD_o is the sum of a contribution from this error curve and from the 0.001" mentioned above.

The sensitivities are given as:

$$\frac{\partial (B/Y_o)}{\partial \gamma} = \left[\frac{2\,B/Y_o}{1 - \gamma^2}\right] \frac{1}{n^2}$$

$$\frac{\partial (B/Y_o)}{\partial D_{OC}} = -\frac{\partial (B/Y_o)}{\partial D_o} = \varkappa (B/Y_o)^2 \left[\frac{\gamma^2 - \alpha^2}{\gamma^2 - 1}\right]\left[\frac{\alpha^2 + 1}{\alpha^2}\right]$$

$$\frac{\partial n}{\partial \gamma} = \left[\frac{\gamma^2 - \alpha^2}{\gamma^2 + \alpha^2}\right] \frac{n}{2\gamma}$$

$$\frac{\partial n}{\partial D_{OC}} = -\frac{\partial n}{\partial D_o} = n\,\alpha\,\varkappa \left[\frac{\gamma^2 - 1}{\gamma^2 + \alpha^2}\right]$$

TABLE 4-II

SLOT-COUPLED E PLANE TEE

Experimental Results

The data correspond to the invariant equivalent circuit representation shown in Figure 4.16(b).

λ = 1.2606 inches

a = 0.900 inches , b = 0.400 inches

2ℓ and ℓ' are in inches ; all 2ℓ values are accurate to $\pm$ 0.003 inches, all ℓ' values are accurate to $\pm$ 0.002 inches.

$\alpha = a'/a$, $\beta = b'/b$; a' and b' are in inches

a'	b'	α	β	2ℓ	ℓ'	B/Y_o	n
.275	.127	.306	.317			-15.1 $\pm$ 2.0	1.20 $\pm$ .50
.368	.126	.409	.315			- 6.40 $\pm$ .40	1.11 $\pm$ .15
.461	.126	.512	.315			- 2.72 $\pm$ .11	1.06 $\pm$ .10
.544	.126	.604	.315			- 0.987 $\pm$ .012	0.99 $\pm$ .04
.722	.126	.802	.315			0.620 $\pm$ .006	1.008 $\pm$ .010
.809	.125	.899	.312			0.970 $\pm$ .01[illegible]	0.994 $\pm$ .010
.900	.125	1.000	.312			1.118 $\pm$ .020	1.012 $\pm$ .015
.276	.121	.307	.302	.0052	-.0024		
.360	.121	.400	.302	.0072	-.0049		
.448	.121	.498	.302	.0085	-.0077		
.544	.120	.604	.300	.0091	-.0116		
.632	.121	.702	.302	.0094	-.0137		
.727	.121	.808	.302	.0085	-.0125		
.810	.121	.900	.302	.0078	-.0126		
.900	.121	1.000	.302	.0065	-.0107		

TABLE 4-II (Continued)

a'	b'	α	β	2ℓ	ℓ'	B/I$_o$	n
.185	.245	.205	.612			-26 ± 14	1.22 ± 1.0
.270	.250	.300	.625			- 8.16 ± .60	1.49 ± .50
.361	.252	.401	.630			- 3.77 ± .20	1.24 ± .06
.451	.254	.501	.635			- 1.82 ± .27	1.15 ± .03
.540	.257	.600	.642			- 0.845± .030	1.065± .020
.633	.257	.703	.642			- 0.201± .020	1.005± .010
.720	.257	.800	.642			0.159± .016	0.967± .010
.810	.257	.900	.642			0.372± .020	0.958± .010
.900	.257	1.000	.642			0.480± .014	0.946± .010
.189	.237	.210	.593	.0098	-.0072		
.275	.240	.306	.600	.0176	-.0109		
.361	.240	.401	.600	.0240	-.0176		
.540	.241	.600	.603	.0331	-.0305		
.721	.241	.801	.603	.0306	-.0310		
.900	.240	1.000	.600	.0263	-.0275		
.101	.400	.112	1.000			-54 ± 22	0.9 ± 1.0
.180	.400	.200	1.000			-25 ± 5	0.94 ± .60
.270	.400	.300	1.000			- 5.65 ± .25	1.54 ± .10
.335	.400	.372	1.000			- 3.51 ± .20	1.39 ± .06
.456	.400	.507	1.000			- 1.58 ± .05	1.22 ± .03
.540	.400	.600	1.000			- 0.93 ± .05	1.086± .025
.719	.400	.799	1.000			- 0.254± .015	0.948± .010
.815	.400	.906	1.000			- 0.033± .008	0.910± .010
.900	.400	1.000	1.000			0.043± .010	0.896± .010
.280	.241	.311	.603	.0180	-.0113		
.281	.400	.312	1.000	.0327	-.0208		
.358	.400	.398	1.000	.0455	-.0341		
.449	.400	.499	1.000	.0572	-.0516		
.545	.400	.606	1.000	.0636	-.0672		
.630	.400	.700	1.000	.0645	-.0761	- 0.554± .030	0.993± .012
.734	.400	.816	1.000	.0604	-.0779		
.807	.400	.897	1.000	.0567	-.0763		
.900	.400	1.000	1.000	.0529	-.0691		

It is seen in Table 4-II that the values for 2ℓ and ℓ' correspond to a slightly different set of aperture dimensions from those for B/Y_o and n. The reason for this is that the values of 2ℓ and ℓ' corresponding to the B/Y_o and n values were obtained using length measurements which were determined mechanically. In addition, the stub guide was unsoldered then resoldered each time the slot width was changed (see part II, Sec. A, 3), resulting in a sporadically fluctuating series of values for ℓ' although the operation negligibly affected the other quantities. An additional run was therefore taken for the ℓ' and 2ℓ parameters where the length measurments were made electrically rather than mechanically, and where the slot size was altered by the use of a mandrel instead of the unsoldering technique mentioned above. The resulting values, which are the ones reported, were much more systematic, and are expected to be more accurate. Since parameters 2ℓ and ℓ' are determined essentially by point measurements, which may be made fairly rapidly, the corresponding B/Y_o and n values were not obtained since their determination requires the complete tangent relation procedure.

The data listed in Table 4-II is given graphically in Figures 4.17 to 4.21. In all of the curves the experimental points are indicated, and solid lines are drawn through the average of the indicated points. The data are plotted as a function of slot width $\alpha = a'/a$, with relative slot height $\beta = b'/b$ as a parameter. Two graphs are necessary to present the data for B/Y_o since the values vary over such a wide range; Figure 4.17 applies for $0.5 \leq \alpha \leq 1.0$, while Figure 4.18 uses semi-log paper for the range $0.3 \leq \alpha \leq 0.6$.

From Figures 4.17 and 4.18, it is seen that the behavior of B/Y_o for various aperture sizes is similar to that for B_t/Y_o and B_r/Y_o as shown in Figures 4.3, 4.4, 4.9 and 4.10. There is again a cross-over region, but it is broader than those for B_t/Y_o and B_r/Y_o and it occurs at a slightly more inductive value. For $\alpha = 1$, B/Y_o is always capacitive, while for $\beta=1$, B/Y_o is inductive over almost the whole range, being slightly capacitive for $\alpha > 0.9$; this behavior is somewhat similar to that for B_t/Y_o, which is always capacitive for $\alpha = 1$ and inductive for $\beta = 1$. However, there is a wider variation with β for B/Y_o than occurs for B_t/Y_o or B_r/Y_o.

The curves for the behavior of parameter n are given in Figure 4.19. The value of n remains substantially in the neighborhood of unity; this is an additional desirable feature of this equivalent circuit representation. Poor precision is obtained for values of relative slot width α less than 0.4; high $\pm$ values are associated with the values of n in that range in Table 4-II because the corresponding sensitivities (see Table 4-I) were large. For this reason data for $\alpha \geq 0.4$ only are plotted.

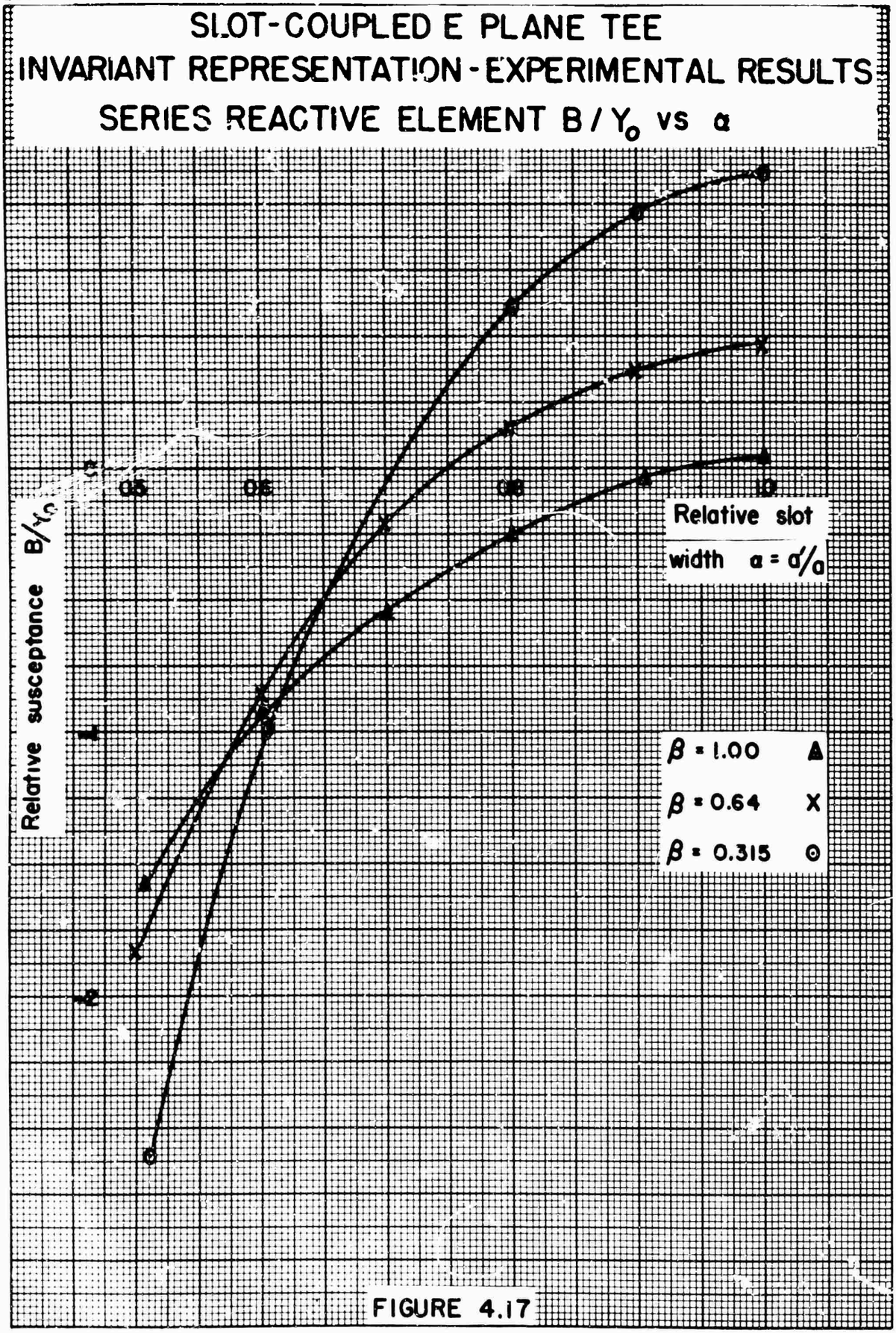
SLOT-COUPLED E PLANE TEE
INVARIANT REPRESENTATION - EXPERIMENTAL RESULTS
SERIES REACTIVE ELEMENT B / Y0 vs α
Relative susceptance B/Y0
0.5
0.6
0.8
1.0
Relative slot
width α = d/a
β = 1.00 ▲
β = 0.64 X
β = 0.315 ⊙

FIGURE 4.17

SLOT-COUPLED E PLANE TEE
INVARIANT REPRESENTATION-EXPERIMENTAL RESULTS
SERIES REACTIVE ELEMENT B / Y_0 vs a

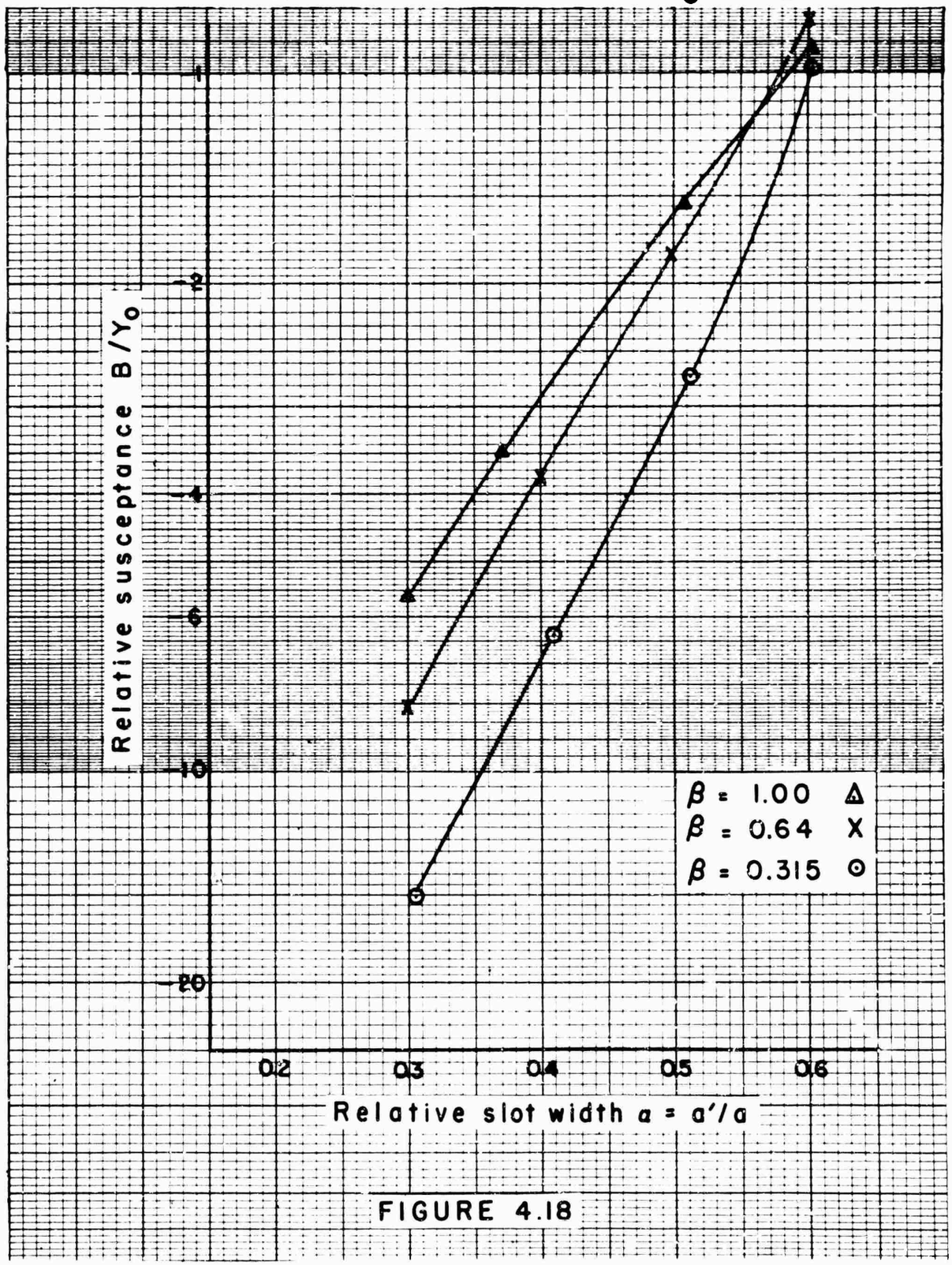

FIGURE 4.18

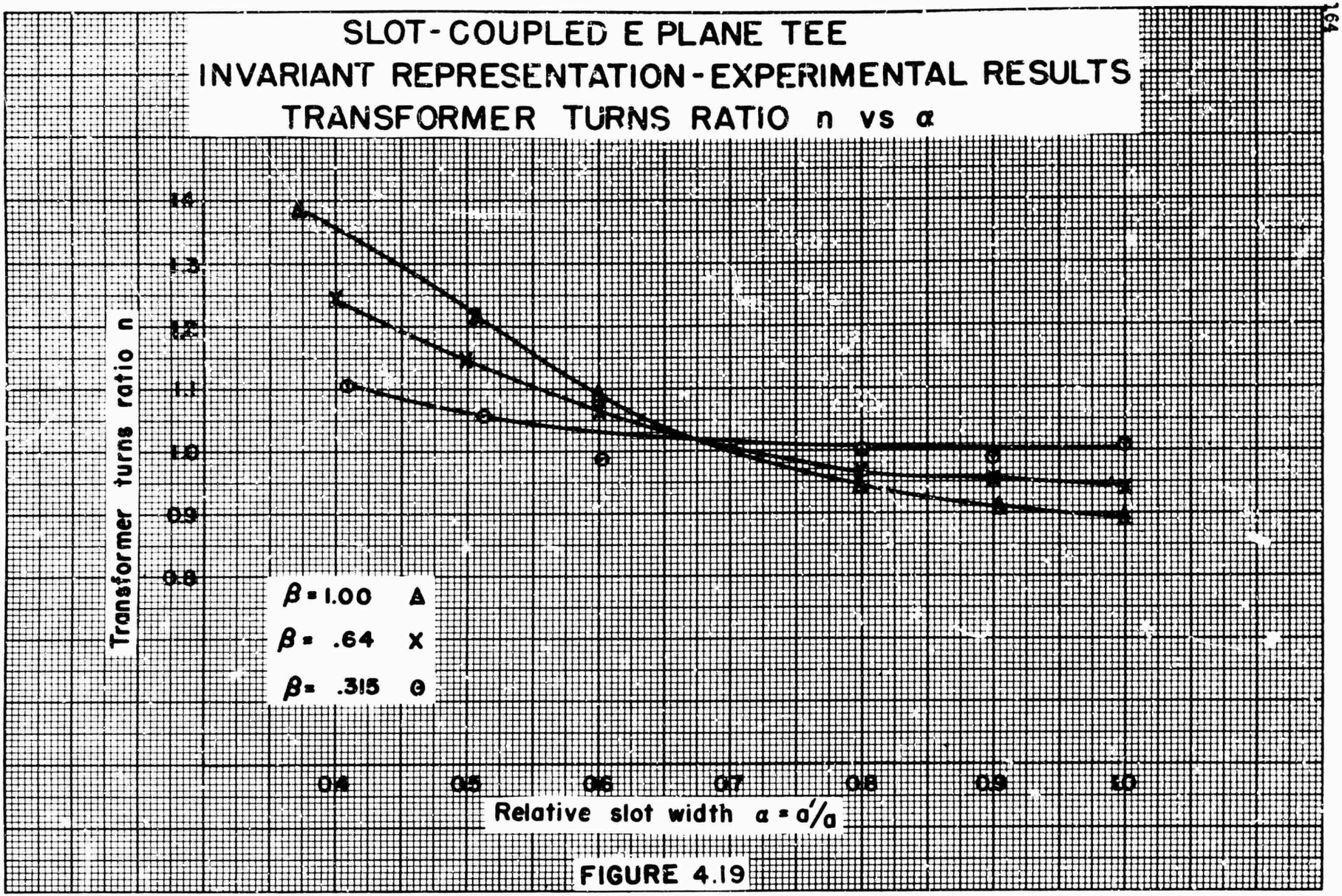
SLOT-COUPLED E PLANE TEE
INVARIANT REPRESENTATION-EXPERIMENTAL RESULTS
TRANSFORMER TURNS RATIO n vs α
Transformer turns ratio n
1.4
1.3
1.2
1.1
1.0
0.9
0.8
β = 1.00 A
β = .64 X
β = .315 0
0.4
0.5
0.6
0.7
0.8
0.9
1.0
Relative slot width α = a'/a

FIGURE 4.19

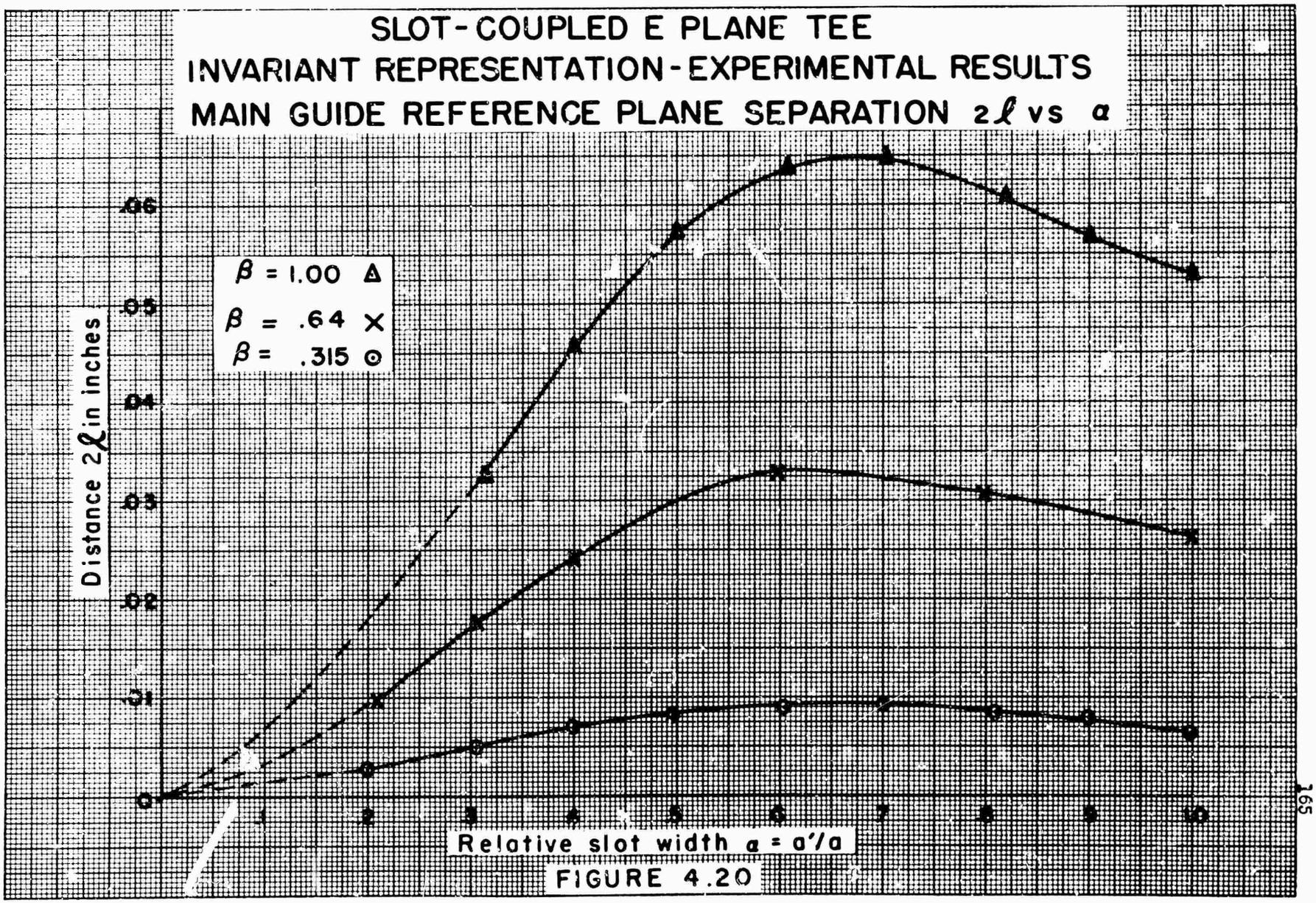
SLOT-COUPLED E PLANE TEE
INVARIANT REPRESENTATION-EXPERIMENTAL RESULTS
MAIN GUIDE REFERENCE PLANE SEPARATION 2ℓ vs α
β = 1.00 Δ
β = .64 ×
β = .315 ⊙
Distance 2ℓ in inches
.06
.05
.04
.03
.02
.01
0
1
2
3
4
5
6
7
8
9
10
Relative slot width α = a'/a

FIGURE 4.20

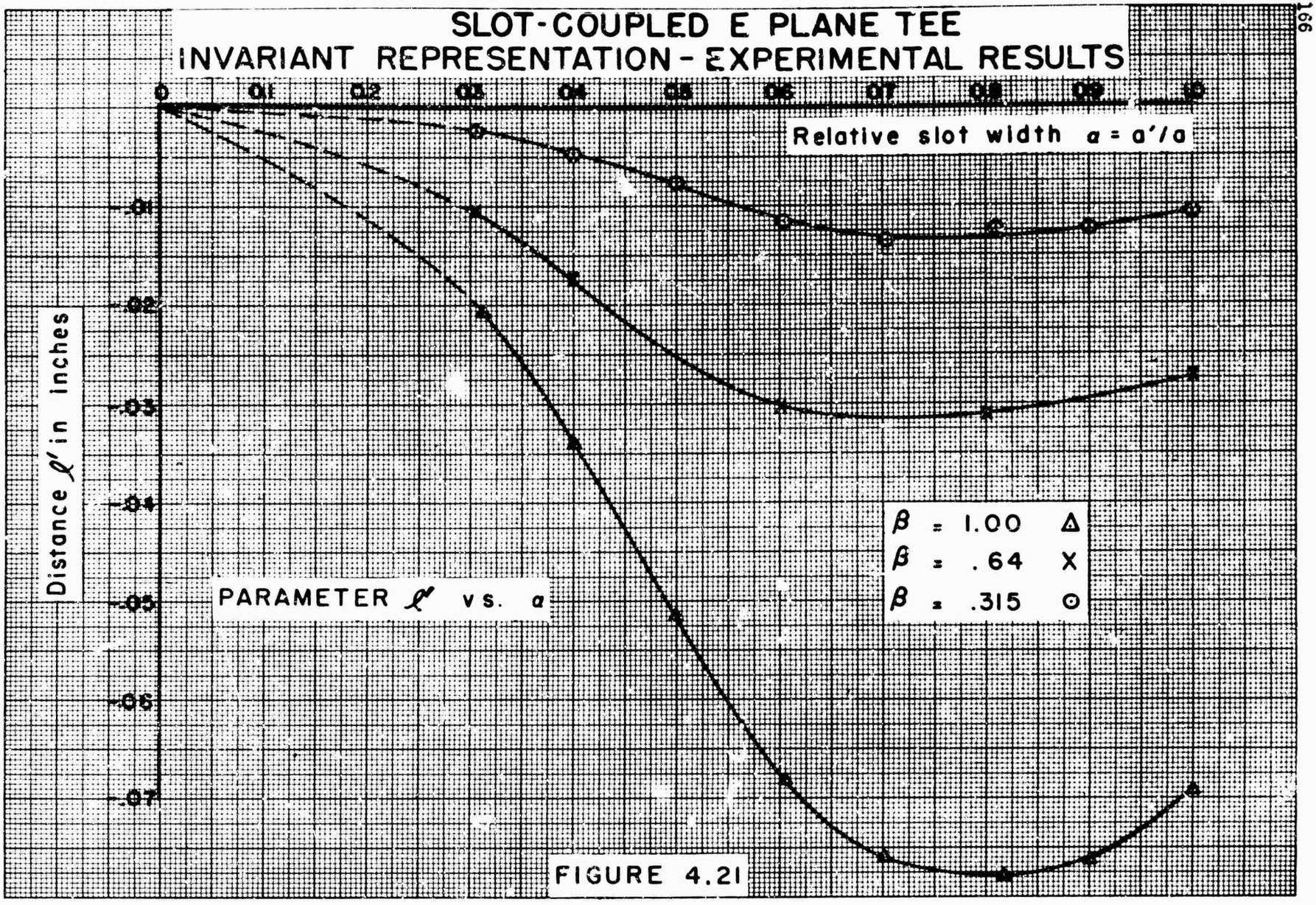
SLOT-COUPLED E PLANE TEE
INVARIANT REPRESENTATION - EXPERIMENTAL RESULTS
0
0.1
0.2
0.3
0.4
0.5
0.6
0.7
0.8
0.9
1.0
Relative slot width a = a'/a
-.01
-.02
-.03
-.04
-.05
-.06
-.07
Distance ℓ' in inches
PARAMETER ℓ' vs. a
β = 1.00 Δ
β = .64 X
β = .315 ⊙

FIGURE 4.21

The values of 2ℓ and ℓ', which locate the reference planes for the equivalent network, are plotted in Figures 4.20 and 4.21. The values of 2ℓ are seen to be always positive, while those for ℓ' are always negative; both are small in absolute value, being less than 0.08" at all times. This means that the reference planes are never displaced from the centerline reference planes by more than 5 percent of a guide wavelength. An error in the electrical lengths L or L_3 of $\pm$ 0.001" to 0.002" is possible (see Table I), resulting in estimated possible errors of $\pm$ 0.003" in 2ℓ and $\pm$ 0.002" in ℓ'. The result of such an error, however, would be to shift bodily up or down a whole curve, rather than to affect individual points. It is also seen that 2ℓ and ℓ' are relatively insensitive to the value of α in the range $0.5 \leq \alpha \leq 0.8$ and $0.6 \leq \alpha \leq 0.9$, respectively, and that the value of α corresponding to maximum 2ℓ and $-\ell'$ is substantially independent of β, being equal to approximately 0.65 for the 2ℓ curves and 0.80 for the ℓ' curves. It might seem from the slope of the curve for ℓ' for $\beta = .30$ that the curve may actually go slightly positive for α approaching zero. However, the extrapolated curve is not given in this manner since a slight error in the electrical length would bring the curve below the axis again. It is difficult to see theoretically whether or not ℓ' must always be negative; 2ℓ must always be positive, however, since it is directly related to parameter B_a/Y_o at the centerline reference planes, and from theoretical considerations this latter parameter is always of the same sign.

In order to permit one to obtain by graphical interpolation the parameter values for a slot size for which data was not taken, Figures 4.22 to 4.25 are included. In these graphs, the parameter values are plotted as a function of relative slot height β, with relative slot width α as a parameter, in contrast to Figures 4.17 to 4.21. The combination of both sets of graphs should permit interpolation to a fair degree of accuracy. Parameter n is not included in this latter set since it is rather insensitive to β.

The theoretical expressions apply to the parameters of the centerline equivalent circuit representation given in Figure 4.16-(a). The parameters are seen to be B_b/Y_o, B_a/Y_o, n_c and X_c/Z_o, where B_b/Y_o is the dominant one; the reference planes are always fixed. Theoretical expressions occur naturally for $(B_b/Y_o + B_a/2\,Y_o)$ and B_a/Y_o, and not for B_b/Y_o separately; these correspond to short - and open - circuit bisections, respectively, of the equivalent network. Parameter X_c/Z_o is expected to be very small, and for first order values it is set equal to zero. Parameter n_c remains around the value unity, but simple expressions which account partly for its deviation from unity are given as Equations (3.123) and (3.125), the different expressions corresponding to different ranges of aperture dimensions. The expression for B_a/Y_o is Equation (3.120), valid for all aperture sizes. Finally, expressions for $(B_b/Y_o + B_a/2\,Y_o)$ are

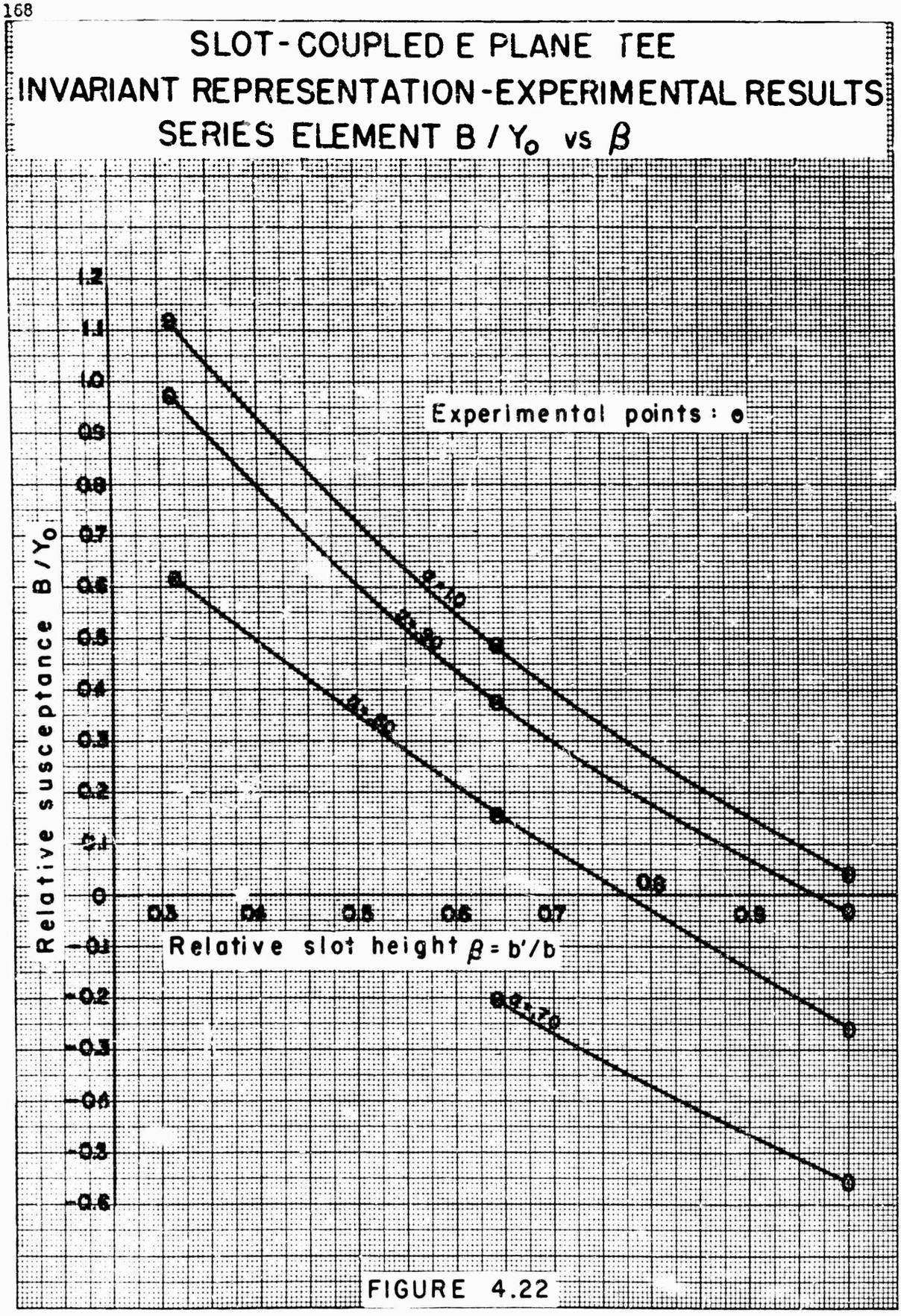
SLOT-COUPLED E PLANE TEE
INVARIANT REPRESENTATION-EXPERIMENTAL RESULTS
SERIES ELEMENT B / Y0 vs β
Experimental points : o
Relative susceptance B/Y0
Relative slot height β = b'/b
1.2
1.1
1.0
0.9
0.8
0.7
0.6
0.5
0.4
0.3
0.2
0.1
0
-0.1
-0.2
-0.3
-0.4
-0.5
-0.6
0.3
0.4
0.5
0.6
0.7
0.8
0.9
θ=10°
θ=20°
θ=30°
θ=70°

FIGURE 4.22

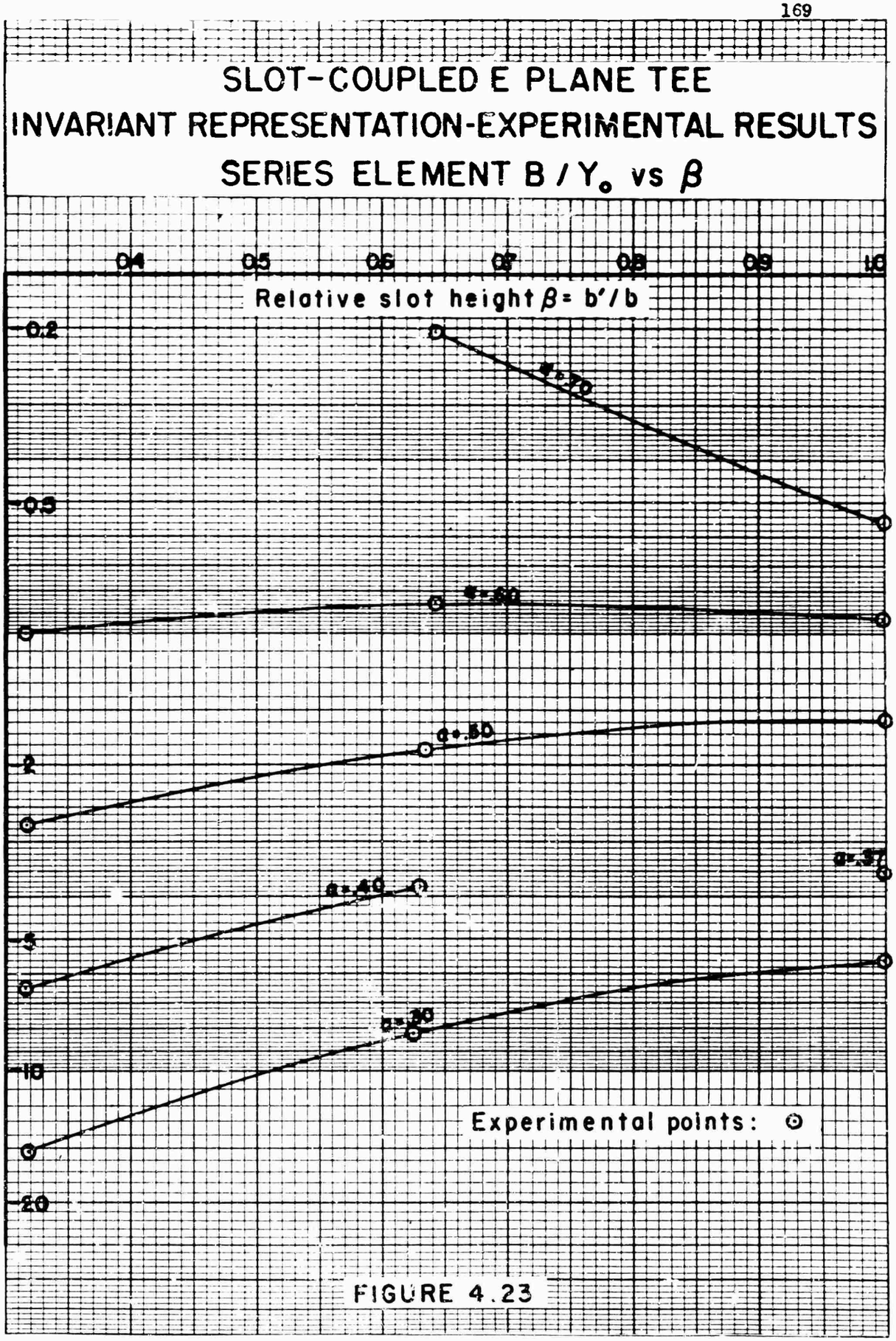
SLOT-COUPLED E PLANE TEE
INVARIANT REPRESENTATION-EXPERIMENTAL RESULTS
SERIES ELEMENT B / Y₀ vs β
Relative slot height β = b'/b
Relative susceptance B/Y₀
Experimental points:

FIGURE 4.23

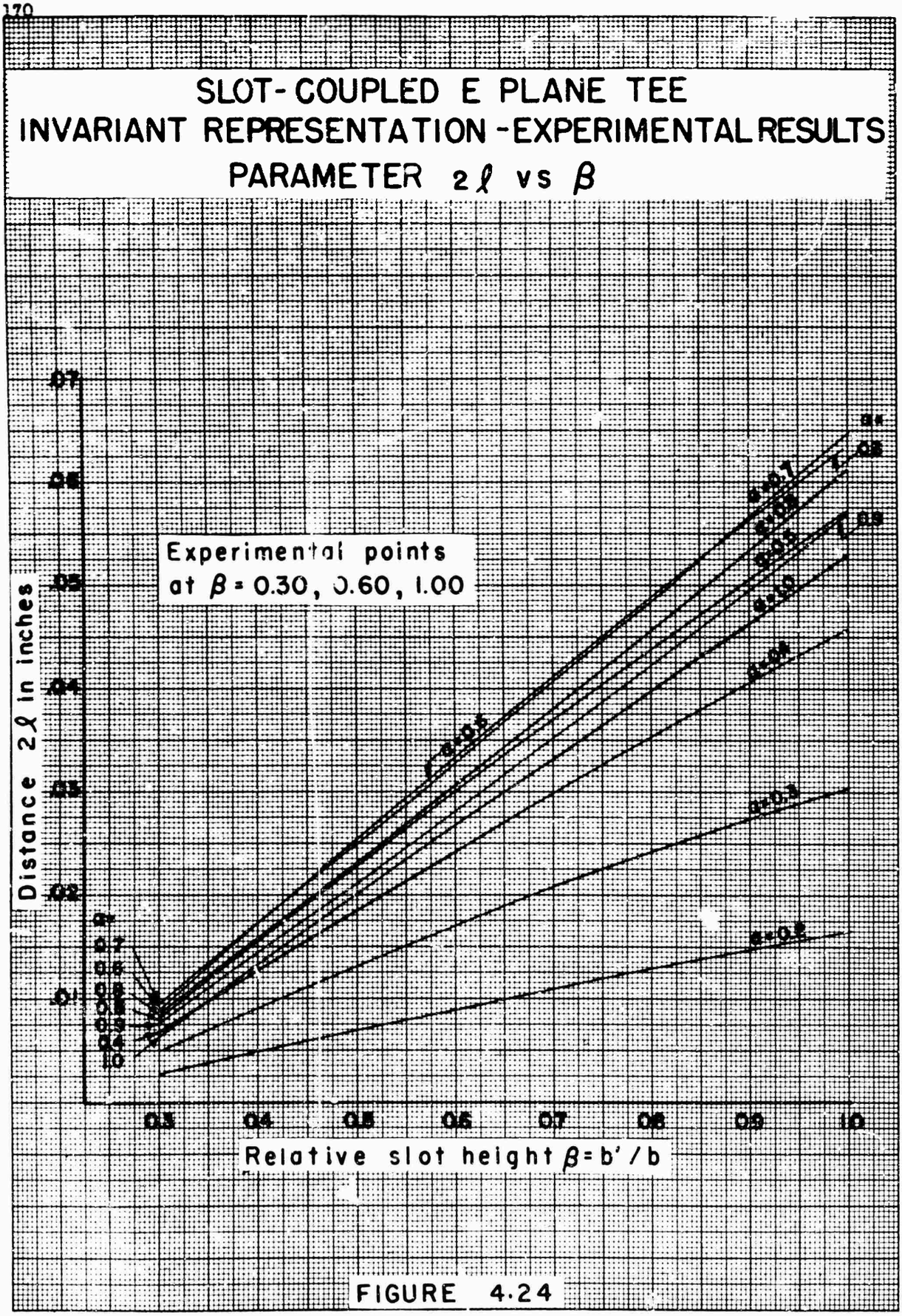
SLOT-COUPLED E PLANE TEE
INVARIANT REPRESENTATION - EXPERIMENTAL RESULTS
PARAMETER 2ℓ vs β
Experimental points
at β = 0.30, 0.60, 1.00
Distance 2ℓ in inches
Relative slot height β = b' / b
0.3
0.4
0.5
0.6
0.7
0.8
0.9
1.0

FIGURE 4.24

SLOT-COUPLED E PLANE TEE
INVARIANT REPRESENTATION - EXPERIMENTAL RESULTS
PARAMETER ℓ' vs β

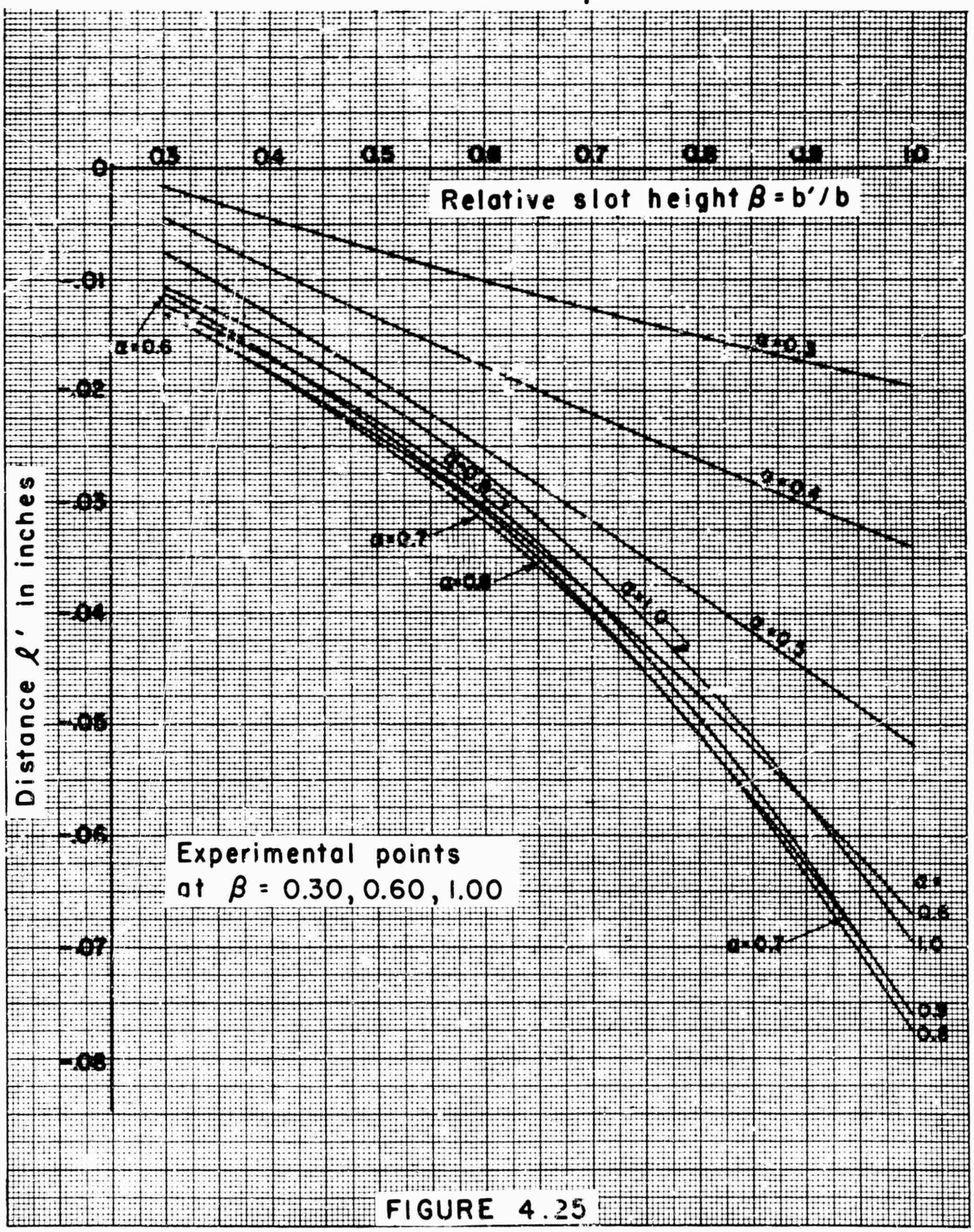

FIGURE 4.25

given by Equations (3.122), (3.124) and (3.126), where the different expressions correspond to different ranges of aperture dimensions.

A comparison of theoretical and experimental results for the parameters discussed above for the centerline representation is given graphically in Figures 4.26 to 4.30. The theoretical data in all the graphs are represented by the solid lines, and the experimental data by the indicated points; both are plotted as a function of relative slot width $\alpha = a'/a$, with relative slot height $\beta = b'/b$ as a parameter. For Figures 4.29 and 4.30 the experimental data are shown by dashed lines in addition to the indicated points.

The experimental data for the centerline representation are obtained from the invariant representation results listed in Table 4-II by applying the appropriate reference plane shifts. The necessary shifting formulae are given in Table 2-I, and the method of derivation is indicated in the Appendix to part II. Parameter B_a/Y_o of the centerline representation is dependent only on 2ℓ of the invariant representation. Parameters B_b/Y_o, X_c/Z_o and n_c involve all of the parameters of the invariant representation; however, they are sensitive to some of them, and insensitive to others. For larger values of α, B_b/Y_o is sensitive to B/Y_o, X_c/Z_o is sensitive to ℓ', and n_c is sensitive to n. For small values of α, an investigation of the shifting formulae of Table 2-I indicates that the product $\lambda(B/Y_o)(2\ell)$ becomes significant. If this product were much less than unity, then, for α approaching zero, B_b/Y_o would approach B/Y_o, X_c/Z_o would approach zero, and n_c would approach n; the effect of the above product is to increase the absolute values of B_b/Y_o and X_c/Z_o, and to decrease n_c. Since the precision of the experimental data is much less for small slots (since they transmit so little power into the stub guide), one must keep the above in mind when comparing the theoretical and experimental values.

In Table 4-II, as mentioned earlier, the data for B/Y_o and n correspond to slightly different values of β and α than the data for ℓ' and 2ℓ. Before shifting the results to the centerline reference planes, the values of ℓ' and 2ℓ were obtained at α and β values corresponding to those for B/Y_o and n by graphical interpolation using Figures 4.24 and 4.25.

Figure 4.26 compares the experimental and theoretical data, at the centerline reference planes, for parameter combination $(B_b/Y_o + B_a/2Y_o)$ for the wider slots, i.e., for $0.6 \leq \alpha \leq 1.0$. The agreement is seen to be quite good. Two theoretical curves are given for $\beta = 0.64$; the upper one corresponds to Equation (3.122), while the lower one is obtained using Equation (3.124). Both are given since the experimental data seem to lie between them. The curve for $\beta = .315$ is obtained from Equation (3.122), and that for $\beta = 1.0$ from Equation (3.127). The prescription given in

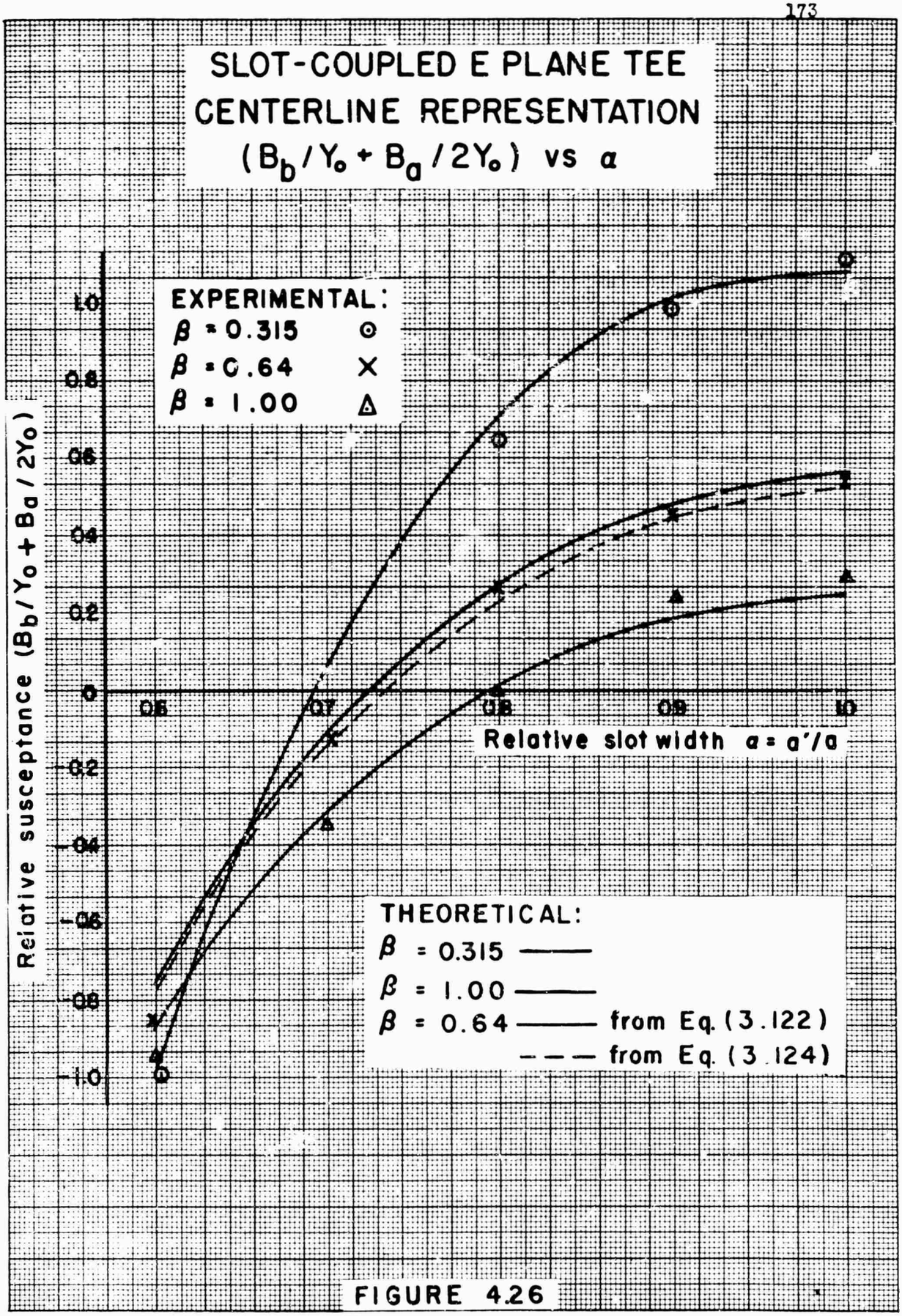
SLOT-COUPLED E PLANE TEE
CENTERLINE REPRESENTATION
$(B_b/Y_o + B_a/2Y_o)$ vs a
EXPERIMENTAL:
β = 0.315 ⊙
β = 0.64 ×
β = 1.00 △
THEORETICAL:
β = 0.315 ——
β = 1.00 ——
β = 0.64 —— from Eq. (3.122)
--- from Eq. (3.124)
Relative susceptance $(B_b/Y_o + B_a/2Y_o)$
Relative slot width $a = a'/a$
1.0
0.8
0.6
0.4
0.2
0
-0.2
-0.4
-0.6
-0.8
-1.0
0.6
0.7
0.8
0.9
1.0

FIGURE 4.26

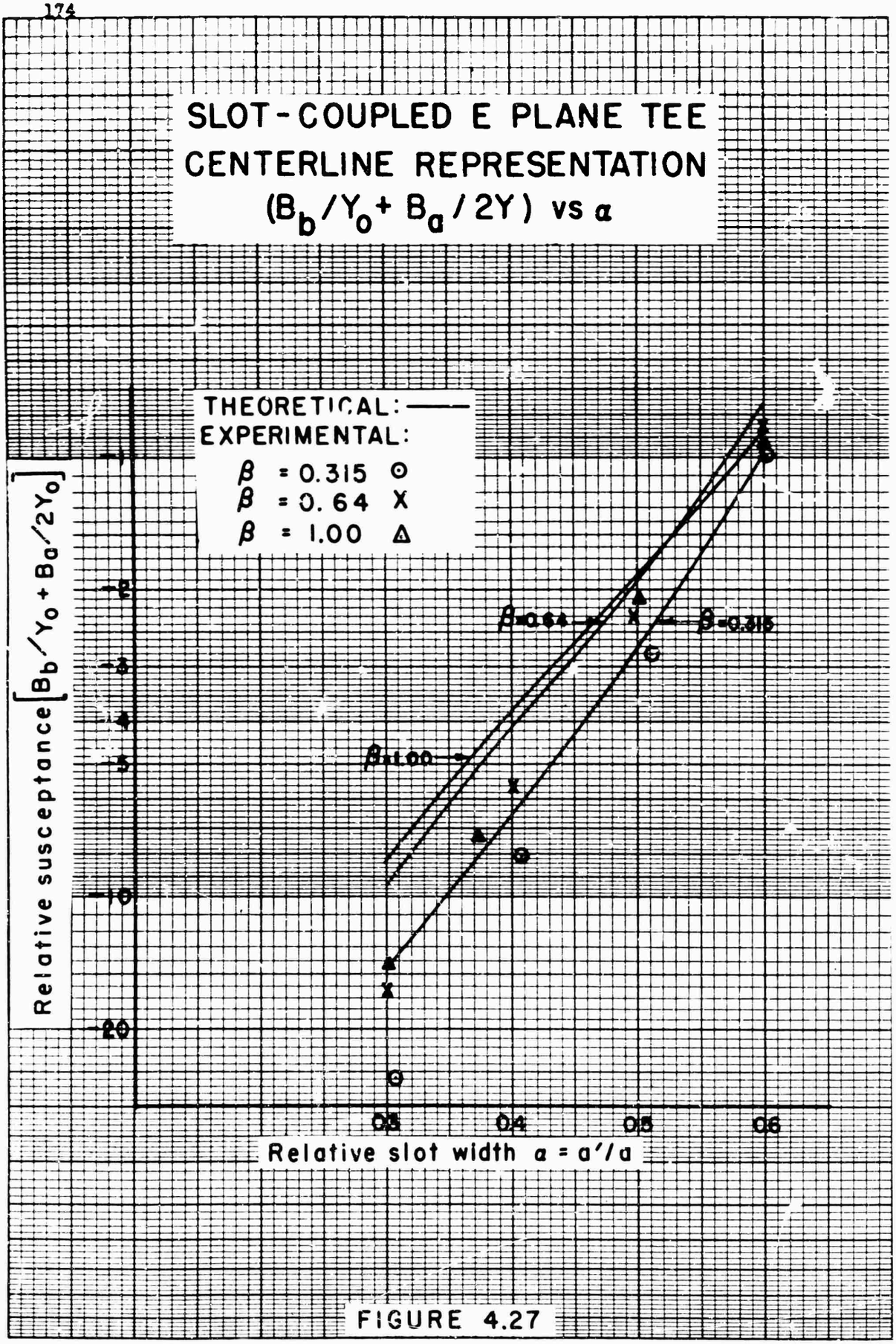
SLOT-COUPLED E PLANE TEE
CENTERLINE REPRESENTATION
$(B_b/Y_0 + B_a/2Y)$ vs α
THEORETICAL: ——
EXPERIMENTAL:
β = 0.315 ⊙
β = 0.64 X
β = 1.00 Δ
β=0.64
β=0.315
β=1.00
Relative susceptance $[B_b/Y_0 + B_a/2Y_0]$
-1
-2
-3
-4
-5
-10
-20
0.3
0.4
0.5
0.6
Relative slot width $\alpha = a'/a$

FIGURE 4.27

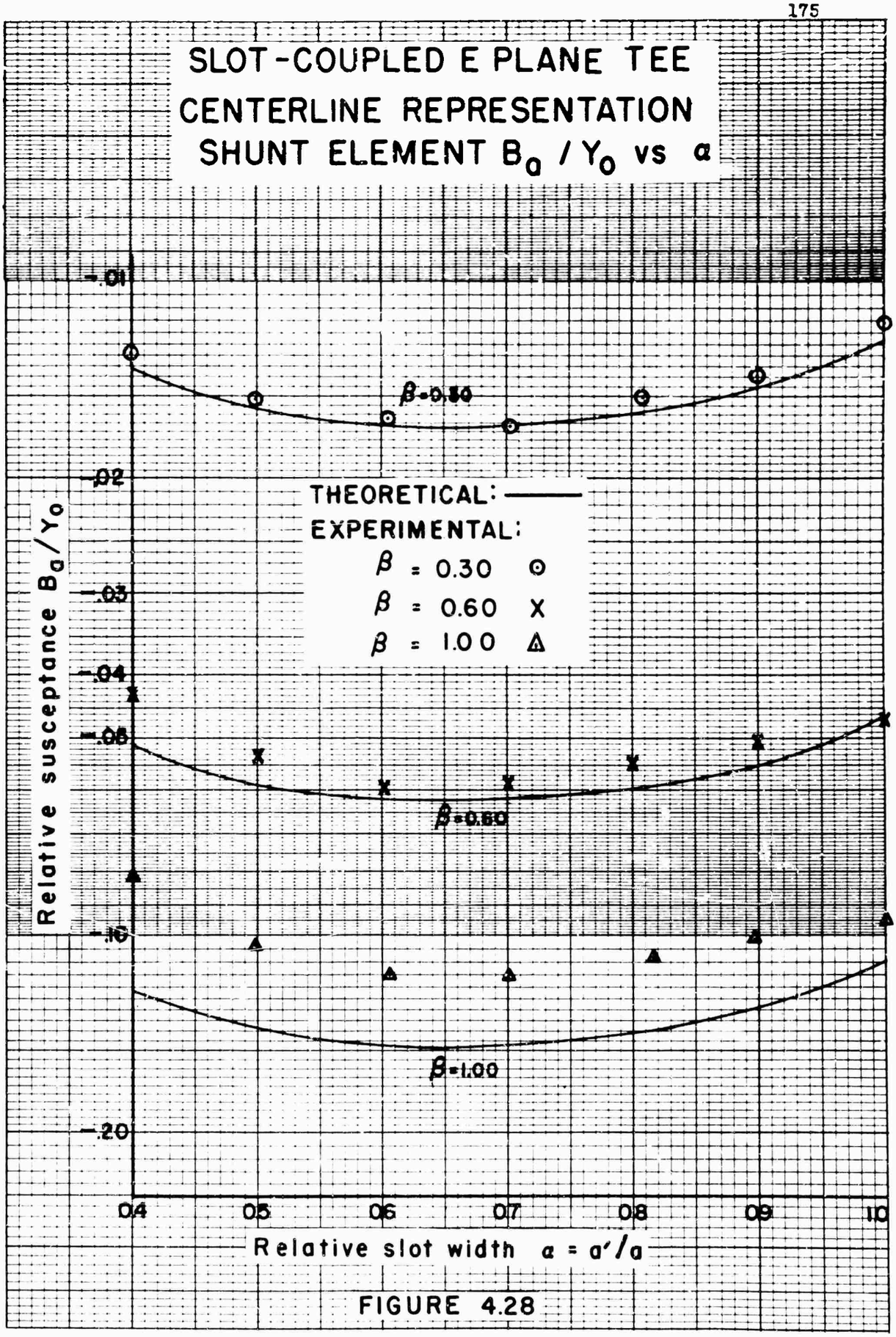
SLOT-COUPLED E PLANE TEE
CENTERLINE REPRESENTATION
SHUNT ELEMENT B_a / Y_o vs α
-.01
-.02
-.03
-.04
-.05
-.10
-.20
Relative susceptance B_a/Y_o
THEORETICAL: ——
EXPERIMENTAL:
β = 0.30 ⊙
β = 0.60 X
β = 1.00 △
β=0.30
β=0.60
β=1.00
04
05
06
07
08
09
10
Relative slot width $\alpha = a'/a$

FIGURE 4.28

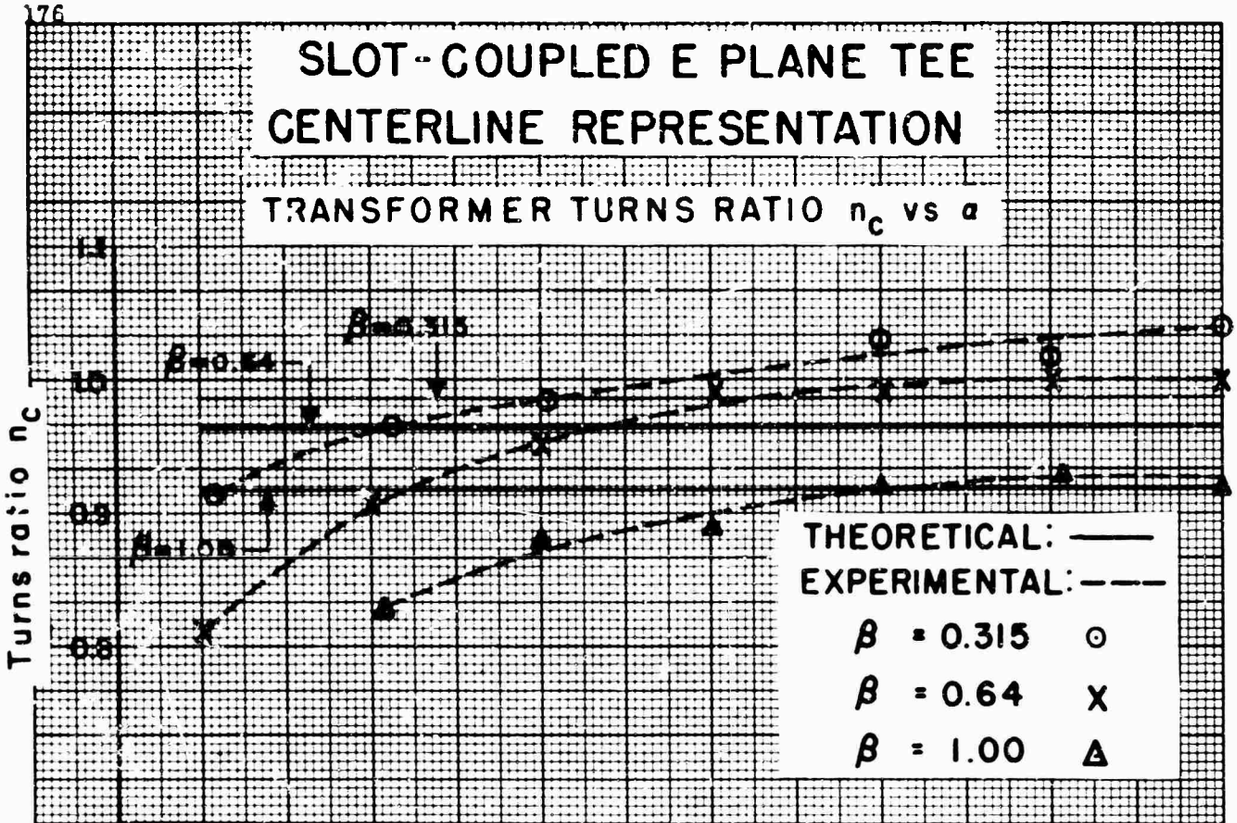

FIGURE 4.29

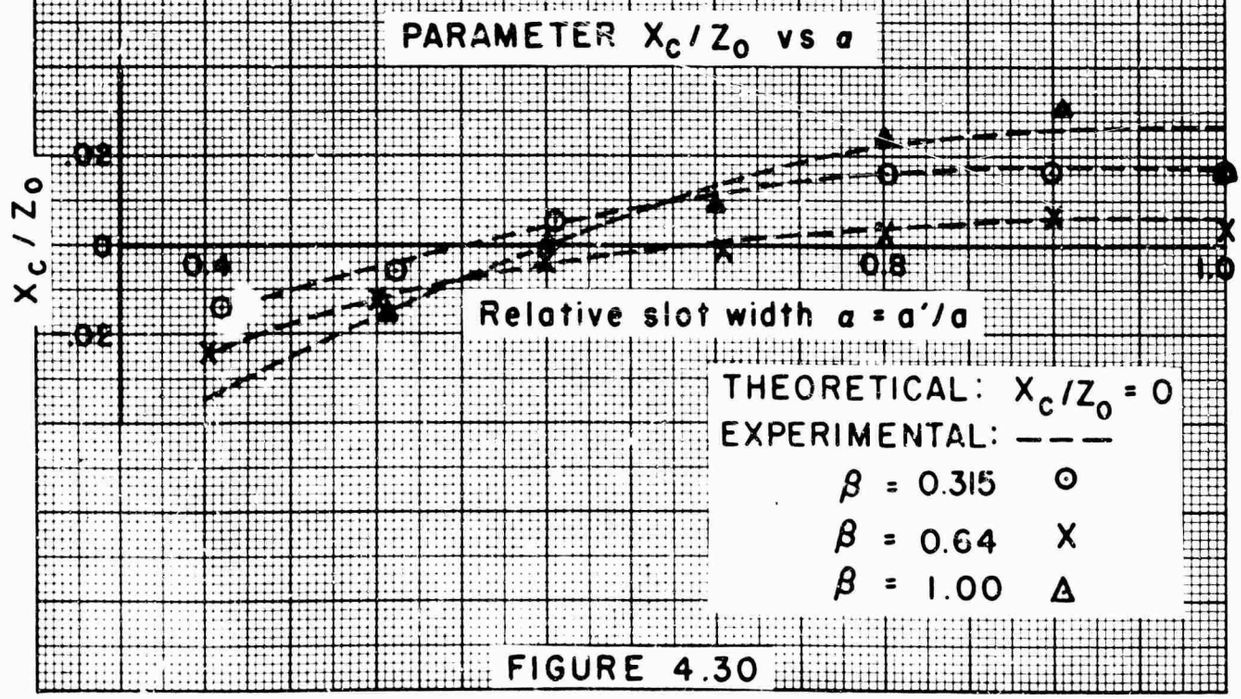

FIGURE 4.30

Sec. E, 4 of part III for which expression to use for a particular range of aperture dimensions is to be altered in the light of Figure 4.26 in only the following respects: Equation (3.122) is valid for $\beta \leq 0.6$, rather than $\beta < 0.5$, while Equation (3.124) applies to the range $0.6 < \beta \leq 0.9$, rather than $0.5 \leq \beta \leq 0.9$. The general behavior for $(B_b/Y_o + B_a/2\,Y_o)$ at the centerline reference planes for $\alpha \geq 0.6$ is also seen to be similar to that for B/Y_o at the invariant reference planes for the same range of α ; the similarity is greater for the smaller values of β.

A comparison between theoretical and experimental values for $(B_b/Y_o + B_a/2\,Y_o)$ for narrower slots, i.e., for $0.3 \leq \alpha \leq 0.6$, is given in Figure 4.27. Only one curve is given for the theoretical values at $\beta = 0.64$ because the results of Equations (3.122) and (3.124) become practically identical. The other curves correspond to the same expressions as for Figure 4.26. The striking feature of these graphs is that the experimental data lie consistently bel w the theoretical data. This is in part due to the sensitivity of the shifting formulae for small values of α, as discussed above, but it cannot be completely explained by it. One concludes that the theoretical expressions, while very satisfactory for large α, are less accurate for small α. This is not surprising, however, as the field assumption used in the variational expression is no longer valid for small values of α, as discussed in part III. In the summary, Sec. E of part III, the expressions are stated as applicable for $\alpha > 0.5$ only.

A comparison of theoretical and experimental data for B_a/Y_o appears in Figure 4.28. Since the values for B_a/Y_o depend only on 2ℓ, the original, rather than the interpolated, data for 2ℓ was used; comparison is made at $\beta = 0.30$ and 0.60, rather than at 0.315 and 0.64. Agreement between theory and experiment is reasonably good for $\beta = 0.3$ and 0.6, and is fair for $\beta = 1.0$. The agreement seems to be poorer for very large β and for very small α. When it is considered, however, that B_a/Y_o is itself a small quantity, the agreement from a practical standpoint is quite satisfactory.

In Figure 4.30, the experimental data for X_c/Z_o are plotted, and dashed lines are drawn through the average of the points; the theoretical prediction for X_c/Z_o, admittedly a first order one, is zero. It is seen that the plotted values are very small in magnitude and lie on both sides of the zero axis, indicating that zero is an acceptable first order result. The experimental points are very sensitive to the initial data, involving differences between much larger numbers. This fact might explain the overlap apparent in the curves; furthermore, for more accurate data, the values of X_c/Z_o may be smaller in magnitude.

A comparison of theoretical and experimental data for n_c appears in Figure 4.29. The theoretical data is represented by the solid lines and the experimental data by the dashed lines. Agreement seems only fair, but it is seen that the ordinate scale is enlarged. The value of n_c is approximately unity, and the theoretical results are first order ones which account somewhat for the deviation from unity; the variation with β is approximately accounted for. The theoretical expression does not anticipate a variation with α ; the variation with α of the experimental data may be in part due to the sensitivity of the shifting formulae discussed earlier. The field assumption used in the theoretical expression for n_c is no longer valid for small α, as discussed in part III, and this may explain the lack of variation with α for small α. The summary, Sec. E of part III, lists the expressions for n_c as valid for $\alpha > 0.5$ only. From a practical standpoint, however, for $\alpha \geq 0.5$, the agreement is satisfactory; if necessary, a more accurate theoretical expression can be derived.

4.) The E Plane Radiating Slot

The E plane radiating slot denotes a slot located in the broad face of rectangular waveguide, and coupling the waveguide to a half space. The slot is rectangular and centered, with its sides parallel to the waveguide walls; the geometry is indicated in Figure 4.31. Of a variety of

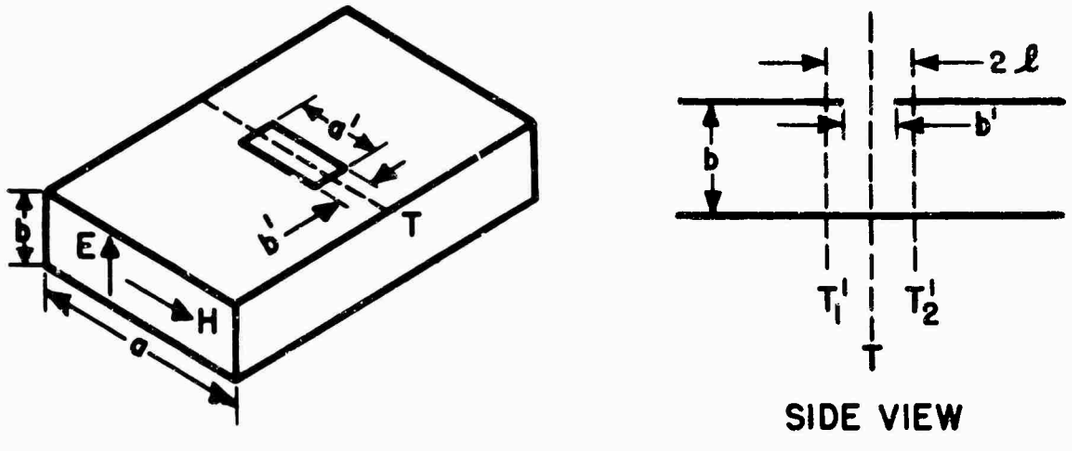

Figure 4.31 - Geometry of the E Plane Radiating Slot.

possible equivalent circuit representations, two are chosen: the "centerline", at reference planes T_1 and T_2, and the "invariant", at reference planes T_1' and T_2'. The centerline representation is the one at which the theoretical formulae apply; the invariant representation, as discussed in Part II, Sec. B, 1), is so chosen as to reduce to a purely series circuit for thick slots and for slots with negligible loss. These two equivalent circuit representations are presented in Figure 4.32 (a) and (b). The four parameters for the centerline circuit are G_b/Y_o, B_b/Y_o, R_a/Z_o and X_a/Z_o; those for the invariant circuit are G_b'/Y_o, B_b'/Y_o, G_a'/Y_o and 2ℓ, where the reference planes are spaced 2ℓ apart. All parameters have been normalized to the characteristic admittance of the waveguide.

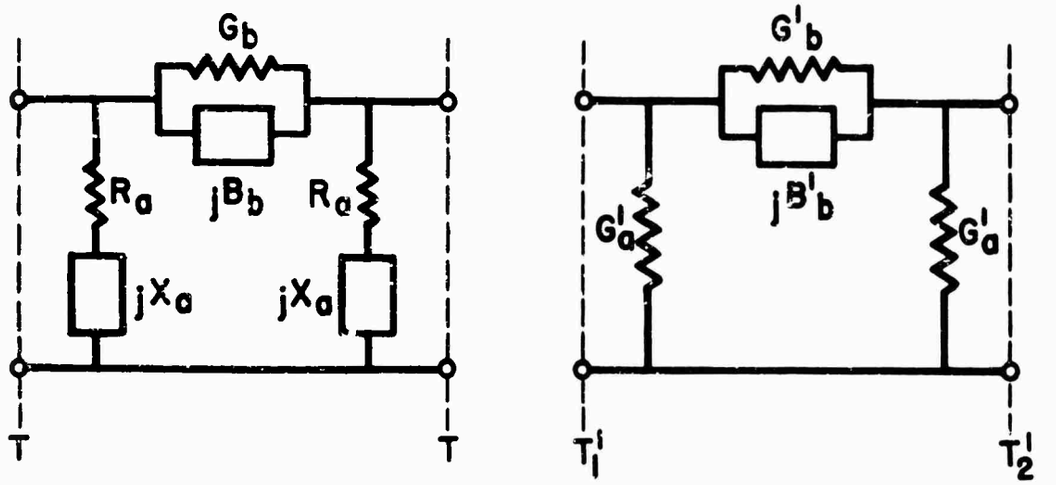

CENTERLINE REPRESENTATION (a)

INVARIANT REPRESENTATION (b)

Figure 4.32 - Equivalent circuit representation for the E plane radiating slot.

At the time at which the data reported here were taken, there was no precision method available for the measurement of dissipative structures. One has been devised since, however, and new data are being taken utilizing this procedure, but the new data will not be reported here. The radiating

slots measured can be roughly classified as "lossless" and "having appreciable loss", the latter occurring when a measurable (non-infinite) VSWR is produced by the slot for some location of the variable short-circuiting plunger placed in back of it. The former category (where the VSWR's produced are too high to be measured) occure for very small slots, permitting a purely lossless equivalent circuit representation. These small slots can therefore be analyzed by means of the tangent relation procedure, utilizing an equivalent circuit analogous to Figure 4.1-(b) for a finite thickness transverse slot. The difference is that a series, rather than a shunt, element is utilized, and parameters B_t/Y_o and x are replaced by B_t'/Y_o and 2ℓ, respectively. It is noted that the circuit of Figure 4.32-(b) reduces to this for no loss.

The latter category (for measurable loss) applies to the larger slots. Since no precision method was available, the parameters for these slots were measured at the centerline reference planes by the two-point method (described in the Final Report, Chap. II, Sec. C). These latter data are therefore admittedly approximate.

Measurements were taken for the following range of slot sizes: relative slot width $\alpha = a'/a$ varying in steps by 0.1 from 0.1 to 0.5, for relative slot heights $\beta = b'/a$ equal to 0.6 and 1.0, and for α varying in steps of 0.1 from 0.3 to 1.0 for $\beta = 0.3$. In addition, measurements were made at $\alpha = 1.0$ for $\beta = 0.4$ and 0.6. The data were obtained by varying the slot width while maintaining the slot height constant. For these measurements, however, the waveguide was not coupled to an actual half space. For the $\beta = 0.3$ run, the slot radiated directly into space, as shown in Figure 4.33-(a). For the larger slot heights, i.e., for $\beta = 0.6$ and 1.0, a metal plate was attached to the guide to approximate a large baffle, as shown in Figure 4.33-(b). (A more detailed drawing of this attached plate is given in Figure 2.4. The air chuck included in the figure is not used for the radiating measurements.) Further details concerning the experimental techniques are given in Part II, Sec. B, 3).

For the slots for which there is negligible radiation, the effect of the surrounding space is small, and, as mentioned before, the data were analyzed by means of the tangent relation method. For such slots the results to be given should be fairly reliable. However, for the larger slots, for which appreciable radiation occurs, the lack of a proper half space will be more significant, and, in addition, only two point measurements were taken. For the larger slots, therefore, the results to be quoted must be considered as first order values only.

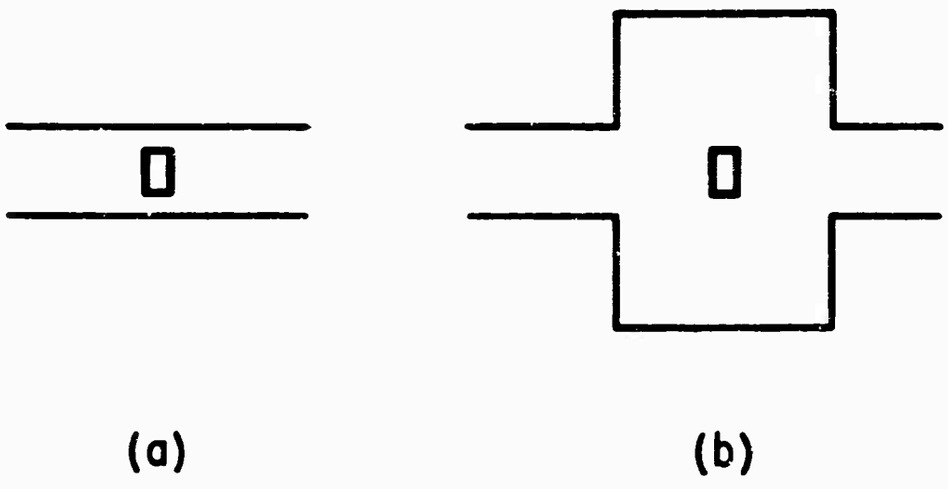

Figure 4.33 - Approximations to the half space.

The experimental results are listed in Table 4-III. As mentioned above, the "lossless" data occur at the invariant reference planes of Figure 4.31, so that the parameters are B_b'/Y_o and 2ℓ ; the results for the slots for which there is appreciable loss are obtained directly at the centerline reference planes, and the corresponding parameters are, therefore, B_b/Y_o , G_b/Y_o , R_a/Z_o and X_a/Z_o . The last two parameters are also alternatively presented as G_a/Y_o and B_a/Y_o .

The theoretical expressions for most of the parameters at the centerline representation are obtained from those for the parameters of slots in other locations, and from certain microwave network considerations. These considerations are discussed in Part III, Sec. D, 5). The exception to the above is R_a/Z_o, the expression for which is given by Equation (3.135). The expressions for the other parameters are given as Equations (3.133), (3.132) and (3.134) for B_b/Y_o , G_b/Y_o and X_a/Z_o , respectively. Equation (3.133) for B_b/Y_o may be written in terms of other parameters as:

$$\frac{B_b}{Y_o} = \left(\frac{B_b}{Y_o} + \frac{B_a}{2Y_o}\right)_{Tee} - \left(\frac{B_a}{2Y_o}\right)_{Tee} + \frac{1}{n_c^2}\left(\frac{B_h}{Y_o} - \frac{B_t}{2Y_o}\right) \qquad (4.5)$$

TABLE 4-III

E PLANE RADIATING SLOT

Experimental Results

λ = 1.2606" , a = 0.900" , b = 0.400"

$\alpha = a'/a$, $\beta = b'/b$; 2ℓ, a' and b' are in inches

1. "Lossless" slots (at invariant reference planes):

a'	b'	α	β	B_b'/Y_o	2ℓ
.300	.100	.333	.250	- 9.8	.019
.360	.120	.400	.300	- 5.40	.025
.450	.120	.500	.300	- 2.45	.023
.100	.245	.111	.612	- 70	.009
.185	.245	.205	.612	- 16	.023
.270	.250	.300	.625	- 6.75	.032
.360	.252	.400	.630	- 3.16	.044
.451	.254	.501	.635	- 1.68	.044
.101	.400	.112	1.000	- 34	.013
.180	.400	.200	1.000	- 12.2	.034
.270	.400	.300	1.000	- 5.01	.043
.335	.400	.372	1.000	- 2.96	.055
.456	.400	.507	1.000	- 1.41	.055

2. "Lossy" slots (at centerline reference planes):

a'	b'	α	β	G_b/Y_o	B_b/Y_o	G_a/Y_o	B_a/Y_o	R_a/Z_o	X_a/Z_o
.54	.12	.60	.30	.782	-0.547	-.0009	-.058	- .265	17.2
.63	.12	.70	.30	.788	0.430	.0005	-.046	.236	21.7
.72	.12	.80	.30	.699	1.108	.0039	-.052	1.44	19.2
.81	.12	.90	.30	.682	1.415	.0240	-.055	6.66	15.3
.90	.12	1.00	.30	.712	1.696	.0001	-.067	.023	15.0
.90	.16	1.00	.40	.746	1.469	.0006	-.051	.228	19.5
.90	.24	1.00	.60	.836	1.117	.0005	-.075	.090	13.4

where the notation has been discussed earlier in this section. It is noted that the expression for B_b/Y_o involves the term $(B_b/Y_o + B_a/2Y_o)$ for the E plane Tee. Since in the discussion above for the E plane Tee the theoretical results for small α were consistently higher in value than the corresponding experimental results, one would expect a similar behavior here for B_b/Y_o for small α.

Since for the "lossless" data, the experimental results are at the invariant reference planes, while the theoretical results are at the centerline ones, one must utilize the appropriate shifting formulae in order to compare results. These formulae are given in Tables 2-VII and 2-VIII, wherein one simply sets the conductances to zero.

For comparison between theoretical and experimental data at the centerline reference planes the experimental data were shifted through the length ℓ of transmission line. However, the resultant values of B_b/Y_o were not reasonable, indicating an error in 2ℓ. The reasons why 2ℓ is suspected rather than B_b'/Y_o are first that the latter is determined by the slope of the D vs. S curve which is generally accurately known, then that 2ℓ involves a mechanically measured length for the slot structure, which is not as accurate as an electrically measured length, and finally that the resultant B_b/Y_o values are very sensitive to slight errors in 2ℓ. Because of the above, comparison is made between the theoretical and experimental values of B_b'/Y_o, where the theoretical values are shifted from the centerline reference planes, using

$$\frac{B_b'}{Y_o} = \frac{B_b/Y_o}{1 + \frac{B_a}{Y_o}\left(\frac{B_a}{Y_o} + 2\frac{B_b}{Y_o}\right)} \tag{4.6}$$

This comparison is given in Figure 4.34, where the experimental points are indicated, and solid lines are drawn through their average, and where the theoretical values are indicated by the dashed lines. The data are plotted as a function of relative slot width $\alpha = a'/a$, with relative slot height $\beta = b'/b$ as a parameter. It is seen that the agreement is good for $\beta = 0.3$, but that for $\beta = 0.6$ and 1.0 the theoretical data lie above the experimental data, as expected. (Actually, the expectation applied to B_b/Y_o, but similar behavior should occur here as seen from Equation (4.6).) As mentioned earlier, the theoretical data apply to a half space coupled to the waveguide, while the experimental data do not. Even though negligible radiation occurs, there exists stored higher mode energy in the neighborhood of the slot outside of the guide, and the distribution

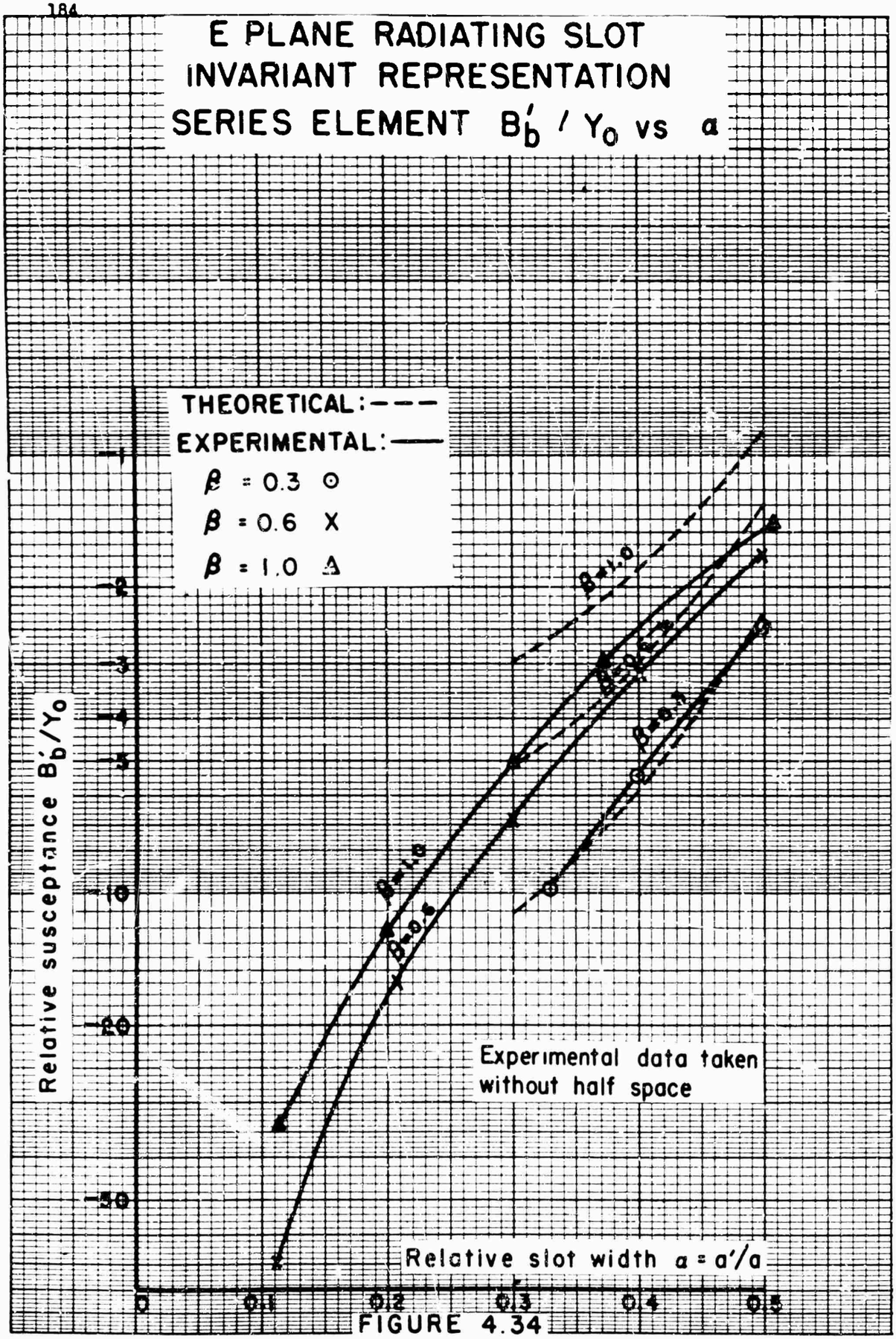
E PLANE RADIATING SLOT
INVARIANT REPRESENTATION
SERIES ELEMENT B'_b / Y_0 vs a
THEORETICAL: - - -
EXPERIMENTAL: ——
β = 0.3 ⊙
β = 0.6 X
β = 1.0 Δ
Relative susceptance B'_b/Y_0
-1
-2
-3
-4
-5
-10
-20
-50
β=1.0
β=0.6
β=0.3
Experimental data taken without half space
Relative slot width $a = a'/a$
0
0.1
0.2
0.3
0.4
0.5

FIGURE 4.34

of this stored energy will be somewhat affected by the lack of a large baffle. The value of the susceptance B_b/Y_o will therefore be affected; it is difficult to know, however, if the effect is negligible or not.

The theoretical and experimental values for B_b/Y_o for $\alpha \geq 0.6$ are compared in Figure 4.35, where the theoretical data are represented by the solid lines, and the experimental data by indicated points, which for $\beta=0.3$ are also connected by a dashed line. The data are plotted as a function of α, with β as a parameter. The experimental points are seen to lie consistently lower than the theoretical values. Since for these slot dimensions appreciable radiation occurs, the behavior mentioned above may be due to the lack of a large baffle or may be due to the flanges which couple the structure containing the slot to the slotted section on one side and to the variable short on the other. The effect of the flanges may be greater than that of the lack of a baffle because most of the radiated power occurs in the direction of the flanges. However, their effect on the susceptance is difficult to investigate as one must know their exact distance from the slot and how their phasing affects the susceptance value.

The general shape of the curves of B_b/Y_o vs. α is similar to that obtained for B_t/Y_o, B_r/Y_o and $(B_b/Y_o + B_a/2Y_o)_{Tee}$. As was found for the others, the susceptance value is capacitive for $\alpha = 1.0$. For $\beta = 1.0$, however, the slot may be either capacitive or inductive, depending upon the value of α. There is again a cross-over region, which occurs for α between 0.6 and 0.7, as has been true for the other susceptances, and which is a broad region, as for the E plane Tee. It is more capacitive in content that the E plane Tee, just as the transverse radiating slot was more capacitive in content than the transverse slot. This latter fact results in the cross-over region for B_b/Y_o occurring very near resonance, so that for α lying between 0.63 and 0.67 the slot is resonant for all values of β. (The small shunt susceptance B_a/Y_o has been neglected in this discussion on resonance; B_b/Y_o is the dominant susceptance term.)

A comparison between theoretical and experimental values for the dominant conductance term G_b/Y_o, at centerline reference planes, is given in Figure 4.36; the results are plotted as a function of α with β as a parameter. The theoretical results are represented by solid lines and the experimental data by indicated points. The experimental data seem rather poor, but this is not surprising in view of the circumstances. First, as mentioned earlier, these data are only first order ones, since they were obtained by a two-point procedure. Then, conductance values are generally less accurate than susceptance ones since they are masked by the latter; the same situation arose in connection with the transverse radiating slot. In addition, the conductance values vary only over a small range and the ordinate scale is enlarged; the discrepancy between the theoretical and experimental values

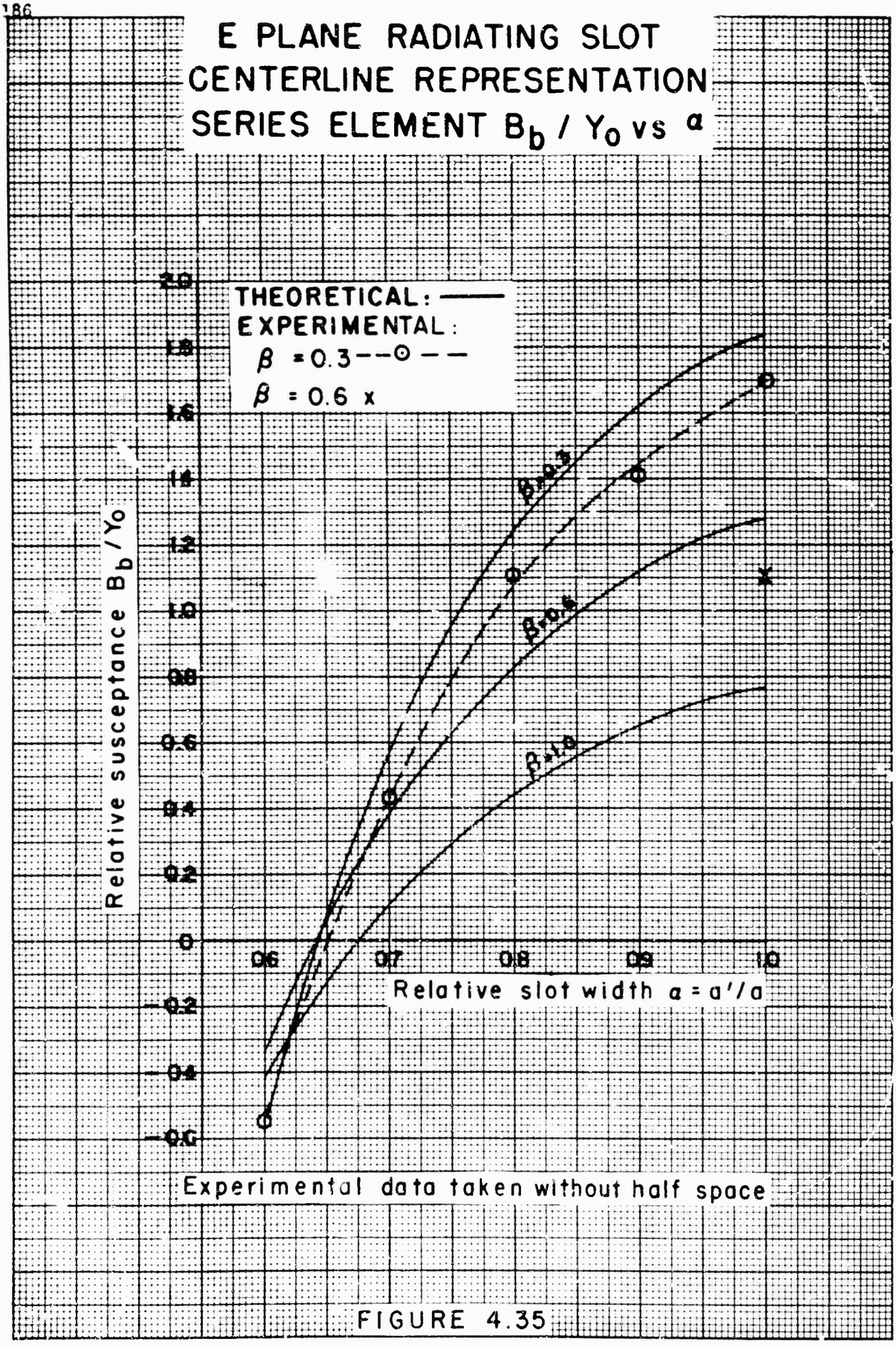
E PLANE RADIATING SLOT
CENTERLINE REPRESENTATION
SERIES ELEMENT B_b / Y_0 vs a
THEORETICAL: ——
EXPERIMENTAL:
β = 0.3 --⊙--
β = 0.6 x
Relative susceptance B_b / Y_0
2.0
1.8
1.6
1.4
1.2
1.0
0.8
0.6
0.4
0.2
0
-0.2
-0.4
-0.6
0.6
0.7
0.8
0.9
1.0
Relative slot width $a = a'/a$
β=0.3
β=0.6
β=1.0
Experimental data taken without half space

FIGURE 4.35

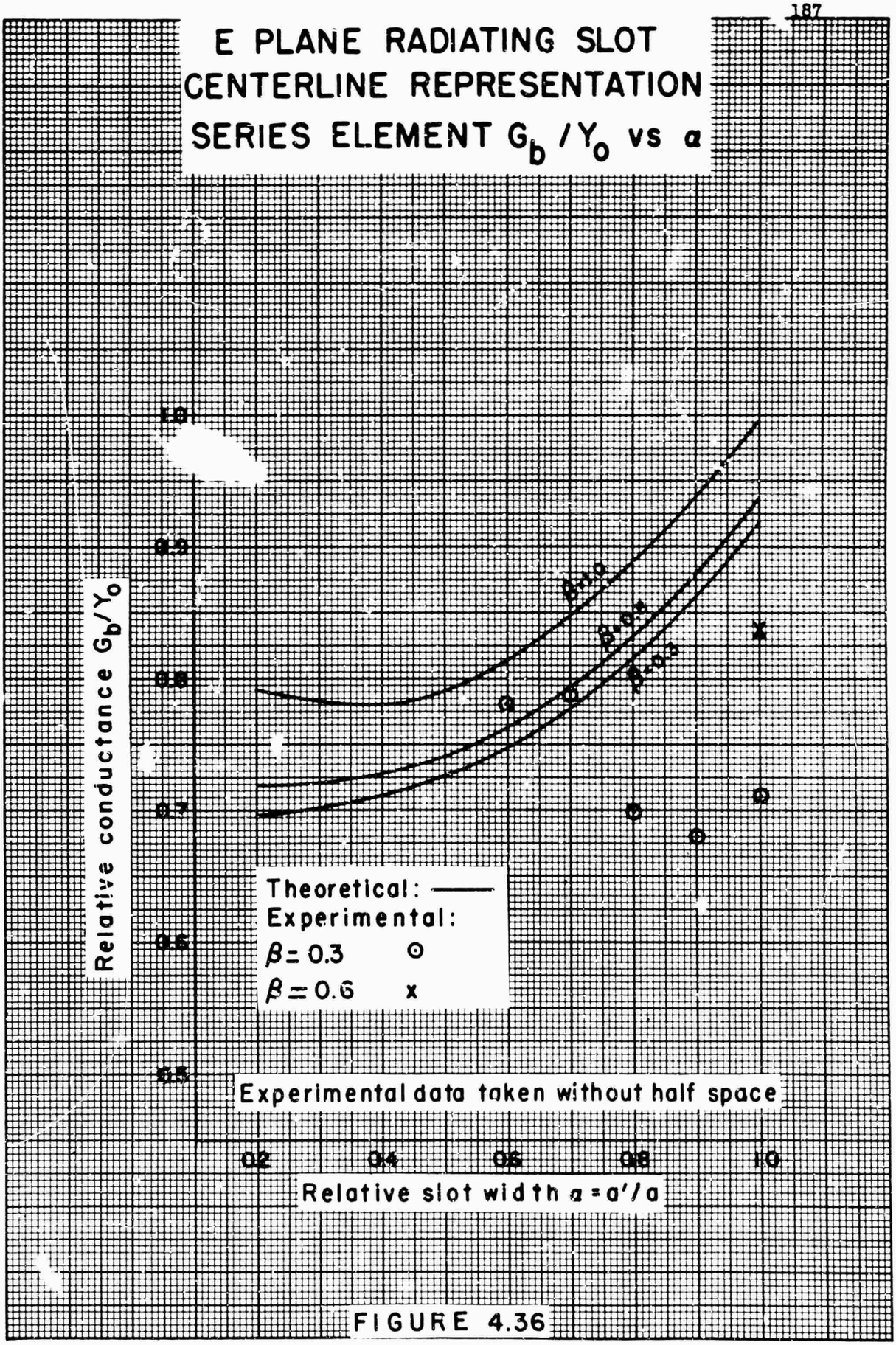
E PLANE RADIATING SLOT
CENTERLINE REPRESENTATION
SERIES ELEMENT G_b / Y_0 vs a
Relative conductance G_b/Y_0
1.0
0.9
0.8
0.7
0.6
0.5
β=1.0
β=0.6
β=0.3
Theoretical: ——
Experimental:
β = 0.3 ⊙
β = 0.6 x
Experimental data taken without half space
0.2
0.4
0.6
0.8
1.0
Relative slot width $a = a'/a$

FIGURE 4.36

is never greater than 20 percent. The effect of the lack of an adequate baffle, and of the flanges, may likewise affect this discrepancy, where, generally, the experimental values are smaller than the theoretical ones. The variation with α of the theoretical values of G_b/Y_o is similar to that for G_r/Y_o, for the transverse radiating slot. However, the variation with β is seen to be opposite to that for B_r/Y_o; the reason lies in the factor $1/n_c^2$, which increases with increasing β.

The shunt parameters of the centerline representation are R_a/Z_o and X_a/Z_o. These two parameters are specified rather than the alternative G_a/Y_o and B_a/Y_o because theoretical expressions for the former arise naturally. The theoretical expression for R_a/Z_o was given earlier as Equation (3.135); the theoretical expression for X_a/Z_o was not evaluated directly, but rather is given in Equation (3.134) as $-1/(B_a/Y_o)$ for the E plane Tee, which is approximately valid if $(B_a/Y_o)^2 >> (G_a/Y_o)^2$. Actually, therefore, theoretical expressions are available for R_a/Z_o and B_a/Y_o. For this reason, comparison between theory and experiment will be made for these parameters. If $(R_a/Z_o)^2 (B_a/Y_o)^2 << 1$, it follows that

$$\frac{X_a}{Z_o} = -\frac{1}{B_a/Y_o} \tag{4.7}$$

$$\frac{G_a}{Y_o} = \frac{R_a}{Z_o}\left(\frac{B_a}{Y_o}\right)^2 \tag{4.8}$$

This condition is fulfilled for the data here, as seen from Table 4-III.

Comparison between the experimental and theoretical values for B_a/Y_o is afforded by Figure 4.37, where the values are plotted as a function of α, with β as a parameter. The theoretical values are those for B_a/Y_o of the E plane Tee, and are represented by the solid lines. The experimental data are given by the indicated points, and are connected by the dashed lines. The experimental data for $\alpha \geq 0.6$ correspond to the slots with appreciable loss, parameters of which were evaluated by the two-point method directly at the centerline reference planes; that for $\alpha \leq 0.5$ correspond to the "lossless" data evaluated at the invariant reference planes and shifted to the centerline reference planes. For $\alpha \leq 0.5$, the experimental B_a/Y_o values are then dependent only on the 2ℓ data reported in

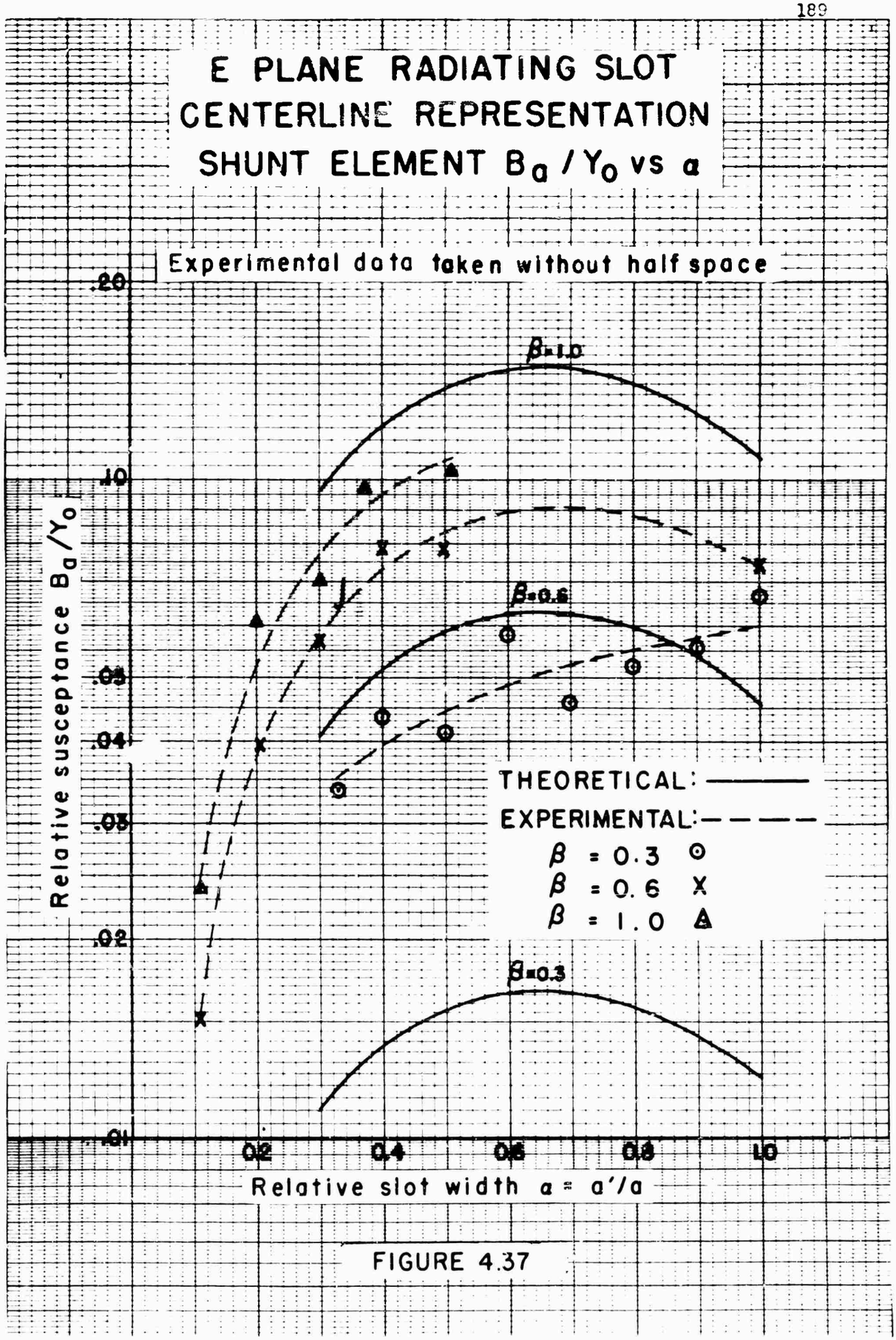
E PLANE RADIATING SLOT
CENTERLINE REPRESENTATION
SHUNT ELEMENT B_a / Y_0 vs α
Experimental data taken without half space
Relative susceptance B_a/Y_0
.20
.10
.05
.04
.03
.02
.01
β=1.0
β=0.6
β=0.3
THEORETICAL: ———
EXPERIMENTAL: — — — —
β = 0.3 ⊙
β = 0.6 X
β = 1.0 Δ
0.2
0.4
0.6
0.8
1.0
Relative slot width α = a'/a

FIGURE 4.37

Table 4-III, which, as discussed above, are questionable. As seen in Figure 4.37, agreement is obtained on the general variation with both α and β and on the order of magnitude. Since this parameter is not dominant in determining the slot behavior, and since the magnitudes involved are small, the disagreement is not as bad as implied. In addition, it is recalled that the experimental data for this parameter are not as reliable as for the other parameters.

In Figure 4.38, the theoretical values of R_a/Z_o are plotted as a function of α. There is no variation with β indicated; the dependence on β is negligible. The experimental data is not plotted because of the large scatter obtained, as seen in Table 4-III. Since the value of X_a/Z_o are much greater than those of R_a/Z_o, the latter are effectively masked by the former, so that it is almost impossible to obtain accurate experimental values for R_a/Z_o. The theoretical curve for R_a/Z_o is seen to behave similarly to those for G_r/Y_o and G_b/Y_o, being of the same order of magnitude and varying similarly with α.

Theoretical data for G_a/Y_o are given in Figure 4.39, where the data are plotted as a function of α. The experimental points are not plotted because of the scatter mentioned above for R_a/Z_o. Comparison with Table 4-III, however, indicates an order of magnitude agreement. It is seen that the values of G_a/Y_o are very small. The values of X_a/Z_o are not plotted since they are essentially negative reciprocals of B_a/Y_o.

Since the conductance values are masked by the (larger) susceptance values, with the result that it is difficult to measure accurately the conductance values, it is generally better to trust a theoretical result for the conductance than an individual experimental result. This general comment, although especially true for the shunt resistance R_a/Z_o, also applies to G_b/Y_o, and G_r/Y_o for the transverse radiating slot.

As mentioned earlier, because much of the data reported in Table 4-III was obtained by a two-point method and because an adequate "infinite" baffle was not employed, another set of data is being taken which answers these criticisms.

B. Thick Slots

The equivalent circuit parameters for slots of finite thickness are obtainable from the parameters of slots of infinitesimal thickness by means of appropriate microwave network considerations. The thick slot is considered in terms of its constituent elements, namely, junctions and lengths of transmission line. The junction parameters are generally

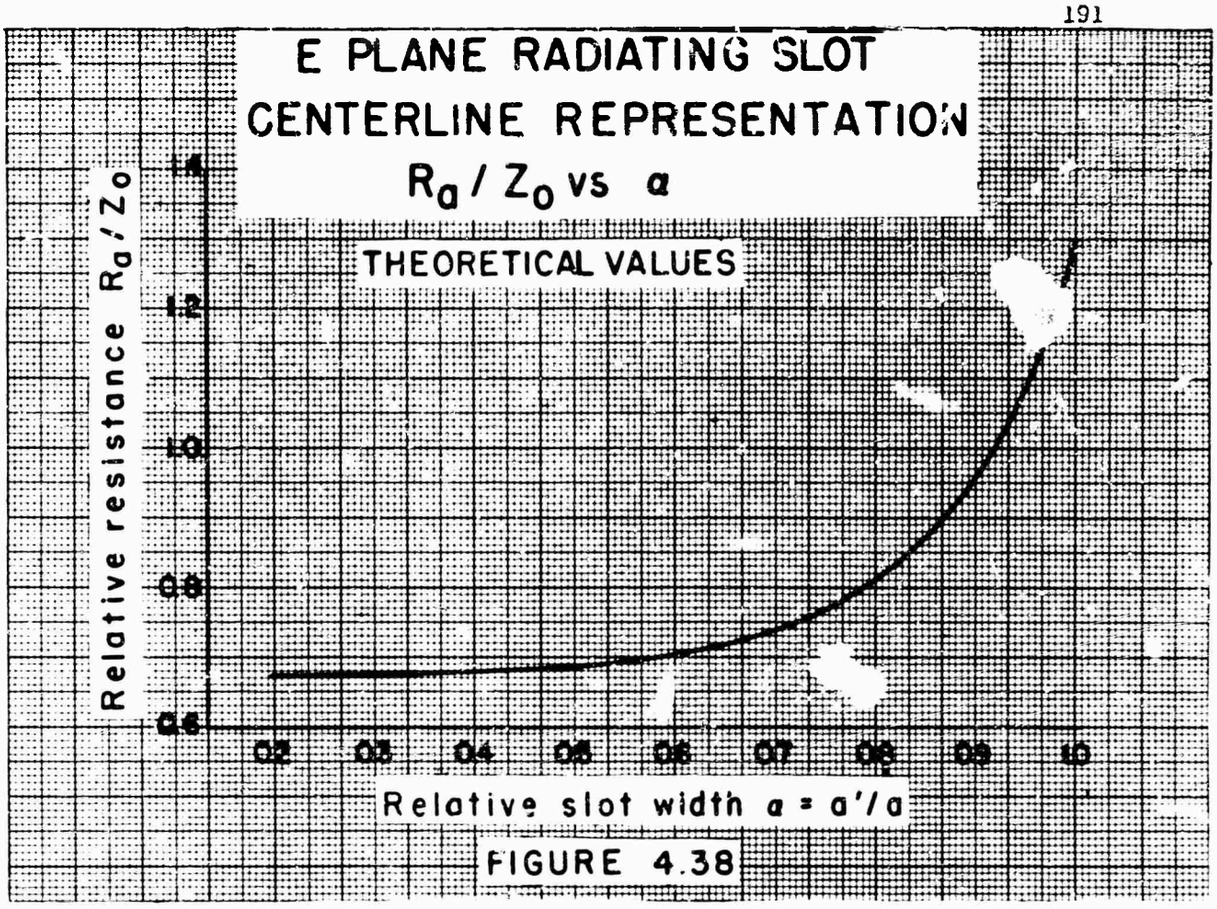

FIGURE 4.38

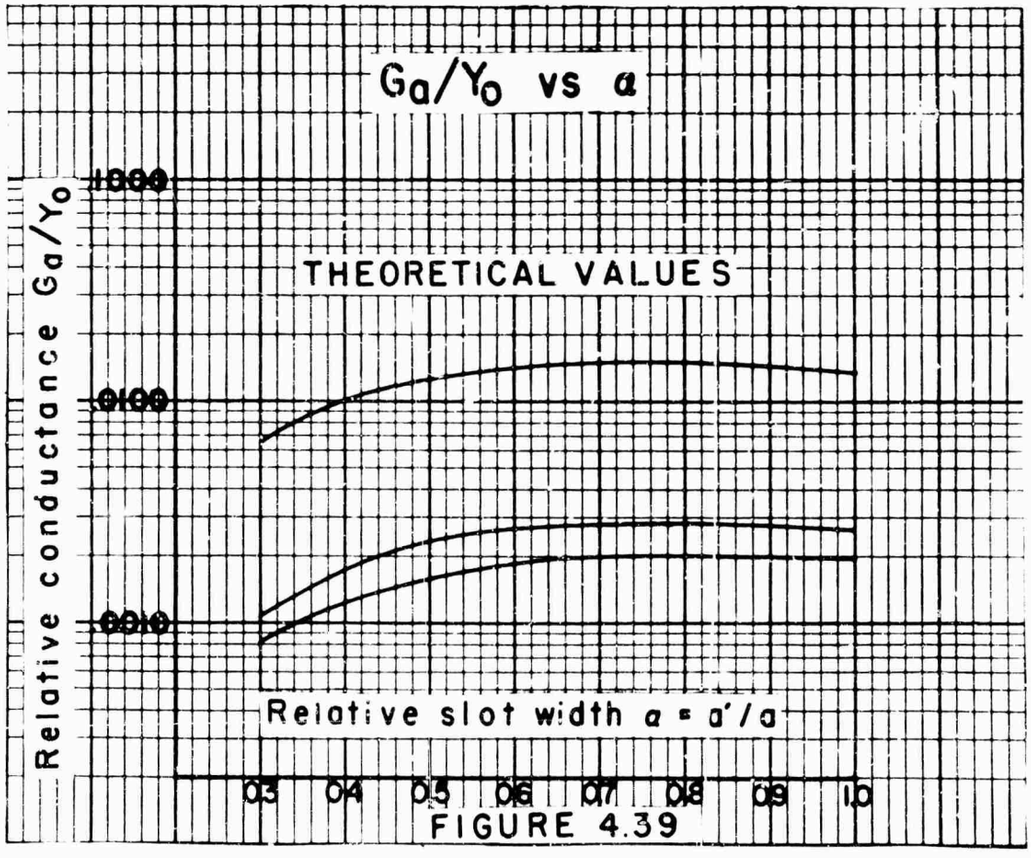

FIGURE 4.39

expressible in terms of the parameters of corresponding infinitesimally thick slots. The parameters for a number of such junctions have been given in Part III, Sec. E. It should be recognized, however, that the junction parameters were obtained by microwave network considerations from the parameters of slots of infinitesimal thickness; only the latter parameters were determined from the variational expressions.

The thick slots discussed below are the transverse radiating slot, the slot-coupled E plane Tee and the E plane radiating slot. The experimental data taken for them directly yield the parameters of the overall thick structure as a function of slot thickness. Such data are given in both tabular and graphical form. The measurement methods involved, and the experimental techniques necessary for obtaining the data, are discussed in Part II. The thick transverse slot coulping identical waveguides is omitted here since it has been fully discussed in the above-mentioned Final Report.

The data are treated in two ways. The first is to insert the theoretical values for the parameters of the junctions and lengths of transmission line in the composite equivalent network for the thick slot, and to compute from this a theoretical prediction for the parameters of the overall thick slot. These theoretical results are then graphically compared with the corresponding experimental data; the agreement has been found to be very satisfactory. The second method of treating the data is based upon the understanding that the parameters of a component junction of the thick slot will not change as the slot thickness is varied. The parameters of this junction are computed from the experimental data of the overall thick slot and the theoretical results for the remaining junctions and lengths of transmission line of the composite network. A plot of the parameters of this junction as a function of slot thickness should yield a horizontal line. The latter way of treating the data serves both to check the internal consistency of the data, and as a semi-experimental means of determining the junction parameters. The check, however, is a very sensitive one, and produces a scatter in the above-mentioned plot. The scatter has been investigated and is found to be completely explained by the possible errors in the experimental data. The composite and overall equivalent networks for the various thick slots are given in Part II, together with all the pertinent relations allowing one to treat the data in the two fashions described above. Consistent notation has been employed, wherein the parameters of the thick slot have the additional subscript "tk", and those of the junction the subscript "j".

1.) The Transverse Radiating Slot

The geometry of the thick slot under consideration is given in Figure 4.40, together with its overall equivalent circuit representation.

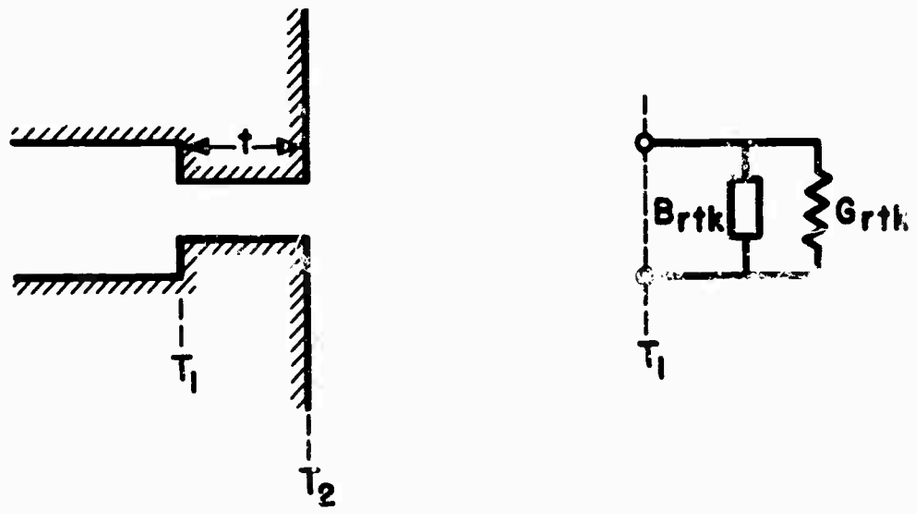

GEOMETRY OVERALL EQUIVALENT NETWORK

Figure 4.40 - The thick transverse radiating slot.

As is shown in Figure 4.40, the equivalent network is referred to plane T_1. Experimental data were taken of the input admittance at plane T_1, yielding the values of $G_{rtk}/Y_o + j\, B_{rtk}/Y_o$, for slots of three different aperture dimensions as a function of thickness t of the slot. Details of the experimental techniques involved have been given in the Final Report, Chap. IV, and in Part II, C, of this report.

The three thick slots on which measurements were taken are numbered I, II and III, and have the following cross-section dimensions:

I) $a' = .811"$, $b' = .161"$

II) $a' = .631"$, $b' = .321"$

III) $a' = .269"$, $b' = .320"$

The notation has been used consistently in previous sections, and is given explicitly in Figure 2.20. The waveguide formed by the thick slot itself is a propagating one for slot I, a guide at a very near cut-off for slot II, and a below cut-off guide for slot III. These considerations are with respect to the dominant mode, of course. The experimental results are listed in Table 4-IV for the three slots. For slot III, which is below cut-off, the VSWR was not measurable so that susceptance values only are reported.

The theoretical values for G_{rtk}/Y_o and B_{rtk}/Y_o are obtained from the composite equivalent circuit representation shown in Figure 4.41. The component junctions are shown in Figure 4.42, (a) and (b). It is seen that the characteristic admittance of the slot guide is not $Y'_o = \kappa'/\omega\mu$, but is rather $\tilde{Y}_o$, which is given by:

$$\frac{\tilde{Y}_o}{Y_o} = \frac{1}{n_t^2}\,\frac{Y'_o}{Y_o} \tag{4.9}$$

where $Y'_o/Y_o = \lambda_g/\lambda'_g$, and n_t^2 is given by Equation (2.1). The term $\tilde{Y}_o/Y_o$ is explicityly given in Equation (2.4). The use of $\tilde{Y}_o$ instead of Y'_o eliminates the use of a transformer in the equivalent circuit of Figure 4.42-(a) for the transverse junction (cf. Figure 2.9-(a)), and is used because of this simplification. These matters are further discussed in Part II, Sec.C.

The parameters B_{rtk}/Y_o and G_{rtk}/Y_o of the overall structure are obtained from the components of the composite representation by the use of Equation (2.9). The theoretical expression for B_{tj}/Y_o is taken as $0.55\ B_t/Y_o$; a slightly less accurate but simpler expression would be $B_t/2Y_o$. Parameter B_t/Y_o is given by Equation (3.107) or (3.108), depending on the slot dimensions; values in graphical form appear in Figures 4.3, 4.4, 4.6 and 4.7, valid at $\lambda = 3.20$ cms. The theoretical expressions for $\tilde{G}_{rj}/Y_o$ and $\tilde{B}_{rj}/Y_o$ are

$$\tilde{G}_{rj}/Y_o = G_r/Y_o \tag{4.10a}$$

$$\tilde{B}_{rj}/Y_o = B_r/Y_o - B_{tj}/Y_o \tag{4.10b}$$

which are deduced from the composite network of Figure 4.41. If the alternative composite network of Figure 2.21-(a) is used, then

TABLE 4-IV

THICK TRANSVERSE RADIATING SLOT

Experimental Results

Slot I: $a' = .811"$, $b' = .161"$, $\lambda = 1.259"$

$a'/a = .901$, $b'/b = .402$; $\lambda'_g = 2.00"$

$\tilde{Y}_o/Y_o = 2.21$; t and d are in inches.

t	r	d	G_{rtk}/Y_o	B_{rtk}/Y_o
1.199	4.9	.067	2.14	2.31
1.100	3.88	.110	1.28	1.63
.999	2.56	.161	0.97	0.96
.901	1.44	.251	0.87	0.32
.801	1.47	- .290	0.79	- 0.28
.701	2.52	- .154	1.02	- 0.97
.600	3.83	- .088	1.63	- 1.74
.501	4.79	.043	3.16	- 2.19
.401	8.26	- .006	5.43	- 0.64
.202	5.95	.065	2.10	2.73
.102	4.34	.112	1.18	1.73
.077	4.10	.123	1.07	1.58
.050	3.45	.137	1.01	1.33

Slot II: $a' = .631"$, $b' = .321"$; $\lambda = 1.259"$

$a'/a = .701$, $b'/b = .802$; $\lambda'_g = 21.6"$

$\tilde{Y}_o/Y_o = .113$; t and d in inches.

TABLE 4-IV (continued)

t	r	d	G_{rtk}/Y_o	B_{rtk}/Y_o
.999	5.6	- .285	.24	- .59
.900	4.9	- .282	.28	- .60
.801	4.3	- .275	.33	- .62
.700	3.8	- .265	.39	- .65
.601	3.42	- .258	.44	- .66
.500	2.9	- .258	.52	- .63
.401	2.40	- .253	.60	- .57
.300	2.09	- .254	.66	- .53
.249	1.94	- .261	.70	- .51
.201	1.77	- .265	.74	- .42
.151	1.62	- .286	.74	- .34
.101	1.49	- .307	.76	- .25
.076	1.39	- .322	.78	- .20
.051	1.40	- .335	.76	- .18
.026	1.37	- .364	.76	- .13

Slot III: $a' = .269"$, $b' = .\,:0"$; $\lambda = 1.259"$

$a'/a = .299$, $b'/b = .802$; $\lambda'_g = j\ .595"$

$\tilde{Y}_o/Y_o = -j\ 7.95$; t and d are in inches.

r = VSWR > 30 over most of the range.

t	d	B_{rtk}/Y_o
.501	- .023	- 12.3
.450	- .023	- 12.4
.400	- .021	- 13.7
.347	- .023	- 12.2
.299	- .023	- 12.0
.251	- .021	- 13.3
.201	- .023	- 12.3
.151	- .021	- 13.5
.102	- .023	- 12.3
.074	- .022	- 12.6
.048	- .026	- 10.8
.025	- .032	- 8.8

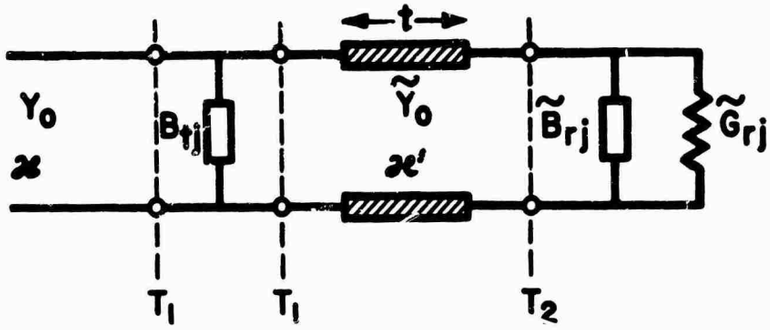

Figure 4.41 - Composite network for thick transverse radiating slot.

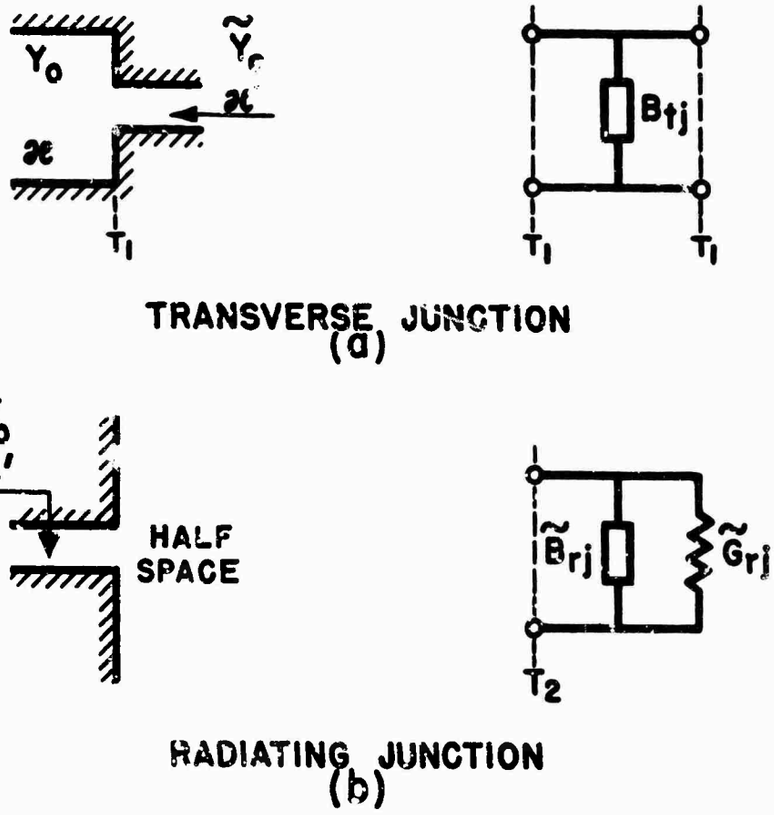

Figure 4.42 - Component junctions of the thick transverse radiating slot.

$$G_{rj}/Y_o = n_t^2 \; G_r/Y_o \qquad (4.11a)$$

$$B_{rj}/Y_c = n_t^2 \left[B_r/Y_o - B_{tj}/Y_o \right] \qquad (4.11b)$$

Parameter B_{tj}/Y_o has been discussed above, and expressions for parameters G_r/Y_o and B_r/Y_o are given in Part III, Sec. E, 3); numerical values at $\lambda = 3.20$ cms. are reported graphically in Figures 4.9, 4.10, 4.12 and 4.13 for B_r/Y_o and in Figure 4.14 for G_r/Y_o. Expressions for γ' and $\tilde{Y}_o/Y_o$ are given, respectively, in Equations (2.5a) and (2.4). The length t of the intervening transmission line is simply the slot thickness.

The theoretical values for these component parameters for the three slots are obtained as:

TABLE 4-V

SLOT	B_{tj}/Y_o	$\tilde{G}_{rj}/Y_o$	$\tilde{B}_{rj}/Y_o$	λ'_g	$\tilde{Y}_o/Y_o$
I	.204	.84	.77	2.000"	2.21
II	- .267	.73	.13	21.6"	.113
III	-4.5	.66	-4.5	j .595"	j 7.95

The last slot has imaginary values for λ'_g and $\tilde{Y}_o/Y_o$ because it is below cut-off.

A comparison of theoretical and experimental values for B_{rtk} and G_{rtk} is given graphically in Figures 4.43 to 4.47. The theoretical values obtained from the component theoretical values listed in Table 4-V are represented by solid lines; the experimental values by the indicated points. The agreement is seen to be quite satisfactory, although slightly better agreement is obtainable if some of the component parameter values are changed slightly. The results of such changes for some of the graphs are shown by the dashed lines; the changes involved are given in the respective figures.

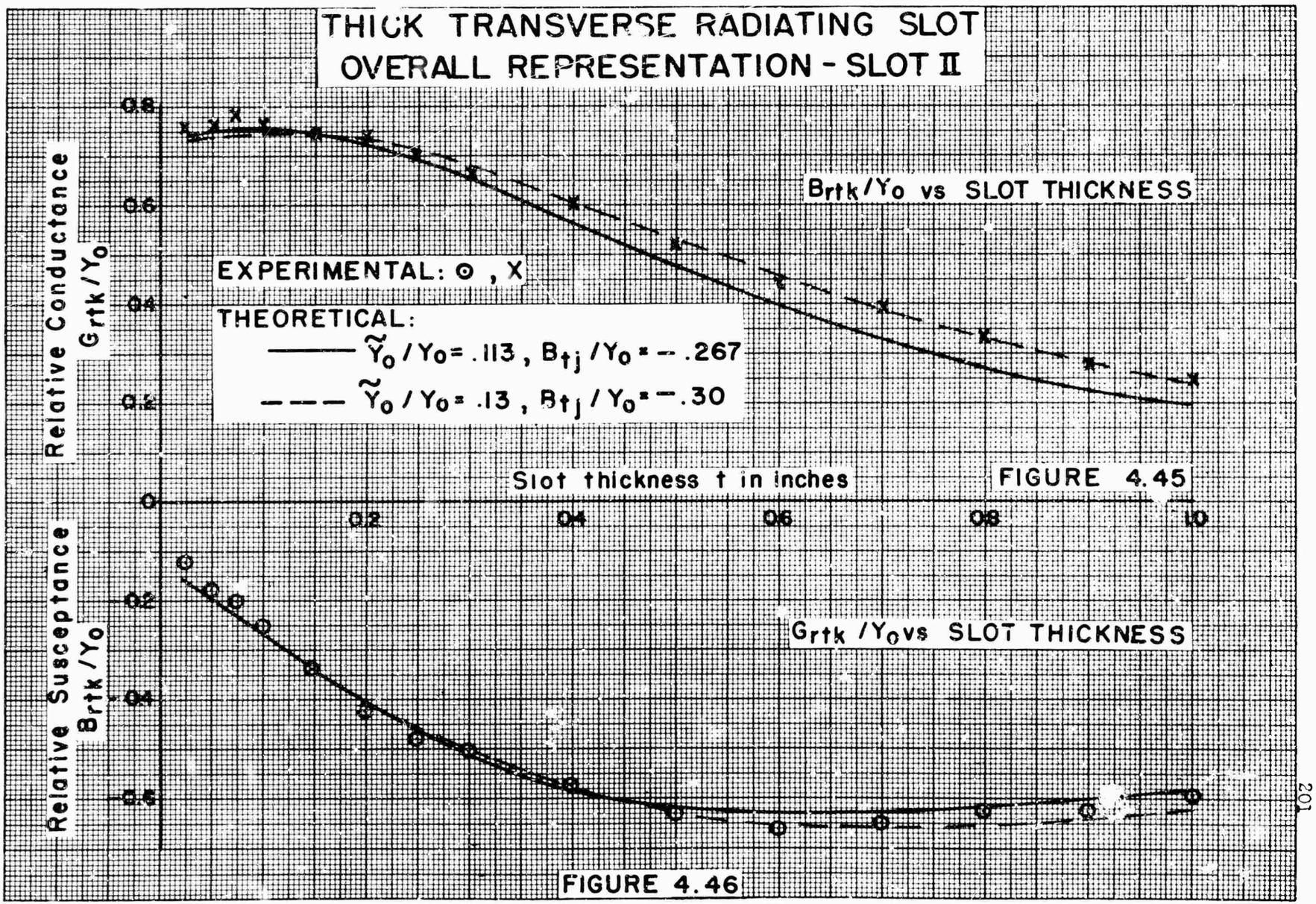
THICK TRANSVERSE RADIATING SLOT
OVERALL REPRESENTATION - SLOT II
Brtk/Yo vs SLOT THICKNESS
EXPERIMENTAL: ⊙ , X
THEORETICAL:
——— Ỹo / Yo = .113 , Btj / Yo = – .267
– – – Ỹo / Yo = .13 , Btj / Yo = – .30
Relative Conductance Grtk / Yo
Slot thickness t in inches
0.2
0.4
0.6
0.8
1.0
FIGURE 4.45
Grtk /Yo vs SLOT THICKNESS
Relative Susceptance Brtk / Yo
FIGURE 4.46

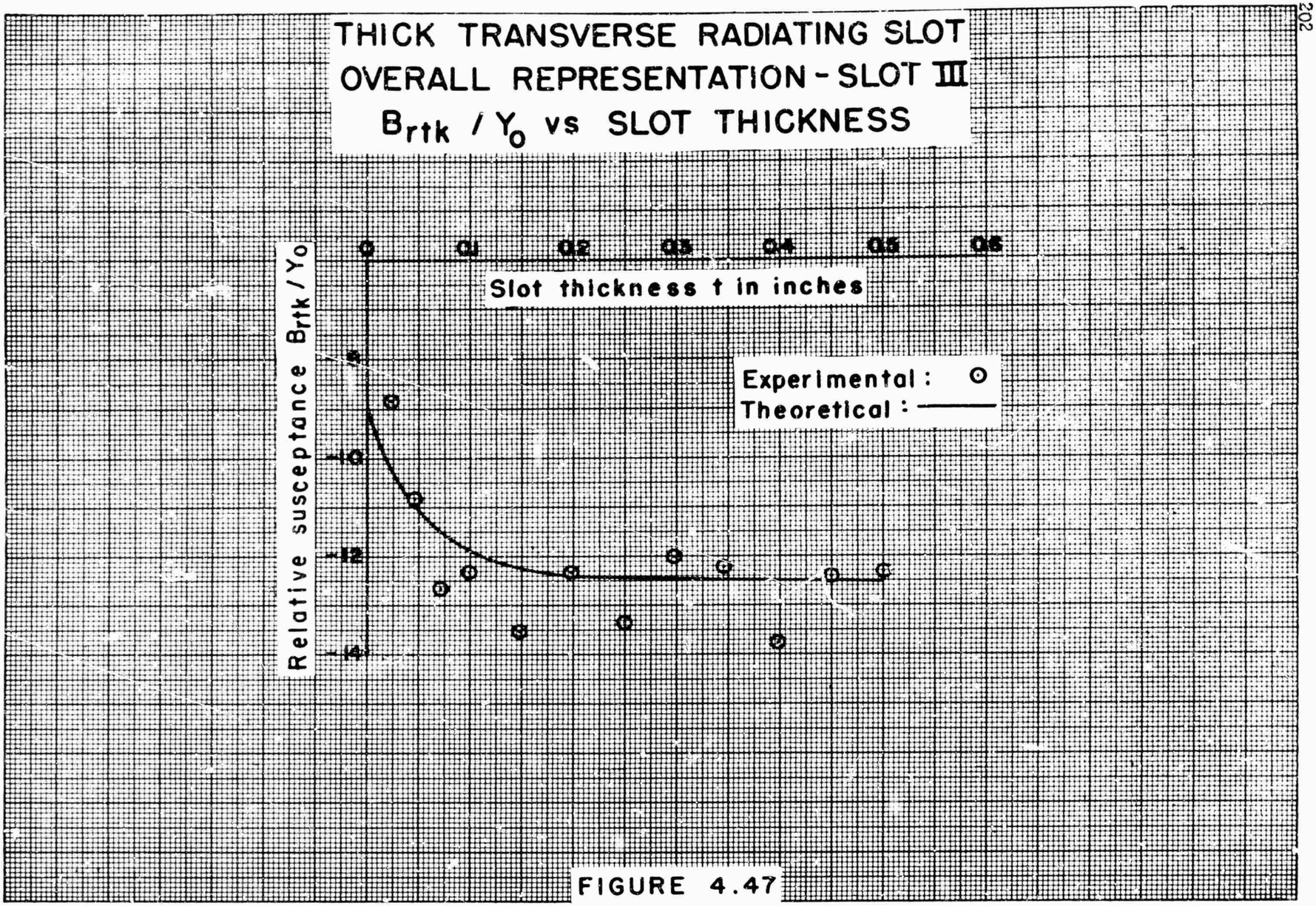
THICK TRANSVERSE RADIATING SLOT
OVERALL REPRESENTATION - SLOT III
B_{rtk} / Y_0 vs SLOT THICKNESS
Relative susceptance B_{rtk} / Y_0
Slot thickness t in inches
0
.01
.02
.03
.04
.05
.06
-.8
-1.0
-1.2
-1.4
Experimental : ⊙
Theoretical : ——

FIGURE 4.47

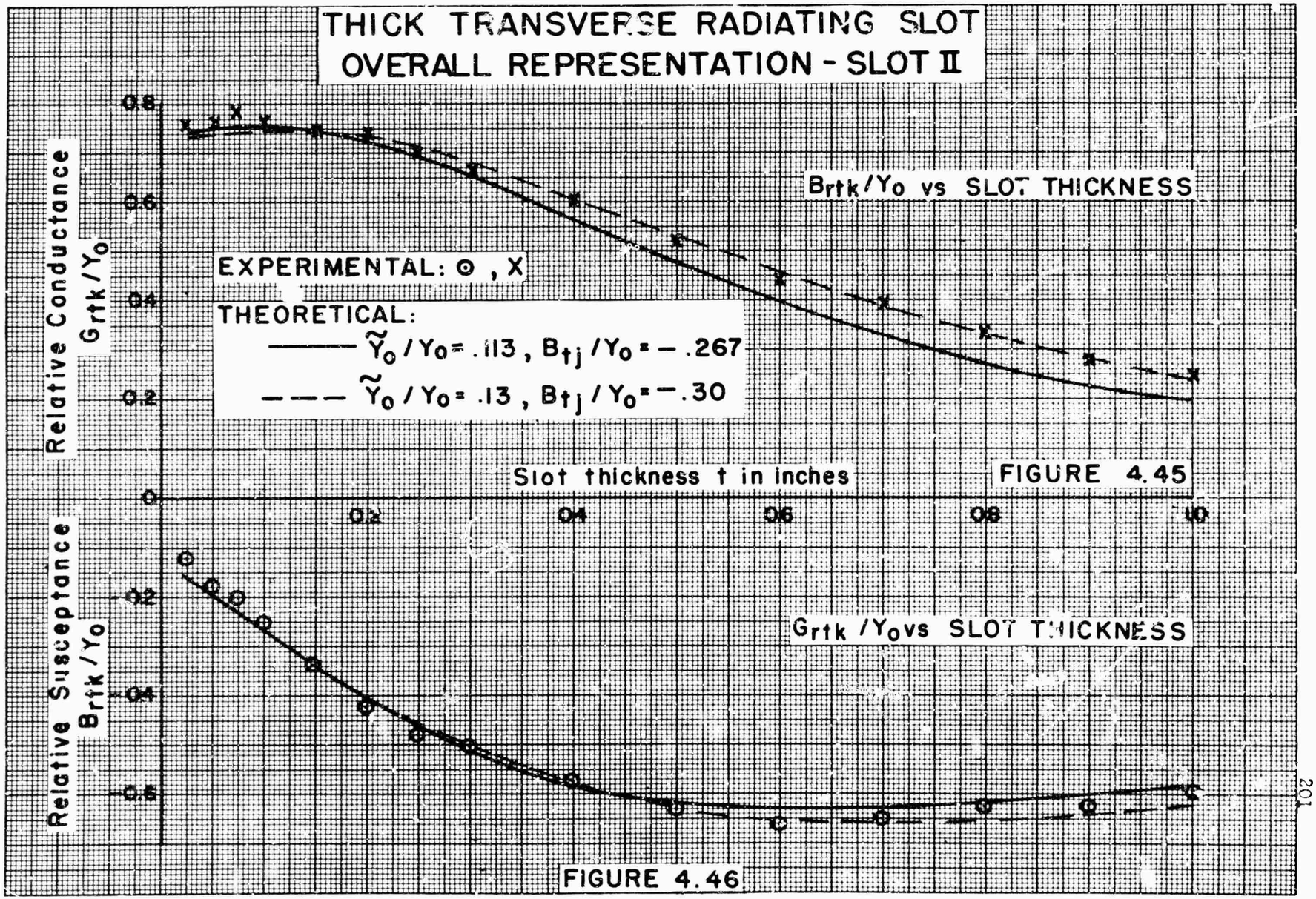

FIGURE 4.45

FIGURE 4.46

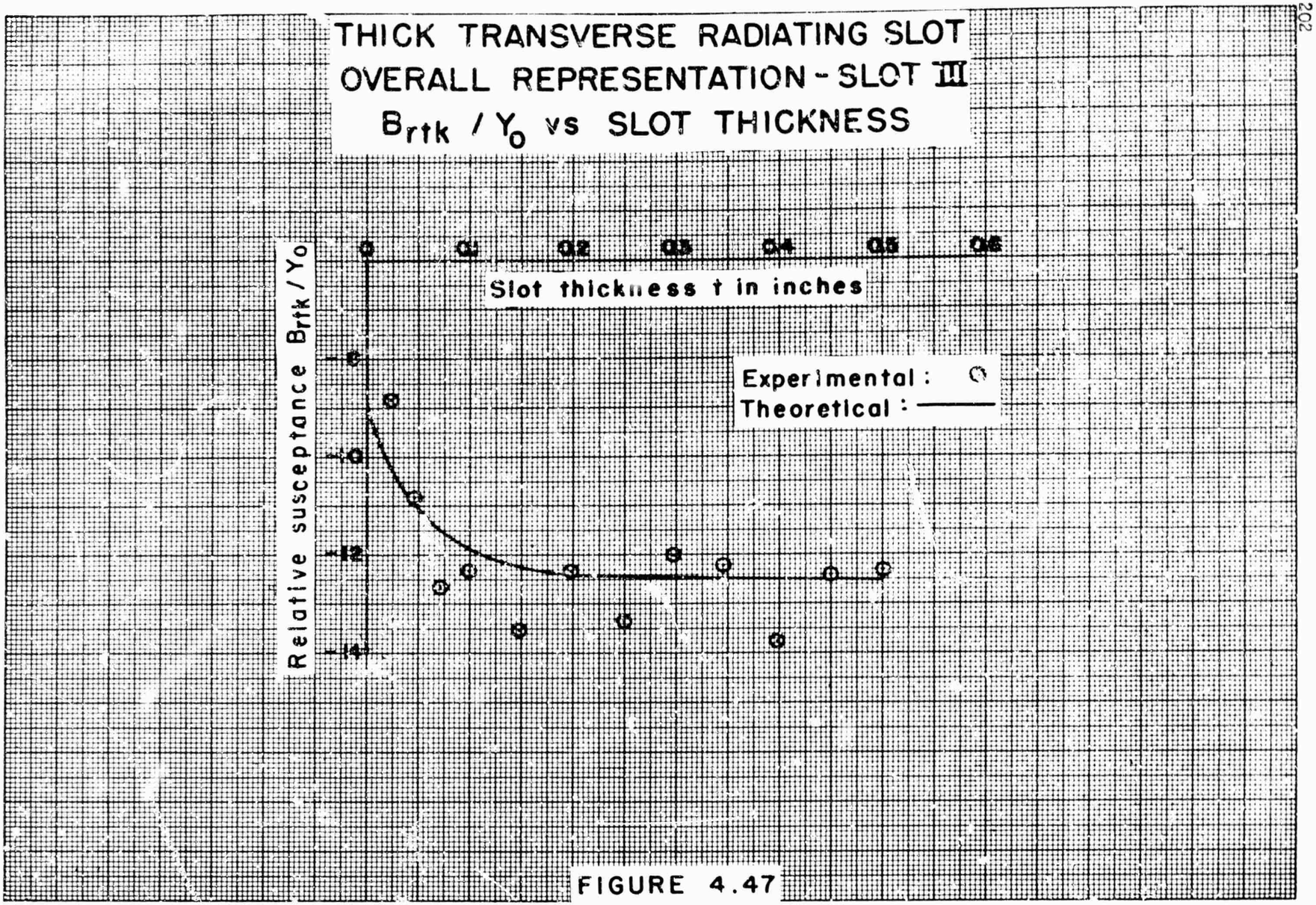
THICK TRANSVERSE RADIATING SLOT
OVERALL REPRESENTATION - SLOT III
B_{rtk} / Y_o vs SLOT THICKNESS
Slot thickness t in inches
Relative susceptance B_{rtk} / Y_o
Experimental :
Theoretical :
0
0.2
0.3
0.4
0.5
0.6
-12
-14

FIGURE 4.47

No comparison is made for G_{rtk}/Y_o for slot III because the experimental VSWR values were not measurable. However, it was ascertained that the VSWR was above 30 over most of the range so that the computation of G_{rtk}/Y_o and B_{rtk}/Y_o from the measurements is particularly simple, since

$$G_{rtk}/Y_o = 0 \quad , \quad B_{rtk}/Y_o = \cot \beta d \tag{4.12}$$

if $r^2 \gg 1$, $r^2 \gg \cot^2 \beta d$ (r = VSWR). The theoretical values of B_{rtk}/Y_o are likewise simply computed from Equation (2.7). The difference in the shape of the curves for the various slots is due to the value of the slot guide wavelength, λ_g'. For slot I, $\lambda_g' = 2.00"$, so that the curves will be repetitive with a period of 1.00" ; this is seen to be the case. Since $\lambda_g' = 2.16"$ for slot II, only a slow variation of the input admittance values is obtained. The behavior for slot III occurs because the slot guide is beyond cut-off. In all instances, however, very satisfactory approximations to the input admittance values for the thick slot are obtained by the use of the composite network of Figure 4.41, employing the theoretical expressions for the junction parameters.

The experimental data and a portion of the theoretical data for the component junctions can be treated in another fashion. The equivalence between the overall network of Figure 4.40 and composite network of Figure 4.41 can be used to obtain a semi-experimental value for the parameters of the radiating junction, shown in Figure 4.42-(b). The results for slots I and II are given in Figures 4.48 and 4.49, where the theoretical and semi-experimental values of $\tilde{B}_{rj}/Y_o$ and $\tilde{G}_{rj}/Y_o$ are compared. Corresponding results for slot III were not computed, since the slot is below cut-off and the conditions set down in Equations (2.6) and (2.7) apply over most of the range. The semi-experimental values of the radiating junction parameters were computed using Equations (2.5).

In Figures 4.48 and 4.49 the theoretical values, obtained from Table 4-V, are represented by the solid straight line as the value is independent of slot thickness t. The "experimental" values are shown by the indicated points, which are seen to fluctuate somewhat. They scatter about some constant value which in some cases does not agree well with the theoretical one, although in most cases the agreement is good. In order to be able to determine the cause of these fluctuations, it is desirable to find the effect of individual errors in measurements or incorrect theoretical values for the junction parameters on the radiating junction admittance $\tilde{Y}_{rj}/Y_o$.

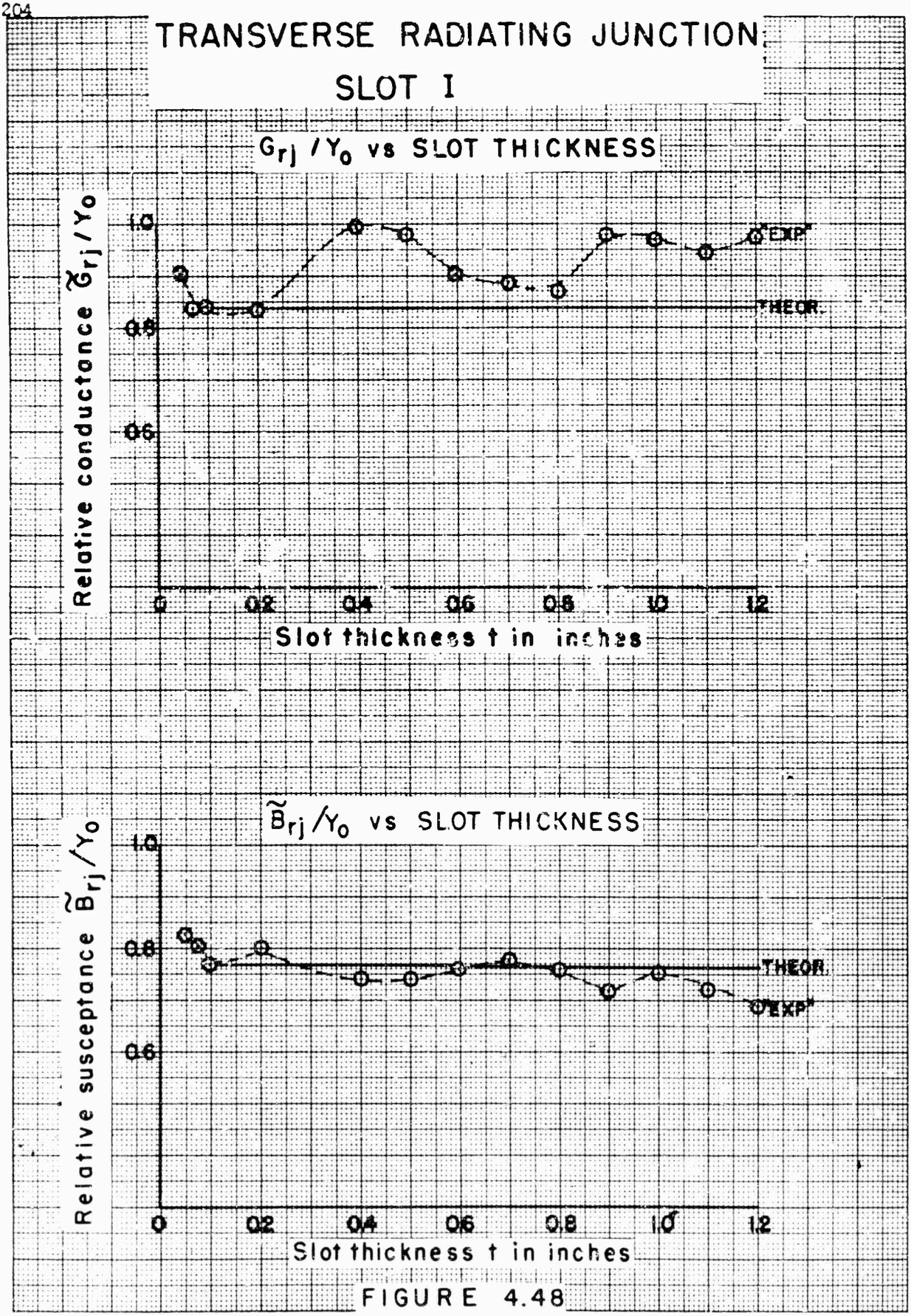
TRANSVERSE RADIATING JUNCTION
SLOT I
G_{rj}/Y_0 vs SLOT THICKNESS
Relative conductance $\tilde{G}_{rj}/Y_0$
1.0
0.8
0.6
EXP
THEOR.
0
0.2
0.4
0.6
0.8
1.0
1.2
Slot thickness t in inches
$\tilde{B}_{rj}/Y_0$ vs SLOT THICKNESS
Relative susceptance $\tilde{B}_{rj}/Y_0$
1.0
0.8
0.6
THEOR.
EXP
0
0.2
0.4
0.6
0.8
1.0
1.2
Slot thickness t in inches

FIGURE 4.48

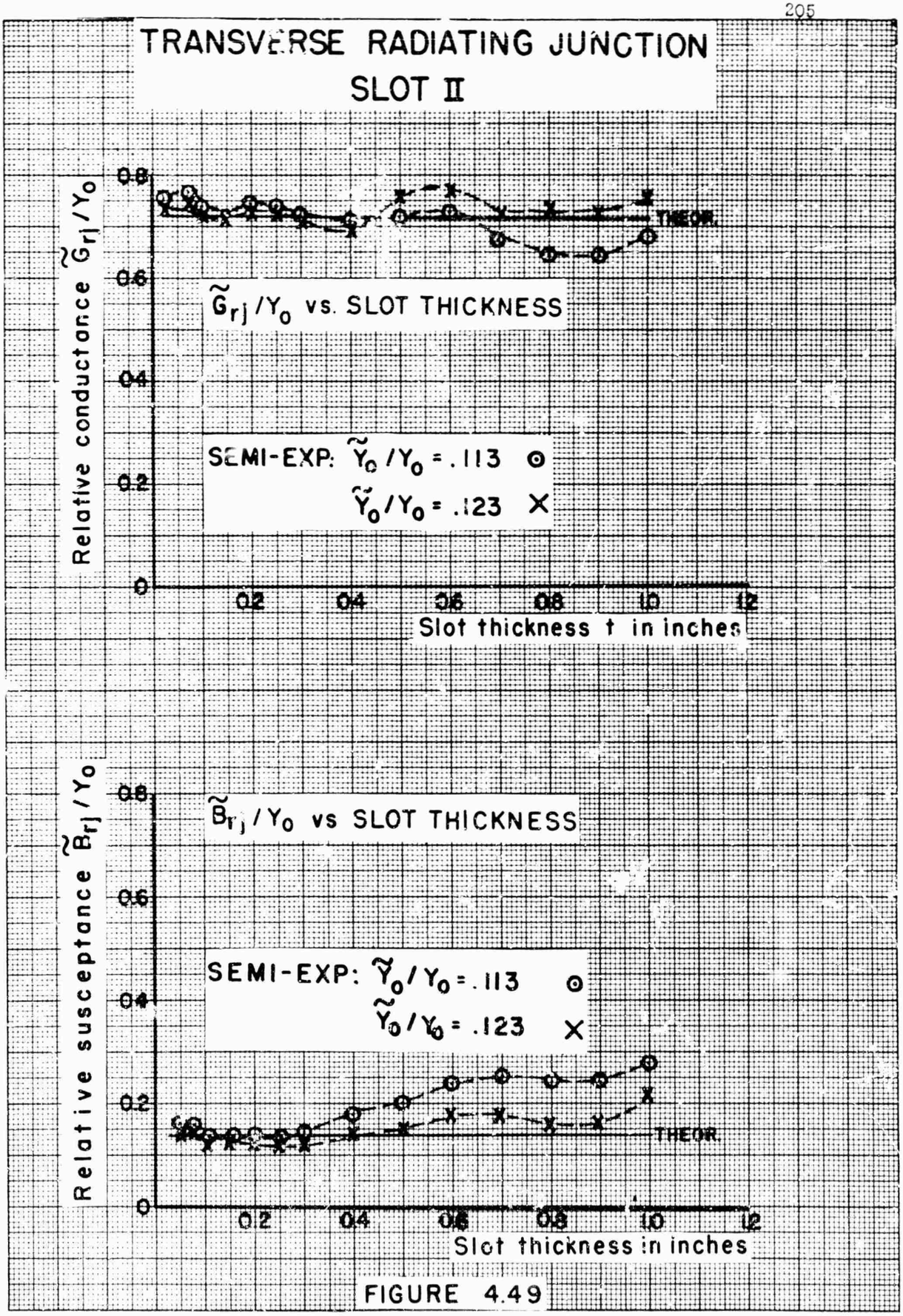
TRANSVERSE RADIATING JUNCTION
SLOT II
Relative conductance $\tilde{G}_{rj}/Y_0$
0.8
0.6
0.4
0.2
0
THEOR.
$\tilde{G}_{rj}/Y_0$ vs. SLOT THICKNESS
SEMI-EXP: $\tilde{Y}_0/Y_0 = .113$ ⊙
$\tilde{Y}_0/Y_0 = .123$ X
0.2
0.4
0.6
0.8
1.0
1.2
Slot thickness t in inches
Relative susceptance $\tilde{B}_{rj}/Y_0$
$\tilde{B}_{rj}/Y_0$ vs SLOT THICKNESS
SEMI-EXP: $\tilde{Y}_0/Y_0 = .113$ ⊙
$\tilde{Y}_0/Y_0 = .123$ X
THEOR.
Slot thickness in inches

FIGURE 4.49

The admittance $\tilde{Y}_{rj}/Y_o$ computed from Equations (2.5) is directly affected by errors in a) Y_{rtk}/Y_o which, in turn, depends on the measured VSWR and location of voltage minimum, b) slot thickness t, c) the value of $\tilde{Y}_o/Y_o$, and d) the value of B_{tj}/Y_o. The sensitivity of $\tilde{Y}_{rj}/Y_o$ to these errors is a function of thickness and may be so calculated. In addition, there may be mechanical factors, such as imperfect centering of the slot, variations in the cross-sectional dimensions of the slot, or such electrical imperfections as poor contact between vacuum chuck and slot and between slot and infinite plane (see Part II, Sec. C) which are not easily taken into account theoretically.

The effect of small deviations in the values of the first-mentioned quantities, however, is readily accounted for in the manner shown in Table 4-VI. The possible errors in the experimental quantities are arrived at from experience with the performance of the measuring equipment, while the possible range of variation in the network parameters is determined from the tolerances put on those values. A short discussion is given below of these possible errors.

a) VSWR: The inability to determine high VSWR's accurately when the measurements were first begun was a considerable source of error. The measuring equipment was improved, however, at a later date so that higher accuracy could be achieved. The following limits of accuracy are based on repeated checks against standard mismatches. For approximately the first half of the measurements (before the equipment was improved), $\Delta r = \pm .07\ r$, $r > 4$; $\Delta r = \pm .05\ r$, $4 > r > 3$; $\Delta r = \pm .03\ r$, $r < 3$; while the remaining data was taken with a tolerance of $\Delta r = \pm .02\ r$, $r < 5$.

b) Location of voltage minimum: The accurate location of voltage minima in the guide becomes increasingly difficult at low VSWR's. The procedure (employed in measurements of lossless discontinuities) of accentuating the "dip" in the voltage curve by raising the gain of the detector to any desired value cannot be applied here to the same degree because of the non-zero level of the voltage minimum which will go off scale for too great an amplification. However, it was found that even for VSWR's as low as 1.4, the voltage minimum could be located to within 2 mils, i.e., $\Delta d = \pm .002"$.

c) Slot thickness: To achieve different slot thicknesses the slots were cut down on a lathe after each measurement.

TABLE 4-VI

Estimates of Error for the Radiating Junction

The maximum total error in $\tilde{Y}_{rj}/Y_o$ introduced by individual small errors in the measurements of V.S.W.R. r and distance d to the voltage minimum from terminal plane T_1, and in the values of $\tilde{Y}_o/Y_o$, $\omega' t$, and B_{tj}/Y_o is given by:

$$\left|\Delta \tilde{C}_{rj}\right| = \left|\frac{\partial \tilde{C}_{rj}}{\partial r}\Delta r\right| + \left|\frac{\partial \tilde{C}_{rj}}{\partial d}\Delta d\right| + \left|\frac{\partial \tilde{C}_{rj}}{\partial (\omega' t)}\Delta (\omega' t)\right| + \left|\frac{\partial \tilde{C}_{rj}}{\partial \left(\frac{\tilde{Y}_o}{Y_o}\right)}\Delta \left(\frac{\tilde{Y}_o}{Y_o}\right)\right| + \left|\frac{\partial \tilde{C}_{rj}}{\partial \left(\frac{B_{tj}}{Y_o}\right)}\Delta \left(\frac{B_{tj}}{Y_o}\right)\right|$$

where $\tilde{C}_{rj}$ stands for either $\tilde{G}_{rj}/Y_o$ or $\tilde{B}_{rj}/Y_o$, and where

$$\frac{\partial \tilde{C}_{rj}}{\partial r,\, d} = \frac{\partial \tilde{C}_{rj}}{\partial G_{rtk}}\frac{\partial G_{rtk}}{\partial r,\, d} + \frac{\partial \tilde{C}_{rj}}{\partial B_{rtk}}\frac{\partial B_{rtk}}{\partial r,\, d}$$

The most probable error, rather than the maximum error, is obtained by taking the square root of the sum of the squares.

To evaluate the actual estimates of error, the sensitivity of $\tilde{G}_{rj}$ to variations in the quantities listed above must be computed. These sensitivities are found to be:

$$\frac{\partial (\tilde{G}_{rj}/Y_o)}{\partial (\omega' t)} = 2\,\frac{\tilde{G}_{rj}}{Y_o}\left[A\,\frac{\tilde{G}_{rj}}{G_{rtk}} - \cot \omega' t\right]$$

TABLE 4-VI (Continued)

$$\frac{\partial\left(\tilde{B}_{rj}/Y_o\right)}{\partial\left(\alpha' t\right)} = 2A\,\frac{\tilde{G}_{rj}}{G_{rtk}}\,\frac{\tilde{B}_{rj}}{Y_o} - \csc 2\alpha' t\left[\frac{\tilde{B}_{rj}}{Y_o} + \frac{\bar{B}}{Y_o}\,\frac{\tilde{G}_{rj}}{G_{rtk}}\right]$$

$$\frac{\partial\left(\tilde{G}_{rj}/Y_o\right)}{\partial\left(Y_o/\bar{Y}_o\right)} = -\frac{2}{A^2+B^2}\,\frac{\tilde{G}_{rj}}{Y_o}\left\{\frac{\bar{B}}{Y_o}\cot\alpha' t + \frac{Y_o}{\bar{Y}_o}\left[\left(\frac{G_{rtk}}{Y_o}\right)^2 + \left(\frac{\bar{B}}{Y_o}\right)^2\right]\right\}$$

$$\frac{\partial\left(\tilde{B}_{rj}/Y_o\right)}{\partial\left(Y_o/\bar{Y}_o\right)} = \frac{1}{A^2+B^2}\left\{\cot\alpha' t\left[\left(\frac{G_{rtk}}{Y_o}\right)^2 + \left(\frac{\bar{B}}{Y_o}\right)^2 + \left(\frac{\tilde{Y}_o}{Y_o}\right)^2\right] - 2\,\frac{\tilde{B}_{rj}}{Y_o}\left[A\,\frac{\bar{B}}{Y_o} + B\,\frac{G_{rtk}}{Y_o}\right]\right\}$$

$$\frac{\partial\left(\tilde{G}_{rj}/Y_o\right)}{\partial\left(B_{tj}/Y_o\right)} = \frac{2AB}{A^2+B^2}\,\frac{\tilde{G}_{rj}}{G_{rtk}} = -\frac{\partial\left(\tilde{G}_{rj}/Y_o\right)}{\partial\left(B_{rtk}/Y_o\right)} = \frac{\partial\left(\tilde{B}_{rj}/Y_o\right)}{\partial\left(G_{rtk}/Y_o\right)}$$

$$\frac{\partial\left(\tilde{G}_{rj}/Y_o\right)}{\partial\left(G_{rtk}/Y_o\right)} = \frac{A^2-B^2}{A^2+B^2}\,\frac{\tilde{G}_{rj}}{G_{rtk}} = \frac{\partial\left(\tilde{B}_{rj}/Y_o\right)}{\partial\left(B_{rtk}/Y_o\right)} = -\frac{\partial\left(\tilde{B}_{rj}/Y_o\right)}{\partial\left(B_{tj}/Y_o\right)}$$

$$\frac{\partial\left(G_{rtk}/Y_o\right)}{\partial r} = \frac{1}{r^2}\left(\frac{G_{rtk}}{Y_o}\right)^2\left(\cos^2\alpha\, d - r^2\sin^2\alpha\, d\right)$$

$$= \frac{1}{\alpha\left(r^2-1\right)}\,\frac{\partial\left(B_{rtk}/Y_o\right)}{\partial d}$$

TABLE 4-VI (Continued)

$$\frac{\partial (B_{rtk}/Y_o)}{\partial r} + \frac{2}{r^2 - 1} \frac{G_{rtk}}{Y_o} \frac{B_{rtk}}{Y_o} = - \frac{1}{\pi(r^2 + 1)} \frac{\partial(G_{rtk}/Y_o)}{\partial d}$$

where $A = \cot \pi t + \frac{Y_o}{\tilde{Y}_o} \frac{\bar{B}}{Y_o}$

$$B = \frac{Y_o}{\tilde{Y}_o} \frac{G_{rtk}}{Y_o}$$

$$\frac{\bar{B}}{Y_o} = \frac{B_{rtk}}{Y_o} - \frac{B_{tj}}{Y_o}$$

Care was taken to turn down the same face of the slot each time, and the turned-down surface was lapped afterwards to remove any high spots. After lapping, the slot thickness was measured with a micrometer to within 1 mil so that $\Delta t = \pm .001"$.

d) $\tilde{Y}_o/Y_o$ and B_{tj}/Y_o : From previously reported agreement between theory and experiment on the values of $\tilde{Y}_o/Y_o$ and B_{tj}/Y_o the tolerances on these parameters can be taken as $\pm$ 3 percent for B_{tj}/Y_o , and $\pm$ 2 percent for $\tilde{Y}_o/Y_o$. These estimated errors are approximate and are not as small as indicated in some ranges of slot dimensions.

A complete error analysis has been carried through for slot I; for a range of slot thicknesses from .5" to 1.2"; the sensitivities of $\tilde{G}_{rj}/Y_o$ and $\tilde{B}_{rj}/Y_o$ to errors in the above-mentioned quantities are plotted as functions of t in Figure 4.50. The values of $\tilde{G}_{rj}/Y_o$ and $\tilde{B}_{rj}/Y_o$, together with the estimated errors as obtained from Figures 4.50 and the estimated component errors above, are given in Table 4-VII.

TABLE 4-VII

Semi-experimental values of $\tilde{Y}_{rj}/Y_o$ for slot I

$a' = .811"$, $b' = .161"$, $\lambda'_g = 2.00"$

Theoretical value of $\tilde{Y}_{rj}/Y_o = .84 + j\ .77$

t = slot thickness in inches.

t	$\tilde{G}_{rj}/Y_o$	$\tilde{B}_{rj}/Y_o$
1.199	.97 $\pm$ .09	.69 $\pm$ .08
1.100	.94 $\pm$ .06	.72 $\pm$ .07
.999	.97 $\pm$ .02	.76 $\pm$ .05
.901	.98 $\pm$ .02	.72 $\pm$ .06
.801	.87 $\pm$ .04	.76 $\pm$ .05
.701	.88 $\pm$ .06	.77 $\pm$ .08
.600	.91 $\pm$ .08	.76 $\pm$ .08
.501	.98 $\pm$ .13	.74 $\pm$ .07
.401	.99	.74
.202	.84	.80
.102	.85	.77
.077	.84	.81
.050	.91	.83

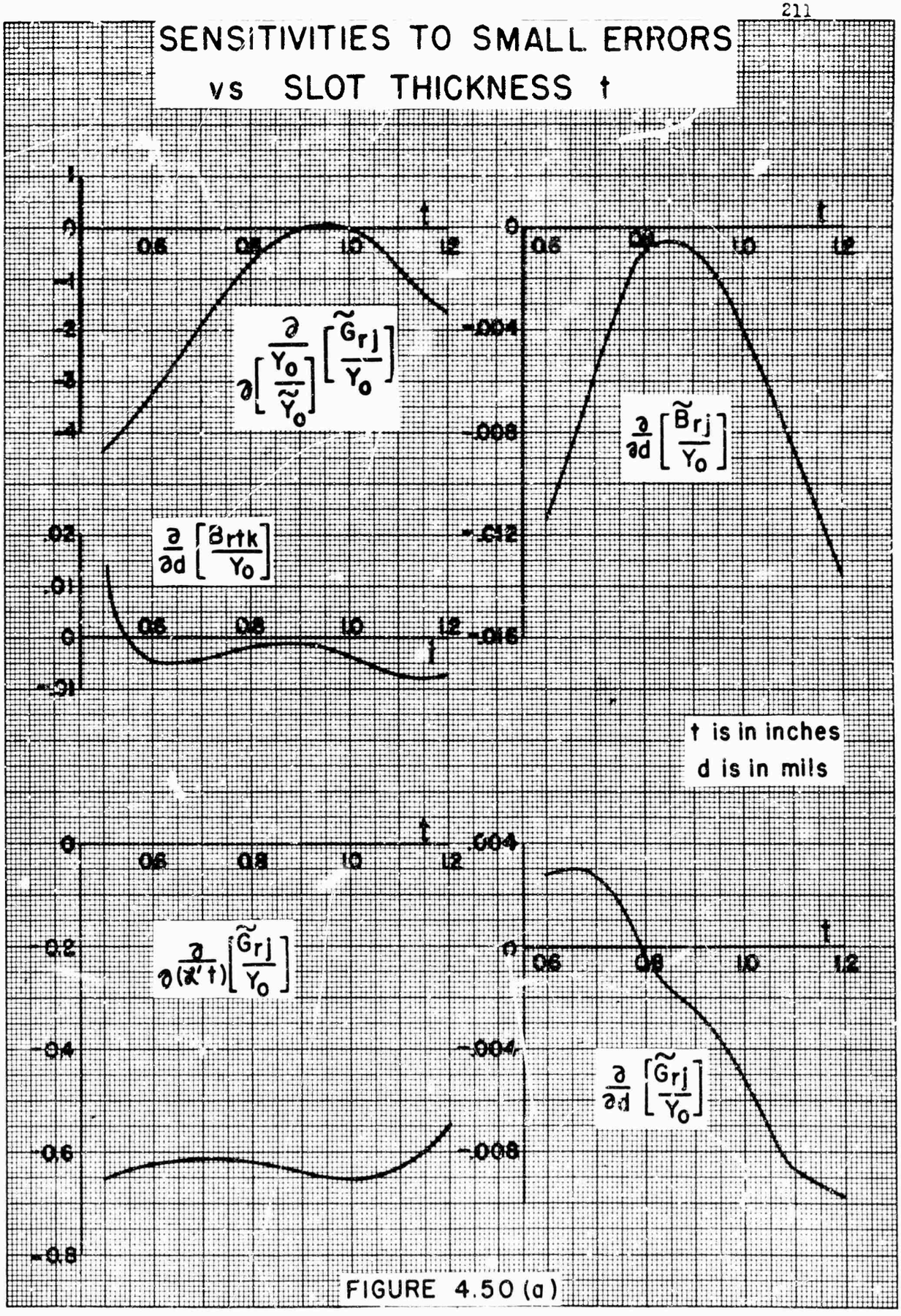
SENSITIVITIES TO SMALL ERRORS
vs SLOT THICKNESS t
$\frac{\partial}{\partial\left[\frac{Y_0}{\tilde{Y}_0}\right]}\left[\frac{\tilde{G}_{rj}}{Y_0}\right]$
$\frac{\partial}{\partial d}\left[\frac{\tilde{B}_{rj}}{Y_0}\right]$
$\frac{\partial}{\partial d}\left[\frac{B_{rtk}}{Y_0}\right]$
$\frac{\partial}{\partial(\alpha' t)}\left[\frac{\tilde{G}_{rj}}{Y_0}\right]$
$\frac{\partial}{\partial d}\left[\frac{\tilde{G}_{rj}}{Y_0}\right]$
t is in inches
d is in mils
t
0.6
0.8
1.0
1.2

FIGURE 4.50 (a)

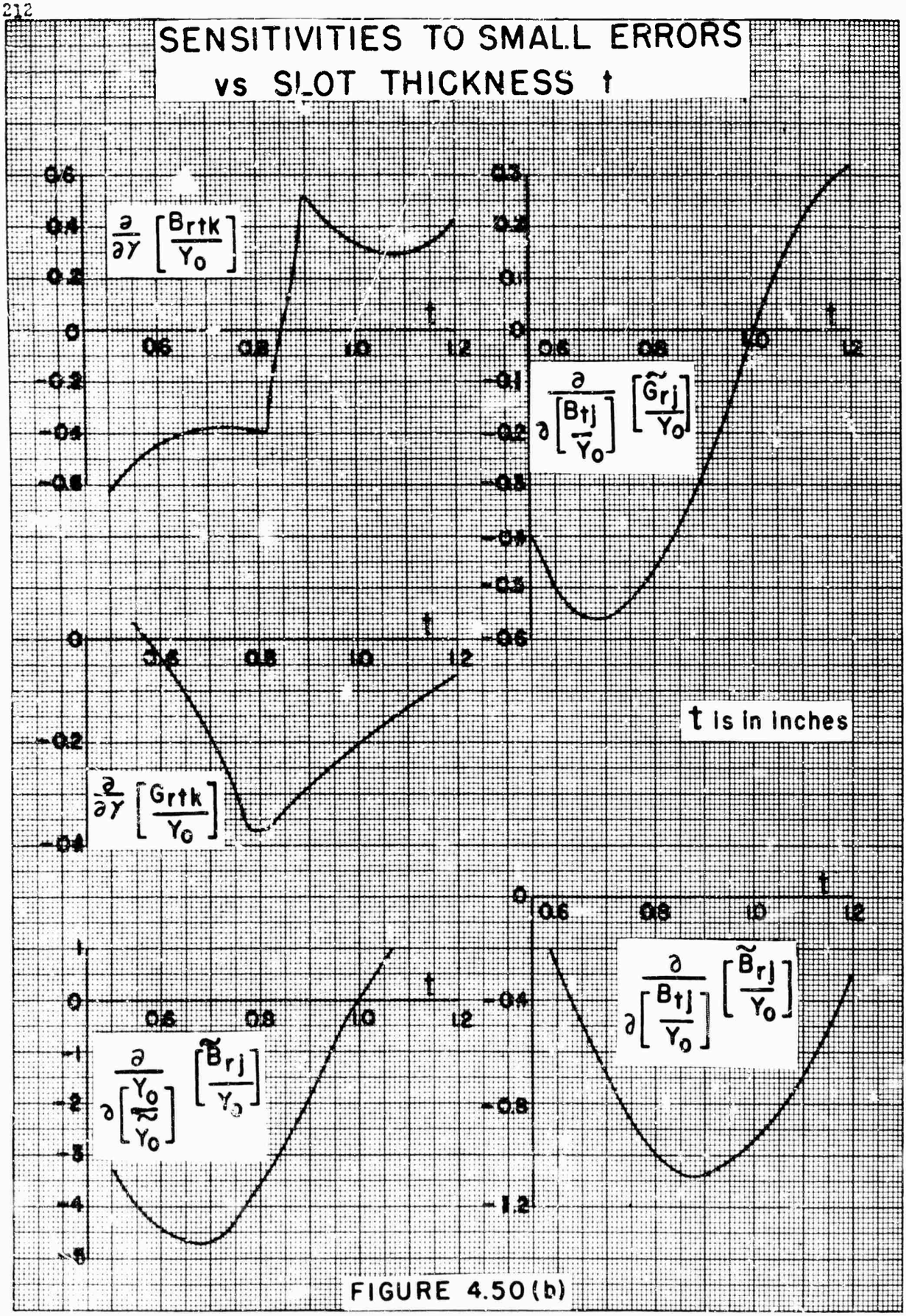
SENSITIVITIES TO SMALL ERRORS
vs SLOT THICKNESS t
$\frac{\partial}{\partial \gamma}\left[\frac{B_{rtk}}{Y_0}\right]$
$\frac{\partial}{\partial\left[\frac{B_{tj}}{Y_0}\right]}\left[\frac{\tilde{G}_{rj}}{Y_0}\right]$
$\frac{\partial}{\partial \gamma}\left[\frac{G_{rtk}}{Y_0}\right]$
$\frac{\partial}{\partial\left[\frac{B_{tj}}{Y_0}\right]}\left[\frac{\tilde{B}_{rj}}{Y_0}\right]$
$\frac{\partial}{\partial\left[\frac{Y_0}{\tilde{Y}_0}\right]}\left[\frac{\tilde{B}_{rj}}{Y_0}\right]$
t
t is in inches

FIGURE 4.50 (b)

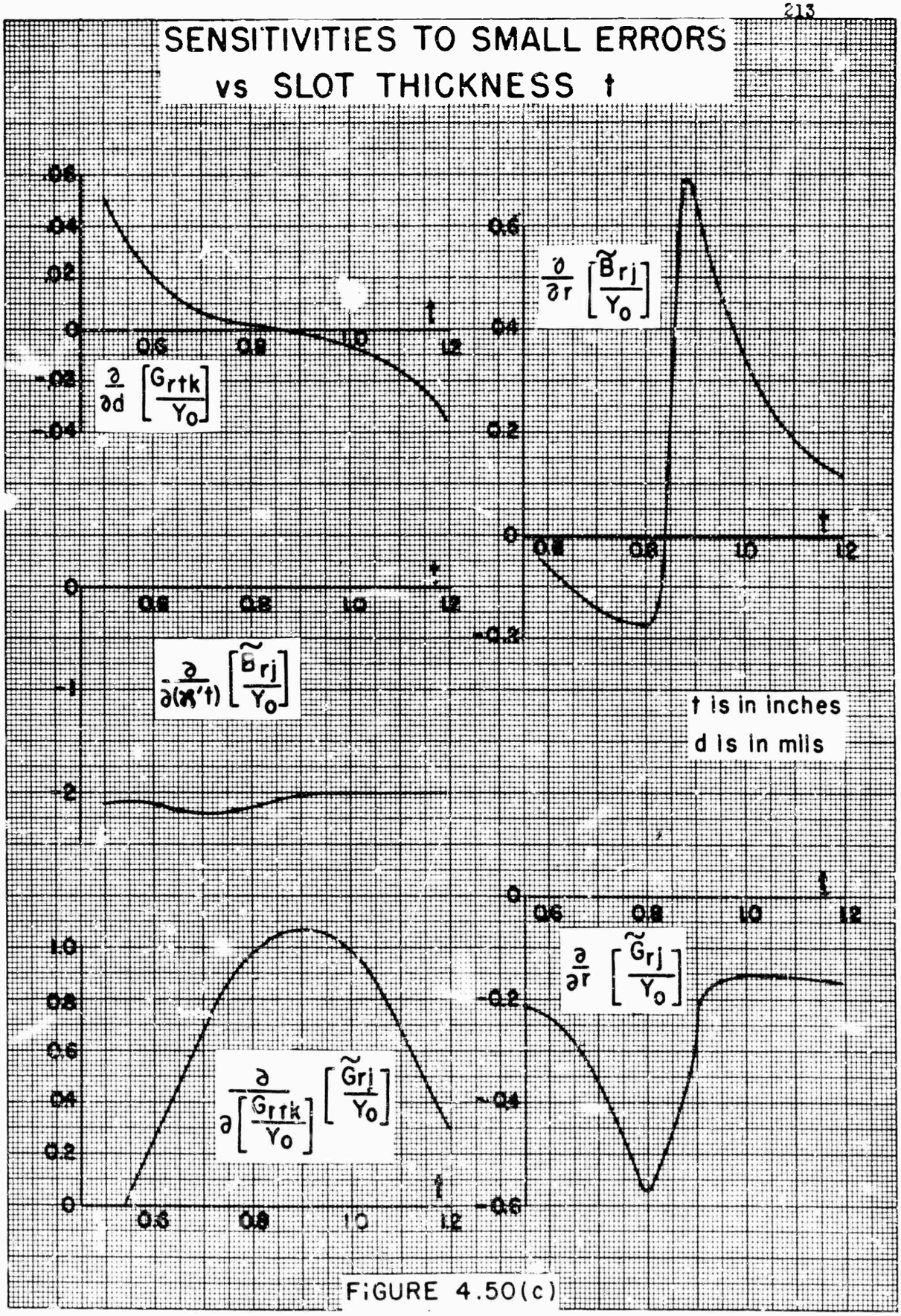
SENSITIVITIES TO SMALL ERRORS
vs SLOT THICKNESS t
$\frac{\partial}{\partial d}\left[\frac{G_{rtk}}{Y_0}\right]$
$\frac{\partial}{\partial r}\left[\frac{\tilde{B}_{rj}}{Y_0}\right]$
$\frac{\partial}{\partial(\pi' t)}\left[\frac{\tilde{B}_{rj}}{Y_0}\right]$
$\frac{\partial}{\partial r}\left[\frac{\tilde{G}_{rj}}{Y_0}\right]$
$\frac{\partial}{\partial\left[\frac{G_{rtk}}{Y_0}\right]}\left[\frac{\tilde{G}_{rj}}{Y_0}\right]$
t is in inches
d is in mils
t
0.6
0.8
1.0
1.2
0.4
0.2
0
-0.2
-0.4
-0.6
-1
-2

FIGURE 4.50(c)

It is seen from Figure 4.48 that the tolerances on $\tilde{B}_{rj}/Y_0$ cover the entire range of scatter from some constant value, while those on $\tilde{G}_{rj}/Y_0$ do so except for two points.

A similar error analysis has been worked through for slot II but the details will not be presented; similar results are obtained. It is thus confirmed that the expectation of a constant value for $\tilde{Y}_{rj}/Y_0$ constitutes a very severe check of all the parameters involved, in that slight errors in otherwise reasonable data may give rise to a considerable scatter in the result.

In Figure 4.49, two sets of points are given corresponding to the semi-experimental data. The circled points correspond to a $\tilde{Y}_0/Y_0$ value equal to that given in Table 4-V, while the crosses correspond to a slight change in that value. The exact amounts are given on the figure; all of the other quantities are the same for both sets of points. The circled points indicate a slight slope which is largely eliminated by the better choice for $\tilde{Y}_0/Y_0$. However, the original choice is actually quite adequate for obtaining satisfactory engineering results for the parameters of the overall network, as seen in Figures 4.45 and 4.46, where such severe demands are not made on the accuracy of all the components of the composite network.

2.) The Slot-coupled E Plane Tee

The geometry of the thick slot-coupled E plane Tee is given in Figure 4.51, together with its overall equivalent circuit representation at invariant reference planes. It is at these reference planes that the experimental data for this thick slot were taken. The parameters are B_{tk}/Y_0, n_{tk}, $2\ell_{tk}$ and ℓ'_{tk}. The measurement procedure used to determine the parameters of the thick slot are similar to those for the thin slot. The pertinent experimental techniques are discussed in Part II, Sec. A, 3). Measurements were taken on a slot of cross-section dimensions a' = .809", b' = .159" in X band waveguide at a wavelength of 3.20 cms., as a function of the slot thickness t.

The theoretical parameters for the overall network of Figure 4.51-(b) are obtained by the use of the composite network given in Figure 2.10. The overall thick slot structure is considered to consist of an E plane Tee junction coupled to a transverse junction, or change of cross-section, by means of a length of guide equal to the slot thickness. The E plane Tees junction is shown in Figures 2.9-(b) and (c), with regard to its geometry and its equivalent network at both the centerline and invariant reference planes. The notation associated with the parameters of the networks is also given in the figures. The geometry and equivalent network for the transverse junction are given in Figure 2.9-(a). The text associated with these figures includes further information concerning these components of the composite network.

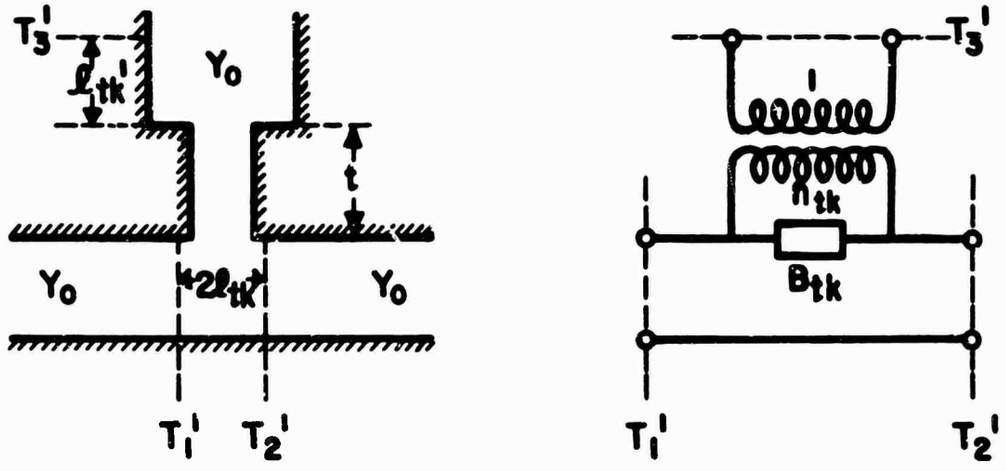

Figure 4.51 - The thick slot-coupled E plane Tee.

The composite network is partly at centerline and partly at invariant reference planes; it is chosen in this manner to simplify the calculations. The E plane Tee junction component of it is that at invariant reference planes and is the one shown in Figure 2.9-(c). However, the theoretical parameters for this junction are available directly for the centerline representation of Figure 2.9-(b), thus requiring the shifting of these values to the invariant reference planes. The necessary relations are given in Table 2-V. The shift of the reference plane in the stub guide from T_4 to T_3 is accounted for by altering the length of the coupling transmission line, as shown in Figure 2.10; the network of Figure 2.9-(a) may then be used directly.

The parameters of the Tee junction of Figure 2.9-(b) are obtained theoretically as follows: B_{bj}/Y_o is equal to B_2/Y_o which is given by Equation (3.129), B_{aj}/Y_o is given by Equation (3.120), X_{cj}/Z_o is taken as zero, and n_{cj} is equal to $n_c\, n_t$, where n_c is given by Equation (3.123) or (3.125), depending on the slot dimensions, and n_t by Equation (2.1). The theoretical values for the parameters of the transverse junction of Figure 2.9-(a) are obtained as: n_t is given by Equation (2.1), δ is taken as zero, and B_{tj}/Y_o is equal to $B_t/2\ Y_o$, where B_t/Y_o is given by Equation (3.107) or (3.108), depending on the slot dimensions. For the particular slot on which measurements were taken, the above component parameter values were determined as:

$$B_{bj}/Y_o = .609 \quad , \quad B_{aj}/Y_o = -.026$$

$$n_{cj} = .617 \quad , \quad n_t = .630$$

$$B_{tj}/Y_o = .212$$

When the Tee junction parameters are shifted to the invariant reference planes, they become:

$$B_j/Y_o = .319 \quad , \quad n_j = .602$$

$$\ell'_j = -.0396 \quad , \quad 2\ell_j = .0146$$

Parameter $2\ell_j$ depends only on B_{aj}/Y_o, but the other parameters are related to all the parameters of centerline representation and sensitive to small changes in any of them. Once all the component parameters of the composite representation of Figure 2.10 are known, the parameters of the overall network of Figure 4.51 may be obtained by means of the relations given in Table 2-III.

Theoretical values in graphical form for most of the parameters discussed above are given in Sec. A of this part of the report. However, since values of n_t^2 are not given there they are now given in Figure 4.52. The values are plotted as a function of relative slot width $\alpha = a'/a$, with relative slot height $\beta = b'/b$ as a parameter; the values are valid for X band waveguide at a wavelength of 3.20 cms., as were the other numerical values quoted. It may be noted that when $\alpha = 1$, $n_t^2 = \beta$, and if α is small,

$$n_t^2 = 4\,\alpha\,\beta/\pi^2 \qquad (4.13)$$

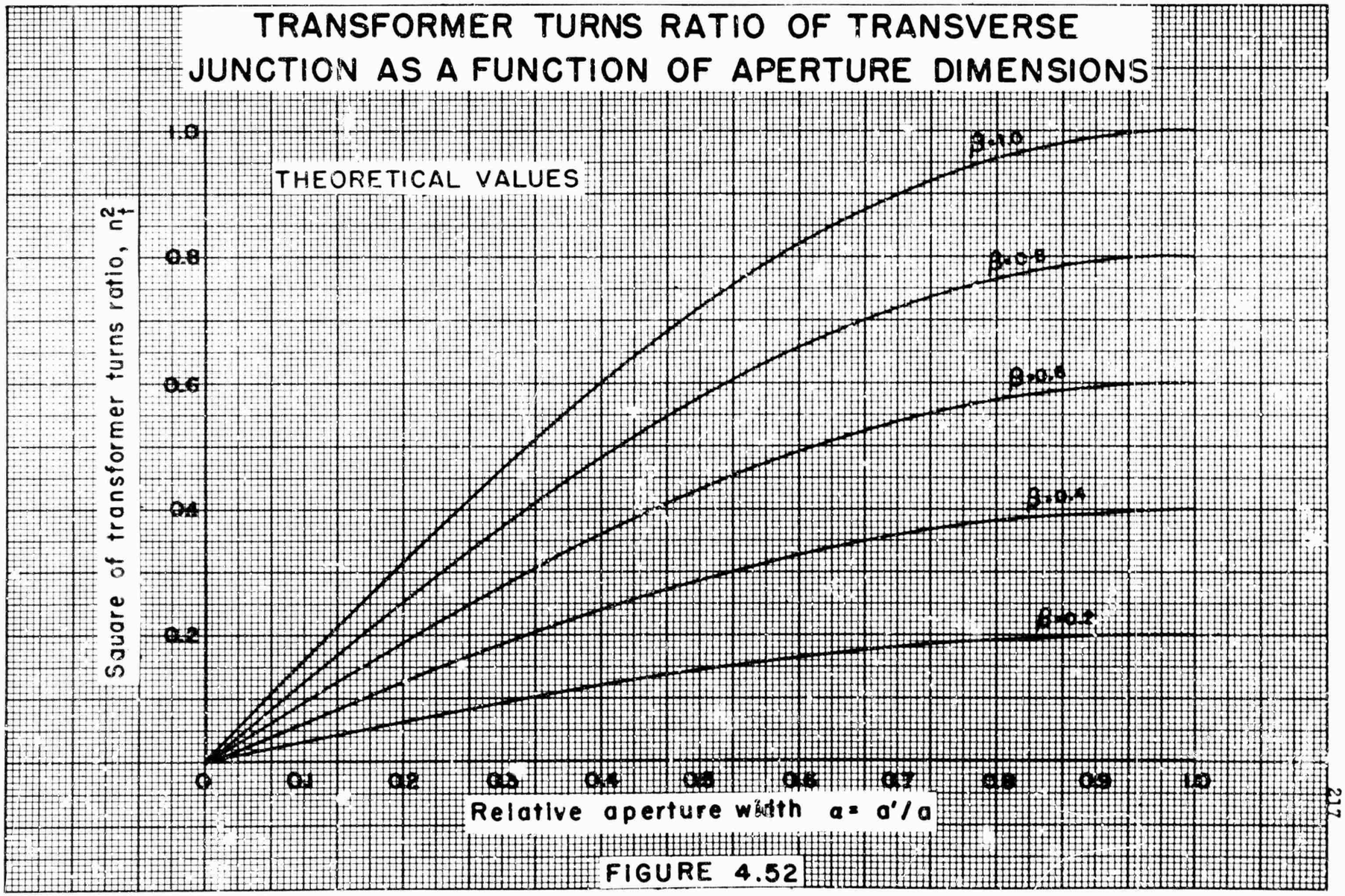
TRANSFORMER TURNS RATIO OF TRANSVERSE JUNCTION AS A FUNCTION OF APERTURE DIMENSIONS
THEORETICAL VALUES
Square of transformer turns ratio, n_t^2
1.0
0.8
0.6
0.4
0.2
0
0.1
0.2
0.3
0.4
0.5
0.6
0.7
0.8
0.9
1.0
β=1.0
β=0.8
β=0.6
β=0.4
β=0.2
Relative aperture width a = a'/a

FIGURE 4.52

The experimental results for the parameters of the overall equivalent network are listed in Table 4-VIII.

TABLE 4-VIII

THICK SLOT-COUPLED E PLANE TEE

Experimental Results

$a' = .809''$, $b' = .159''$; $\lambda_g = 1.7644$, $\alpha = 3.5611$

$a'/a = .899$, $b'/b = .398$; $\lambda'_g = 2.0108$, $\alpha' = 3.1247$

$$Y'_o/Y_o = \alpha'/\alpha = .8775$$

t , ℓ'_{tk} and $2\ell_{tk}$ are in inches.

t	B_{tk}/Y_o	n_{tk}	ℓ'_{tk}	$2\ell_{tk}$
.900	0.140	.979	- .851	.010
.801	- 0.478	.910	- .810	.011
.801	- 0.472	.910	- .810	.011
.700	- 1.114	.771	- .755	.011
.700	- 1.167	.777	- .760	.011
.599	- 1.804	.603	- .682	.012
.499	- 1.202	.457	- .543	.009
.499	- 1.272	.458	- .547	.010
.361	2.317	.477	- .284	.011
.361	2.229	.475	- .286	.011

For four of the thickness values, two sets of results are given; the second set in each case is obtained by reversing the structure and repeating the measurements. The reversals serve both as a check on the results and as a rough guide to their precision. As seen, parameter $2\ell_{tk}$ does not vary with the slot thickness.

Comparisons between the experimental results listed in Table 4-VIII and the theoretical results as computed from the composite network and discussed above are given in Figures 4.53 to 4.55. The comparison is made for parameters B_{tk}/Y_o , n_{tk} and ℓ'_{tk} , all as a function of slot thickness. The

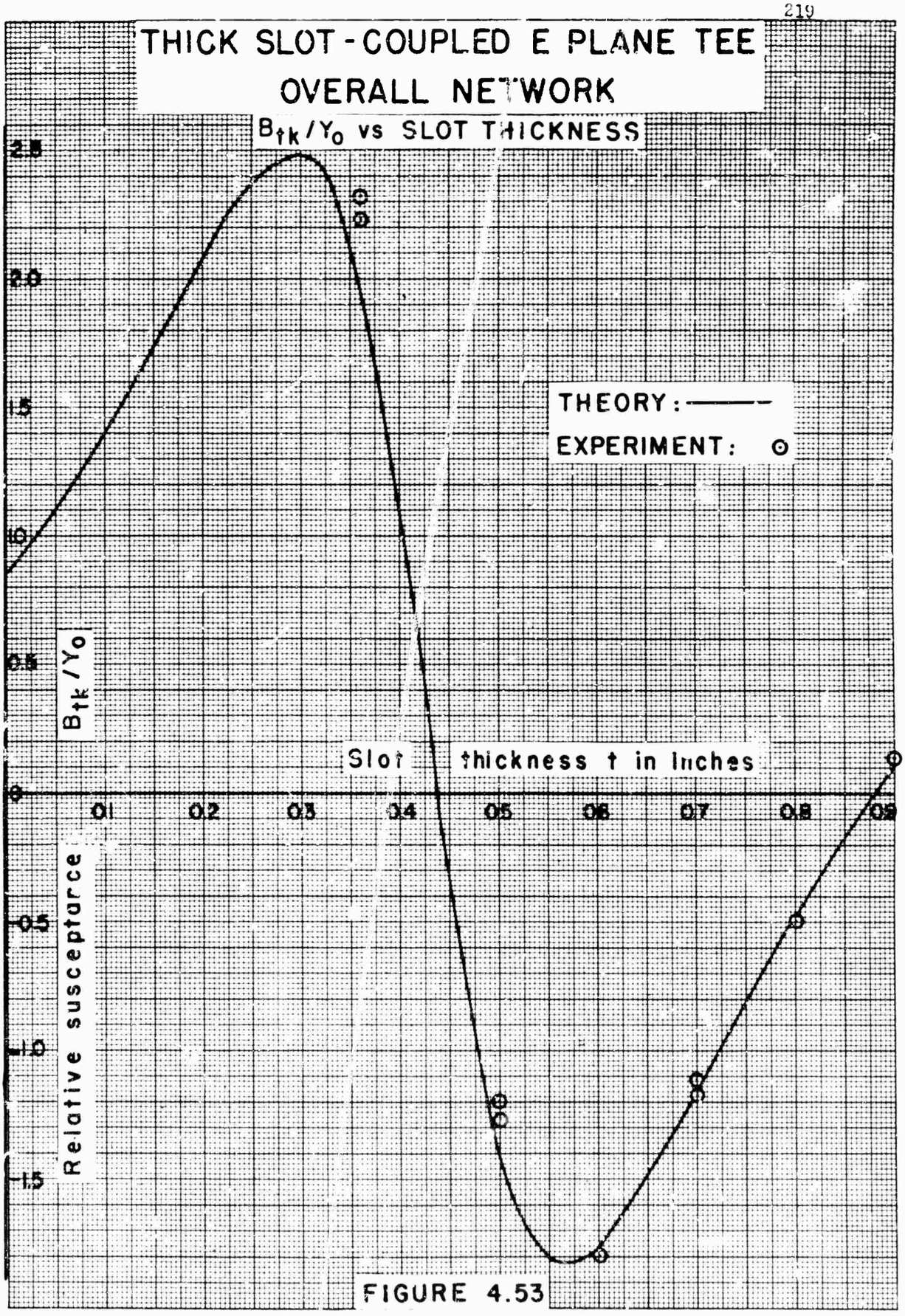
THICK SLOT-COUPLED E PLANE TEE
OVERALL NETWORK
B_{tk}/Y_0 vs SLOT THICKNESS
THEORY: ———
EXPERIMENT: ⊙
B_{tk}/Y_0
Relative susceptance
Slot thickness t in Inches
2.5
2.0
1.5
1.0
0.5
0
-0.5
-1.0
-1.5
0.1
0.2
0.3
0.4
0.5
0.6
0.7
0.8
0.9

FIGURE 4.53

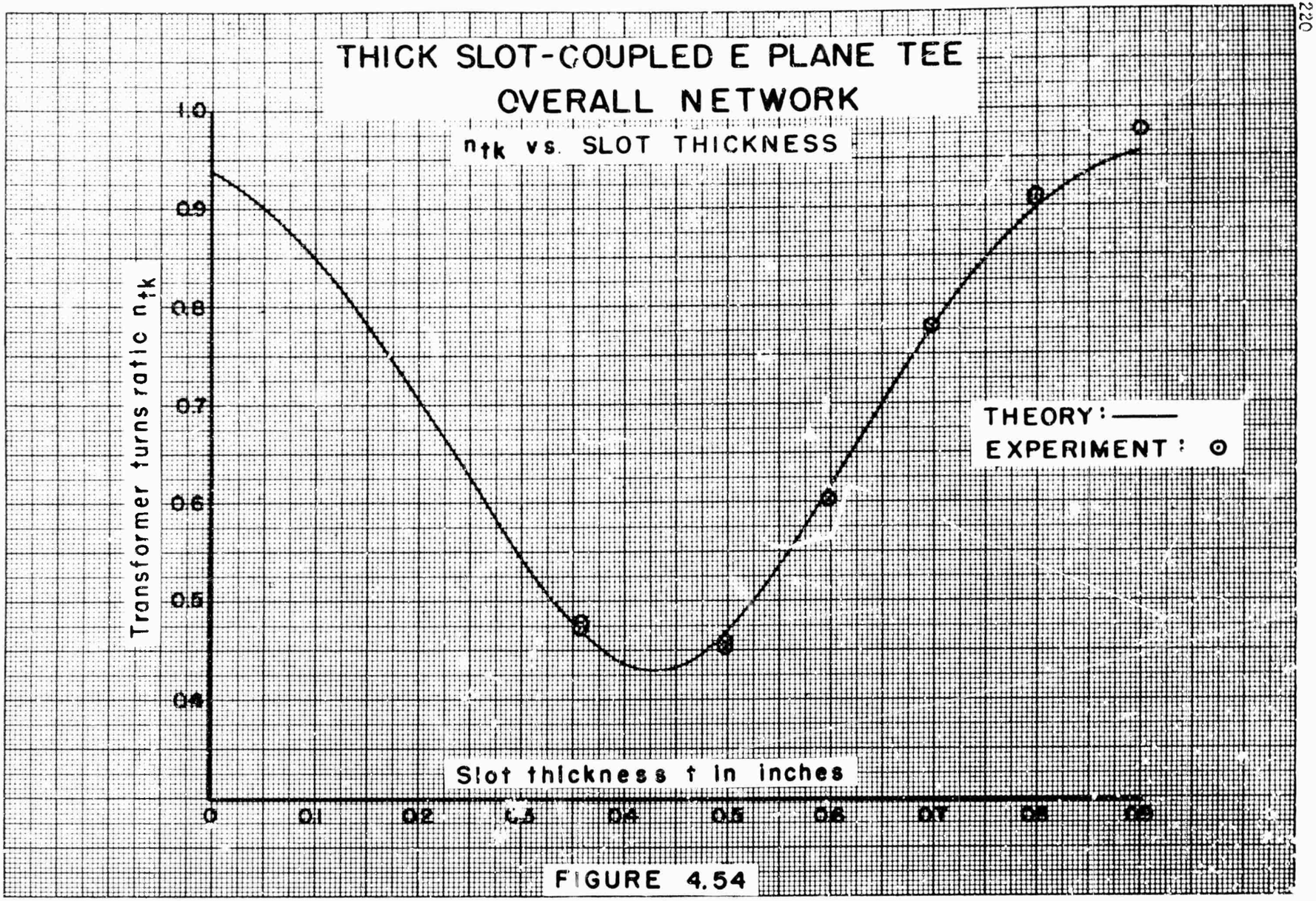
THICK SLOT-COUPLED E PLANE TEE
OVERALL NETWORK
n_{tk} vs. SLOT THICKNESS
Transformer turns ratio n_{tk}
1.0
0.9
0.8
0.7
0.6
0.5
0.4
Slot thickness t in inches
0
0.1
0.2
0.3
0.4
0.5
0.6
0.7
0.8
0.9
THEORY: ——
EXPERIMENT: ⊙

FIGURE 4.54

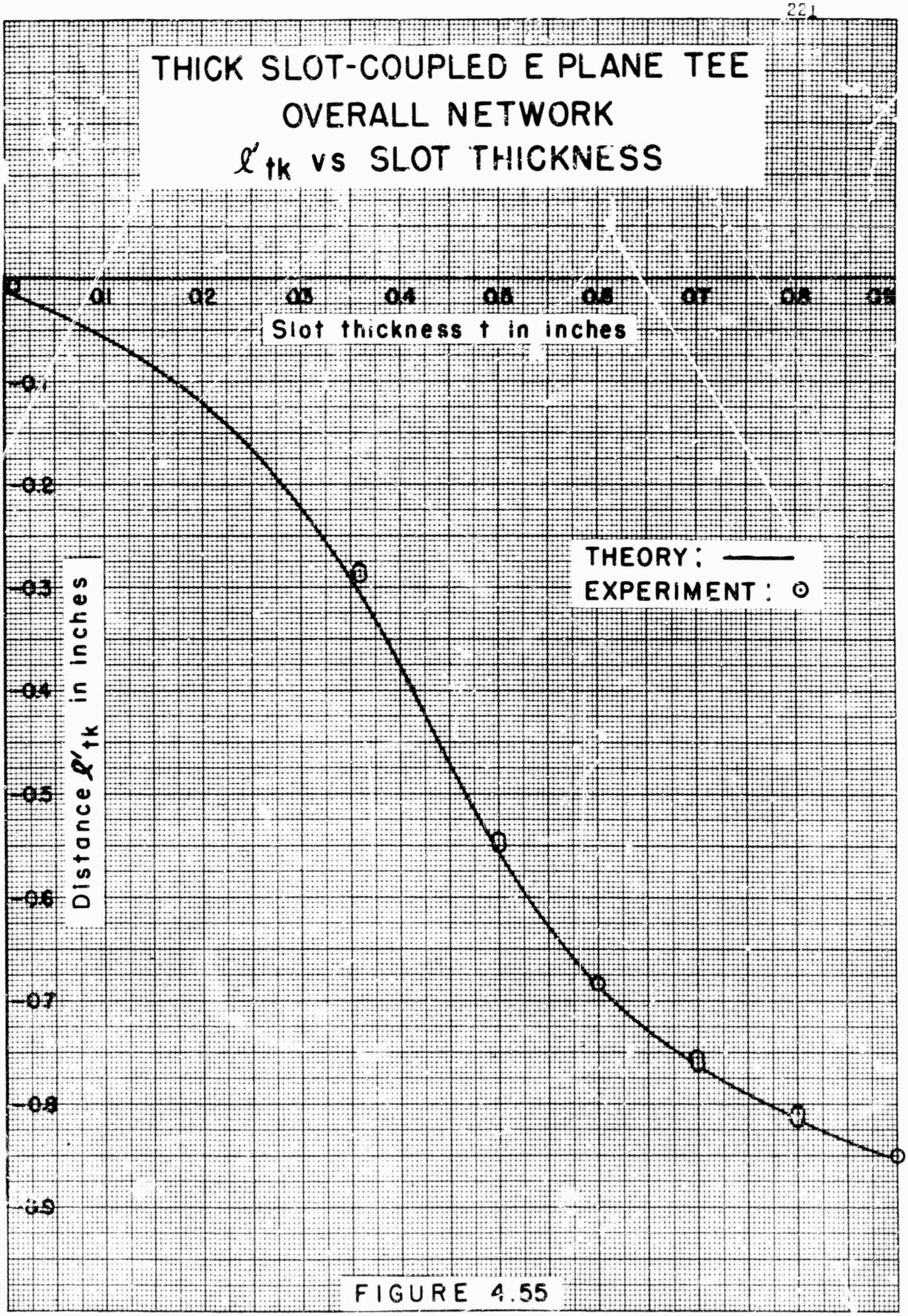
THICK SLOT-COUPLED E PLANE TEE
OVERALL NETWORK
ℓ'_{tk} vs SLOT THICKNESS
Slot thickness t in inches
Distance ℓ'_{tk} in inches
THEORY: ——
EXPERIMENT: ⊙

FIGURE 4.55

theoretical predictions are represented by the solid lines and the experimental data by the indicated points. The reason for some points appearing as pairs is mentioned above. It is seen that the agreement between theoretical and experimental values is very satisfactory. In certain ranges, the parameters plotted are sensitive to some of the component parameters and not to others; in other ranges this is reversed. Generally, however, the range of thickness from 0.3" to 0.6" is the most sensitive.

The experimental data and a portion of the theoretical data for the component junctions may be combined to yield a semi-experimental value for the E plane Tee junction parameters. The relations between the parameters of the composite and overall networks that are required for the determination of the Tee junction parameters are given in Table 2-IV. The results of such calculations as a function of slot thickness are given in Figures 4.56 and 4.57. Two sets of points are given for the semi-experimental data; the encircled points utilize the theoretical values for the transverse junction employed for Figures 4.53 to 4.55, while the crosses use $n_t = .625$, rather than .630, the other theoretical values remaining the same. The actual points are connected by dashed lines; a solid horizontal line is drawn through the average of the points for which $n_t = .625$. The reason for the latter is, of course, that theoretically one expects the values to remain constant independent of thickness.

It is seen that a scatter is obtained for the plotted points in Figures 4.56 and 4.57; from experience with the thick transverse radiating slot and the thick transverse slot coupling identical guides the scatter occurs because this method of utilizing the data is one which is very sensitive to small errors in the initial data. The value of $n_t = .625$ is seen to reduce the scatter somewhat and it is for this reason that the solid line is drawn through the average of the corresponding points. Only one set of points appears for parameter $2\ell_j$ since it is directly equal to $2\ell_{tk}$ and is therefore independent of n_t.

By means of Table 2-VI, the semi-experimental parameters obtained above for the E plane Tee junction can be shifted to the centerline reference planes, to the representation of Figure 2.9-(b), thereby permitting direct comparison with the theoretical values given earlier. These shifted semi-experimental values are plotted in Figures 4.58 and 4.59 as a function of slot thickness. A solid horizontal line is drawn through the average of the points. These average values, together with the theoretical predictions for these parameters, are compared in Table 4-IX. The $\pm$ values associated with the average values represents the scatter shown in Figures 4.58 and 4.59.

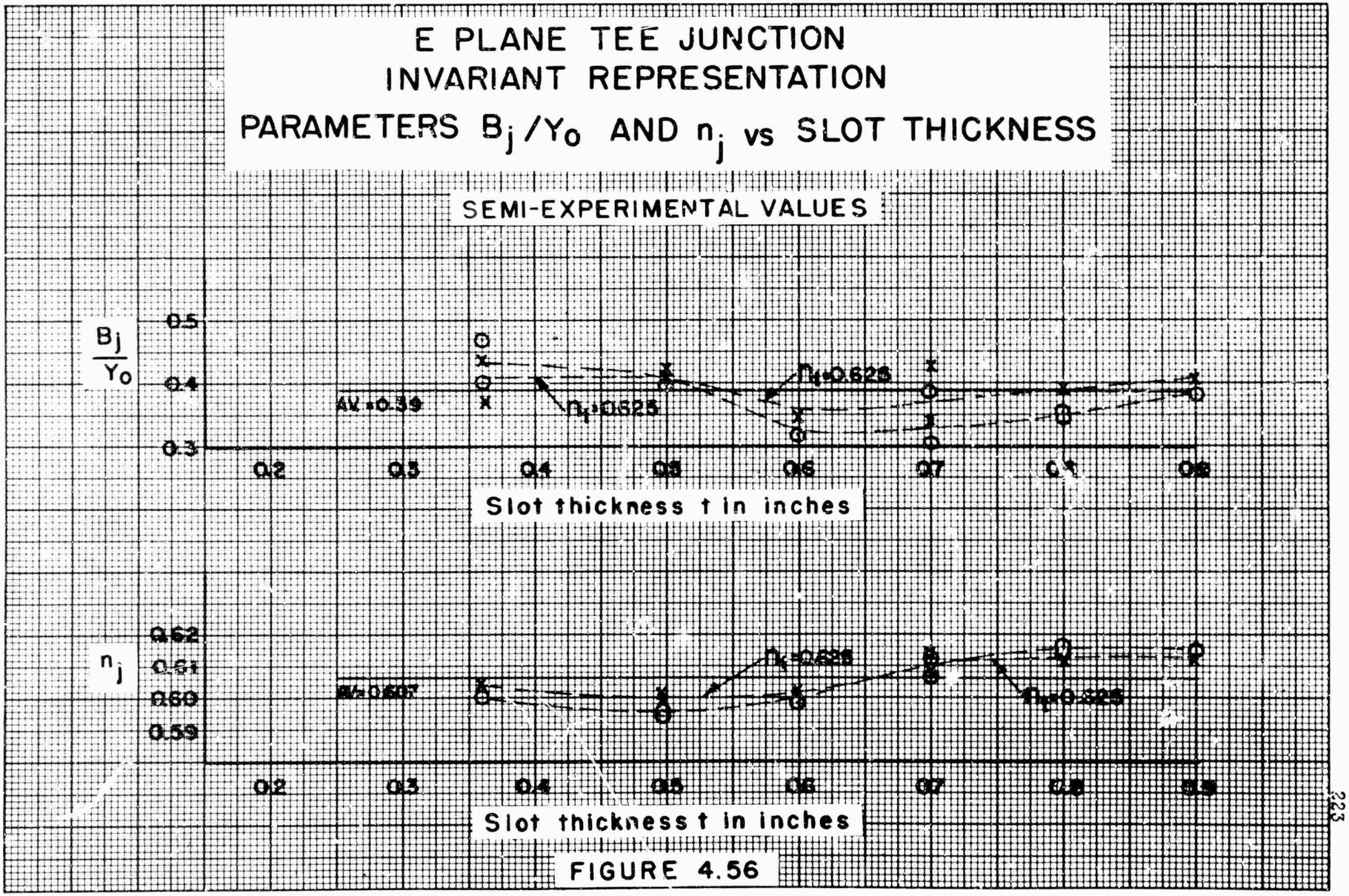
E PLANE TEE JUNCTION
INVARIANT REPRESENTATION
PARAMETERS B_j/Y_o AND n_j vs SLOT THICKNESS
SEMI-EXPERIMENTAL VALUES
$\frac{B_j}{Y_o}$
0.5
0.4
0.3
Av = 0.39
n_1=0.625
n_1=0.625
0.2
0.3
0.4
0.5
0.6
0.7
0.8
0.9
Slot thickness t in inches
n_j
0.62
0.61
0.60
0.59
Av=0.607
n_1=0.625
n_1=0.625
0.2
0.3
0.4
0.5
0.6
0.7
0.8
0.9
Slot thickness t in inches

FIGURE 4.56

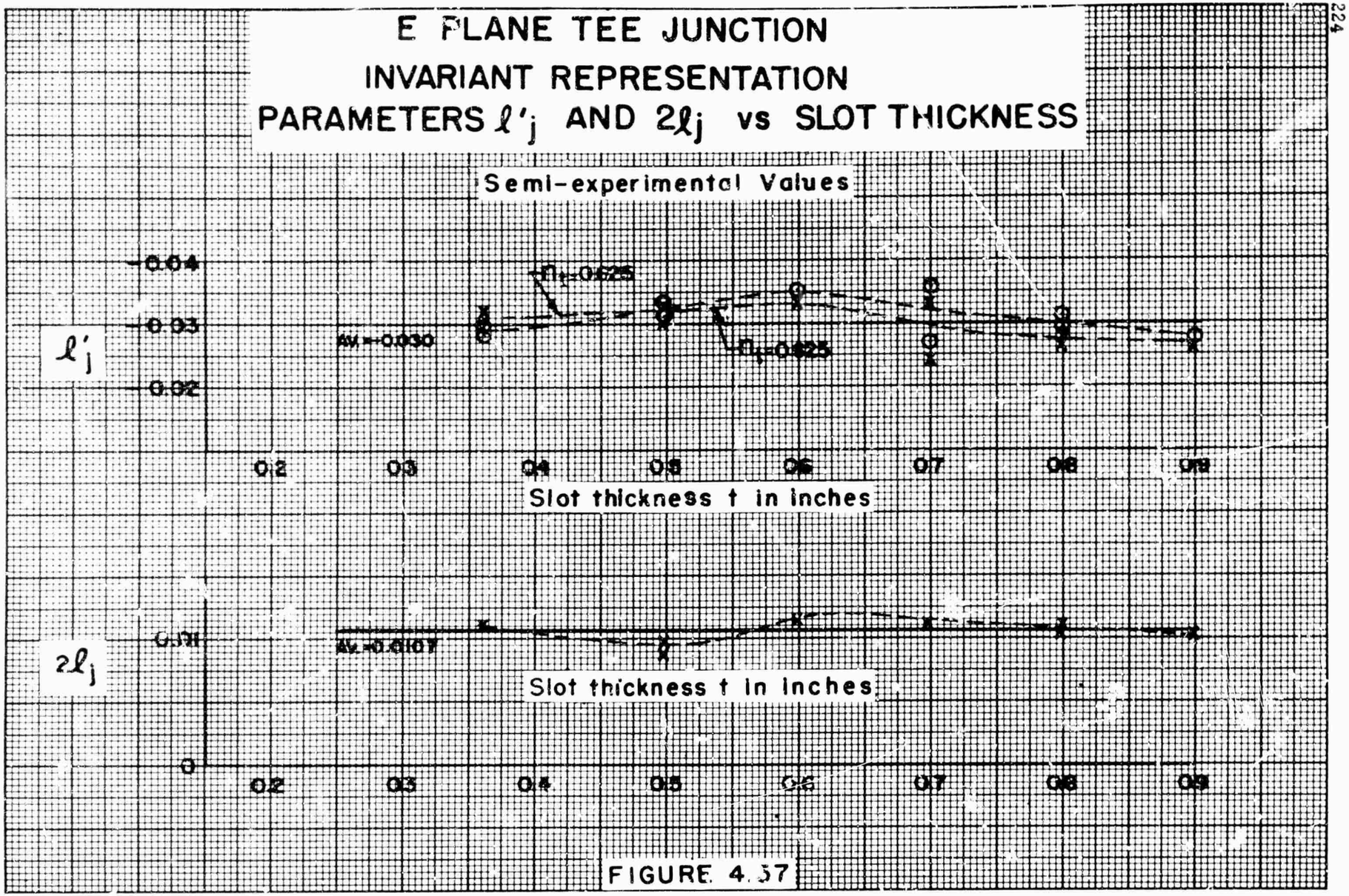
E PLANE TEE JUNCTION
INVARIANT REPRESENTATION
PARAMETERS ℓ'_j AND $2\ell_j$ vs SLOT THICKNESS
Semi-experimental Values
ℓ'_j
0.04
0.03
0.02
$\Delta\ell'_j$=0.030
$\Delta\ell'_j$=0.025
$\Delta\ell'_j$=0.025
0.2
0.3
0.4
0.5
0.6
0.7
0.8
0.9
Slot thickness t in inches
$2\ell_j$
0.031
$\Delta 2\ell_j$=0.0107
0
0.2
0.3
0.4
0.5
0.6
0.7
0.8
0.9
Slot thickness t in inches

FIGURE 4.37

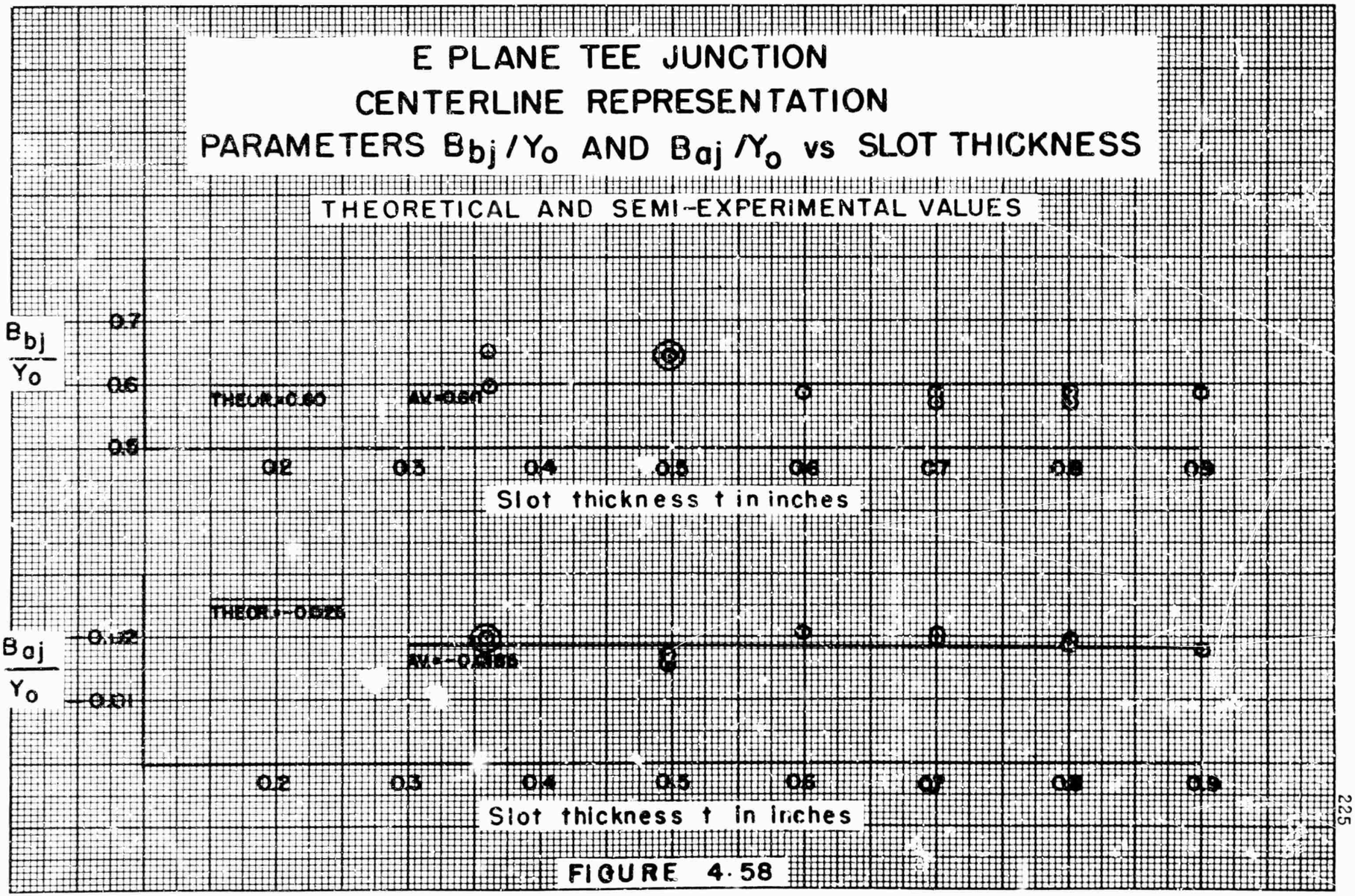
E PLANE TEE JUNCTION
CENTERLINE REPRESENTATION
PARAMETERS B_{bj}/Y_o AND B_{aj}/Y_o vs SLOT THICKNESS
THEORETICAL AND SEMI-EXPERIMENTAL VALUES
$\frac{B_{bj}}{Y_o}$
0.7
0.6
0.5
THEOR.=0.60
AV.=0.64
0.2
0.3
0.4
0.5
0.6
0.7
0.8
0.9
Slot thickness t in inches
THEOR.=0.025
$\frac{B_{aj}}{Y_o}$
0.02
0.01
AV.=0.035
0.2
0.3
0.4
0.5
0.6
0.7
0.8
0.9
Slot thickness t in inches

FIGURE 4.58

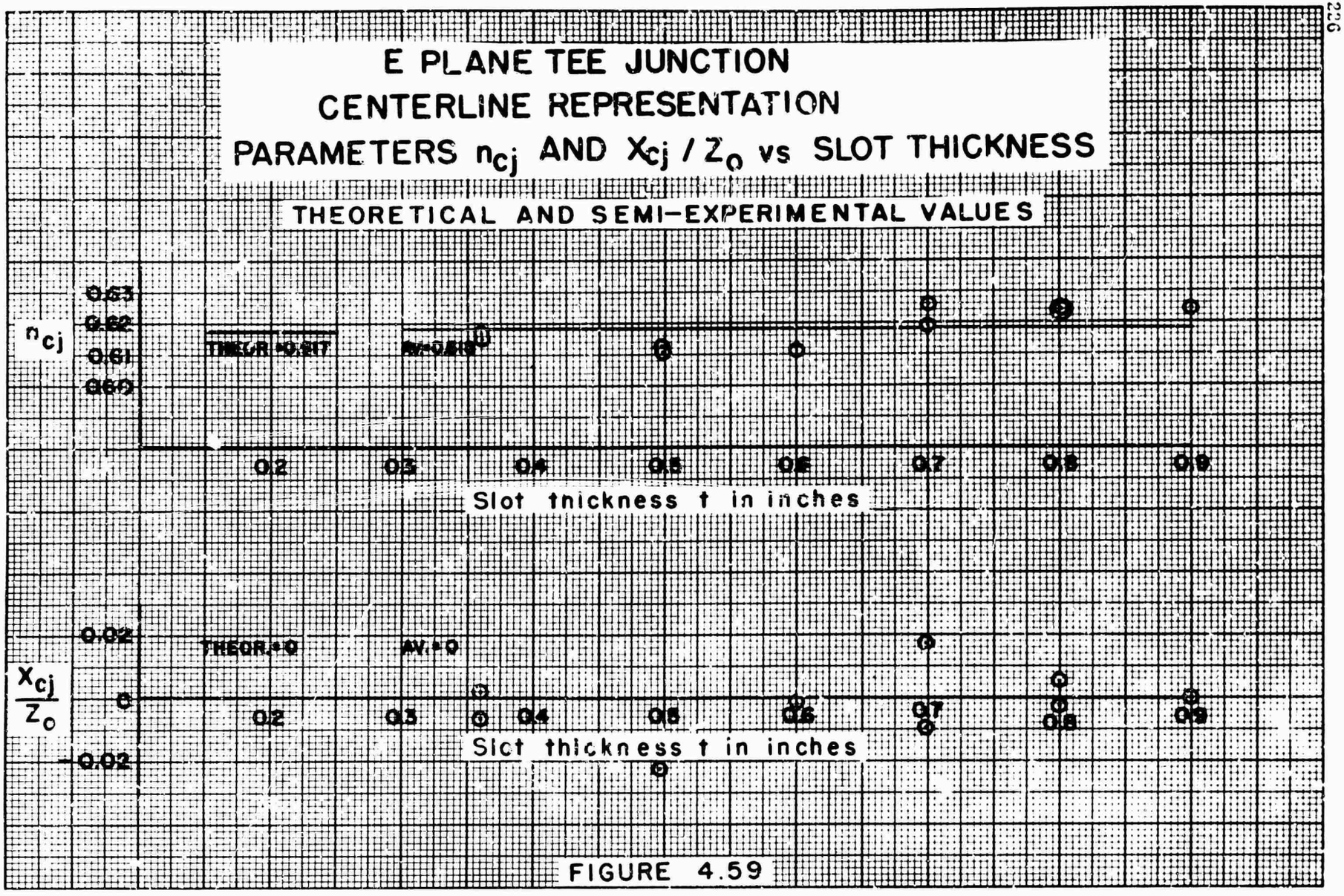
E PLANE TEE JUNCTION
CENTERLINE REPRESENTATION
PARAMETERS n_{cj} AND X_{cj}/Z_o vs SLOT THICKNESS
THEORETICAL AND SEMI-EXPERIMENTAL VALUES
n_{cj}
0.63
0.62
0.61
0.60
THEOR.=0.617
AV.=0.618
0.2
0.3
0.4
0.5
0.6
0.7
0.8
0.9
Slot thickness t in inches
$\frac{X_{cj}}{Z_o}$
0.02
0
-0.02
THEOR.=0
AV.=0
0.2
0.3
0.4
0.5
0.6
0.7
0.8
0.9
Slot thickness t in inches

FIGURE 4.59

TABLE 4-IX

E PLANE TEE JUNCTION

Centerline Representation

Parameter	Semi-experimental	Theoretical
B_{bj}/Y_o	.60 ± .04	.609
B_{aj}/Y_o	- .0185 ± .002	- .026
n_{cj}	.618 ± .006	.617
X_{cj}/Z_o	0 ± .01	0

It is seen from Table 4-IX that the theoretical values for the centerline parameters of the Tee junction are in good agreement with the semi-experimental values, except for B_{aj}/Y_o. The theoretical value for the latter parameter lies outside of the scatter indicated and is about 30 percent too high. Since it is such a small quantity, this discrepancy is not serious. It seems, however, that a 30 percent lower value for the theoretical prediction for B_{aj}/Y_o should be recommended in view of the above, and also because the B_{aj}/Y_o value was assumed theoretically to be identical with the B_a/Y_o value, i.e., it was assumed to depend only upon the size of the slot as seen from the main guide and independent of the dimensions of the stub guide. The calculation of B_a/Y_o involved a free space spatial admittance, with the tacit assumption, therefore, that the waveguide walls were not too near; for the Tee junction, however, they are right next to the slot and one can expect a change in the B_a/Y_o value. The change is difficult to estimate, and further theoretical investigation was not considered worthwhile because the susceptance value itself is so small. Using Table 4-IX as a basis, a semi-theoretical prediction for B_{aj}/Y_o may therefore be given as

$$B_{aj}/Y_o = 0.7 \; B_a/Y_o \tag{4.14}$$

when the slot size is identical in both cases.

When theoretical values of B_{tk}/Y_0 , n_{tk} and ℓ'_{tk} for the overall network are obtained using the B_{aj}/Y_0 value given by Equation (4.14), the agreement with experiment becomes even closer than that shown in Figures 4.53 to 4.55. This is, of course, to be expected, since the latter value for B_{aj}/Y_0 is obtained from an average of the experimental data. Graphs illustrating this improved agreement will not be given here, however.

3.) The E Plane Radiating Slot

The geometry of the thick E plane radiating slot is given in Figure 4.60, together with its overall equivalent circuit representation at invariant reference planes. It is at these reference planes that the experimental data for this thick slot were taken. The paramters are G_{tk}/Y_0 , B_{tk}/Y_0 and $2\ell_{tk}$. The measurement procedure and the experimental techniques

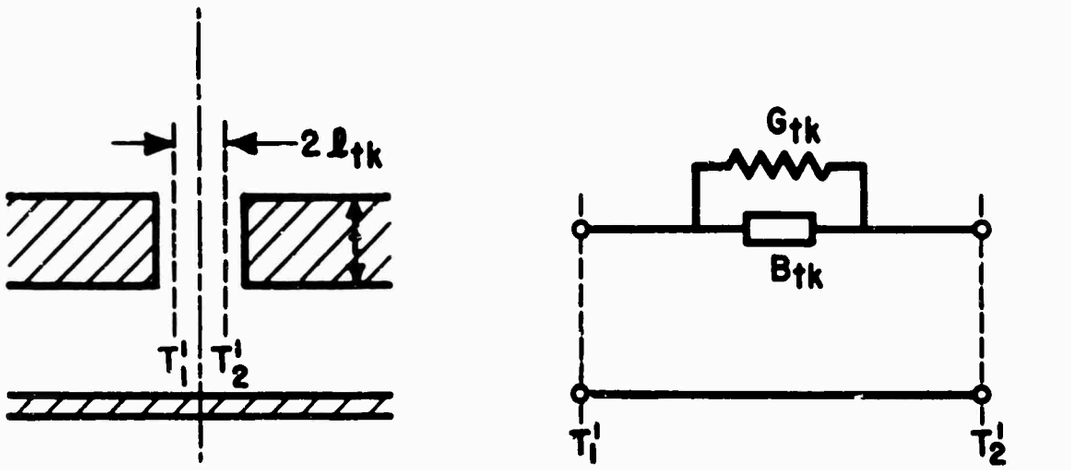

Figure 4.60 - The thick E plane radiating slot

employed are discussed in Part II, Sec. B, in 4) and 3), respectively. The thick slot upon which measurements were taken is identically the one used for investigating the thick slot-coupled E plane Tee. In fact, immediately after each Tee measurement, the slot was arranged to radiate into a half

space and the appropriate measurements were taken. This means that not only are the cross-section dimensions the same, but the slot thickness values at which data are available are the same also, for the most part. (For two thickness values only Tee data were taken, while at one value measurements were made only on the radiating slot.) The dimensions are a' = .809" by b' = .159", and the slot thickness was varied from .80" to .40", approximately.

The theoretical parameters for the overall network of Figure 4.60-(b) are obtained by use of the composite network given in Figure 2.19. The overall thick slot structure is considered to consist of an E plane Tee junction coupled to a transverse radiating junction by means of a length of guide equal to the slot thickness. The E plane Tee junction is shown in Figures 2.9-(b) and (c), where the physical structure and the equivalent networks at both the centerline and invariant reference planes, respectively, are given. The geometry and equivalent network for the transverse radiating junction are shown in Figure 2.18. The notation associated with the parameters of these networks is also given in the figures. The text associated with these figures include further information concerning these components of the composite network.

The composite network of Figure 2.19 is at the invariant reference planes; the E plane Tee junction component of it is also shown in Figure 2.9-(c). However, the theoretical parameters for this junction are available directly for the centerline representation of Figure 2.9-(b), thus requiring the shifting of these values to the representation at the invariant reference planes. The necessary relations are given in Table 2-V. The network of Figure 2.18 connects directly to the other end of the intervening transmission line representing the slot thickness.

The equations to use in order to obtain the theoretical values for the parameters of the E plane Tee junction at centerline reference planes are discussed in the previous section, i.e., on the thick slot-coupled E plane Tee. Also given there are the numerical values for the slot under consideration. However, attention is called to Equation (4.14), which relates B_{aj}/Y_o to B_a/Y_o on the basis of the experimental investigation described in the previous section, rather than by theoretical considerations alone. It is pointed out there that $B_{aj}/Y_o = 0.7\ B_a/Y_o$ yields a better value than $B_{aj}/Y_o = B_a/Y_o$, which is the approximate theoretical prediction. Using the 0.7 factor, the centerline representation parameters for the E plane Tee junction are:

$$B_{bj}/Y_o = .609 \quad , \quad B_{aj}/Y_o = -.018$$

$$n_{cj} = .617 \quad , \quad X_{cj}/Z_o = 0$$

where all parameters except B_{aj}/Y_o are the same as those used for thick slot-coupled Tee. When the network is shifted to the invariant reference planes, however, the values are slightly different from those used for the thick Tee; they become:

$$B_j/Y_o = .405 \quad , \quad n_j = .606$$

$$\ell'_j = -.0278 \quad , \quad 2\ell_j = .0104$$

The theoretical values for the parameters of the transverse radiating junction are obtained from:

$$G_{rj}/Y_o = n_t^2 \; G_r/Y_o \tag{4.15a}$$

$$B_{rj}/Y_o = n_t^2 \; B_h/Y_o \tag{4.15b}$$

Expressions for G_r/Y_o and B_h/Y_o are given in Part III, Sec. E, 3) ; n_t is given by Equation (2.1).

For the particular slot on which measurements were taken, the parameters of the component transverse radiating junction are:

$$G_{rj}/Y_o = .333 \quad , \quad B_{rj}/Y_o = .305$$

Once all the component parameters of the composite representation of Figure 2.19 are known, the parameters of the overall network of Figure 4.60 may be obtained by means of the relations given in Table 2-IX.

Experimental results for the parameters of the overall equivalent network are listed in Table 4-X.

TABLE 4-X

THICK E PLANE RADIATING SLOT

Experimental Results

$a' = .809"$, $b' = .159"$; $\lambda_g = 1.7644$, $\lambda_c = 3.5611$

$a'/a = .899$, $b'/b = .398$; $\lambda_g' = 2.0108$, $\lambda_c' = 3.1247$

$$Y_o'/Y_o = \lambda_c'/\lambda_c = .8775$$

Slot thickness t is in inches.

t	G_{tk}/Y_o	B_{tk}/Y_o	R_{tk}/Z_o	X_{tk}/Z_o
.801	0.769	0.018	1.30	- .031
.801	0.819	0.029	1.22	- .043
.700	0.956	- 0.683	0.693	.495
.700	0.957	- 0.675	0.698	.492
.599	1.22	- 1.45	0.341	.404
.499	2.73	- 2.34	0.212	.181
.499	2.89	- 2.40	0.205	.170
.400	5.71	- 1.59	0.163	.045
.400	5.81	- 1.37	0.163	.038

The reason for the two sets of values for most of the thicknesses was given in the discussion on the thick slot-coupled Tee. The values of $2\ell_{tk}$ are the same as those for the thick Tee, and therefore are not reported here. Their measurement from the Tee structure is the more accurate one, since it is obtained directly from a (sensitive) zero power measurement. Parameters R_{tk}/Z_o and X_{tk}/Z_o are included as alternative parameters, in series from (see Figure 2.16), to G_{tk}/Y_o and B_{tk}/Y_o in parallel form.

Comparisons between the experimental results listed in Table 4-X and the theoretical results as computed from the composite network and discussed above are given in Figures 4.61 and 4.62, for B_{tk}/Y_o and G_{tk}/Y_o, respectively. The theoretical predictions are represented by the solid lines and the experimental data by the indicated points; both are plotted as a function of slot thickness. The reason for most of the points appearing as pairs is mentioned above. It is seen that the agreement is quite

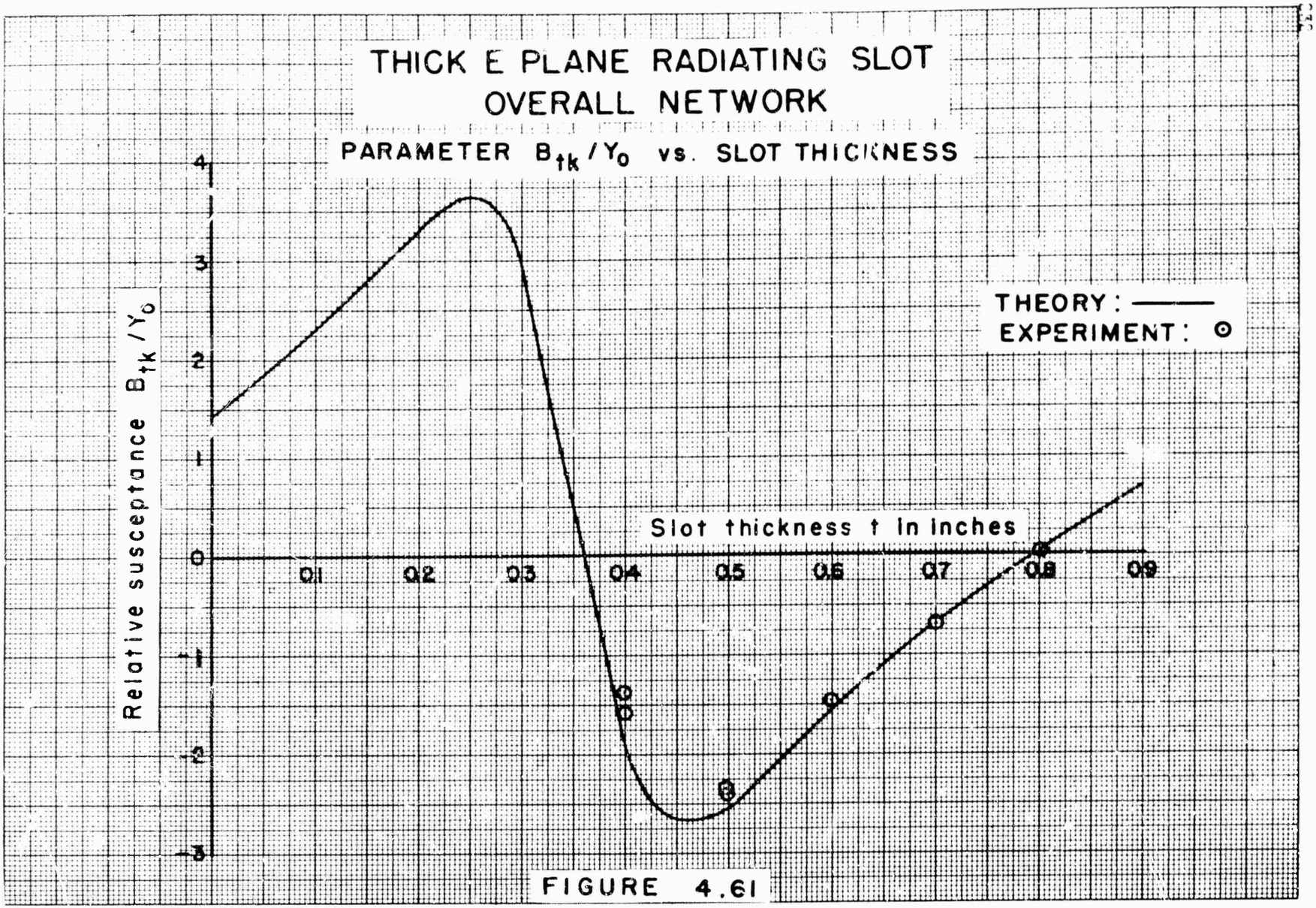
THICK E PLANE RADIATING SLOT
OVERALL NETWORK
PARAMETER B_{tk}/Y_0 vs. SLOT THICKNESS
THEORY: ——
EXPERIMENT: ⊙
Relative susceptance B_{tk}/Y_0
Slot thickness t in inches
4
3
2
1
0
-1
-2
-3
0.1
0.2
0.3
0.4
0.5
0.6
0.7
0.8
0.9

FIGURE 4.61

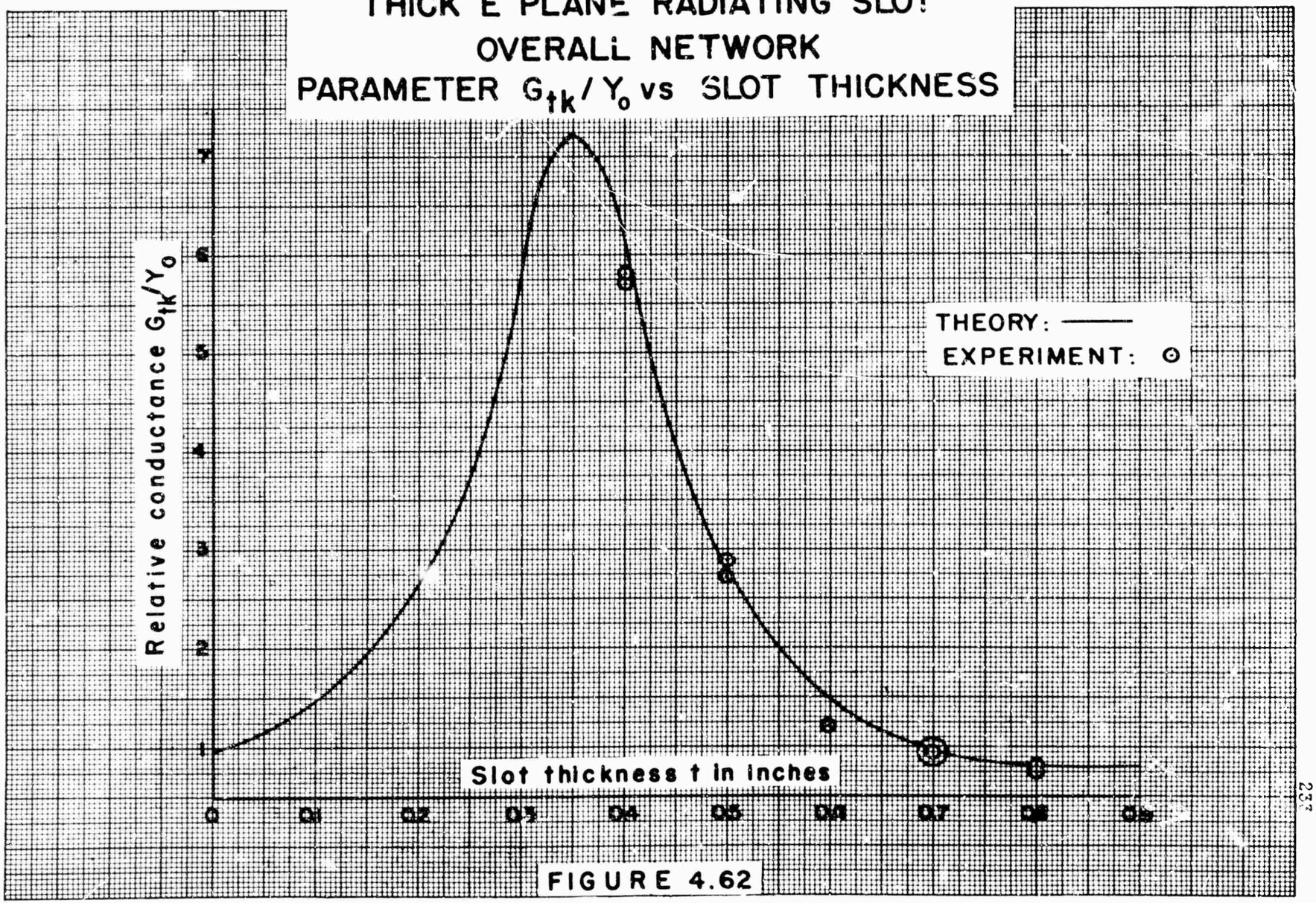
THICK E PLANE RADIATING SLOT
OVERALL NETWORK
PARAMETER G_{tk}/Y_o vs SLOT THICKNESS
Relative conductance G_{tk}/Y_o
THEORY: ——
EXPERIMENT: ⊙
Slot thickness t in inches
0
0.1
0.2
0.3
0.4
0.5
0.6
0.7
0.8
0.9
1
2
3
4
5
6

FIGURE 4.62

satisfactory. The curves are repetitive for each inch of slot thickness because the slot guide wavelength is approximately two inches. In the range shown, the region from t = 0.25" to 0.55" is most sensitive to slight variations in the parameters of the component junctions; outside of this range, the results are relatively insensitive to them.

The experimental data for the overall network and the theoretical data for the E plane Tee junction may be combined to yield semi-experimental values for the parameters of the transverse radiating junction. The relations between the parameters of the composite and overall networks that are required for this determination are given in Table 2-X. The results of such calculations as a function of slot thickness are given in Figures 4.63-(a) and (b). The semi-experimental data are represented by the indicated points, and dashed lines are drawn connecting these points. A solid horizontal line is superimposed on the curves to indicate the average values. Results for t = 0.6" are indicated, but are excluded from the dashed line average because of their large deviation. Since it happens coincidentally that only one set of data was obtained for t = 0.6", there is no check available on its accuracy. It may also be seen from Figure 4.62 that the experimental value of G_{tk}/Y_o for t = 0.6" shows a larger deviation from the theoretical curve than any of the other values, even though it is just outside of the sensitive region.

The scatter evident in these curves is similar to that appearing in corresponding curves for the thick transverse radiating slot and the thick slot-coupled E plane Tee; the scatter is due to the great sensitivity of the results cast in this form to small errors in the initial data. The average of the semi-experimental results is compared with the theoretical predictions in Table 4-XI; the $\pm$ values associated with the semi-experimental results are indicative of the scatter. Also included in the table are the corresponding semi-experimental results for B_{rj}/Y_o and G_{rj}/Y_o obtained from the thick transverse radiating slot. (The values of $\tilde{B}_{rj}/Y_o$ and $\tilde{G}_{rj}/Y_o$ given there (in Figure 4.48) become those of B_{rj}/Y_o and G_{rj}/Y_o upon multiplication by $n_t^2 = 0.396$.)

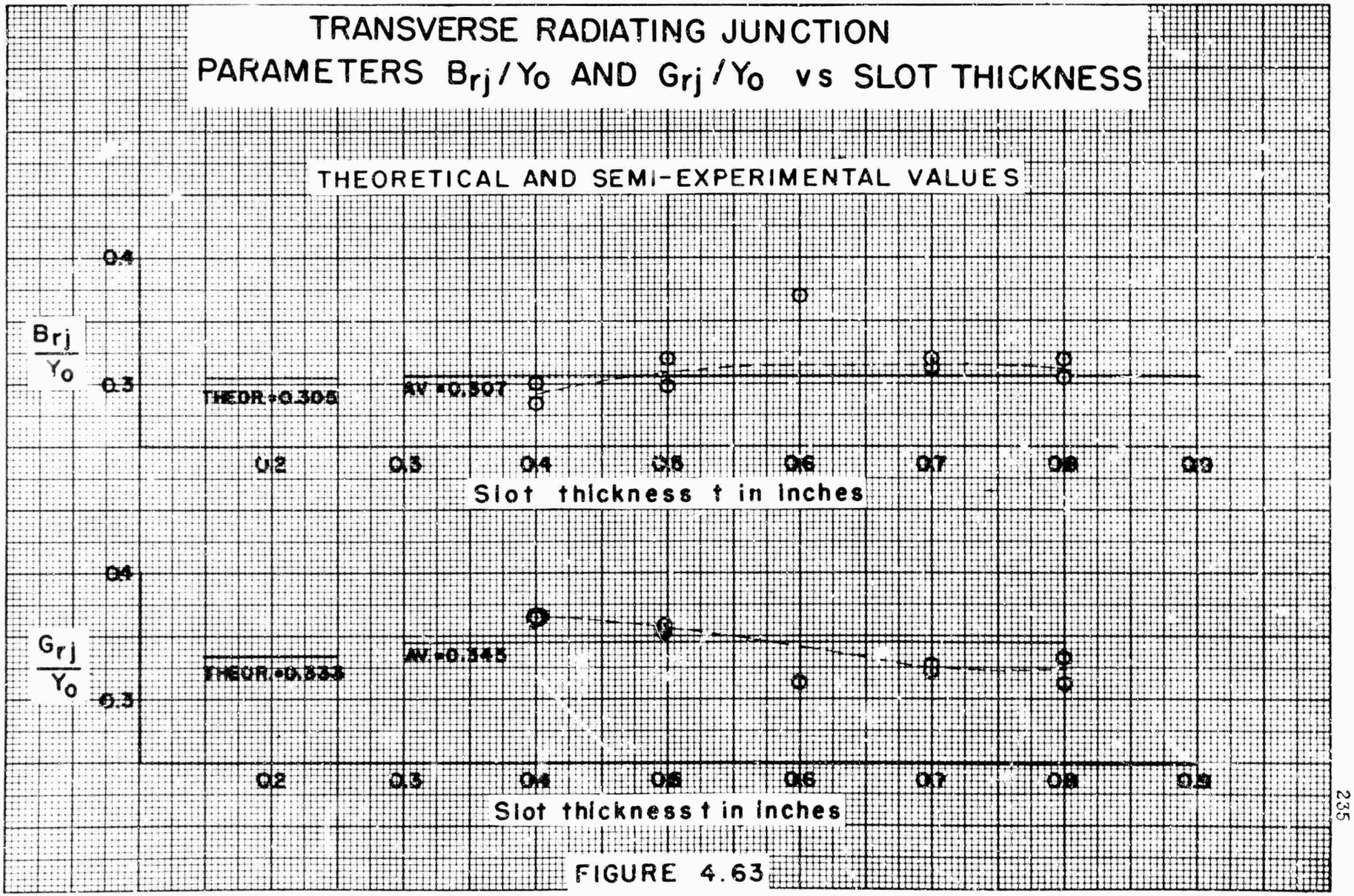
TRANSVERSE RADIATING JUNCTION
PARAMETERS B_{rj}/Y_o AND G_{rj}/Y_o vs SLOT THICKNESS
THEORETICAL AND SEMI-EXPERIMENTAL VALUES
$\frac{B_{rj}}{Y_o}$
0.4
0.3
THEOR.=0.305
AV.=0.307
0.2
0.3
0.4
0.5
0.6
0.7
0.8
0.9
Slot thickness t in inches
$\frac{G_{rj}}{Y_o}$
0.4
0.3
THEOR.=0.333
AV.=0.345
0.2
0.3
0.4
0.5
0.6
0.7
0.8
0.9
Slot thickness t in inches

FIGURE 4.63

TABLE 4-XI

TRANSVERSE RADIATING JUNCTION

Parameter	Semi-experimental		Theoretical
	From Figs. 4.63	From Figs. 4.48	
B_{rj}/Y_o	.307 ± .010	.300 ± .015	.305
G_{rj}/Y_o	.345 ± .020	.360 ± .030	.333

It is evident from the table that the theoretical values lie within the scatter indicated, although the theoretical value for G_{rj}/Y_o lies just at the lower limit of the scatter for Figure 4.48. The agreement for B_{rj}/Y_o is very good. The semi-experimental data for G_{rj}/Y_o are consistently slightly higher than the theoretical prediction, implying that a somewhat better theoretical value for G_{rj}/Y_o is obtainable from

$$G_{rj}/Y_o = 1.05\ n_t^2\ G_r/Y_o \qquad (4.16)$$

rather than from Equation (4.15a). The scatter for the conductance values is also seen to be greater than that for the susceptance values. The scatter for the data of Figures 4.63 is also less than that for Figures 4.48, because the latter involves two point data only, while the former employs an averaging procedure for the data.

V. THE STUDY OF A HALF SPACE IN TERMS OF SPHERICAL TRANSMISSION LINES

(L. Felsen)

A. The Utility of a Spherical Transmission Line Description

In describing the effect of an obstacle on the field in a given region excited by an electromagnetic source, it is often advantageous to regard the field as a superposition of an infinite number of modes whose amplitudes satisfy transmission line equations characteristic of the given region. Such a representation is particularly useful if it is found that, for a given geometry, the field can be very closely approximated by three, two, or perhaps even one so-called propagating modes. In that case the infinite-mode space is replaced by three, two, or one transmission lines, respectively, propagating the modes in question. Since for each mode a mode voltage, mode current, and mode characteristic impedance is specified, the impedance offered to each propagating mode by an obstacle can be conveniently defined. This impedance takes into account the effect of higher, "non-propagating" modes which are generated by induced currents on the obstacle.

For the case of the far field set up in a half-space by a radiating slot in an infinite plane, a spherical mode description is especially convenient since far from the aperture, which is centered about the origin of coordinates, the source looks like a point so that the far fields are essentially transverse, i.e. true spherical waves, centered at the origin. The spherical line representation of the half-space, however, can be of practical value only if it were found that a small number of modes suffices to give a close approximation to the field, making possible the replacement of the half-space by this small number of transmission lines. This problem was investigated[1] for the case of narrow rectangular slots ($b'/a' < .4$) in an infinite plane excited by a cosine electric field. Details of this investigation are given in Sec. B. It was found that, far from the aperture, the field can be reproduced almost exactly by the H_{11}, H_{13}, and H_{33} spherical modes. In the neighborhood of the Z - axis (see Figure 5.1) only the H_{11} and H_{13} modes are important.

---

[1] L. Felsen, "Spherical Mode Representation of the Field Excited by a Rectangular Slot in an Infinite Plane", Thesis for M.E.E. Degree, P.I.B., 1949.

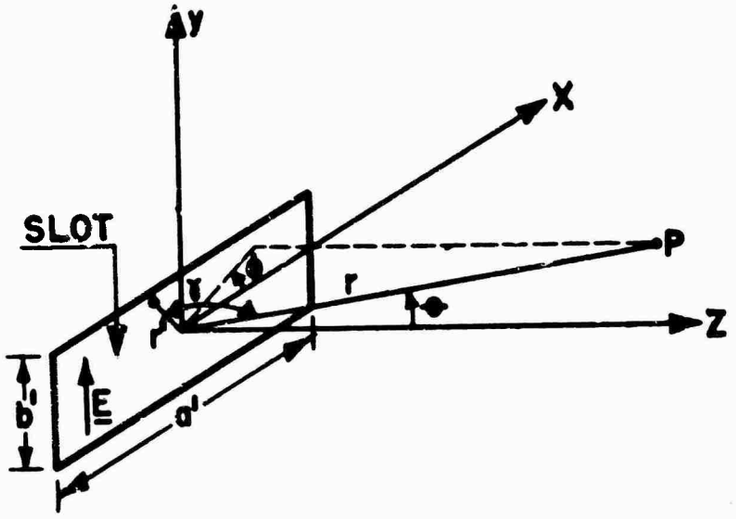

Figure 5.1

For very small slots the H_{11} mode alone is sufficient. In all cases, the H_{11} mode is by far the most important one; it carries practically the entire power radiated from the slot.

The knowledge of the equivalent network for a slot coupling a rectangular waveguide to a spherical waveguide is necessary for the formulation of impedances in a spherical line from measurements in rectangular guide. With the results of the previous paragraph in mind it is reasonable to represent the half-space as a good approximation by a single spherical transmission line propagating the H_{11} mode only. This principle has been applied to finding the equivalent four-terminal circuit for a thin transverse slot radiating into a half-space from the end of a rectangular waveguide. Before discussing possible representations for the coupling effect of the slot, some of the basic considerations underlying the spherical transmission line approach will be dealt with.

B. Spherical Mode Representation of the Fields in a Half-Space

The electromagnetic fields in the half-space are uniquely determined by specification of either the tangential electric or magnetic field components along all bounding surfaces of the region. Thus, for the given case it suffices to specify that the tangential electric field $\underline{E} \times \underline{n}$ vanishes along the metal sheet and along an infinite hemisphere centered

about the origin (i.e., no sources at infinity), and has the value $\underline{M}$ in the aperture. The unit vector $\underline{n}$ normal to the bounding surfaces points into the half-space. The exciting field in the aperture region is equivalent to a magnetic surface current distribution on a solid metal plate of density $\underline{M}$, which can be regarded as the result of a superposition of magnetic current elements distributed over the aperture. Consider one such element located at $(r', \pi/2, \phi')$ (cf. Figure 5.1). Since its vector direction lies in the plane of the metal sheet, the field it produces at (r, θ, ϕ) is identical with its free space field save for a factor of two because of the imaging effect of the plate. If the element oscillates with angular frequency ω, it has a magnetic dipole moment $(-j/\omega)\ \underline{M}\ (r')$,[2] and its free space Hertz vector is

$$\underline{\Pi}(\underline{r}, \underline{r}') = \frac{-j}{4\pi\omega\mu}\ \underline{M}(\underline{r}')\ \frac{e^{-jk\,|\underline{r}-\underline{r}'|}}{|\underline{r}-\underline{r}'|}$$

where a time dependence $e^{j\omega t}$ is implied.

The magnetic field due to this single element is given by

$$\underline{\mathcal{H}}(\underline{r}, \underline{r}') = (\nabla\nabla + k^2\,\underline{\underline{\epsilon}}) \cdot \underline{\Pi}(\underline{r}, \underline{r}')$$

where $\underline{\underline{\epsilon}}$ is a unit dyadic such that $\underline{\underline{\epsilon}} \cdot \underline{A} = \underline{A} \cdot \underline{\underline{\epsilon}} = \underline{A}$. The total field due to all the source elements is then found by superposing contributions from the entire aperture (taking account of the imaging due to the screen):

$$\underline{H}(\underline{r}) = \frac{-j\omega\epsilon}{2\pi} \iint_{ap} \left(\underline{\underline{\epsilon}} + \frac{\nabla\nabla}{k^2}\right) \frac{e^{-jk\,|\underline{r}-\underline{r}'|}}{|\underline{r}-\underline{r}'|} \cdot \underline{M}(\underline{r}')\ dS' \qquad (5.1)$$

where the vector differential operator $\nabla\nabla\cdot$ operates only on the unprimed (field point) coordinates.

If $r \gg r'$, then $|\underline{r}-\underline{r}'| \approx r - r'\cos\gamma$, and one obtains for the far field, neglecting all terms decaying more rapidly than $1/r$:

$$\underline{H}(\underline{r})_{far} = \underline{H}_t(\underline{r})_{far} = \frac{jk\epsilon}{2\pi}\ \frac{e^{-jkr}}{r}\ (\underline{\underline{\epsilon}} - \underline{r}_o\,\underline{r}_o) \cdot \iint_{ap} \underline{n}\times\underline{E}(\underline{r}')\ e^{jkr'\cos\gamma}\ dS' \qquad (5.2)$$

---

[2] T. A. Stratton, "Electromagnetic Theory", Secs. 8.4 and 8.5 (by duality)

which yields a purely transverse vector in spherical coordinates, since $\underline{\epsilon} - \underline{r}_o \underline{r}_o = \underline{\theta}_o \underline{\theta}_o + \underline{\phi}_o \underline{\phi}_o$. For the magnetic density $\underline{M}$, its value $\underline{E} \times \underline{n}$ in terms of the slot electric field has been substituted. $\underline{r}_o$, $\underline{\theta}_o$, and $\underline{\phi}_o$ are unit vectors in the r, θ, and ϕ directions, while γ is the angle between vectors $\underline{r}$ and $\underline{r}'$ which connect the origin with the observation point $P(r, \theta, \phi)$ and the source point $(r', \pi/2, \phi')$ in the aperture, respectively (see Figure 5.1). If the field in the aperture is assumed as

$$\underline{E}(\underline{r}') = \underline{y}_o E_o \cos \frac{\pi x'}{a'} = E_o \cos \frac{\pi x'}{a'} (\underline{r}_o \sin \phi' + \underline{\phi}_o \cos \phi') \qquad (5.3)$$

then integration of (5.2) yields for the squared field amplitudes (we substitute $r' \cos \gamma = x' \sin \theta \cos \phi + y' \sin \theta \sin \phi$, and integrate over x' and y'):

$$H_t^2 = H_t'^2 \left| \frac{j \omega \epsilon E_o e^{-j k r}}{2 \pi r} \right|^2 \left(\frac{4 a'}{k\pi}\right)^2 \left(\frac{k b'}{2}\right)^2$$

$$H_t'^2 = (\cos^2\theta \cos^2\phi + \sin^2\phi) \frac{\sin^2 \left(\frac{k b'}{2} \sin\theta \sin\phi\right) \cos^2 \left(\frac{k a'}{2} \sin\theta \cos\phi\right)}{\left(\frac{kb'}{2}\right)^2 \sin^2\theta \sin^2\phi \left[1 - \left(\frac{ka'}{\pi}\right)^2 \sin^2\theta \cos^2\phi\right]^2} \qquad (5.4)$$

where $H_t'^2$ is normalized so that its maximum value (for $\theta = 0$) is unity. a' and b' are the aperture dimensions parallel to the X and Y axis, respectively.

In accord with the field assumption in Equation (5.3) the magnetic current elements are directed along the X axis. If the slot is long and narrow (under these conditions the assumed field choice is most reliable if the slot is excited appropriately from a rectangular guide) the E lines are approximately circular about the X axis. Thus, any radial vector will intersect the E lines orthogonally so that the problem can be analyzed approximately in terms of H modes alone. In general, the spherical mode representation for the transverse magnetic field is given by:[3]

$$\underline{H}_t(\underline{r}) = \sum_i \left[\frac{I_i'(r)}{r} \underline{h}_i'(\theta, \phi) + \frac{I_i''(r)}{r} \underline{h}_i''(\theta, \phi) \right] \qquad (5.5)$$

---

[3] N. Marcuvitz, "Waveguide Handbook", McGraw-Hill Book Co., New York; 1951. Secs. 1.5 and 2.5.

where the single primes denote E modes and the double primes denote H modes. For this analysis, the double primed quantities alone are excited, and in the following the primes will be omitted altogether since only H modes are considered. The i-th mode current far from the slot is given by (i stands for a double index mn)[4]:

$$I_i(r) = \eta\, H_n'^{(2)}(kr)\, E_o \int_{-\frac{b'}{2}}^{\frac{b'}{2}} \int_{-\frac{a'}{2}}^{\frac{a'}{2}} \frac{\cos \frac{\pi x'}{a'}}{r'^2} \left\{ \frac{x'}{k} \hat{J}_n(kr')\, \nabla_t \cdot \underline{h}_i(\phi') + y' \hat{J}_n'(kr')\, \underline{\phi}_o \cdot \underline{h}_i(\phi') \right\} dx'\, dy' \qquad (5.6)$$

and $r'^2 = x'^2 + y'^2$. For i = (1,1), i = (1,3), i = (3,3), the $\hat{J}_n$ functions under the integral in Equation (5.6) are

$$\hat{J}_1(kr) = \frac{\sin kr}{kr} - \cos kr \; ; \quad \hat{J}_3(kr) = \left[1 - \frac{15}{(kr)^2}\right] \cos kr - \left[\frac{6}{kr} - \frac{15}{(kr)^3}\right] \sin kr$$

while the terms involving the mode functions $\underline{h}_i(\theta, \phi)$ become (for $\theta' = \frac{\pi}{2}$):

$$\nabla_t \cdot \underline{h}_{1,1} = -\sqrt{\frac{2}{\pi}} \frac{\cos \phi'}{r'} \qquad \underline{\phi}_o \cdot \underline{h}_{1,1} = -\frac{1}{2}\sqrt{\frac{3}{\pi}} \sin \phi'$$

$$\nabla_t \cdot \underline{h}_{1,3} = \frac{3}{2}\sqrt{\frac{7}{\pi}} \frac{\cos \phi'}{r'} \qquad \underline{\phi}_o \cdot \underline{h}_{1,3} = \frac{1}{8}\sqrt{\frac{7}{\pi}} \sin \phi' \qquad (5.7)$$

$$\nabla_t \cdot \underline{h}_{3,3} = -\frac{15}{2}\sqrt{\frac{7}{15\pi}} \frac{1}{r'}(4\cos^3\phi' - 3\cos\phi') \qquad \underline{\phi}_o \cdot \underline{h}_{3,3} = -\frac{15}{8}\sqrt{\frac{7}{15\pi}} (3\sin\phi' - 4\sin^3\phi')$$

$$\cos \phi' = x'/r' \qquad \sin \phi' = y'/r'$$

---

[4] This expression and others are derived in a forthcoming report on spherical transmission lines.

PLOT OF SQUARED FIELD AMPLITUDES $H_t'^2$
AGAINST POLAR ANGLE θ FOR TWO DIFFERENT VALUES OF ϕ
SLOT DIMENSIONS: $a'=.630"$, $b'=.120"$

LEGEND
- —— —— H_{11} MODE.
- ——— ——— $(H_{11}+H_{13})$ MODES.
- ——— ——— ——— $(H_{11}+H_{13}+H_{33})$ MODES.
- ——————— EXACT.

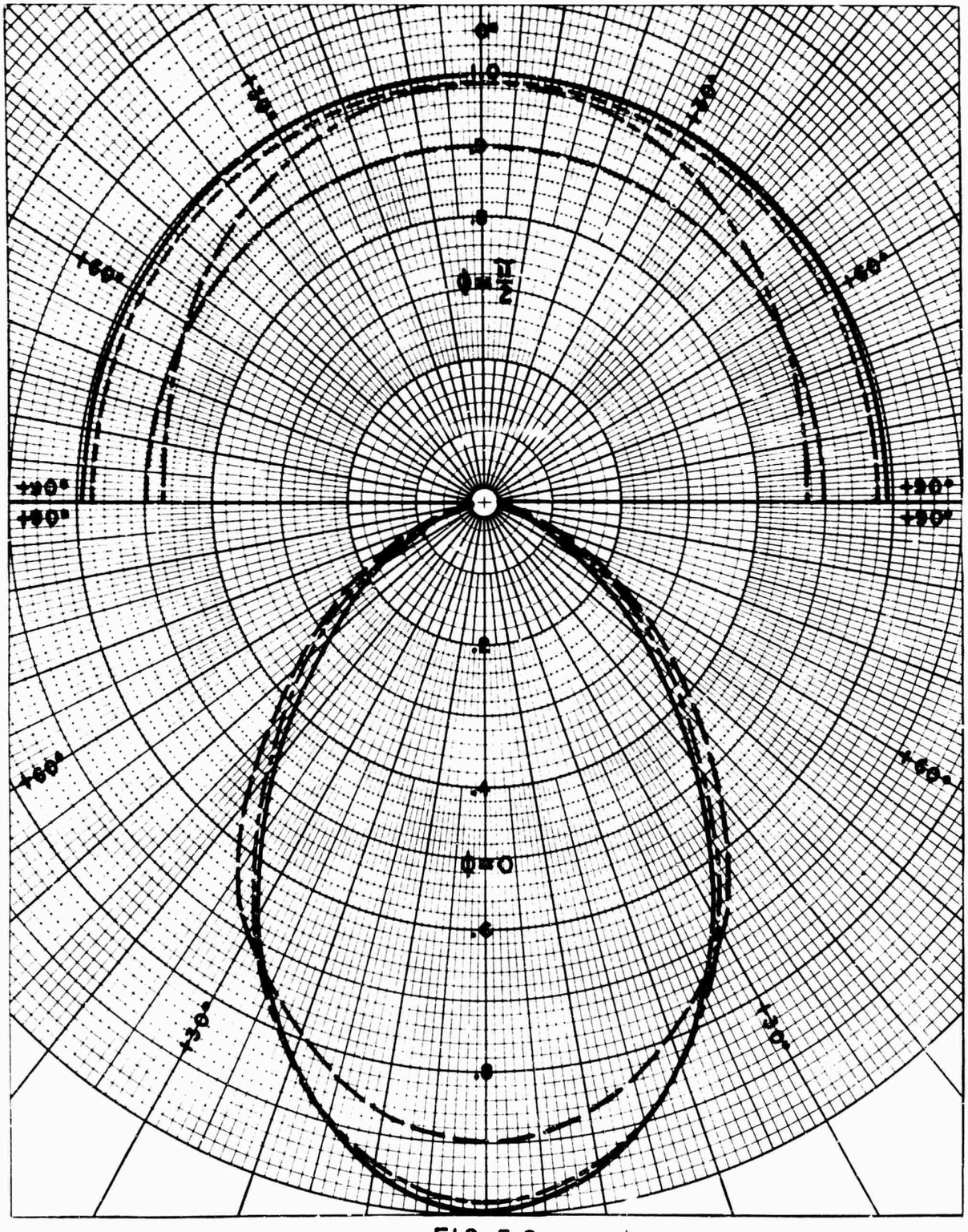

FIG. 5.2

In order to check how many terms in the spherical mode expansion (5.5) are necessary for slots of different sizes to closely reproduce the exact result in (5.4), three apertures with the following dimensions were chosen: I) $a' = .630" = \lambda/2$, $b' = .120"$; II) $a' = .315"$, $b' = .120"$; III) $a' = .900"$, $b' = .120"$. It was found that the H_{11}, H_{13}, and H_{33} modes yield a close approximation in all cases. The degree of approximation achieved with the H_{11} mode alone varies with the shape of the slot. For the small slot (II), the H_{11} mode contribution alone represents the entire field for most practical purposes, while for the large slot (III), the discrepancy between that lowest mode and the exact result is appreciable. To demonstrate the shape of the field amplitude curves, the pattern obtained from slot (I) is plotted in Figure 5.2 in two mutually perpendicular planes ($\phi = 0$ and $\phi = \pi/2$) together with the exact solution. It is to be noted that only the H_{11} and H_{13} modes contribute to the field in the vicinity of the $\theta = o$ axis; the effect of the H_{33} mode is most pronounced near the infinite plane. In the $\phi = o$ plane, the field due to the combined effects of the H_{11}, H_{13}, and H_{33} modes has not been plotted since it agrees very closely with the exact result. Therefore, the field incident from the slot on an obstacle confined to a small region about the $\theta = o$-axis is conveniently expressed as the contribution from two modes, or, as a first approximation, as a one-mode field.

If the slot in the infinite plane is now regarded as a transverse discontinuity terminating a rectangular waveguide the analysis is exactly as pointed out above except that the cosine aperture field is now only a good guess value. To determine the true field requires the solution of an integral equation which poses prohibitive difficulties. A variational formulation for the field in the half-space might be attempted in which first order errors in the guessed slot field introduce only second order errors in the space field. However, it is felt that such a formulation, though quantitatively more accurate, will not radically change the results obtained from a Kirchhoff-type integration of the cosine guess field over the aperture. The main purpose of the investigation was to determine whether a single mode representation of the half-space is feasible. As a first approximation this certainly appears to be the case.

It is interesting to note that the power radiated from the slot is almost entirely carried by the H_{11} spherical mode regardless of slot size. This brings out the important fact that although three modes are necessary in general to closely specify the field at points far from the aperture, the integrated effect of the field (namely the power) is given by one mode alone. To demonstrate the relative magnitude of the portions of radiated power carried by the three above-mentioned modes the results of the calculation for slot (I) are given below. The radiated power obtained by integrating the far field over a transverse cross-section is given by

$$P = \mathcal{S} \int_{\phi=0}^{2\pi} \int_{\theta=0}^{\pi/2} H_t^2 \, r^2 \sin\theta \, d\theta \, d\phi \cong \mathcal{S} \, (I_{11}^2 + I_{13}^2 + I_{33}^2) \qquad (5.8)$$

where $\mathcal{S} = 1/\eta = \sqrt{\mu/\epsilon}$, the series for $(r \underline{H}_t)$ has been substituted from (5.5), and the expression for I_i is given in Equation (5.6). For slot (I), the result for the radiated power is

$$P = \text{Const. x } (1 + .00094 + .00136) \qquad (5.9)$$

The numbers inside the bracket on the right-hand side of (5.9) are, respectively, the relative contributions from the H_{11}, H_{13}, and H_{33} modes. A constant has been factored out to compare the higher mode contributions with unit power carried by the H_{11} mode.

The correctness of the radiated power derived on a spherical mode basis is conveniently checked by computing the conductance offered by the slot to the rectangular guide which it terminates. The effect of the slot radiating into the matched half-space is a simple two-terminal network problem and can be represented by a susceptance B and a conductance G as shown in Figure 5.3. The conductance G is attributable entirely to the

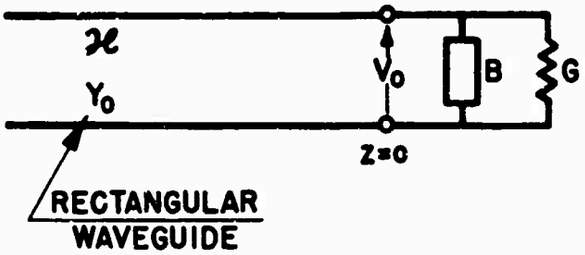

Equivalent Circuit for Slot Radiating into Unbounded Half-Space from End of Rectangular Guide

Figure 5.3

dissipative properties of the (matched) half-space, and can be expressed in terms of the radiated power and the voltage V_o (with respect to rectangular guide) in the plane of the slot as

$$G = \frac{P}{V_o^2} \qquad (5.10)$$

The voltage V_o in the aperture plane is given by

$$V_o = \iint_{ap} \underline{E}_t \cdot \underline{e}_g \, dS \quad ; \quad \underline{e}_g = \sqrt{\frac{2}{a\,b}} \cos\frac{\pi x}{a} \, \underline{Y}_o \tag{5.11}$$

where $\underline{E}_t$ is the aperture field, $\underline{e}_g$ is the vector mode function for the dominant (H_{10}) mode in rectangular guide, and a and b are the rectangular waveguide dimensions parallel to the X and Y axis, respectively. If G is evaluated from Equation (5.10) for slot (I) it is found that

$$\frac{G}{Y_o} = \frac{S}{Y_o} \frac{(I_{11}^2 + I_{13}^2 + I_{33}^2)}{V_o^2} = .76 \quad ; \quad Y_o = \frac{1}{S} \frac{\alpha}{k} \tag{5.12}$$

where the values of P and V_o have been computed from Equations (5.8) and (5.11), respectively, and a normalization with respect to the characteristic admittance Y_o of the rectangular guide has been carried out in order to permit direct comparison with the measured value. The conductance measured for slot (I) is .78 (Final Report, Chap. V, Table VI). It is seen that the agreement is quite good. For slots (II) and (III) the conductances calculated from Equation (5.12) were compared with computed variational results since no measurements were made on those slot sizes. Here, too, close agreement was noted. The conductances obtained from the spherical mode analysis were always slightly smaller than the experimental or variational results.

The results listed above indicate that although an infinity of modes propagate in the half-space a single-mode description of the field yields a good approximation to the actual conditions. Certainly, a single-mode analysis for transmitted power appears justified. To replace the half-space by a single spherical transmission line is a most useful concept if it is desired to find the scattering properties of obstacles placed therein. The impedance of such obstacles could then be found from measurements in the rectangular guide which are very conveniently performed. To allow a transition from rectangular-guide to spherical-line quantities, and vice versa, it is necessary, however, to know the network coupling the two waveguides. In the next section, a discussion of the theoretical determination of the equivalent circuit for the slot is given.

C. Theoretical Evaluation of the Slot Equivalent Circuit Parameters

In order to find the equivalent circuit for the slot radiating from the end of the guide it is necessary to relate the voltages and currents on one side of the discontinuity to those on the other. Since the half-space is to be represented as a spherical waveguide, expressions for voltage and current (i.e. transverse electric and magnetic field) in a spherical guide in terms of known excitations will have to be derived. Suppose that a spherical wave is incident from infinity upon the aperture in the infinite plane. This wave will induce a field in the aperture and electric currents in the metal plane. The total field in the half-space is uniquely given by the specification of either electric or magnetic tangential field components along the bounding surfaces. Thus, the problem can be solved uniquely with the following boundary conditions:

1) $\underline{H}_t = \underline{H}_u$ along a hemispheric shell far from the origin
2) $\underline{E}\underline{n} = \underline{M}$ in the aperture
3) $\underline{E}\underline{n} = 0$ along the metal plane.

$\underline{n}$ is a unit vector normal to the plane and pointing into the half-space. Since the spherical waveguide region is taken as one whose transverse cross-sections are bounded by a metallic surface, and since the mode functions are so defined as to satisfy boundary conditions on a metallic boundary, the aperture constitutes a (longitudinal) discontinuity on the boundary which can be taken into account by replacing the slot by an equivalent magnetic current excitation of magnitude $\underline{M}$. Thus, the field in the half-space is formed by superposing the responses due to excitations 1) and 2) above.

The total magnetic field in the half-space can be represented as:[4]

$$\underline{H}(\underline{r}) = \sum_i \left[\underline{H}_i'(\underline{r}) + \underline{H}_i''(\underline{r}) \right] \tag{5.13}$$

where

$$r\underline{H}_i(\underline{r}) = I_i(r)\, \underline{h}_i(\theta, \phi) + Y_{si}\, V_i(r)\, \underline{h}_{ri}(\theta, \phi)$$

for E and H modes, and

$$Y_{si} = Y_i \Big|_{k=0} = \frac{-j\, k_{ci}}{r\, \omega\, \mu} \quad , \quad k_{ci}^2 = n(n+1) \; ; \quad \underline{h}_{ri} = \underline{r}\, \frac{\nabla_t \cdot \underline{h}_i}{k_{ci}}$$

It was shown in Sec. B that for the slot field of Equation (5.3), only H modes are excited. Thus, an H mode incident from infinity may be taken to excite a slot field which, in turn, radiates only H modes so that the entire problem is analyzed in terms of H modes alone. All transmission line quantities from now on will be understood to refer to H modes. The mode voltages and currents satisfy inhomogeneous transmission line equations[4]

$$\frac{d V_i (r)}{dr} = - j \varkappa_i (r) Z_i (r) I_i (r) + v_i (r)$$

$$\frac{d I_i (r)}{dr} = - j \varkappa_i (r) Y_i (r) V_i (r) + i_i (r) \tag{5.14}$$

where $\varkappa_i$, Y_i, Z_i are as defined in Equation (1) of the Appendix, and v_i and i_i are "source terms" arising from the presence of apertures in the bounding plane and are given by[4]

$$v_i (r) = - \int_0^{2\pi} \underline{M} (r', \phi') \cdot \underline{h}_i (\phi) \, d\phi$$

$$i_i (r) = Y_{si} \int_0^{2\pi} \underline{M} (r', \phi') \cdot \underline{h}_{ri} (\phi) \, d\phi \tag{5.15}$$

where the magnetic source current $\underline{M}$ is equal to $\underline{E} \times \underline{n}$.

To find the unperturbed field, i.e. the field due to an incoming spherical H mode wave with no aperture present, we can use the solutions for V and I from Equation (3) of the Appendix, because $v_i = i_i = 0$ for this case. Since then the line is terminated by a short-circuit at the origin, we obtain

$$V_{ui} (r) = V_{ui} \hat{J}_n (kr) \, , \; V_{ui} = 2 C_i$$

$$I_{ui} (r) = j \eta \, V_{ui} \hat{J}'_n (kr) \tag{5.16}$$

where the subscript u designates unperturbed quantities (with aperture absent). The scattered mode voltages and currents (due to the aperture magnetic source current $\underline{M}$ alone) are:[4]

$$V_{si}(r) = -j \hat{H}_n^{(2)}(kr) \int_0^r \int_0^{2\pi} \underline{n} \times \underline{E}(\underline{r}') \cdot \underline{h}_i^{(1)}(\underline{r}')\, d S'$$

$$- j \hat{J}_n(kr) \int_r^{\square} \int_0^{2\pi} \underline{n} \times \underline{E}(\underline{r}') \cdot \underline{h}_i^{(-)}(\underline{r}')\, d S' \qquad (5.17)$$

$$I_{si}(r) = \eta \hat{H}_n'^{(2)}(kr) \int_0^r \int_0^{2\pi} \underline{n} \times \underline{E}(r') \cdot \underline{h}_i^{(1)}(\underline{r}')\, d S'$$

$$+ \eta \hat{J}_n'(kr) \int_r^{\square} \int_0^{2\pi} \underline{n} \times \underline{E}(\underline{r}') \cdot \underline{h}_i^{(-)}(\underline{r}')\, d S'$$

where $\square$ denotes the aperture boundary, and

$$r \underline{h}_i^{(-)}(\underline{r}) = \hat{H}_n'^{(2)}(kr)\, \underline{h}_i(\theta, \phi) - j \varsigma Y_{si} \hat{H}_n^{(2)}(kr)\, \underline{h}_{ri}(\theta, \phi)$$

$$r \underline{h}_i^{(1)}(\underline{r}) = \hat{J}_n'(kr)\, \underline{h}_i(\theta, \phi) - j \varsigma Y_{si} \hat{J}_n(kr)\, \underline{h}_{ri}(\theta, \phi) \qquad (5.18)$$

$$d S' = r' dr' d \phi'$$

By superposing solutions (5.16) and (5.17) the magnetic field per mode anywhere in the half-space is given by Equation (5.13) in terms of the incident and aperture fields as:

$$\mathbf{r}\,\underline{H}_1(\underline{r}) = V_{ui}\left[j\,\eta\,\hat{J}_n'(kr)\,\underline{h}_1(\theta,\phi) + Y_{si}\,\hat{J}_n(kr)\,\underline{h}_{r1}(\theta,\phi)\right]$$

$$+\int_0^{r}\int_0^{2\pi} \underline{n}\times\underline{E}(\underline{r}')\cdot\Big[\eta\,\hat{H}_n'^{(2)}(kr)\,\underline{h}_1^{(1)}(\underline{r}')\,\underline{h}_1(\theta,\phi)$$

$$-j\,Y_{si}\,\hat{H}_n^{(2)}(kr)\,\underline{h}_1^{(1)}(\underline{r}')\,\underline{h}_{r1}(\theta,\phi)\Big]\,dS'$$

$$+\int_r^{\infty}\int_0^{2\pi} \underline{n}\times\underline{E}(\underline{r}')\cdot\Big[\eta\,\hat{J}_n'(kr)\,\underline{h}_1^{(-)}(\underline{r}')\,\underline{h}_1(\theta,\phi)$$

$$-j\,Y_{si}\,\hat{J}_n(kr)\,\underline{h}_1^{(-)}(\underline{r}')\,\underline{h}_{r1}(\theta,\phi)\Big]\,dS'$$

Or, for the total field,

$$\underline{H}(\underline{r}) = j\,\eta\,V_u\,\underline{h}^{(1)}(\underline{r}) + \iint_{ap} \underline{n}\times\underline{E}(\underline{r}')\cdot\underline{Y}_h(\underline{r},\underline{r}')\,dS' \qquad (5.19)$$

where $$\underline{Y}_h(\underline{r},\underline{r}') = \begin{cases} \sum_i \eta\,\underline{h}_1^{(-)}(\underline{r})\,\underline{h}_1^{(1)}(\underline{r}') & r > r' \\ \sum_i \eta\,\underline{h}_1^{(1)}(\underline{r})\,\underline{h}_1^{(-)}(\underline{r}') & r < r' \end{cases} \qquad (5.20)$$

The incident field in (5.19) is taken to consist of an H_{11} mode only, which is dominant in the spherical guide under consideration (see the remarks in Sec. B). The equivalent circuit is to be evaluated with respect to this mode, and with this understanding, the modal subscripts are omitted. However, the scattered field (the integral in (5.19) can also be represented in closed form by (cf. Equation (5.1))

$$\underline{H}_s(\underline{r}) = \iint_{ap} \underline{n} \times \underline{E}(\underline{r}') \cdot \underset{\sim}{Y}_h(\underline{r}, \underline{r}')\, dS' \tag{5.21}$$

where $\underset{\sim}{Y}_h(\underline{r}, \underline{r}') = \frac{j\omega\epsilon}{2\pi}\left(\underset{\sim}{\epsilon} + \frac{\nabla\nabla}{k^2}\right)\frac{e^{-jk|\underline{r}-\underline{r}'|}}{|\underline{r}-\underline{r}'|}$

Thus, the expressions for the half-space dyadic spatial admittance in (5.20) and (5.21) are identical, representing, respectively, its modal expansion in spherical vector modes and its closed form. The dyadic kernel $\underset{\sim}{Y}_h$ contains conductive and reactive parts for all scattered modes. Since we consider only one mode to propagate in the half-space we would like to determine the equivalent circuit to that mode. For this purpose we separate out the conductive part of the dominant mode term in the kernel since no real dominant mode power is then dissipated in the discontinuity. This real part of the dominant mode field (capable of carrying real power) can then be combined with the unperturbed magnetic field.

The dominant mode part of the kernel is given by $\eta\, h^{(-)}(\underline{r})\underline{h}^{(1)}(\underline{r}')$ for $r > r'$, and by $\eta\, \underline{h}^{(1)}(\underline{r})\underline{h}^{(-)}(\underline{r}')$ for $r < r'$. From Equations (5.18) it is seen that $\underline{h}^{(1)}$ is real and $\underline{h}^{(-)}$ is complex. In fact

$$\underline{h}_1^{(-)}(\underline{r}) = \underline{h}_1^{(1)}(\underline{r}) - j\,\underline{h}_1^{(2)}(\underline{r}) \tag{5.22}$$

where $r\,\underline{h}_1^{(2)}(\underline{r}) = \hat{H}_n'(kr)\,\underline{h}_1(\theta, \phi) - j \sum Y_{s1}\,\hat{N}_n^{(2)}(kr)\,\underline{h}_{r1}(\theta, \phi)$

so that $\underline{h}^{(2)}(\underline{r})$ is also real. Therefore, the real part of the dominant mode in the kernel is $\eta\, \underline{h}^{(1)}(\underline{r})\, \underline{h}^{(1)}(\underline{r}')$ so that Equation (5.19) can be written as:

$$\underline{H}(\underline{r}) = j\eta\, \nabla_1 \underline{h}^{(1)}(\underline{r}) + \iint_{ap} \underline{n} \times \underline{E}(\underline{r}') \cdot \left[\eta\, \underline{h}^{(1)}(\underline{r}')\, \underline{h}^{(1)}(\underline{r})\right] dS' \tag{5.23}$$

$$+ \iint_{ap} \underline{n} \times \underline{E}(\underline{r}') \cdot \left[\underset{\sim}{Y}_h(\underline{r}, \underline{r}') - \eta\, \underline{h}^{(1)}(\underline{r})\, \underline{h}^{(1)}(\underline{r}')\right] dS'$$

The unperturbed voltage amplitude V_u can be broken down as follows. The total dominant mode voltage and current are expressible as (see Appendix):

$$V(r) = A \hat{J}_n(kr) + B \hat{N}_n(kr) = V_u \hat{J}_n(kr) + j B \hat{H}_n^{(2)}(kr) \; ; \; V_u = A - j B$$

$$-j \zeta I(r) = A \hat{J}_n'(kr) + B \hat{N}_n'(kr) = V_u \hat{J}_n'(kr) + j B \hat{H}_n^{(2)}{}'(kr) \qquad (5.24)$$

Equations (5.24) represent correctly the voltage and current behavior off the source region, i.e. for points for which r is greater than the distance from the origin to the furthest point on the aperture boundary. This can also be seen by comparing with the total voltage and current obtained from superposition of the results in (5.16) and (5.17), since for such points the integrals in (5.17) multiplied by $\hat{J}_n(kr)$ and $\hat{J}_n'(kr)$ vanish. Equating identical coefficients in Equations (5.16), (5.17), and in Equations (5.24) we obtain

$$V_u = A - j B \; ; \quad B = - \iint_{ap} \underline{n} \times \underline{E}(\underline{r}') \cdot \underline{h}^{(1)}(\underline{r}') \, dS' \qquad (5.25)$$

so that (5.23) becomes, finally:

$$\underline{H}(\underline{r}) = j \eta A \underline{h}^{(1)}(\underline{r}) + \iint_{ap} \underline{n} \times \underline{E}(\underline{r}') \cdot \left[\underset{\sim}{Y}_h(\underline{r}, \underline{r}') - \eta \underline{h}^{(1)}(\underline{r}') \underline{h}^{(1)}(\underline{r}) \right] dS' \qquad (5.26)$$

In order to formulate an equivalent circuit for the slot we must relate the fields on both sides of the discontinuity. The transverse magnetic field in the rectangular guide ($z < 0$) propagating the dominant mode is given by (cf. Final Report, Ch. I, Secs. 2a and b)

$$\underline{H}_t(\underline{r}_g) = I_g(z) \underline{h}_g(\rho) - \iint_{ap} \underline{n} \times \underline{E}(\underline{r}') \cdot \underset{\sim}{\mathcal{B}}_g(\underline{r}, \underline{r}') \, dS' \qquad (5.27)$$

where the subscript g refers to rectangular guide, and $\underline{\rho} = (x,y)$. Since the transverse magnetic field must be continuous in the aperture we can equate, from (5.26) and (5.27):

$$\left[I_g(0)\, \underline{h}_g(\rho) - j\eta A\, \underline{h}^{(1)}(\underline{r}) \right] \times \underline{n} =$$

$$= \iint_{ap} \underline{n}\times\underline{E}(\underline{r}') \cdot \left[\underline{\underline{Y}}_+(\underline{r},\underline{r}') - \eta\, \underline{h}^{(1)}(\underline{r}')\underline{h}^{(1)}(\underline{r}) + \underline{\underline{\mathcal{B}}}_g(\underline{r},\underline{r}') \right] \times \underline{n}\, dS' \qquad (5.28)$$

Equation (5.28) is the integral equation for the slot electric field. If Equation (5.28) is now multiplied in dot product fashion by $\underline{E}(\underline{r})$ and the result is integrated over the aperture, one obtains

$$I_g(0)\, V_g(0) + j\eta A B = \iint_{ap} dS \iint_{ap} dS'\, \underline{n}\times\underline{E}(\underline{r}') \cdot \underline{\underline{K}}(\underline{r},\underline{r}') \cdot \underline{n}\times\underline{E}(\underline{r}) \qquad (5.29)$$

where $\underline{\underline{K}}(\underline{r},\underline{r}') = \underline{\underline{Y}}_g(\underline{r},\underline{r}') - \eta\, \underline{h}^{(1)}(\underline{r}')\, \underline{h}^{(1)}(\underline{r}) + \underline{\underline{\mathcal{B}}}_g(\underline{r},\underline{r}')$

$$V_g(0) = \iint_{ap} \underline{n}\times\underline{E}(\underline{r}) \cdot \underline{h}_g(\rho)\, dS$$

and Equation (5.25) has been employed. Upon dividing both sides of Eq. (14) by

$$\left[V_g(0) \right]^2$$

we finally obtain a relationship that expresses the equivalent circuit for the slot:

$$\frac{I_g(0)}{V_g(0)} + j\eta \frac{A}{B} \left[\frac{B}{V_g(0)} \right]^2 = \frac{\iint_{ap} dS \iint_{ap} dS'\, \underline{n}\times\underline{E}(\underline{r}') \cdot \underline{\underline{K}}(\underline{r},\underline{r}') \cdot \underline{n}\times\underline{E}(\underline{r})}{\left[\iint_{ap} \underline{n}\times\underline{E}(\underline{r}) \cdot \underline{h}_g(\rho)\, dS \right]^2} \qquad (5.30)$$

The two quantities on the left-hand side of (5.30) have the dimensions of admittance. The first term represents the input admittance to the structure as seen from the rectangular guide. The second term is readily interpreted if the output terminal plane is chosen not at $r = 0$ but rather at $r = (2q + 1)\lambda/4$, q = large integer. For large values of r the asymptotic representations for the spherical functions apply (see Appendix), and Equation (5.24) can be written as (for $n = 1$):

$$V(r) = -A \cos kr - B \sin kr$$
$$-jS\, I(r) = A \sin kr - B \cos kr \qquad (5.31)$$

If r is now chosen as $r_o = (2q+1)\lambda/4$, and the ratio of I to V is formed, one obtains for the output admittance at r_o:

$$\frac{I(r_o)}{V(r_o)} = -j\eta \frac{A}{B} \quad ; \quad |V(r_o)| = |B| \qquad (5.32)$$

Equation (5.30) becomes, in terms of admittances,

$$Y_g(0) - Y(r_o) \left[\frac{V(r_o)}{V_g(0)}\right]^2 = Y_1 \qquad (5.33)$$

where Y_1 stands for the right-hand side of (5.30). If the equivalent circuit is now assumed to be shunt (rigorously this implies that the fields excited in the slot by an incoming dominant mode wave from the rectangular or the spherical guide are identical to within a constant factor) then Equation (5.33) allows the simple physical interpretation illustrated in Figure 5.4, and the network

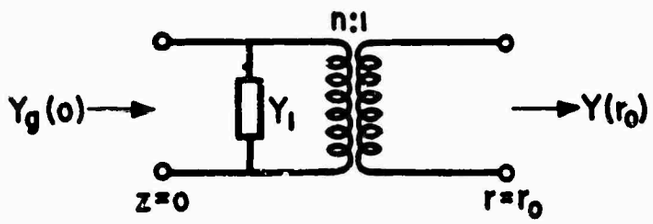

Figure 5.4
Equivalent Circuit

parameters can be determined as follows:

$$|n| = \left|\frac{V_g(0)}{V(r_o)}\right| = \left|\frac{\iint_{ap} \underline{n} \times \underline{E}(\underline{r}) \cdot \underline{h}_g(\underline{\rho})\, dS}{\iint_{ap} \underline{n} \times \underline{E}(\underline{r}) \cdot \underline{h}^{(1)}(\underline{r})\, dS}\right| \qquad (5.34)$$

$$Y_1 = \frac{\iint_{ap} dS \iint_{ap} dS' \; \underline{n} \times \underline{E}(\underline{r}') \cdot \underset{\sim}{K}(\underline{r}, \underline{r}') \cdot \underline{n} \times \underline{E}(\underline{r})}{\left[\iint_{ap} \underline{n} \times \underline{E}(\underline{r}) \cdot \underline{h}_g(\underline{\rho}) \, dS \right]^2} \tag{5.35}$$

$$= Y_t - \frac{1}{n^2}\eta$$

$$\text{where } Y_t = \frac{\iint_{ap} dS \iint_{ap} dS' \; \underline{n}\underline{x}\underline{E}(\underline{r}') \cdot \left[\underset{\sim}{Y}_h(\underline{r},\underline{r}') + \underset{\sim}{\beta}_g(\underline{r},\underline{r}') \right] \cdot \underline{n}\underline{x}\underline{E}(\underline{r})}{\left[\iint_{ap} \underline{n} \times \underline{E}(\underline{r}) \cdot \underline{h}_g(\underline{\rho}) \, dS \right]^2}$$

Y_1 is given in a variational form. The term Y_t represents exactly the two-terminal input admittance to a thin slot radiating into a half space from the end of a rectangular guide. Results for this have been worked out and measured elsewhere (Part III, Sec. D., also Final Report, Ch. V, Table VI). Therefore, the only parameter that needs to be evaluated is the transformer turns ratio n as given in (5.34).[5]

The term $(1/n^2)\eta$ in (5.35) is the conductance as seen from the rectangular guide due to the matched dominant-mode spherical line, and is therefore subtracted from the two-terminal admittance so that a four-terminal equivalent circuit is obtained. If the half space could be represented rigorously by a single transmission line propagating only the dominant mode then Y_1 would be purely reactive. However, the half-space is capable of propagating an infinity of spherical modes each of which can carry real power. Thus, the subtraction of only the dominant mode conductance will leave a conductive part in Y_1 which represents the power radiated by the higher modes. But it was pointed out in Sec. B that the portion of power carried by the higher modes is very small in comparison with that of the dominant mode so that the real part of Y_1 should be very small. This is confirmed by the calculations.

Since the slot is rectangular it is best to express all variables in Cartesian coordinates. The functions involved are the following (evaluated in the aperture):

---

[5] The results in (5.35) are valid also for wider slots scattering E modes as well since $\underset{\sim}{Y}_h$ in its closed form (5.21) contains all scattered modes. For E mode scattering the spherical mode representation (5.20) of $\underset{\sim}{Y}_h$ includes additional terms.

$$\underline{h}_g(x, y) = \sqrt{\frac{2}{ab}} \cos \frac{\pi x}{a} \underline{x}_0$$

$$\underline{h}^{(1)}(r, \tfrac{\pi}{2}, \phi) = \frac{1}{r}\left[\hat{J}_1'(kr)\, \underline{h}(\tfrac{\pi}{2}, \phi) - j\varsigma Y_s \hat{J}_1(kr)\, \underline{h}_r(\tfrac{\pi}{2}, \phi)\right]$$

$$\underline{h}(\tfrac{\pi}{2}, \phi) = -\frac{1}{2}\sqrt{\frac{3}{\pi}} \sin\phi\, \underline{\phi}_0$$

$$Y_s = \frac{-j}{r\omega\mu} k_c \quad ; \quad \underline{h}_r(\tfrac{\pi}{2}, \phi) = \underline{r}\, \frac{1}{k_c} \nabla_t \cdot \underline{h}$$

$$\nabla_t \cdot \underline{h}\,\Big|_{\theta = \pi/2} = -\frac{1}{r}\sqrt{\frac{3}{\pi}} \cos\phi \qquad (5.36)$$

$$r = \sqrt{x^2 + y^2} \quad ; \quad \cos\phi = x/r \quad ; \quad \sin\phi = y/r$$

$$\underline{\phi}_0 \cdot \underline{x}_0 = -\sin\phi \quad ; \quad \underline{r}_0 \cdot \underline{x}_0 = x/r$$

$$\hat{J}_1(kr) = \frac{\sin kr}{kr} - \cos kr = .333\,(kr)^2 - .0333(kr)^4 + .00119(kr)^6 - + \ldots\ldots$$

and a and b are the rectangular guide dimensions. The integration over the aperture extends from $-a'/2$ to $a'/2$ in x and from $-b'/2$ to $b'/2$ in y. Since the integral equation (5.28) for the aperture field cannot be solved, a guess value for the field will be employed. A simple guess value is

$$\underline{E}(\underline{r}) = \underline{y}_0 \cos \frac{\pi x}{a'} \qquad (5.37)$$

The evaluation of the numerator integral in the expression of n is straight-forward. The denominator integral, on the other hand, involves trigonometric functions whose arguments are square roots and, thus, is not easily evaluated. However, this difficulty can be avoided by employing the series expansion for $\hat{J}_1(kr)$ and its derivative. It is found that the resulting series of terms converges very rapidly over the range of apertures

considered (for $\lambda = 1.26''$) so that only two or three terms need be taken. The integrals now reduce to those where the integrands are trigonometric functions multiplied by powers of the variable and are easily found. Thus, the result for n is calculated to be:

$$|n| = \frac{\sqrt{\frac{2a}{b}}\ \frac{a'b'}{\pi}\ \frac{2a}{a^2 - a'^2}\ \cos\left(\frac{\pi a'}{2a}\right)}{1.3\left(\frac{a'}{\lambda}\right)b'\left[1 - .188\left(\frac{a'}{\lambda}\right)^2 - .658\left(\frac{a'}{\lambda}\right)^2\left(\frac{b'}{a'}\right)^2 + .0093\left(\frac{a'}{\lambda}\right)^4 + \ldots\right]} \qquad (5.38)$$

The numerator and denominator of (5.38) represent directly the results of the numerator and denominator integrals in Equation (5.34).

The parameters n and Y_1 have been computed from Equation (5.38) and (5.35), and are given in Table I. The terminal admittances Y_1 were taken from the experimental results on .005" thick slots as the most reliable available values (see Final Report, Chap. V, Table VI). The results of the calculation are listed in Table II in Sec. D, where they can be compared directly with measured values.

D. Experimental Determination of the Slot Equivalent Circuit Parameters

1. The Scattering Matrix for the Slot

Since the H_{11} spherical mode almost completely characterizes propagation in the half-space, the equivalent circuit defining the effect of the presence of the slot on the dominant modes in both the rectangular and spherical guides will be practically lossless. The circuit parameters of the general lossless four-pole can be determined most precisely from a series of D vs. S measurements (see Final Report, Chap. II). Such measurements, however, require a movable short which is not readily constructable for a spherical line. (In the spherical waveguide the transverse cross-sections over which the voltage and current are constant are hemispheres centered about the origin and bounded by the infinite baffle.) Therefore, three fixed metal hemispheres with different radii were constructed to serve as individual terminations of the spherical line. From the three corresponding input measurements in rectangular guide, the equivalent

circuit for the slot can be determined. The circuit parameters so obtained can then be checked against a fourth measurement with the slot radiating into the unterminated half-space, i.e., a matched spherical line.

The representation of the slot parameters was first attempted on a scattering basis since the reflection coefficient (unlike the input impedance) in a spherical guide is well behaved at the origin. The virtue of such a representation is that it makes the origin the input terminal to the spherical line. With the directions of incident and reflected waves in both guides chosen as in Figure 5.5, the relationship between the (voltage)

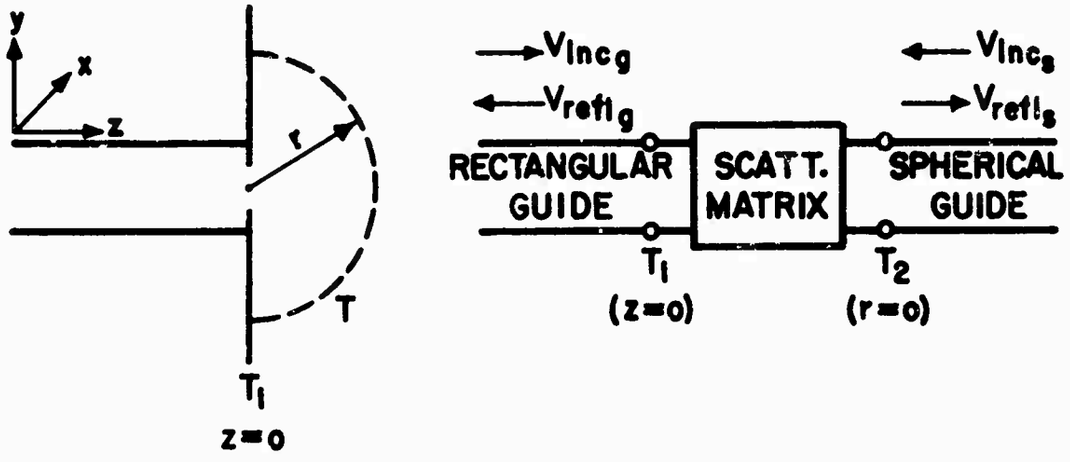

Representation of the Configuration

Figure 5.5

reflection coefficients looking to the right on both sides of the network is given by:

$$\Gamma_g(z)\Big|_{z=0} = S_{11} - \frac{S_{12}^2}{S_{22} - \dfrac{1}{\Gamma_s(r)\Big|_{r=0}}} \qquad (5.39)$$

where S_{11}, S_{12}, S_{22} are the scattering coefficients for the iris, and the subscripts g and s refer to the rectangular and spherical guides, respectively (cf. Final Report, Chap. II, Eq. (12)).

If r_o is taken as the radius of the metallic hemispheric terminations, then ${}^{o}\Gamma_{sn}(r_o)$ in Equation (7) of the Appendix is equal to - 1. r_o can now be chosen to make $\Gamma_{gn}(o)$ particularly simple. We are concerned here with only the H_{11} mode, i.e., $n = m = 1$. Thus, Equation (7) of the Appendix becomes:

$$\Gamma_g(o) = e^{-j\,2\eta_1(kr_o)} \tag{5.40}$$

If $\eta_1(kr_o)$ is now chosen as $-\pi/4$, 0, $\pi/4$, the corresponding values for the reflection coefficient at the origin are:

$$\text{a) } \Gamma_g(o) = +j \quad ; \quad \text{b) } \Gamma_g(o) = +1 \quad ; \quad \text{c) } \Gamma_g(o) = -j \tag{5.41}$$

For the given wavelength $\lambda = 2\pi/k = 1.260''$, the radii are found to be:

$$\text{a) } r_o = 1.067'' \quad ; \quad \text{b) } r_o = 1.228'' \quad ; \quad \text{c) } r_o = 1.390'' \tag{5.42}$$

The values in (5.42) are, of course, not unique. However, they were chosen because this range fitted the physical outlay of the measuring equipment. In the rectangular waveguide, the reflection coefficient corresponding to each of the terminations a), b), c) is given in terms of the distance d of the voltage minimum from plane T_1 as

$$\Gamma_g(o)_{a,b,c} = -e^{j\left[\frac{4\pi}{\lambda g}\right]d_{a,b,c}} \tag{5.43}$$

The scattering coefficients can now be determined from (5.39). (For explicit formulae for S_{11}, S_{12}, S_{22} in terms of Γ_g and Γ_s see the Final Report, Chap. II, Eqs. (36).) For the case of the unterminated half-space, $\Gamma_s(r)=0$, so that the corresponding Γ_g yields S_{11} directly as an independent check. The results of measurements on five slots are given in Table I.

TABLE I

Slot Size	3 - cup measurements			No Termination
	S_{11}	S_{22}	S_{12}^2	S_{11}
a' = .354" b' = .158"	.960 | 162.6°	.960 | 164.7°	.078 | 147.3°	1 | 162.7°
a' = .448" b' = .159"	.909 | 141.0°	.909 | 141.1°	.174 | 102.0°	1 | 140.7°
a' = .54" b' = .16"	.407 | 94.1°	.406 | 123.7°	.835 | 37.5°	.373 | 92.1°
a' = .60" b' = .09"	.146 | 21.0°	.146 | 161.6°	.979 | 2.7°	.131 | 18.4°
a' = .630" b' = .160"	.158 | -34.8°	.158 | -163.2°	.975 | -17.7°	.149 | -46.1°

For small slot sizes ($|S_{12}|$ small) the value of S_{11} obtained from measurements with the hemispheric terminations checks well with the independently determined one (first two apertures listed in Table I). Actually, only the phase of S_{11} can be compared since the V.S.W.R. for the latter measurements was too high to be determined accurately, and was thus arbitrarily taken as infinite. For larger slot widths the agreement, though reasonable, is not as good. This is to be expected since the single mode representation of the half-space, on the basis of which the measurements and analysis are undertaken, holds best for small apertures, and cannot be expected to yield accurate results for large slots.

The internal consistency of the calculations of the scattering coefficients was checked by making use of the following relationship which the scattering matrix for a lossless four-pole coupling two uniform trans-

mission lines is known to satisfy:[6]

$$\begin{bmatrix} S_{11}^* & S_{12}^* \\ S_{12}^* & S_{22}^* \end{bmatrix} \begin{bmatrix} S_{11} & S_{12} \\ S_{12} & S_{22} \end{bmatrix} = \begin{bmatrix} 1 & 0 \\ 0 & 1 \end{bmatrix} \tag{5.44}$$

so that

$$|S_{11}| = |S_{22}| \quad ; \quad |S_{12}|^2 = 1 - |S_{11}|^2 \quad ; \quad \gamma = \tfrac{1}{2}\left[\theta + \phi \pm \pi\right]$$

where

$$S_{11} = |S_{11}| \angle\theta \quad ; \quad S_{22} = |S_{22}| \angle\phi \quad ; \quad S_{12} = |S_{12}| \angle\gamma \ .$$

Inspection of Table I shows that the values listed there meet the conditions (5.44). A point of interest in connection with Equation (5.44) is that the derivation of the unitary character of the scattering matrix for a lossless structure is based on the ability to write the total incident power in terms of the incident and reflected waves as follows:

$$P = \mathrm{Re}\left[\sum_{n=1}^{2} V_n I_n^*\right] = \sum_{n=1}^{2}\left[|V_{\mathrm{inc}\ n}|^2 - |V_{\mathrm{refl}\ n}|^2\right] \tag{5.45}$$

where V_n and I_n are RIS values. This can always be done for a uniform waveguide but not, in general, for the spherical guide. That is, for the spherical guide (from Equations (3b) and (5) of the Appendix, after normalizing to unit characteristic impedance)

$$\mathrm{Re}\ |V_n I_n^*| = -\left(|C|^2 - |D|^2\right)\frac{1}{r} - \left(|V_{\mathrm{inc}\ s}|^2 - |V_{\mathrm{refl}_s}|^2\right). \tag{5.46}$$

The minus sign in front of the brackets arises from the choice of direction of incident wave in the spherical line in the direction of decreasing r. Equation (5.46) states that the power flow across any hemispheric cross-section is constant, which it should be since no power is dissipated in any finite region. On the other hand, the amplitudes of incident and reflected waves depend on r. However, far from the origin the Hankel functions vary

---

6 C.G. Montgomery, "Principles of Microwave Circuits", MIT Rad. Lab. Series, Vol. 8. McGraw-Hill Co., New York, 1948. Sec. 5.16.

as $\exp\left[\mp j\,(kr - \pi/2)\right]$ (cf. Eq. (9) of the Appendix), so that the inequality in (5.46) can be removed for $kr \gg 1$. Therefore, the scattering matrix for a network between terminal planes $z = o$ and $r = (2q + 1)\lambda/4$, where q is a large integer, is unitary. But it was shown in Eq. (13b) of the Appendix that, for a mode with n odd, such as the H_{11} mode, the reflection coefficients (from which the S matrix is computed) at $r = o$ and $r = (2q + 1)\lambda/4$ are identical. Thus, the scattering matrices are identical and unitary between both reference planes.

The three hemispheric terminations, shown in Figure 5.6(a), were made by boring a hemispheric cavity into solid brass stock on a lathe. The rims of the cups were insulated with thin mica in order to eliminate the possibility of non-uniform contact between the rim and the aperture plane.

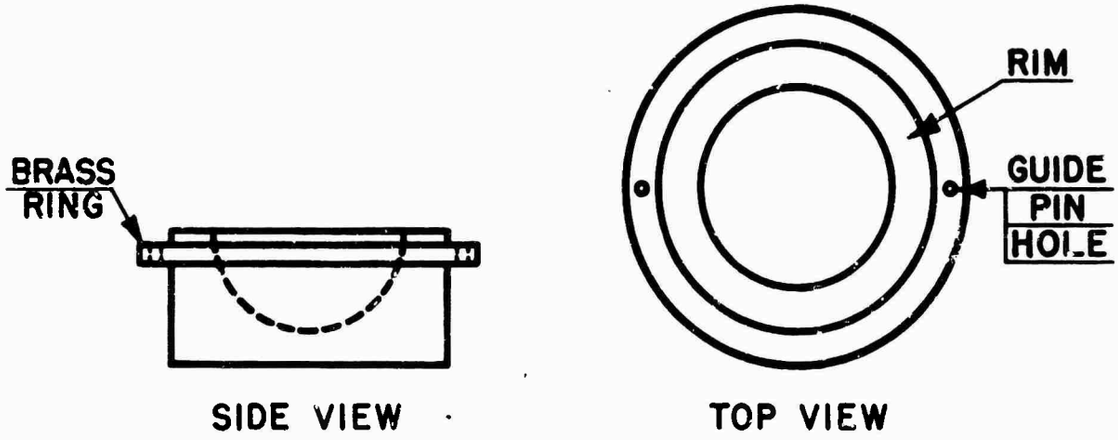

Figure 5.6 (a)

Hemispheric Terminations

The aperture structure iself was made especially rigid by first milling the slot into a thick brass plate, soldering the waveguide to it, and then turning the face of the plate down on the lathe until the aperture thickness was about 10 mils. A diagram of the slot structure is given in Figure 5.6(b), and a photograph of the hemispheric terminations and the slot appears in Figure 5.7. In this manner, possibility for uneven contact between the insulated cup rims and the slot plane was minimized. The cups were centered with respect to the slot by the use of guide pins and were held to the plane with C - clamps.

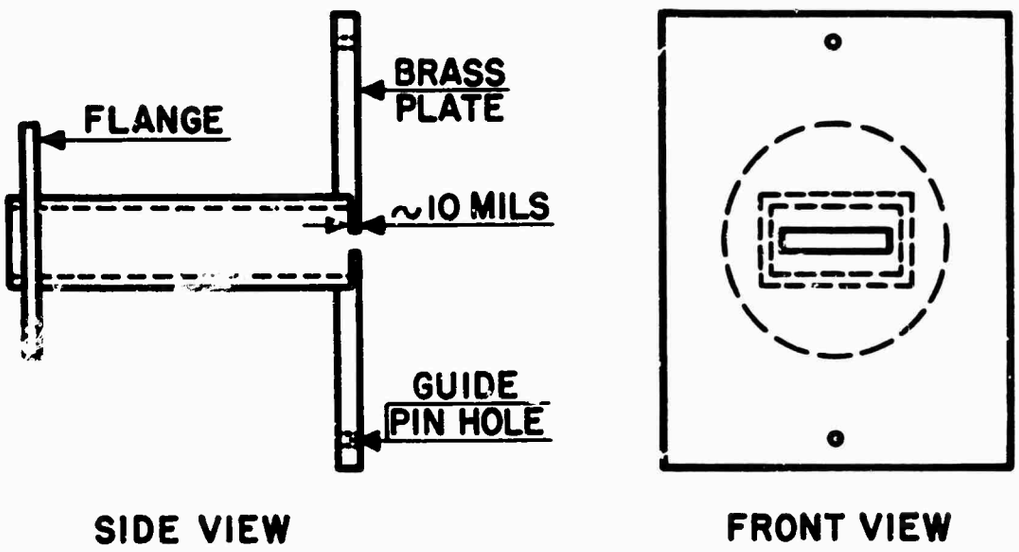

Picture of the Slot Structure

Figure 5.6 (b)

Figure 5.7

2. The Equivalent Circuit for the Slot

In view of the fact that the relationship of input (rectangular guide) to output (spherical guide) quantities by means of Equation (5.39) is rather cumbersome, it was attempted to find a representation which offers a simpler method of transforming input quantities into output quantities, and vice versa. Such a representation was obtained by formulating an equivalent admittance network for the slot between terminal planes z = o on the left and r = (2q + 1)λ/4 on the right (see Figure 5.8), where q is a large integer. If the H_{11} mode only is taken to propagate in the half-space then the equivalent circuit is lossless. Furthermore, under the assumption leading to the interpretation of Equation (5.33), the admittance Y_2' in Figure 5.8 is infinite.

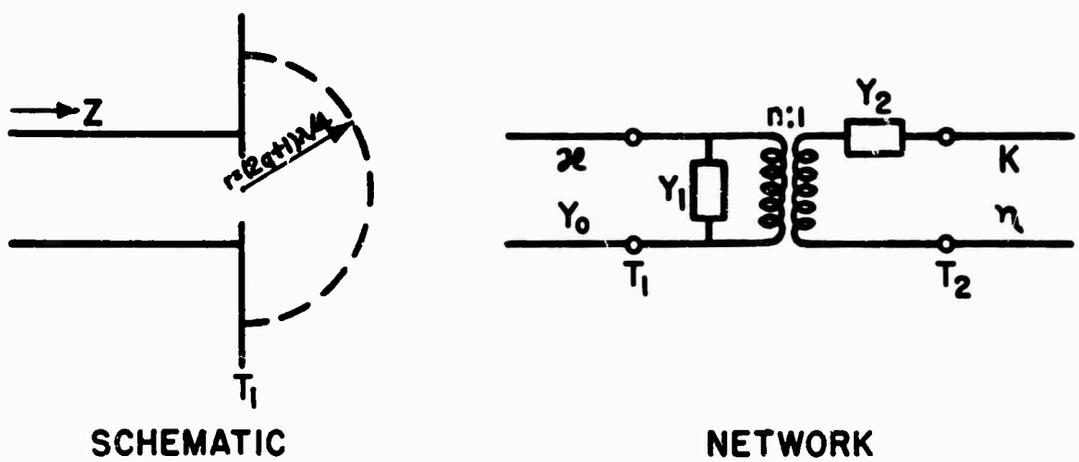

Admittance Representation for the Slot

Figure 5.8

The lossless equivalent circuit of Figure 5.8 can now be computed from three output - input measurements. Using relation (13b) of the Appendix, the terminal impedance in the direction of increasing r relative to the characteristic impedance ζ of the half-space far away can be expressed in terms of the reflection coefficient at r = o as:

$$\left.\frac{Z(r)}{\zeta}\right|_{r=(2q+1)\lambda/4} = \frac{1+\Gamma(0)}{1-\Gamma(0)} \qquad (5.47)$$

Employing the same sequence as that in Equation (5.41) these impedances become:

$$a)\ \frac{Z_{out}}{S} = +j\ ,\quad b)\ \frac{Z_{out}}{S} = \infty\ ,\quad c)\ \frac{Z_{out}}{S} = -j\ . \qquad (5.48)$$

In terms of the input reflection coefficient, from (5.43), the corresponding input impedances are:

$$Z'_{in_{a,b,c}} = -j\ \tan\left[\left(\frac{\theta_{a,b,c}}{2}\right)\right]\ ,\quad \theta = \frac{4\pi d}{\lambda_g} \qquad (5.49)$$

where the prime denotes normalization with respect to Z_0 in rectangular guide. With these relationships applied to Eqs. (32), Chap. II, of the Final Report, the relative equivalent circuit parameters Z'_{11}, Z'_{12}, Z'_{22} can be found, which, in turn, determine the equivalent transformer network as:

$$Y'_1 = \frac{1}{Z'_{11}}\ ;\quad Y'_2 = \frac{Z'_{11}}{Z'_{11}\,Z'_{22} - Z'^{2}_{12}}\ ;\quad n = \frac{Z'_{11}}{Z'_{12}}\ . \qquad (5.50)$$

The network so obtained is checked against a fourth measurement which yields the input admittance for the slot radiating into the unterminated half-space. These results, together with theoretical results obtained as discussed in Sec. C, are listed in Table II.

The theoretical value of Y'_2 in Table II is infinite under the assumptions in Sec. C for a zero thickness slot. The theoretical value of Y'_1 is listed as purely reactive. Actually slight real parts of the order of .02 were obtained but discarded, since that order of magnitude corresponds to the tolerances put on the measured values of Y_t as taken from Final Report, Chap. V, Table VI. The finite measured value for Y'_2 as well as the discrepancy between theoretical and experimental Y'_1 is at least partly due to the physical thickness of the slot (see Sec. E). There also exist differences between the directly measured input admittances for the unterminated half-space and those obtained by terminating the equivalent circuit in a spherical line match. (Where the directly measured input admittances in Table II do not have real parts, the V.S.W.R. was too high to be measured accurately and was arbitrarily taken to be infinite.) The differences between the two results can be attributed to a great extent to the tolerances on the equivalent circuit parameters. The tolerances due to error in the input data alone were obtained by computing the sensitivity of each parameter to small deviations in location of the voltage minimum in the rectangular guide, and multiplying by the expected possible error.

TABLE II

Experimentally Obtained Network Parameters For Radiating Slots

The parameters are those for the circuit in Figure 5.6.

$$Y_1' = \frac{Y_1}{Y_o} \quad ; \quad Y_2' = \frac{Y_2}{Y_o} \quad ; \quad \gamma\ell = \frac{2\pi}{\lambda_g} \quad ; \quad k = \frac{2\pi}{\lambda} \quad ; \quad Y_o = p\frac{\lambda}{\lambda_g} \quad ; \quad \lambda = 1.26'' \quad ; \quad \lambda_g = 1.76''$$

The results in the last column are computed by placing a match on the output terminals of the measured equivalent circuit.

Slot Size	3 - cup measurements			Theoretical evaluation		Input Admittance	
	Y_1'	n	Y_2'	Y_1'	n	Measured	Computed from equiv. circuit
a' = .354" b' = .158"	- j 6.41	1.35	- j 83	- j 5.75	1.44	- j 6.58	.75 -j 6.43
a' = .448" b' = .159"	- j 2.59	1.35	- j 21	- j 2.30	1.42	- j 2.80	.76 -j 2.64
a' = .54" b' = .16"	- j .680	1.36	- j 21	- j .61	1.40	.77 -j .67	.75 -j .72
a' = .60" b' = .09"	- j .064	1.35	- j 83	j .02	1.37	.78 -j .064	.76 -j .077
a' = .63" b' = .16"	j.196	1.34	- j 27	j .18	1.35	.81 +j .18	.77 +j .16

These tolerances were found to be of the order of $\pm$ .01 on Y_1', of the order of $\pm$ .02 on n, and of the order of $\pm$ (.25 Y_2') on Y_2'. The high sensitivity of Y_2' to experimental errors is not too critical since Y_2' is a series admittance of large magnitude so that its reciprocal is the pertinent quantity in a network calculation. In addition to errors in the input data there is the possibility of error in the output quantities such as to make the output impedances different from those listed in Equation (5.48). Such deviations can be brought about by a slightly different radius or non-spherical shape for the spherical cups, or by noting the effect of the thin insulating mica strip on the cup rims. Computations to take into account the former sources of output error could be made, but it was felt that the non-precision nature (three-point method) of the measurements did not warrant it. At any rate, the agreement between the quantities compared in Table II is considered reasonable.

E. Effect of Slot Thickness on the Equivalent Circuit Parameters

The schematic and equivalent circuit representations for the thick rectangular slot radiating from the end of rectangular waveguide are given in Figure 5.9. The thick slot is taken to be a transmission line of length t and constants γ' and Y_o' coupling the rectangular guide with constants γ and Y_o to the spherical guide with constants k and γ. The network between terminals T_1 in Figure (5.9-b) represents the effect of change in cross-section of the rectangular guide, while the network between terminals T_3 and T_2 in the same figure takes into account the coupling between the slot and the spherical guide. The parameters B_{tj}/Y_o and n' have been encountered on numerous occasions before (See Part II; n'^o is equal to $1/n_t$) and are given by

$$\frac{B_{tj}}{Y_o} = .5 \times \text{(Admittance of thin slot of same dimensions coupling two identical rectangular guides)}$$

(5.51)

$$n' = \frac{\pi}{4}\sqrt{\frac{a\,b}{a'\,b'}}\left[\frac{1-(\frac{a'}{a})^2}{\cos(\frac{\pi\,a'}{2a})}\right]$$

where a' and b' are the dimensions of the slot parallel to the guide dimensions a, b, respectively. The parameters n and B'/Y_o are obtained from

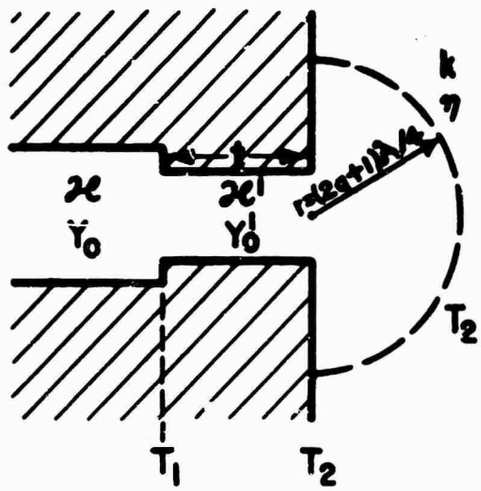

SCHEMATIC
(a)

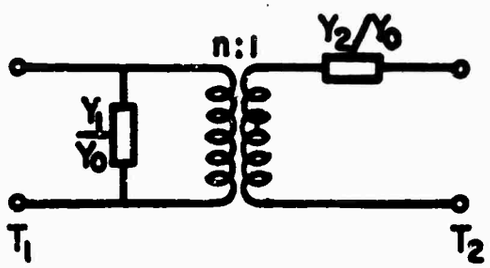

REDUCED FORM OF CIRCUIT (b)
(c)

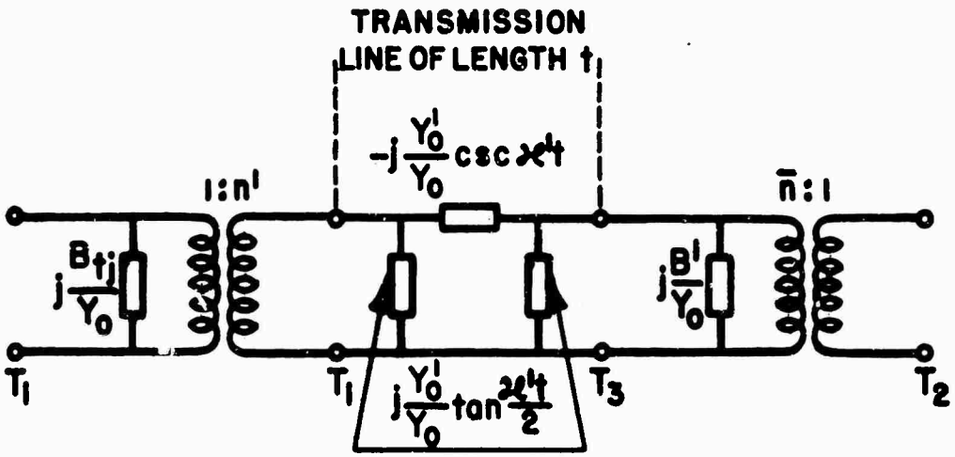

EQUIVALENT CIRCUIT IN COMPONENT FORM
(b)

Representation for the Thick Slot

Figure 5.9

Sec. C, Equations (5.34) and (5.35), respectively, from the theoretical circuit for the junction effect for a thick slot radiating into a half-space. In this case Y_1 corresponds to B', Y_t represents the terminal admittance Y_{rtk} of a thick slot radiating into a match (see Part IV), and

$$\underline{h}_g = \sqrt{\frac{2}{ab}} \cos\left(\frac{\pi x}{a'}\right) \underline{x}_o \qquad \text{so that} \qquad |\bar{n}| = \sqrt{\frac{a' b'}{2}} / D \ ,$$

where D is the same demoninator as in Equation (5.28). Since the transformer with turns ratio n' has been retained in the equivalent circuit formulation for the change in cross-section in rectangular guide, the characteristic admittance Y_o' is defined in the usual manner as

$$Y_o' = \frac{\varkappa'}{\omega \mu} \tag{5.52a}$$

so that

$$\frac{Y_o'}{Y_o} = \frac{\varkappa'}{\varkappa} = \frac{\lambda_g}{\lambda_g'} \tag{5.52b}$$

In order to determine how the theoretically derived circuit in Figure 5.4 is affected by physical thickness of the slot it is desirable to transform the equivalent circuit of Figure 5.9-(b) into the form given in Figure 5.9-(c) so that direct comparison with the theoretical (and measured) networks is easily achieved. The conversion to the simple form of Figure 5.9-(c) is brought about by first changing circuit 5.9(b) into the standard π form of Figure 5.10.

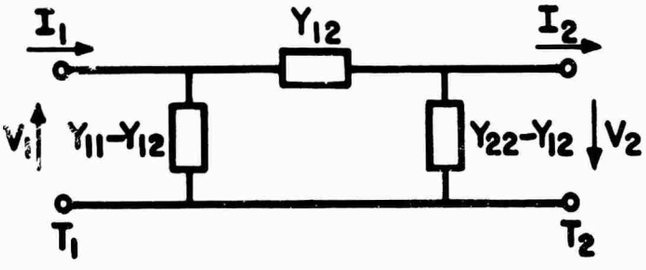

π - Representation for Thick Slot

Figure 5.10

The π parameters are found from short-circuit terminations as follows:

$$Y_{11} = \left(\frac{I_1}{V_1}\right)_{V_2=0} \quad ; \quad Y_{22} = \left(\frac{I_2}{V_2}\right)_{V_1=0} \quad ; \quad Y_{12} = \left(\frac{I_2}{V_1}\right)_{V_2=0} = \left(\frac{I_1}{V_2}\right)_{V_1=0} \tag{5.53}$$

which, in terms of the quantities in Figure 5.9-(b), become:

$$\frac{Y_{11}}{Y_o} = j\left[\frac{B_{t1}}{Y_o} - n'^2\,\frac{Y_o'}{Y_o}\cot \varphi' t\right]$$

$$\frac{Y_{22}}{Y_o} = j\,\bar{n}^2\left[\frac{B'}{Y_o} - \frac{Y_o'}{Y_o}\cot \varphi' t\right] \tag{5.54}$$

$$\frac{Y_{12}}{Y_o} = -j\,\bar{n}\,n'\,\frac{Y_o'}{Y_o}\csc \varphi' t$$

from which the parameters in Figure 5.9-(c) are determined as

$$Y_1 = \frac{\Delta}{Y_{22}} \quad ; \quad Y_2 = Y_{22} \quad ; \quad n = \frac{Y_{22}}{Y_{12}} \quad ; \quad \Delta = Y_{11}\,Y_{22} - Y_{12}^2 \tag{5.55}$$

For small thicknesses,

$$\frac{Y_1}{Y_o} \longrightarrow \frac{B^*}{Y_o} + n'^2\,\frac{B'}{Y_o}$$

$$n \longrightarrow \frac{\bar{n}}{n'}\cos \varphi' t \tag{5.55a}$$

$$\frac{Y_2}{Y_o} \longrightarrow -j\,\bar{n}^2\,\frac{Y_o'}{Y_o}\cot \varphi' t$$

The parameters Y_1/Y_0, Y_2/Y_0, and n have been computed for thicknesses up to .5" for four different slot dimensions and are plotted in Figure 5.11. Since the thick slot circuit parameters depend on the values of B_{t_1}/Y_0 and B'/Y_0, the accuracy of the former can be no better than that of the latter. In addition, the replacement of the thick slot by a length t of single-mode transmission line can no longer be justified for small thicknesses because of higher mode interaction effects. In spite of these inaccuracies in the small-thickness range the curves in Figure 5.11 indicate the trend of change in the parameters with thickness. Thus, the element Y_2/Y_0 is always large and negative; this is borne out by the measurements (cf. Table II). Also, the absolute value of Y_1/Y_0 should increase with slot thickness; this trend is also confirmed by the experimental values if one compares the Y_1/Y_0 parameter from the 3-cup measurements on "thick" (about 10 or 15 mil) slots with the value of B_r/Y_0 found previously for 5 mil slots, in the Final Report, Chap. V, Table VI. On the other hand, there exist no experimental values for n for the 5 mil slots so that no thickness comparison can be made here. It is apparent, however, that for small slots the theoretical values for n are higher than the experimental ones, thus opposing the trend predicted for n by Equations (5.55a). But for small slots, the cosine field assumption is not too accurate and may cause deviations since the expression for n is not variational. The different curve shapes of Figure 5.11 obtained for different slots are due primarily to different guide wavelengths for the slot guides of thickness t.

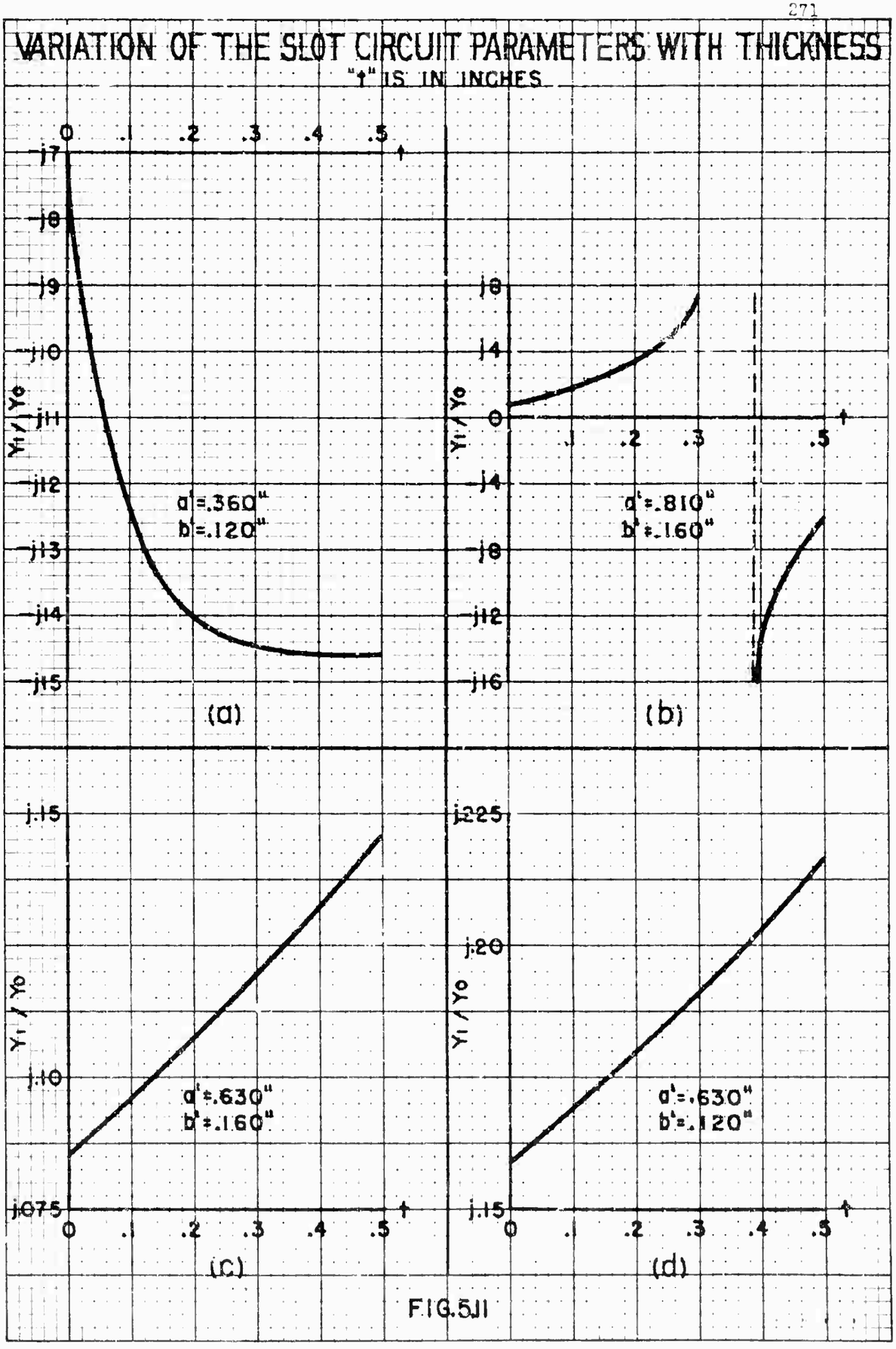
VARIATION OF THE SLOT CIRCUIT PARAMETERS WITH THICKNESS
"t" IS IN INCHES
Y1 / Yo
t
0 .1 .2 .3 .4 .5
-j7
-j8
-j9
-j10
-j11
-j12
-j13
-j14
-j15
a'=.360"
b'=.120"
(a)
j8
j4
0
-j4
-j8
-j12
-j16
a'=.810"
b'=.160"
(b)
j.15
j.10
j.075
a'=.630"
b'=.160"
(c)
j.25
j.20
j.15
a'=.630"
b'=.120"
(d)

FIG.5.11

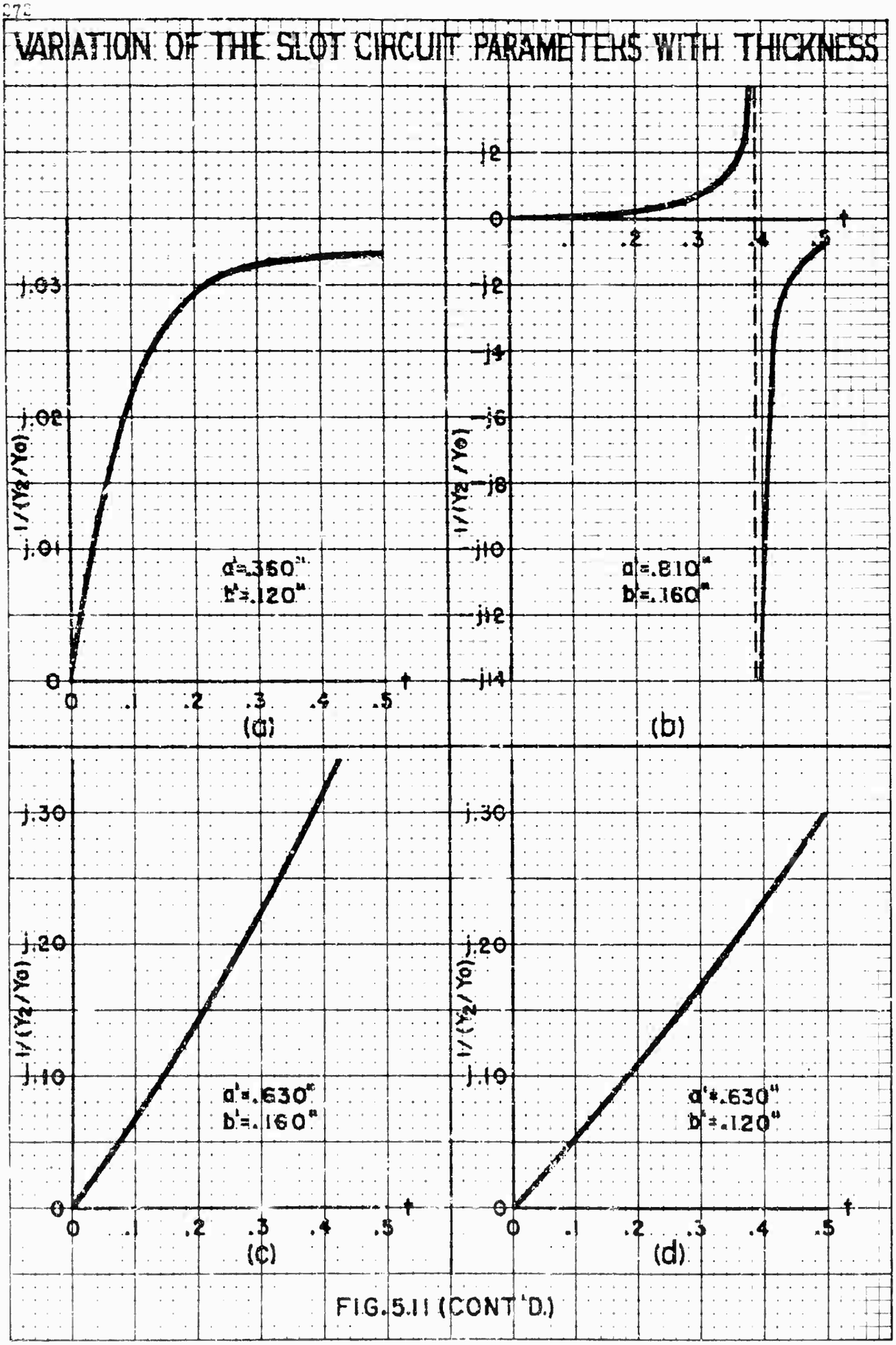

FIG. 5.11 (CONT'D.)

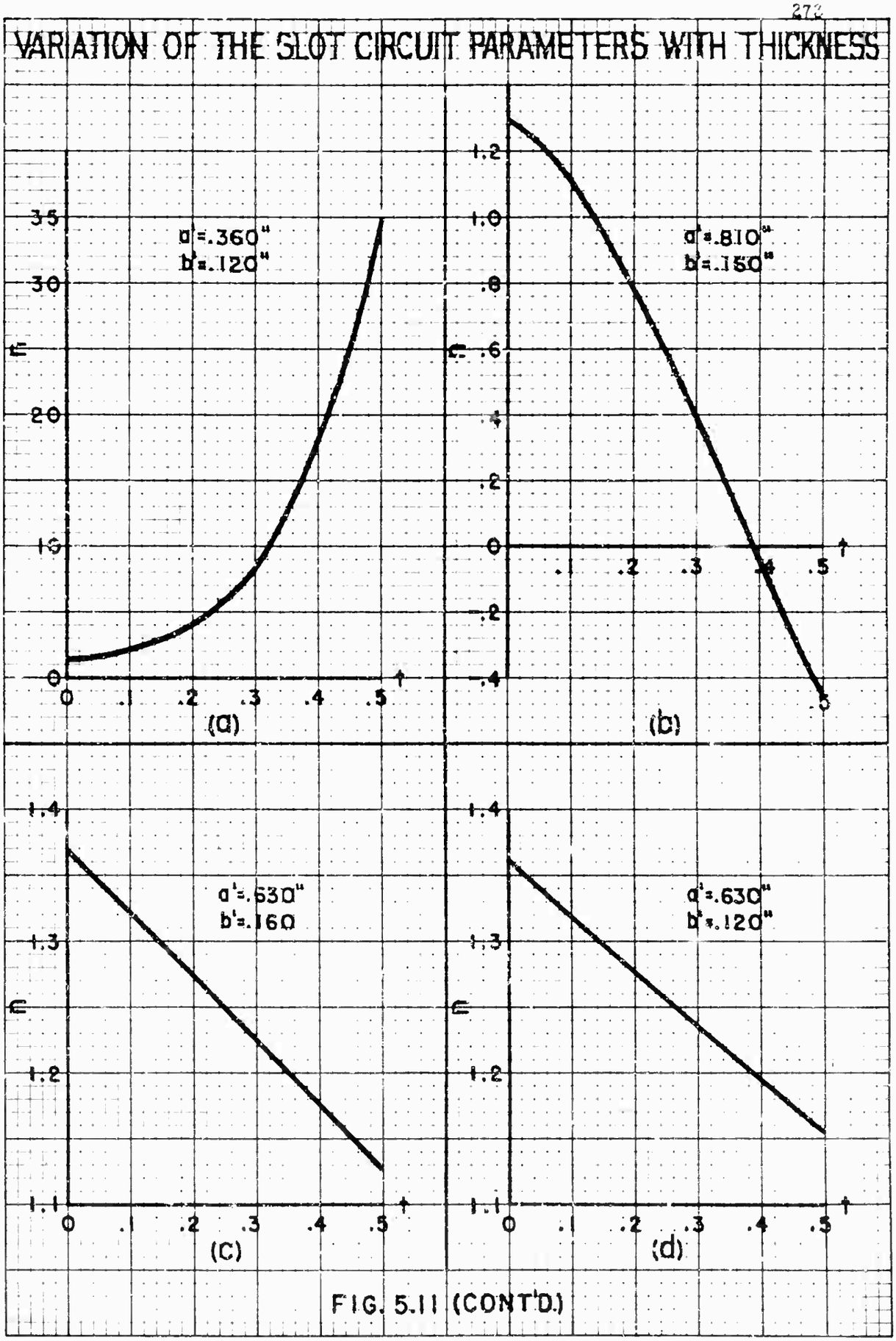

FIG. 5.11 (CONT'D.)

APPENDIX: Fundamental Relationships in Spherical Transmission Lines

The homogeneous transmission line equations for the i-th mode in a spherical line are the following:[3]

$$\frac{d V_i(r)}{dr} = -j \gamma_i(r) Z_i(r) I_i(r)$$

$$\frac{d I_i(r)}{dr} = -j \gamma_i(r) Y_i(r) V_i(r) \qquad (1)$$

where $\gamma_i = \sqrt{k^2 - \frac{k_{ci}^2}{r^2}}$; $k_{ci}^2 = n(n+1)$

$$Z_i = \frac{1}{Y_i} = \zeta \frac{k}{\gamma_i} \quad \text{for H modes}$$

$$\zeta = \sqrt{\frac{\mu}{\epsilon}} \; ; \quad k = \omega\sqrt{\mu\epsilon} = \frac{2\pi}{\lambda}$$

γ_i, k_{ci}, Z_i and Y_i are, respectively, the propagation constant, "cutoff" wavenumber, characteristic impedance, and characteristic admittance, for the i-th mode. i stands for the double index (m, n). Equation (1) can be expressed in terms of V_i alone as:

$$\frac{d^2 V_i}{d(kr)^2} + \left[1 - \frac{n(n+1)}{(kr)^2}\right] V_i = 0 \qquad (2)$$

which is a modified form of Bessel's equation, with solution either as

$$V_i(r) = A_i \hat{J}_n(kr) + B_i \hat{N}_n(kr) \qquad (3a)$$

or

---

[3] N. Marcuvitz, "Waveguide Handbook", McGraw-Hill Book Co., New York; 1951. Secs. 1.8 and 2.8.

$$V_i(r) = C_i \hat{H}_n^{(1)}(kr) + D_i \hat{H}_n^{(2)}(kr) = V_{inc_i} + V_{refl_i} \qquad (3b)$$

where $$\hat{H}_n^{(1)}(kr) = \hat{J}_n(kr) \pm j \hat{N}_n(kr)$$

Equation (3a) is the standing wave solution while Equation (3b) is the traveling wave solution, with $\hat{H}_n^{(1)}$ and $\hat{H}_n^{(2)}$ representing waves traveling toward, and away from the origin, respectively, for an assumed time variation of $e^{+j\omega t}$. The $\hat{J}_n$, $\hat{N}_n$, $\hat{H}_n^{(1)}$, $\hat{H}_n^{(2)}$ functions are, respectively, the spherical Bessel, Neumann, and Hankel functions of the 1st and 2nd kind. The spherical Bessel and Neumann functions are related to the ordinary Bessel and Neumann functions as follows:

$$\hat{J}_n(kr) = \sqrt{\frac{\pi kr}{2}}\, J_{n+1/2}(kr) \quad ; \quad \hat{N}_n(kr) = \sqrt{\frac{\pi kr}{2}}\, N_{n+1/2}(kr) \qquad (4)$$

Upon using the first of Equations (1) and (3b) we find the corresponding current solution:

$$-j\zeta I_i(r) = C_i \hat{H}_n^{(1)\prime}(kr) + D_i \hat{H}_n^{(2)\prime}(kr) = A_i \hat{J}_n'(kr) + B_i \hat{N}_n'(kr) \qquad (5)$$

where the prime denotes the derivative with respect to the argument.

From (3b), we can define the voltage reflection coefficient $\Gamma_n(r)$, looking in the direction of increasing r, as follows:

$$\Gamma_n(r) = \frac{C_i \hat{H}_n^{(1)}(kr)}{D_i \hat{H}_n^{(2)}(kr)} = \frac{C_i}{D_i}\, e^{j2\hat{\eta}_n(kr)} =$$

$$= \Gamma_n(r_o) e^{j2\left[\hat{\eta}_n(kr) - \hat{\eta}_n(kr_o)\right]} \quad ; \hat{\eta}_n(kr) = \tan^{-1}\left[\frac{\hat{N}_n'(kr)}{\hat{J}_n'(kr)}\right] \qquad (6)$$

In particular:

$$\Gamma_n(0) = -\Gamma_n(r_o)\, e^{-j\,2\,\hat{\eta}_n(kr_o)} \tag{7}$$

since, for $r \to o$: $\hat{N}_n(kr) \to \infty$, $\hat{J}_n(kr) \to o$; $n > o$. For the H_{11} mode in spherical guide (i.e., $n = 1$), the spherical functions are given by:

$$\hat{J}_1(kr) = \frac{\sin kr}{kr} - \cos kr \quad ; \quad \hat{N}_1(kr) = -\sin kr - \frac{\cos kr}{kr} \tag{8}$$

Since the Neumann functions become infinite at the origin it is desirable to relate solutions for specific quantities at the origin to those far removed therefrom. Such a relationship can be derived for the voltage reflection coefficient. For $kr >> 1$, the spherical Bessel and Neumann functions reduce to

$$\hat{J}_n(kr) \cong \sin(kr - n\pi/2) \quad ; \quad \hat{N}_n(kr) \cong -\cos(kr - n\pi/2) \tag{9}$$

so that the phase function $\hat{\eta}_n$ for the Hankel function $\hat{H}_n$ becomes

$$\hat{\eta}_n(kr) \cong \tan^{-1}\left[\cot(n\pi/2 - kr)\right] = kr - (n+1+2p)\pi/2, \; p=0, 1, 2 \ldots \tag{10}$$

Suppose, now, that the voltage reflection coefficient $\Gamma(r_o)$ at $r = r_o$ is known. The reflection coefficient at the origin in terms of $\Gamma(r_o)$ is given in (7). Upon substituting (7) into (6) we can write for any r:

$$\Gamma_n(r) = -\Gamma_n(0)\, e^{j\,2\,\hat{\eta}_n(kr)} = -\Gamma_n(0)\, e^{j\,2\left[kr - (n+1)\pi/2\right]}, \; kr >> 1 \tag{11}$$

Equation (11) immediately suggests the selection of two special values of r:

$$a)\ r = q\,(\lambda/2)\ ,\quad b)\ r = (2q+1)(\lambda/4)\ ;\quad q = \text{large integer} \qquad (12)$$

In terms of these radii, Equation (11) reduces to:

$$a)\ \Gamma_n\,(q\lambda/2) \cong (-1)^n\,\Gamma_n(0)\ ,\quad b)\ \Gamma_n\left[(2q+1)\lambda/4\right] \cong (-1)^{n+1}\,\Gamma_n\,(0) \qquad (13)$$

Thus, for the H_{11} mode, the reflection coefficients at the origin and at a radius $r = (2q+1)\lambda/4$, q large integer, are identical (to within the approximation that terms of the order of $1/kr$ and higher can be neglected).